*Conjugated compounds for molecular electronics: from synthesis to conductance studies.*

SANTIAGO MARQUES-GONZALEZ

# Conjugated compounds for molecular electronics:

## *from synthesis to conductance studies*

Santiago Marqués González

This project concerns the synthesis and characterization of linear conjugated compounds, and assessment of their electrical performance. To that end, several oligo(phenylene-ethynylene)s (OPEs) were prepared and the available synthetic procedures reviewed and optimized. Monolayers of these compounds were transferred onto solid substrates by means of the Langmuir-Blodgett technique, and their physical and electrical properties evaluated by Atomic Force Microscopy (AFM) and Scanning Tunnelling Microscopy (STM).

Two novel approaches to the formation of the top electrode on sandwich like metal|molecule|metal devices, based on the in-situ decomposition of gold complexes, are detailed. The synthetic methodologies appropriate for the preparation of gold ethynyl complexes Au(C≡CR)(L) (R = aryl, L= $PPh_3$ and CNR) that are critical to the thermal and photochemical decomposition protocol are described.

A convenient synthesis of bis(ethynyl) complexes *trans*-Ru(C≡CR)$_2$(dppe)$_2$ and unsymmetrically substituted derivatives *trans*-Ru(C≡CR$^1$)(C≡CR$^2$)(dppe)$_2$ is described. A detailed structural and spectroelectrochemical study of the complexes, supported by TD-DFT calculations, demonstrated the relationships between the underlying electronic transitions that are responsible for the NIR absorption band shape and the relative orientations of the metal fragment and arylethynyl moieties in the oxidized species.

Single molecule STM conductance studies were performed on a series of OPE and polyyne derivatives devoting special attention to the role of the molecular linker in the overall performance of the molecular junction. In that regard, a novel molecular linker C≡CSiMe$_3$ was introduced and its electrical and mechanical properties benchmarked against literature known molecular anchoring groups *i.e.* $NH_2$ and SH. Transistor-like behaviour was observed in preliminary electrochemical STM studies performed on complex Ru(C≡CC$_6$H$_4$C≡CSiMe$_3$)$_2$(dppe)$_2$. Finally, the statistical treatment of the conductance (STM) and force (AFM) measurements and the Visual Basic (VBA) codes designed to analyse the large datasets collected are included.

# Conjugated compounds for molecular electronics:

## *from synthesis to conductance studies*

Santiago Marqués González

**PhD THESIS**

Department of Chemistry

University of Durham

2014

## DECLARATION

The material contained in this thesis is, unless stated otherwise through cited reference, the result of the author's work at the University of Durham, Department of Chemistry, between October 2010 and March 2014 and it has not been submitted for a degree at this or any other university.

## STATEMENT OF COPYRIGHT



## PUBLICATION LIST

Martín, S., Pera, G., Ballesteros, L.M., Hope, A. J., **Marqués-González, S.**, Low, P. J., Pérez-Murano, F., Nichols, R. J., Cea, P., *Chem. Eur. J.*, **2014**, accepted in press, DOI: 10.1002/chem.201303967. *"Towards the fabrication of the top-contact electrode in molecular junctions by photoreduction of a metal precursor"*

Li, X.; Zhao, X.; Gao, S.; **Marqués-González, S.**; Yufit, D. S.; Howard, J. A. K.; Low, P. J.; Zhao, Y.; Gan, N.; Guo, Z., *J. Mater. Chem. A*, **2013**, *1*, 9164. "*The structure and coordinative self-assembly of films based on a palladium compound of pyridyl-acetylene platinum and its application in Suzuki and Heck coupling reactions"*

**Marqués-González, S.**; Yufit, D. S.; Howard, J. A. K.; Martin, S.; Osorio, H. M.; Garcia-Suarez, V. M.; Nichols, R. J.; Higgins, S. J.; Cea, P.; Low, P. J., *Dalton Trans.*, **2013**, *42*, 338. **"***Simplifying the conductance profiles of molecular junctions: the use of the trimethylsilylethynyl moiety as a molecule-gold contact*"

Ballesteros , L. M.; Martín , S.; Cortés , J.; **Marqués-González, S.**; Higgins, S. J.; Nichols, R. J.; Low, P. J.; Cea , P., *Chem. Eur. J.*, **2013**, *19*, 5352. "*Controlling the structural and electrical properties of diacid oligo(phenylene ethynylene) Langmuir–Blodgett films*"

Ballesteros, L. M.; Martín, S.; Momblona, C.; **Marqués-González, S.**; López, M. C.; Nichols, R. J.; Low, P. J.; Cea, P., *J. Phys. Chem. C*, **2012**, *116*, 9142. "*Acetylene used as a new linker for molecular junctions in phenylene–ethynylene oligomer Langmuir–Blodgett films*"

# ACKNOWLEDGMENTS

I just cannot believe I am actually here, writing this page, the last before submitting the thesis. I must confess that even after three years, it is rare the day that goes by without my brain going white and after looking around for a couple seconds, ends asking: how on earth did I end here? Hope you understand that, for a Spaniard that never thought about doing a PhD and somehow ended in a lab in Australia, after three years in England, things may feel a bit out of control.

Before exposing the results of the last three years of work, I would like to thank Prof. Paul J. Low's terrible employee selection skills, for giving me the opportunity to waste a considerable amount of his time and money over the last three years, and the chance, to my dislike, to make some good friends along the way: Dr. Phil, Sören, Marie, Dr. Jose, Sam, Dr. Josef, Dr. Ross-Helen, Matthias, Campbell etc… but also, to the other members of the Low family: Sonia, Melissa and James for digging me out of the office to play around making me feel like at home whilst being so far away.

Finally, I would like to dedicate this thesis to my family: my parents, Joaquin and Francisca for being a true life example, thanks for all the love and unconditional support you have given me every single day of my life. To my brother Alfonso, I cannot think of a better person to share life with. To my sister "in-law" Elia, for your patience and contagious happiness. Finally, to the Singaporean side of the family, James and Huitian for your friendship and support that makes this side of the world feel a bit closer to home.

Thanks for your help throughout the last three years of "methodical chaos"…

Would you tell me, please, which way I ought to go from here?

*That depends a good deal on where you want to get to…*

I don't much care where…

*Then it doesn't much matter which way you go.*

…so long as I get somewhere…

*Oh, you're sure to do that, if you only walk long enough…*

**Alice in Wonderland, Lewis Carroll**

# ABBREVIATIONS

| | |
|---|---|
| º | degrees |
| ºC | degrees Celsius |
| δ | chemical shift (ppm) |
| ε | molar extinction coefficient |
| AFM | Atomic Force Microscopy |
| AR-XPS | angle resolved X-ray photoelectron spectroscopy |
| ASAP | atmospheric pressure analysis probe mass spectrometry |
| $\beta$ | tunnelling attenuation factor ($nm^{-1}$) |
| BAM | Brewster angle microscopy |
| BJ | break junction |
| br. | broad |
| $Bu^t$ | *tert*-butyl |
| calcd. | calculated |
| ca. | circa |
| conc. | concentrated |
| CP-AFM | conducting probe atomic force microscope |
| CV | cyclic voltammetry |
| DARPA | Defence Advanced Research Agency (United States) |
| D-B-A | Donor-Bridge-Acceptor |
| dba | dibenzylideneacetone |
| DBU | 1, 8-diazabicyclo[5.4.0]undec-7-ene |
| DFT | Density Functional Theory |

| | |
|---|---|
| DMF | dimethylformamide |
| dppe | 1, 2-bis(diphenylphosphino)ethane |
| E | potential |
| ESI | electrospray ionization |
| Et | ethyl |
| Fc | ferrocene |
| Fc* | decamethylferrocene |
| $G_0$ | conductance quantum (77480 nS) |
| GNPs | gold nanoparticles |
| HOMO | highest occupied molecular orbital |
| HOSO | highest occupied spin orbital |
| IR | infrared |
| $I(s)$ | current-distance STM technique |
| $I(t)$ | current-time STM technique |
| *I-V* | current-voltage |
| IVCT | intervalence charge transfer |
| L | Langmuir |
| LB | Langmuir-Blodgett |
| LCDs | liquid-crystal display |
| LMCT | ligand-to-metal charge transfer |
| LOFO | lift-off-float-on |
| LUMO | lowest unoccupied molecular orbital |
| LUSO | lowest unoccupied spin orbital |

| | |
|---|---|
| *m*- | meta-substituted |
| MCBJ | mechanically controlled break junction |
| Me | methyl |
| MeCN | acetonitrile |
| MeOH | methanol |
| MLCT | metal-to-ligand charge transfer |
| MS | mass spectrometry |
| NIR | near-infrared |
| NLGF | non-linear Green's function |
| NMR | Nuclear Magnetic Resonance |
| $NEt_3$ | triethylamine |
| *o*- | ortho-substituted |
| OAc | acetate |
| OLEDs | Organic Light-Emitting Devices |
| OMe | methoxy |
| OPEs | Oligo(phenylene-ethynylene)s |
| OTf | trifluoromethanesulfonate |
| OTs | 4-toluenesulfonyl |
| *p* - | para-substituted |
| py | pyridine |
| PALO | Polymer-Assisted Lift-Off |
| PEDOT:PSS | poly(3,4-ethylenedioxythiophene):poly(4-styrenesulfonic acid) |
| $PPh_3$ | triphenylphosphine |

| | |
|---|---|
| $Pr^i$ | iso-propyl |
| QCM | Quartz Crystal Microbalance |
| Radar | Radio detection and ranging |
| SA/SAMs | self-assembly / self-assembled monolayers |
| SEM | Scanning Electron Micorscopy |
| SERS | Surface-Enhanced Raman Spectroscopy |
| SPM | Scanning Probe Microscopy |
| STM | Scanning Tunnelling Microscopy |
| STM-BJ | Scanning Tunnelling Microscope controlled Break Junctions |
| TBAF | tetra-*n*-butylamonium fluoride |
| TCB | 1, 2, 4-trichlorobenzene |
| TD-DFT | Time Dependent Density Functional Theory |
| THF | tetrahydrofuran |
| tht | tetrahydrothiophene |
| TLC | Thin Layer Chromatography |
| USAF | United States Air Force |
| UV-Vis | Ultraviolet-visible |
| VBA | Visual Basic |
| WWII | World War II |
| XPS | X-Ray Photoelectron Spectroscopy |

# *TABLE OF CONTENTS*

# 1. GENERAL INTRODUCTION TO MOLECULAR ELECTRONICS

Molecular electronics is an interdisciplinary field that involves the use of molecules as fundamental electronic components such as wires, transistors, memories and gain elements. The field, sometimes called moletronics,[1] is nowadays firing the imagination of a broad cross-section of the scientific community. The great potential of the field to alleviate growing concerns over the future of conventional silicon electronics, and the great interest awakened in the research community by the fundamental scientific challenges can be clearly observed in the marked increase of research articles published during the last decade (Figure 1-1). As it can be seen, 2001 is a critical point in time for the field marking the rapid growth from dozens of publications a year to hundreds. It is no coincidence that, the hook-up of molecules into functional circuits was labelled the breakthrough of the year in 2001 by *Science* magazine.[2]

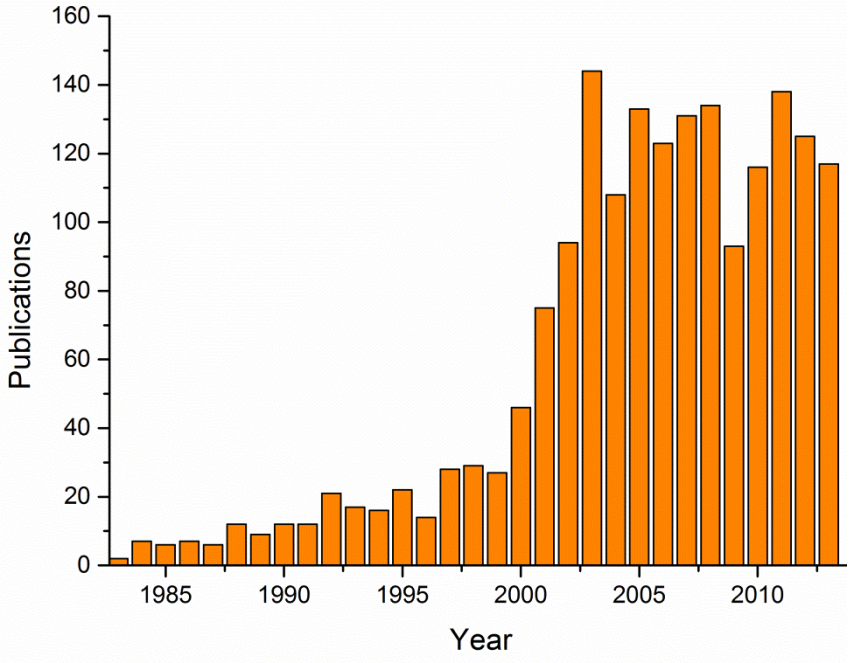


**Figure 1-1.** *"Molecular electronics" bibliometrics. Source: Scifinder at January 2014.*

Before getting into greater detail, a distinction needs to be made between *molecular materials for electronics* and *single molecule electronics*. The use of organic materials for electronic applications that deal with ensembles of several millions of molecules and for which properties are measured on the macroscopic level is nowadays in a mature stage of development and application. Some of the most relevant examples of molecular materials for electronics are the use of liquid crystals in screen displays (LCDs)[3] or the more recent use of organic light emitting diodes (OLEDs).[4] In recent years, the application of molecular materials for electronics has found its way into the market, largely in novel displays, but also in the form of printed and polymer electronics, complementing silicon-based devices allowing for an overall reduction in size and costs, or enhanced performance and consumer appeal of the resulting electronic devices.

However, the sub-field of molecular electronics which this thesis concerns can be summarised as the use of *single molecules* to mimic functional elements in electronic devices. The use of molecules as building blocks to give rise to a more complex system is typically referred to as the "bottom-up" approach, as opposed to the conventional "top-down" lithographic techniques that are employed to etch small features into silicon crystals to build a working device. Despite (or perhaps because of) the great challenges the field of single molecule electronics presents, the enormous benefits of a molecule-based "bottom-up" approach motivates the scientific community to keep moving the field forward. As a clarifying example, a top-end computer microchip nowadays contains $10^9$ transistors in an area of 180 $mm^2$ with typical node sizes *ca.* 22 nm. A single mole of molecular transistors could theoretically provide $10^{23}$ transistors with node sizes up to 20 times smaller. However, to be fair to the fine job of the semiconductor industry, each one of those conventional $10^9$ transistors works in perfect harmony with the rest of the electronic components at the incredible rate of over $10^9$ Hz.[5] The enormous challenge for single

molecule electronics lies in the development of molecular systems that perform better, or perhaps in alternative fashion to these extraordinary solid-state devices. However, before addressing the state-of-the-art in molecular electronics, a look at the field beginnings and development milestones is desirable to fully understand the aims and motivations of this research.

## 1.1. Molecular electronics: the rise of the silicon alternative

Although this section is focused on the rise and development of molecular electronics (Figure 1-2, *right*),[6] the history of the field is incomplete if it neglects the evolution of the silicon microelectronics industry (Figure 1-2, *left*). The first experiments on the electrical properties of semiconductor materials started early in the 19$^{th}$ century. The surprising properties of these materials such as their increased conductance when heated or exposed to light captured the attention of scientists and engineers of the time. Amongst the most renowned contributors of the time are Michael Faraday who first reported the conductance increase with temperature on silver sulfide (1833), Alexandre-Edmond Bequerel father of the photovoltaic effect (1839) and Alexander Graham Bell who employed selenium light sensitivity to transmit sound over a beam of light, the so-called "photophone" (US 235496 A, 1880).

Despite these early experiments, the birth of the semiconductor industry is typically ascribed to the genesis of the first transistor. Before that, electronic devices were based on the use of vacuum tubes to amplify and rectify electrical signals. The first semiconductor based transistor was built at the AT&T Bell labs a couple years after the end of World War II. Despite the great efforts made by both sides of the conflict on the improvement of electronics, as proved by the parallel development of the Radar technology, all the electronic devices used during WWII were based on the use of vacuum tubes.

However, as it happened to many other scientific fields, it is difficult to deny the great influence that WWII had in the quick development of semiconductor technology that followed soon after the conflict ended.

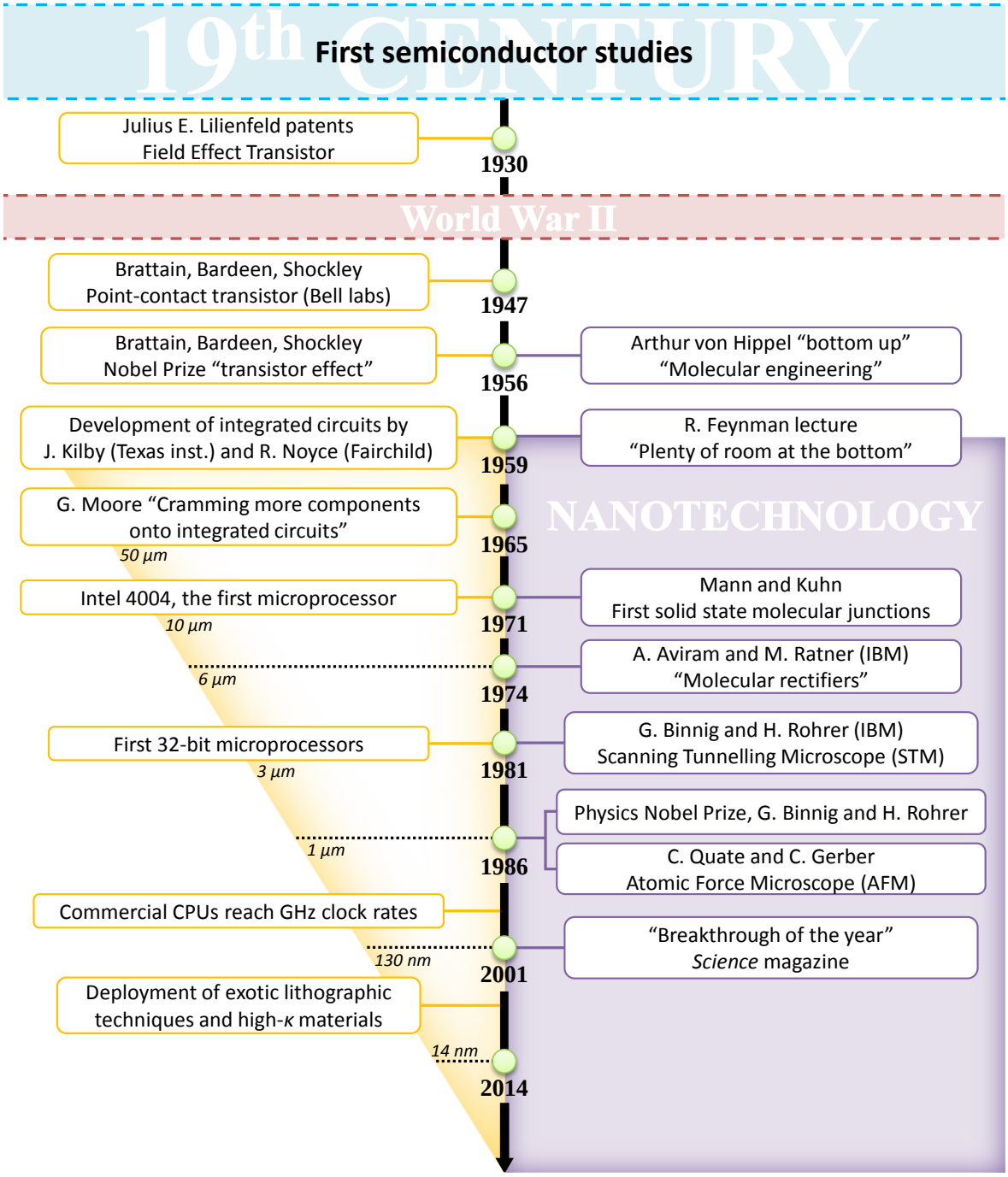


**Figure 1-2.** *Silicon industry (left) and molecular electronics (right) roadmap, from the genesis of the first semiconductor transistor to our days.*

It was Walter Brattain, John Bardeen and William Shockley of Bell laboratories who in 1947 discovered through a series of experiments that by applying a small bias to the surface of a germanium block, the current flow through a second circuit connected to that piece of germanium could be modulated. The device was named the field-effect transistor and with it, solid state electronics were born. However, in an often overlooked episode of the semiconductor history, most of Bell labs initial claims were rejected in benefit of Julius E. Lilienfeld, an Austro-Hungarian physicist best known for the discovery of radiation emitted by a metallic surface when electrons strike it, nowadays known as the Lilienfeld radiation. In 1930, seventeen years before the Bell labs discovery, Lilienfeld patented the field-effect transistor (US1745175 A). Despite his early description of the transistor effect, Lilienfeld's work was largely ignored by the emerging semiconductor industry. The Bell labs found their way around Lilienfeld's patents by presenting their creation as the first point-contact transistor and in 1956, only nine years after the first transistor was built, Brattain, Bardeen and Shockley were awarded the Physics Nobel Prize for their research on semiconductors and discovery of the transistor effect. In recognition of Lilienfeld's sometimes overlooked contribution to science, an annual prize that carries his name was established in 1988 by the American Physical Society to reward a most outstanding contribution to physics.

The 1950s was an era of frenetic activity at the Bell labs at the same time the first transistor was built, Jules Andrus and Walter L. Bond began adapting a photoengraving technique used to print patterns onto integrated circuits to generate sophisticated designs on silicon wafers. Their progress, together with the serendipitous discovery in 1955 of the silicon oxide masking by Carl Frosch also at the Bell labs set the start point for the modern monolithic microelectronics industry.

However, the semiconductor industry was soon a victim of its own success. Almost immediately after the production of the first commercial transistors, the increasing need for computing power became a proxy for a miniaturization race that still lasts to the present day. Transistor sizes dropped dramatically to just a couple centimetres in the year after the Bell work was announced, and the difficulties to further reduce the size of the components would soon occupy most of the industry attention. It is in this context where molecular electronics first came into view. The same year (1956), the Physics Nobel Prize was awarded for the discovery of the transistor effect, a German physicist named Arthur von Hippel then working at MIT proposed a completely different approach:

*"Instead of taking prefabricated materials and trying to devise engineering applications consistent with their macroscopic properties, one builds materials from their atoms and molecules for the purpose at hand ..."*

The notion of "molecular engineering" first introduced by von Hippel is commonly considered the first expression of the "bottom-up" approach and is regarded by many as the starting point of molecular electronics. von Hippels's concept was quickly embraced, and in 1957 a collaboration was set with the Westinghouse company. The successful partnership between Westinghouse and von Hippel ideas captured the attention of the US Air Force (USAF) at the end of the 1950s. At that time, the airborne electronic equipment was growing increasingly complex and vulnerable to failure, as aircraft began flying faster and higher. In 1959, the USAF finally decided to invest US$2 million in a joint USAF-Westinghouse research program for the development of molecular electronics as a possible solution to their problems. Their research proposal "Molecular Electronics – Dendritic Approach" proved successful enough to be funded until 1962. At that point the research program was abandoned mainly due to severe applicability problems.

It is fair to say, that researchers at the Westinghouse labs were the first to encounter what still remains the biggest challenge of the field: the manipulation of matter at the molecular level. The falling interest in molecular electronics in the 1960s was also due in part to the rapid progress being made by the contemporary silicon electronics technology. By the time the USAF became involved in the development of molecular electronics, solid state semiconductor electronics was on the cusp of a seminal breakthrough in integration, which heralded the arrival of the modern semiconductor revolution. In 1959 Jack Kilby at Texas Instruments, and Robert Noyce at Fairchild Camera, developed a solution to integrate even more of the individual components onto a circuit, the so-called solid circuit. In an attempt to reduce the components size, low production costs and increase electronics reliability, they were able to print and wire several electronic components on a silicon substrate. The importance of Kilby's work was recognized later in 2000 when he was awarded the Physics Nobel Prize for his contribution in the invention of the integrated circuit.

Despite the rapid post-war evolution of the silicon industry, the miniaturization race had just begun with the development of the integrated circuit, and the need for smaller electronic components maintained a degree of interest in the concepts of a molecular electronics technology. Two well-known events that gave impetus to molecular and semiconductor electronics took place in the 1960s. The first one was the famous lecture given by physicist Richard Feynman titled "There's plenty of room at the bottom" (December 29$^{th}$ 1959) in which he challenged the whole scientific community to push the miniaturization limits. For many, Feynman's revolutionary ideas exposed in that lecture are the starting point of nanoscience and nanotechnology. The second event has to do with the Intel co-founder Gordon E. Moore who in 1965 published his now famous paper "Cramming more components onto integrated circuits".[7] In his market study, Moore

predicted the growing pace of the number of electronic components, setting the guidelines for the miniaturization race. Only three years later, in 1968, Moore together with Robert Noyce founded the Intel Corporation, and the journey towards the evolution of consumer electronics and the multi-billion dollar semiconductor industry had begun.

In contrast, the ideas of molecular electronics technology had to wait until the 1970s to have a real impact on the scientific community. At that time, establishing electrical contacts across individual molecules was still a dream; however intramolecular electron transfer was being increasingly studied in solution, using the characteristic spectroscopic profiles associated with 'mixed valence' complexes and compounds (*vide infra*). By 1967 Peter Day and colleagues[8] had already prepared a number of mixed-valence systems and showed that in almost every case examined that, the electronic spectrum of the mixed-valence compound was very similar to that obtained from the superposition of the fully oxidized and the fully reduced species. Almost simultaneously with Allen and Hush, Robin and Day published in 1967 an extensive survey of mixed-valence systems and proposed a classification system according to their molecular or crystal structure. The desire to develop well-defined systems to study the electron transfer through bridging ligands lead Creutz and Taube to prepare and characterize the iconic mixed valence cation $[\{(NH_3)_5Ru\}(\mu\text{-py})\{Ru(NH_3)_5\}]^{5+}$ (py = pyrazine) now commonly known as the "Creutz-Taube ion".[9] A detailed overview on the history and foundations of the mixed valence chemistry can be found elsewhere,[10] and the use of mixed-valence systems as models for molecular electronics components continues to this day.[11]

The first direct measurements of through molecule conductance were reported in 1971 when Mann and Kuhn[12] in their pioneering work were able to contrast the already established in-solution electron transfer studies with solid state ones. They prepared a series of well-ordered fatty acid monolayers employing the Langmuir-Blodgett (LB)

technique, sandwiched them between metal electrodes and measured the electrical properties of the systems. Those studies revealed an exponential decay of the conductivity with the molecular length that still remains as one of the field's hot topics nowadays. However, while the scientific community struggled to integrate molecular components into solid-state platforms, the semiconductor industry continued with its relentless miniaturization progress reaching another milestone. In 1971, Intel presented the first ever general purpose microprocessor, the Intel 4004 processor, with over 2000 transistors built on a silicon monolith the size of a fingernail.

The silicon revolution that followed, driven by the then emerging, and now on-going, drive to meet 'Moore's Law', has overseen the growth of one of the most important and dynamic areas of global scientific and technological progress through the following five decades. In 1974, Ari Aviram who at that time worked at the IBM company, and his manager Mark Ratner, who agreed to supervise Aviram's thesis, started working on the theory of electron transfer through single organic molecules. Their efforts crystallized in a now-famous article titled "Molecular Rectifiers".[13] In that document, Aviram and Ratner suggested for the first time the use of a molecule with a modular design based on fragments familiar to chemists as an electronic component (Chart 1-1).

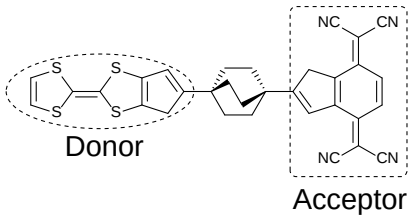


**Chart 1-1.** *Aviram and Ratner proposed a molecular rectifier based on tetrathiafulvalene (donor) and tetracyanoquinodimethane (acceptor) linked via a saturated methylene bridge.*

Curiously enough, Aviram and Ratner never used the words "molecular electronics" in their article; nevertheless, this seminal work became the beginning of the

modern field of molecular electronics. However, Aviram had no answer to the manufacturability problem, in fact he did not even synthesize his proposed rectifier let alone integrate millions of them into a working device. Staggeringly, despite over 2000 citations to the Aviram-Ratner molecular rectifier since 1974, to the best of our knowledge this compound has not yet been synthesized.

Although research efforts at IBM were mainly focused on the pursuit of better silicon processing, researchers there also had their eyes set on the possible future alternatives to the silicon platform. This ambivalent IBM approach resulted in the invention and development of the scanning tunnelling microscope (STM) by Gerd Binnig and Heinrich Rohrer in 1981. While investigating superconductivity and surfaces at the atomic scale they grew increasingly frustrated by the experimental limits of their tools, so they built their own, able to image and manipulate matter at the atomic level. The creation of the STM meant that in 1986, only five years after their invention was presented, Binnig and Rohrer were awarded with the Physics Nobel Prize. That same year (1986), inspired by the development of the STM, G. Binnig, C. Quate and C. Gerber developed the atomic force microscope (AFM). The AFM ability to scan and trace contours of surfaces (not necessarily conductive) revealing their atomic profile was quickly embraced by the scientific community.

With the introduction of the STM and the AFM, the experimental barrier that had frustrated every previous attempt to perform direct measurements of single molecule electronic properties was removed. The maturity of the STM, together with the rise and settlement of nanotechnology[14] and the development of other scanning probe microscopies,[15] such as the conducting probe atomic force microscopy (CP-AFM), brought a renaissance in molecular electronics science throughout the 1990s.

In an echo of the initial USAF-Westinghouse project, modern molecular electronics again managed to capture the attention of the Defence Advanced Research Projects Agency (DARPA) and a proposal by Mark Reed and James Tour, "Spontaneously-assembled molecular transistors and circuit. A quick integration of molecular components on silicon." became DARPA's ULTRA (for ultrafast, ultradense electronics) research theme. After several successful reviews, DARPA consolidated the ULTRA program as a Moletronics research program to provide funding to a multidisciplinary molecular electronics research network from the year 2000, which was overtaken by the Applications of Molecular Electronics (MoleApps) programme in 2004. The renewed interest in molecular electronics in the period is reflected in the growing number of research articles published during the second half of the 1990s lead the *Science* magazine to label the hook-up of molecules into functional circuits the breakthrough of the year in 2001.[2]

A decade after the *Science* declaration of the importance of the advances being made in molecular electronics, the area is making a steady advance towards acceptance as a main stream technology. Efforts to maintain the pace with Moore's law has driven decades of technological achievement and new materials science in the semiconductor industry,[16] and consequently, devices with 22 nm feature sizes are now available (Intel Ivy Bridge and Haswell chips). However, top-down scaling is becoming breathtakingly complex, and increasingly giving way to more complex and lithographically challenging 3D designs (e.g. Intel's 'tri-gate' 22 nm transistors), and conventional materials superseded (e.g. the use of high-$\kappa$ gate dielectrics in place of $SiO_2$).[17] Intel's CEO Brian Krzanich recently announced that the release of the next generation of 14 nm technology (Broadwell architecture) has been pushed back due to problems in yield manufacturing (Intel Developer Forum, 2013). Whilst a miss-step in Intel's production schedule and failure to meet its long standing 'tick-tock' schedule of chip refresh may not seem a major economic

or technological concern, this missed production window is not the first indication of the growing difficulties that conventional semiconductor fabrication methods are now facing. When pressed on this in an interview with the *Wall Street Journal* (21/11/2013), Intel's Executive Vice President of Manufacturing Operations, William Holt, gave the glib, but insightful comment "It's just getting really hard". In fact, the challenges associated with manufacturing advanced electronic circuits are now so great that in 2013 the international community was forced to re-write Moore's Law:

*After 2013, the Moore's Law rate of on-chip transistors slows to 2× every three years.*

***International Technology Roadmap for Semiconductors (2011)***

Molecular electronics has long been touted as a solution to future challenges in the semiconductors industry, and there is now growing industry acceptance of a potential future role for molecular electronics in the sector.

> *Moore's Law is going to hit a wall shortly… Therefore we are currently investigating the role of molecular electronics to potentially offer novel device concepts, which are ultimately scaled and provide electronic functionalities beyond those of the transistor.*
>
> ***IBM Research Laboratories, Zurich (2013)***

Thus with the semiconductor industry slowly struggling to keep up with Moore's predicted pace as they approach the astonishing figure of tenths of nanometres per transistor, molecular electronics seem to be gaining popularity amongst the academic community and the semiconductor industry. However, this time the story seems to have changed, nobody thinks of molecular electronics as a full alternative to silicon but as a complementary technology able to project the electronics industry even further. In other

words, silicon is here to stay; molecular electronics will have to find its way into the current fabrication methods.

> *Computing with molecules as circuit building blocks is an exciting concept with several desirable advantages over conventional circuit elements. Because of their small size, very dense circuits could be built, and bottom-up self-assembly of molecules in complex structures could be applied to augment top-down lithography fabrication techniques. As all molecules of one type are identical, molecular switches should have identical characteristics, thus reducing the problem of variability of components. However, the success of molecular electronics depends on our understanding of the phenomena accompanying molecular switching, where currently many questions remain.*
>
> ***International Technology Roadmap for Semiconductors, 2011***

## 1.2. The experimental barrier

The complex experimental set-up required to perform single molecule studies has historically been, and still remains, one of the most important obstacles to the full development of molecular electronics. However, since the invention of the STM and the AFM and through the great effort made by the scientific community in recent years, several methods that allow the formation of molecular junctions in order to study their physical properties and electronic performance have been firmly established.[18] The main aim of these methods is to assemble one or a small number of molecules between two metallic electrodes to create a junction which allows the electronic properties of the sandwiched molecules to be measured.[19] The most common and important methods for creating these junctions are discussed in the following paragraphs.

### *1.2.1. Break junctions*

This section encompasses the most commonly employed methods for the controlled fabrication of nanogaps not dependent on scanning probe microscopies but rather through the formation of nano-sized junctions by mechanical or electromigration processes. The first mechanically controlled break-junctions were developed by Moreland and Ekin. In their work, Nb-Sn filaments mounted on a flexible glass beam were cleaved by bending the substrate, allowing the formation of well-defined gaps of nanometric dimensions.[20] Their pioneering work was continued by Muller *et al.* who developed the method to form break junctions of metallic (non-brittle) materials.[21] This later setup, depicted in Figure 1-3, is based on the formation of a fine metallic filament bridging the two electrodes which is cleaved by bending the flexible substrate with a pushing rod located beneath the substrate. Recently, lithographic techniques have been used to pattern suspended metallic bridges[22] and systems with a third electrode that can perform as a gate in a transistor-like setup.[23]

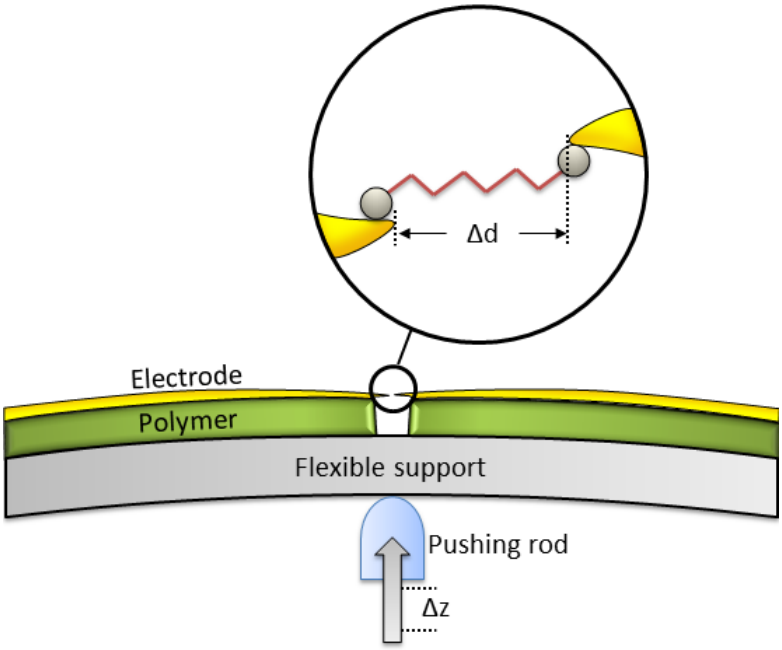


**Figure 1-3.** *Schematic diagram of a mechanically controlled break junction MCBJ.*

The large displacement ratio ($\Delta d/\Delta z$), between the movement of the push rod that bends the system ($\Delta z$) and the displacement of the electrode gap ($\Delta d$), typically $\Delta d/\Delta z \sim 10^{-5}$ allows for a great control over the gap size and makes the system stable against drift and vibrations.

The first experiments involving the use of such mechanically controlled break junctions (MCBJ) concerned the formation and study of atomically thin metallic wires.[24] Importantly, in a series of experiments conducted by van Wees *et al*.[25] on the cleavage of a GaAs-AlGaAs heterojunction, it was found that upon increasing the electrodes separation $\Delta d$ the conductance decreased in quantised steps of $2e^2/h$, corresponding to the conductance quantum $G_0$. Further studies found the same behaviour in several metals including the gold contact.[24, 26] Typically, when two gold electrodes are pulled apart, conductance steps with values close to that of the conductance quantum and its integers are observed. Those experimentally observed conductance jumps were later associated with atomic rearrangements of the gold electrode a proposal that could be supported by theoretical studies.[22a, 27]

In 1997 Reed and Tour,[28] demonstrated that the MCBJ could be employed to form molecular junctions. In that work, a gold wire was coated with a self-assembled monolayer (SAM) of 1,4-benzenedithiol and then pulled apart until cleavage takes place. The two electrodes that resulted from cleavage of the wire were then slowly brought together to form the molecular junction when spanned by one or more 1,4-benzenedithiol molecules. The through-molecule conductance could be recognised by the onset of conductance steps several orders of magnitude lower than the metallic conductance quantum. These novel experiments demonstrated that the electrical properties of a small number of molecules, or even one single molecule could be obtained employing MCBJ methods. In order to determine the number of molecules present in the junction, a growing number of studies

rely on the statistical treatment of the conductance traces and *I*-*V* profiles.[29] The statistical analysis of MCBJ experiments has recently been reviewed (*see* Appendix A).[29f, 30]

### *1.2.2. In-situ break junctions and related methods*

This section encompasses several methods that rely on the use of scanning probe microscopies (STM and CP-AFM), for the study of molecular junctions focusing on the *in-situ* break junction,[31] *I*(*s*) and *I*(*t*) STM techniques.[32]

The STM-break junction (STM-BJ) technique developed by Tao,[31] consists of initially fusing the substrate with the STM tip. As the tip is retracted a metallic filament is formed, the presence of which is typically characterized by large current jumps that relate to integers of the quantum of conductance, $G_0$. Retraction of the tip continues until the metallic contact is cleaved (Figure 1-4, *top*) and the tunnelling current decays exponentially with the distance separating the reformed tips and substrate. When the protocol is repeated in the presence of the target molecules, after the metallic contact is cleaved, molecular junctions can be formed. Conductance through the target molecule can be observed as smaller steps at a fraction of $G_0$ against the otherwise exponential decay of the tunnelling current. The process is repeated until a statistically significant dataset concerning these current plateaus is obtained.

In contrast, the *I*(*s*) and *I*(*t*) methods (Figure 1-4, *bottom*) avoid tip-substrate contact at all times. The *I*(*s*) method introduced by Haiss *et al.*[32a] involves bringing the tip close to the substrate surface and in a manner related to STM-BJ method the exponential decay of the tunnelling current between tip and substrate is registered as the tip is retracted. These blank curves can be used to identify the initial tip-substrate distance (*see* Chapter 2, Eq. 2-1). When the process is repeated in the presence of molecules, there is a finite probability of a molecule becoming electrostatically trapped between the tip and the

substrate. A current plateau is observed when a molecular junction is formed, which both identifies the formation of a junction and permits the electronic characteristics of the molecule to be assessed. Finally, the *I*(*t*) method[32b] monitors the stochastic formation and cleavage of molecular junctions within a period of time. The use of a constant tip-substrate distance in the *I*(*t*) method *vs* the controlled tip approach and retraction in the *I*(*s*) technique distinguishes the two approaches. Under the constant tip-substrate distance conditions that are employed in the *I*(*t*) measurement, the tunnel current is monitored and signal jumps are observed when a molecule bridges the gap resembling telegraphic noise signals.[33]


**Figure 1-4.** *Top to bottom, schematics of STM-BJ, I(s) and I(t) methods.*

Despite the differences in methodology leading to the through-molecule conductance measurements, all three methods STM-BJ, $I(s)$ and $I(t)$ still depend on the statistical treatment of the data (typically consisting in thousands of current-distance traces) as the junction formation ratio can sometimes be low. In order to analyse the STM results with ease, current traces are typically binned into discrete divisions to form histograms, then transformed to electrical conductance $G = I / V$ and finally referenced to the quantum of conductance $G_0$. The preparation of conductance histograms and their significance is discussed in detail in Appendix A.

### *1.2.3. Monolayer matrix isolation*

In this approach developed by Cui *et al.*[34] the molecule of interest, functionalised at each end with gold-binding groups, is isolated within a poorly conductive SAM, typically formed from a long-chain alkanethiol chosen to be slightly shorter in length that the target molecule on a gold substrate. This hybrid monolayer-coated substrate is then immersed into a solution containing gold nano-particles (GNPs) that attach to the available top end linker of the targeted molecule (Figure 1-5). The conductance of the molecular junction is measured by contacting the GNPs on the film surface with the AFM or STM tips. Through statistical treatment of the data distinct conductance values can be identified, and by attributing the lowest conductance peak in the histogram to the conductance of a single molecule, the number of molecules involved in the junctions showing higher conductance peaks could be determined. Despite the apparent simplicity of the technique, several issues need to be considered.[35] Typically, the aggregation of gold nanoparticles in solution is avoided by the use of a stabilising ligand. If the GNPs involved in the molecular junction are coated by a stabilising ligand, the surfactant influence in the junction conductance has to be taken into account. In addition, GNPs with sizes under 5 nm are known to exhibit coulomb blockade,[36] that can be observed at the zero bias region of *I-V* curves presented by

Cui *et al.*[34] Finally addressing the gold nanoparticle with a scanning probe microscope can result in deformation of the under-lying organic film, which in turn can distort the junction characteristics.[35, 37]

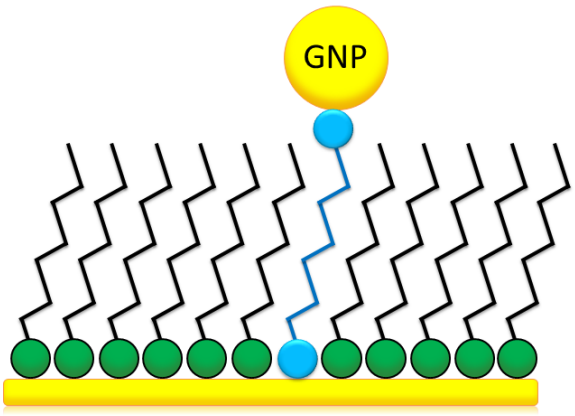


**Figure 1-5.** *Schematic representation of the monolayer matrix isolation.*

### *1.2.4. Nanofabrication*

Despite the great effort made during the last decades, the reliable integration of molecules into complex circuits remains in its infancy.[38] However, those efforts have crystallized in a myriad of nanofabrication methods based on scanning probe microscopies and lithographic protocols that can be used to precisely fabricate nano-sized gaps suitably sized to trap a small number of molecules, or even a single molecule, for their study.[18, 39] Amongst the most relevant nanofabrication processes developed to prepare molecular junctions are: *metal evaporation*; *nanopore architectures*; *mercury drop junction*; *conducting polymer electrodes; soft contact deposition methods (lift-off-float-on and polymer-assisted lift-off); crossed wires*; *nanoparticle bridging (2D array) and nano-printing (dip-pen nanolithography).*

The majority of these techniques were developed as softer alternatives to prepare the junction's "top" electrode, due to the damage caused to the organic film by direct thermal evaporation used to prepare sandwich-like devices from monolayer coated

substrates.[40] Despite metal evaporation being widely used by the semiconductor industry, the metal atoms and clusters evaporated from the heated metal source reach the organic film with enough kinetic energy to penetrate through the molecular layer on the substrate.[40a] Several softer indirect metal evaporation protocols have been developed in an attempt to preserve the integrity of the molecular film. Conducting the evaporation process in the presence of an inert gas can reduce the energy of the evaporated atoms by colliding with the inert gas atoms, turning the organic film away from the metal source or using an electron beam instead of thermal evaporation can all be used to reduce film damage during the deposition of the top-electrode (Figure 1-6).[41]

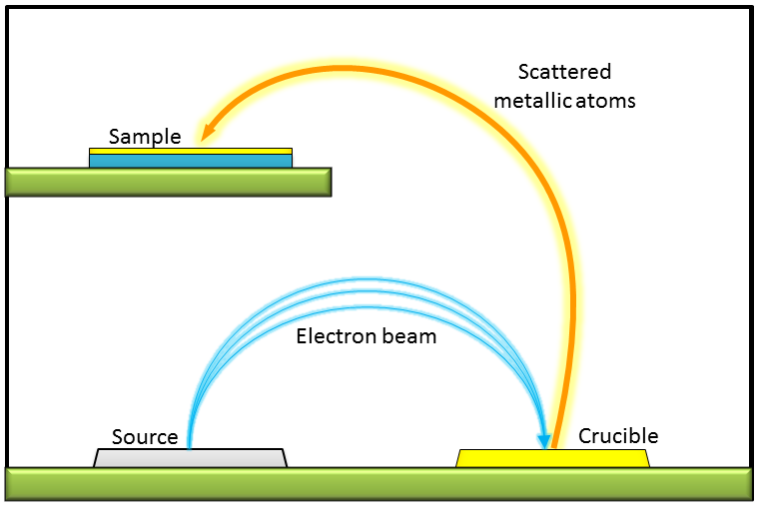


**Figure 1-6.** *Indirect electron beam top-electrode deposition.*

A slightly different approach is the nanopore method. As large area devices are more prone to present short-circuits when the metal electrode is evaporated on the organic film, small area devices can be fabricated to ensure defect free devices.[42] In this method an insulating layer of $SiO_2$ is grown on the electrode and then etched locally to form nano-wells using lithographic techniques.[42-43] A SAM can then be grown on the exposed electrode surface inside the well and a top contact carefully evaporated to complete the junction (Figure 1-7, *left*).

Perhaps the simplest non-destructive top electrode fabrication method is the use of liquid metals, with Hg being the most common choice.[44] Although this technique was first developed to characterise phospholipid monolayers mimicking biological membranes,[45] many variations have been developed.[46] The basic principles of the technique involve a hanging drop of a liquid metal used to softly contact the molecular film completing a sandwich-like device (Figure 1-7, *right*). However, in this method the mercury contact area is not constant and depends on the film topography.[47] In addition, Hg's great affinity for Au can result in amalgamation when Au is employed as the bottom electrode and defects are present in the SAM.[48]

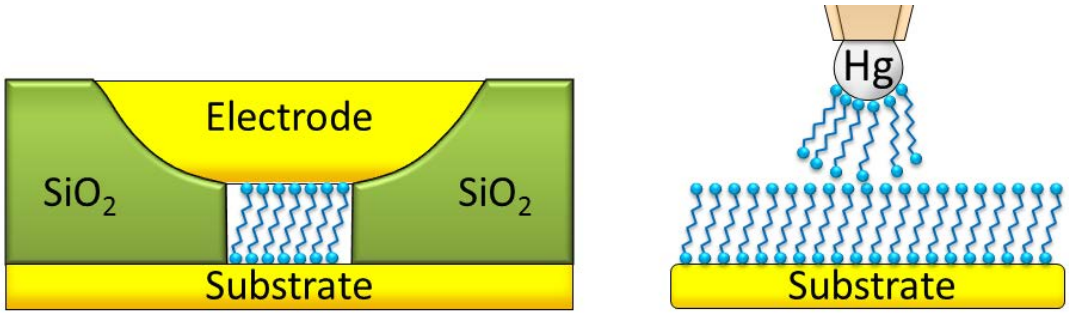


**Figure 1-7.** *Schematic representation of the nanopore (left) and mercury drop (right) molecular junctions.*

A more recent approach towards the formation of molecular junctions involves the use of a conducting polymer as a top electrode.[49] In a similar way to the nanopore protocol, an insulating layer, in this case a photoresist is built (spin-coated) on the gold substrate and wells (10 - 100 μm) are etched by lithographic means. After a SAM is grown in the photoresist gaps a layer of poly(3,4-ethylenedioxythiophene) stabilized with poly(4-styrenesulfonic acid) (PEDOT:PSS) is spin coated on the wafer. Finally a gold top contact is evaporated on top to ensure a good electronic contact. However, due to the large area of the molecular junctions (10 – 100 μm) the formation of short circuits is still high with typical yields ca. 1% of working devices.[40a, 50]

Another alternative method for the fabrication of molecular junctions is the so-called crossed-wire junction.[51] In this technique two metallic wires (10 μm in diameter) are mounted on a crossed geometry. One of the wires is coated with a SAM of the targeted molecule and a perpendicular magnetic field is applied (*B*) (Figure 1-8, *left*). The space between the two electrodes is controlled by the Lorentz force, a small current flowing through one of the wires deflects it in the presence of the external magnetic field, *B*. Although the crossed-wire technique has been successfully employed to study the electrical transport through molecular junctions,[52] the exact number and orientation of molecules contacted between the cross-bars is unknown.

In addition to these methods, the use of metallic nanoparticles as an integral part of the junction formed between two electrodes has been reported (Figure 1-8, *right*).[53] In this case, a nanosized gap is generated between two electrodes by lithographic means and then the electrodes are covered with a SAM. The electrode gap is then bridged with metallic nanoparticles that are trapped between the two coated electrodes by electromagnetic means.[54] The schematic representation of the completed junction can be seen in Figure 1-8, *right*. In contrast to the gold nanoparticles on SAM methods described above, in this case the nanoparticles are not contacted directly but rather form part of the conductive pathway between two lithographically fabricated electrodes. Junctions formed by this method are best modelled as double tunnelling junctions, adding complexity to the interpretation of the electrical data.

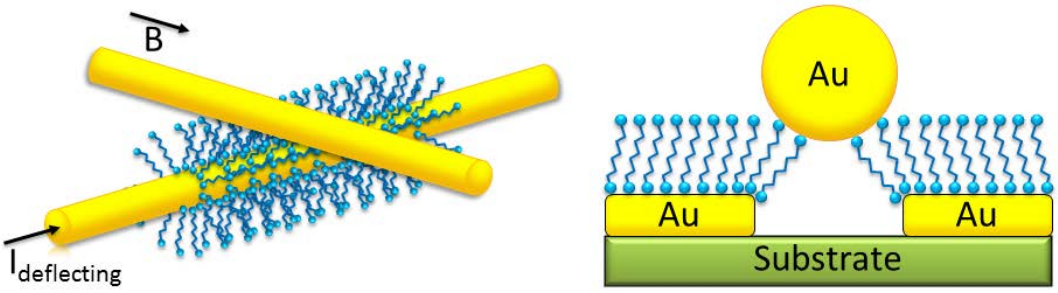


**Figure 1-8.** *Schematic representation of the crossed-wire (left) and GNP (right) junctions.*

Two soft deposition methods have been recently reported for the preparation of large area molecular devices, the lift-off-float-on (LOFO) and the polymer-assisted lift-off (PALO) process. In the LOFO process, a thin metal film is detached from a supporting substrate in a specific solvent.[55] The floating metallic film can then be transferred atop an organic monolayer to complete the molecular device. The PALO process combines the advantages of LOFO with nanotransfer printing.[56] The PALO employs a polymer layer on top of the substrate with the patterned metallic film. The polymer film holding the metallic pattern is detached from the substrate onto a liquid surface and then transferred onto the molecular film to form the junction. A schematic representation of this process can be seen in Figure 1-9 (*left*). The use of the supporting polymeric film allows the simultaneous transfer of multiple metallic patterns while preventing wrinkling of the films.

Finally, nanoprinting technology has been used to transfer a thin metallic layer from lithographically etched stamps onto a molecular film to fabricate junctions.[57] This process developed at the Bell labs, can be seen as variation of a previously developed method to print SAMs on substrates.[58] By bringing the stamp with a thin evaporated metallic layer in contact with the SAM, the metallic layer bonds chemically to the molecular film and detaches from the stamp resulting in precisely patterned junctions over large areas (Figure 1-9, *right*).[59]

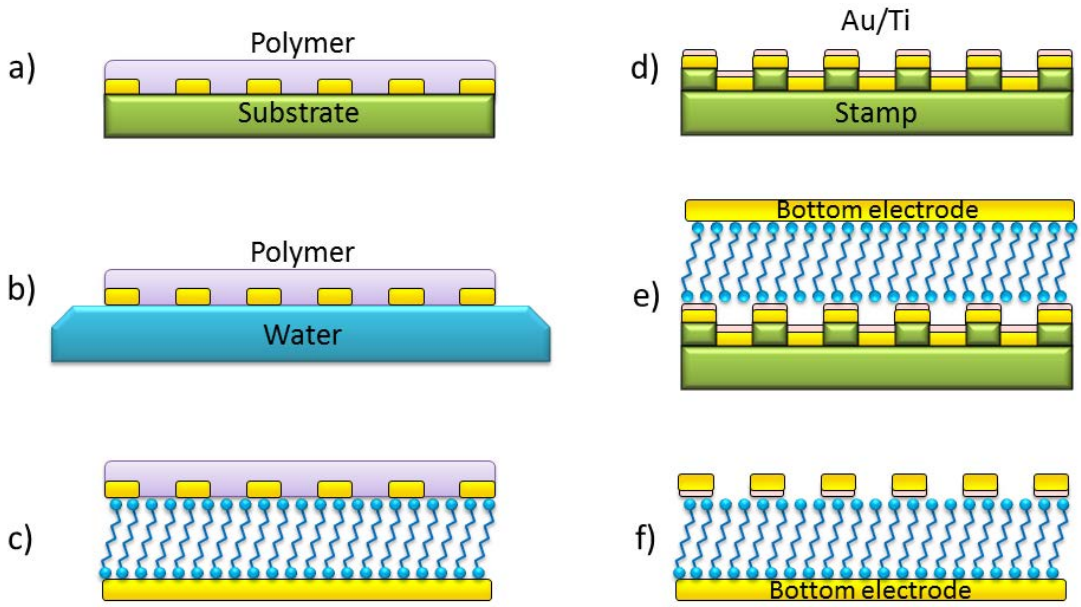


**Figure 1-9.** *Schematic representation of the LOFO process(right): a) a polymeric film is spin-coated on the patterned electrodes on a sacrificial substrate; b) the polymeric film containing the metallic electrodes is transferred on to a water surface; c) the electrodes are transferred onto the molecular film; and electrode nano-printing (right): d) Au and Ti are evaporated on the patterned stamp; e) the stamp and the substrate are brought into contact; c) separating the stamp results in complete transfer of the Au/Ti pattern.*

The decision of which technique to employ ultimately depends on the motivation for the work. Fundamental single molecule studies are typically based on MCBJ or *in-situ* BJ techniques, while application oriented research is clearly focused on the convergence of molecular electronics and modern lithographic techniques. In this thesis, two novel variations of this method that rely on the *in-situ* generation of the top electrode were developed (*see* Chapter 3).

## 1.3. Factors influencing the junction conductance

The development of all techniques for the fabrication and measurements of molecular electronic junctions has meant a wider access to single molecule studies, which in turn is evidenced by the increased number of reporting and analysing these data over the last decade. On the basis of the plethora of studies on molecular junctions that have been reported over the past decade, it has been noted that the conductance of a molecular junction can be affected by several factors such as: the structure and degree of conjugation of the molecular bridge;[60] the nature of the linker group and its geometry;[61] the junction geometry (tilt angles and gap size);[62] and the electronic character of substituents on the molecular backbone.[63]

Our contribution to this field is based on the study of symmetrically and unsymmetrically substituted linear oligo(phenylene-ethynylene) (OPE) derivatives, including organometallic analogues. These highly conjugated derivatives, sometimes referred to as "Tour wires" due to the pioneering studies of these molecules by James M. Tour,[64] have been of significant interest in many different fields of chemistry and physics due to their exceptional properties.[65] Their modular synthesis makes them relatively easy to prepare[66] and OPEs offer a wide range of physical, structural, optical and electronic properties that have been explored in a wide range of contexts and potential applications. For example, OPEs exhibit remarkable thermal stability which has been exploited within thermoset precursors of high performance glassy carbon materials,[67] whilst the rigid rod-like structure and π-π supramolecular interactions offered by the OPE backbone leads to liquid crystalline properties[68] and optoelectronic applications.[67a, 69] However in the context of this thesis, it is the extended, conjugated π-system and good single molecule conductance of the OPEs that merits particular attention.[60a, 70]

Much of the early work in single molecule studies was focused on the molecular backbone assuming that any other factor would have a small influence in the junction electronic performance. However, it is now agreed that, the metal-molecule interface and therefore the molecular anchoring group have a great influence on the global junction behaviour.[61e, f] This area of research has been largely dominated by the –SH linker that, due to its ability to self-assemble on gold has provided a strong test-bed to study the electrical properties of single molecules and ensembles.[71] However, several potential disadvantages have been reported to the use of thiols as molecular linkers. The thiolate-gold bond has a strength similar to that of the gold-gold bond resulting on the electrode surface modification.[24, 72] In addition, at room temperature, stochastic switching of the junction conductance has been observed, ascribed to the mobility of the chemisorbed contacts.[73] Due to the now known influence of the linker on the junction properties, this has become an area of great research activity and several alternative linkers to thiols have been proposed: pyridine;[29c, 31, 74] amines;[61c, 75] selenides;[76] dihydrobenzo[*b*] thiophene;[77] carboxylic acids;[61d, 78] cyanides;[79] isocyanides;[79-80] isothiocyanates;[81] phosphines;[61c] phosphine sulphides;[82] and more recently halides;[83] direct C-Au bonding[61a, 84] and silicon.[61b, 85] As one of the main contributions of the present work, a novel linker $-C{\equiv}CSiMe_3$ was introduced and tested in single molecule studies, the results are shown in Chapter 5.

In addition to the linker, the exact separation between the two electrodes when the molecular bridge is formed can have a pronounced influence in the junction conductance. This is extremely relevant to the development of molecular electronic devices that can show a considerable range of contact-gap separation. Haiss *et al.*[62b] demonstrated that molecular conductance can be measured as a function of electrode gap to sub-nanometre precision. More recently, the effect of the junction gap was also studied for a series of rigid

molecular wires.[62a] In those studies, a substantial conductance increase was found as the gap between the electrodes was closed. DFT studies supported those results proving the significant influence of the molecular tilt angle in the junction conductance.[62b] The influence of the measuring technique on the junction geometry and its impact in the junction conductance is discussed in detail in Chapter 5.

## 1.4. Fundamental aspects of molecular charge transport

### *1.4.1. Transport in Donor-Bridge-Acceptor systems: studies of intramolecular charge transfer in solution*

Intramolecular charge transfer processes have been studied extensively, both theoretically and experimentally, and these studies well precede the studies of through-molecule conductance that form the basis of modern molecular electronics.[86] Nevertheless, investigation of intramolecular charge-transport processes using solution based methods are extremely well developed, with Marcus and Taube both receiving the Nobel Prize for their work unravelling the fundamentals of these elementary processes. Even today, there is considerable emphasis on the role that such solution based methods may play in screening molecular structures for molecular electronic characteristics prior to the more time-consuming junction studies.[11] These in solution studies have largely focused on the rates of transfer in solution between donor (electron source) and acceptor (electron drain) species. By examining the electron transfer rates between covalently linked donor and acceptor units bridged by a molecular spacer with the shape Donor-Bridge-Acceptor (D-B-A) the relevance of the molecular bridge in the electron transport was evaluated.[87] The similarity between a D-B-A system and a metal|molecule|metal junction has led to the use of the term “molecular wire” for the bridging ligand. When the two terminal redox centres present different redox potentials a mixed-valence compound with an odd number of

electrons can be generated chemically, electrochemically or photochemically and the bridge mediated charge transfer between the two redox centres can be studied (Figure 1-10).[88] The inspiration for these D-B-A systems comes from nature, in which many redox biological processes involve molecular systems able to transport charge efficiently over nanometric distances such as the proteins involved in photosynthesis or β-carotene.[89]

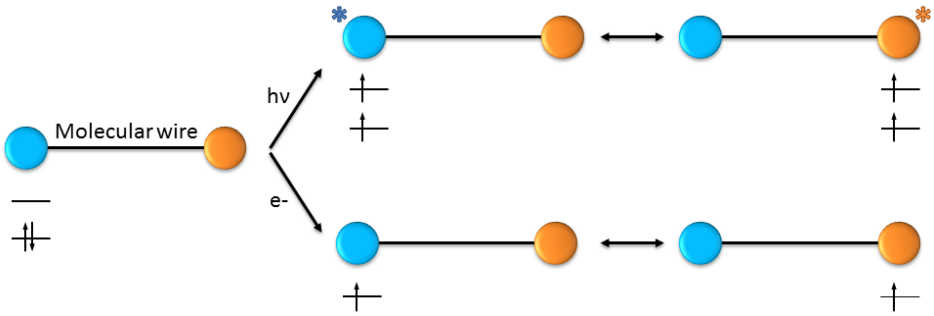


**Figure 1-10.** *Schematic representation of electron conduction in a photonic (top) and redox (bottom) MV system.*

The now well established research field of charge transfer on mixed valence organometallic complexes began with the study of the Creutz-Taube ion.[9] In those early studies, an optically induced intervalence charge transfer (IVCT) absorption band was observed in the near-infrared (NIR) region of the spectra that was not present for the reduced or oxidised species. In addition to the spectroscopic characterization, perhaps the simplest way to examine the electronic interaction between metallic centres in a mixed-valence system is cyclic voltammetry (CV). In a symmetrical bimetallic complex $[M^0M^0]$, in the absence of electronic coupling the two redox centres undergo oxidation at the same potential leading to a single redox wave in the CV ascribed to the formation of $[M^+M^+]$. However, in those cases where a certain degree of through bond or through space electronic interaction is present between the redox sites, two separate $1e^-$ processes are typically observed. However it must be noted that the 'resonance' term is only one of the stabilising factors that contributes to the observed separation of the two redox events, and

more detailed accounts of these factors can be found in several recent reviews.[90] In the potential domain between the two oxidation waves, the system is in the mixed-valence state [$M^+M^0$]. The potential difference between the two oxidation processes $\Delta E_{ox}$, is related to the thermodynamic stability of the mixed-valence state [$M^+M^0$] relative to the fully oxidised [$M^+M^+$] and fully reduced species [$M^0M^0$]. The comproportionation constant $K_c$ can be calculated from $\Delta E_{ox}$ using Eq. 1-1.

$$[M^0M^0] + [M^+M^+] \rightleftharpoons 2[M^+M^0] \qquad \text{where } K_c = \frac{[M^+M^0]^2}{[M^0M^0][M^+M^+]}$$

$$K_c = e^{(F/RT)\,\Delta E_{ox}} = e^{(38.92)\Delta E_{ox}} \text{ (298 K)} \qquad \text{Eq. 1-1}$$

The calculated values of $\Delta E_{ox}$ and $K_c$ have been used in order to evaluate the degree of electronic coupling in mixed-valence complexes,[86, 91] although caution must be exercised in this approach.[90c] In addition, reversible voltammograms at moderate scan rates are a good experimental indication of the stability of the oxidised species.

From the spectroscopic point of view, according to the theoretical model proposed by Hush, the spectral properties of the IVCT absorption bands are linked to the activation barriers for electron transfer described in the Marcus theory, according to Eq. 1-2.

$$\nu_{max} = h\nu = \lambda_i + \lambda_o + \Delta E_0 + \Delta E' \qquad \text{Eq. 1-2}$$

where $\lambda_i$ and $\lambda_o$ are the reorganizational energies of the inner- and outer-sphere respectively, $\Delta E_0$ is the redox asymmetry defined as the energy difference between the initial and final states in the absence of electronic coupling and $\Delta E'$ is an energy factor encompassing spin-orbit contributions and ligand field asymmetry.

The Marcus-Hush theory is typically explained considering the electron transfer reaction in a dinuclear mixed-valence system following the reaction $[M^0M^+] \rightarrow [M^+M^0]$. Upon oxidation of the neutral species $[M^0M^0]$, a MV species is formed with the overall charge +1 that corresponds to $[M^0M^+]$ species in a class-I (fully localized) system or $[M^{1/2}M^{1/2}]$ in a class-III (fully delocalized) system. The symmetrical complex $[M^0M^0]$, can be described by two parabolic potential energy curves (Figure 1-11), where the dotted lines correspond to the wavefunctions $\Psi_a$ and $\Psi_b$ corresponding to the fully localized electronic isomers $[M^0M^+]$ and $[M^+M^0]$ respectively. The wavefunction mixing at the intersection of the diabatic curves gives rise to two new adiabatic surfaces (class-II / blue, class-III / red). The splitting between the surfaces at $X = 0.5$ defines the previously introduced electronic coupling parameter, $H_{ab} = \langle\Psi_a|\hat{H}|\Psi_b\rangle$. The optically induced transition $[M^0M^+] \rightarrow [M^+M^0]^*$ taking place between adiabatic states is the IVCT transition.

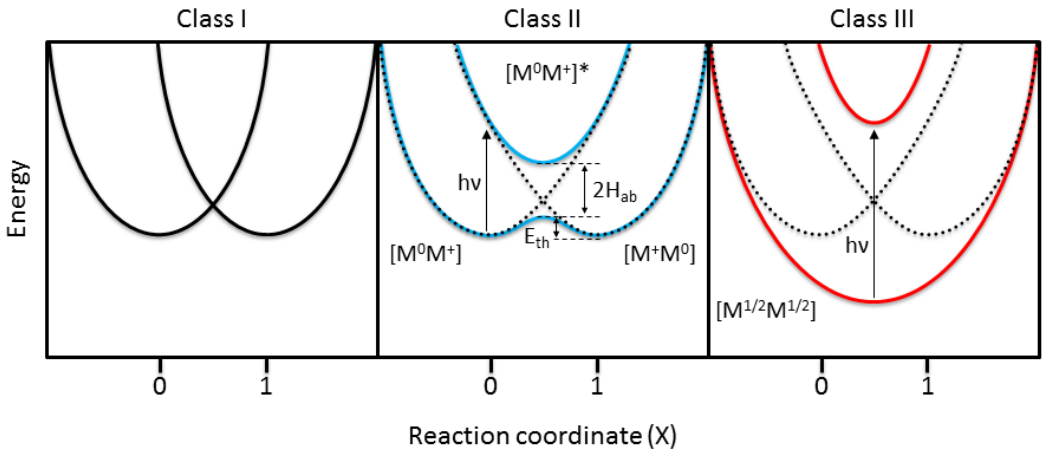


**Figure 1-11.** *Potential energy curves for the electron transfer reaction in ligand-bridged dinuclear complex $[M^0M^+] \rightarrow [M^+M^0]$ with no electronic coupling between sites ($H_{ab}=0$) (class I), weak electronic coupling ($H_{ab}=\lambda/4$) (class II) and strong electronic coupling ($H_{ab}=3\lambda/4$) (class III). Dotted and solid curves represent the diabatic and adiabatic surfaces respectively.*

The classification scheme proposed by Robin and Day, categorizes the mixed valence systems according to the degree of electronic coupling between the two metal centres and the splitting of the resultant adiabatic surfaces.[92] When there is no interaction between the metal centres, the degree of electronic coupling is negligible ($H_{ab}$ = 0) the system is referred to as class-I (Figure 1-11). On the other hand, when the two metallic centres are strongly coupled ($2H_{ab} >> \lambda$), both redox centres present a partial oxidation state [$M^{1/2}M^{1/2}$] the system is referred to as class-III (Figure 1-11). In this case, the IVCT transitions are typically intense ($\varepsilon_{max}$ > 5000 $M^{-1}\cdot cm^{-1}$), solvent independent and narrow ($\Delta\nu_{1/2}$ = 2000 $cm^{-1}$). The coupling parameter $H_{ab}$ can be directly calculated from the IVCT band since $H_{ab} = \nu_{max} / 2$. Finally, the intermediate case where the systems present a moderate electronic coupling between metal centres, is referred to as class-II (Figure 1-11). Due to the limited electronic coupling between the metallic centres present in class-II systems, the IVCT bands are less intense than those of the fully delocalized systems ($\varepsilon_{max}$ < 5000 $M^{-1}\cdot cm^{-1}$). These IVCT bands are also broader ($\Delta\nu_{1/2}$ > 2000 $cm^{-1}$) and solvent dependent. In the two-state limit the IVCT bandwidth can be predicted by using Eq. 1-3.

$$\Delta\nu_{1/2}^{\circ} = \{16RT\ ln2\ (\lambda)\}^{1/2} = \{16RT\ ln2\ (\ \nu_{max} - \Delta E_0 - \Delta E')\}^{1/2} \qquad \text{Eq. 1-3}$$

where $R$ ($K\cdot mol^{-1}$) is the gas constant, $T$ (K) is the temperature, $\Delta E_0$ is the redox asymmetry and $\Delta E'$ is the energy contribution due to spin-orbit coupling and ligand field asymmetry. For a class-II system, where $\Delta E_0 = \Delta E' = 0$ at 298 K, Eq. 1-3 can be simplified into Eq. 1-4.

$$\Delta\nu_{1/2}^{\circ} = (\ 2310\ \nu_{max}\ )^{1/2} \qquad \text{Eq. 1-4}$$

The degree of electronic delocalization in MV systems can be calculated from the spectral characteristics of the IVCT band. The electronic coupling parameter $H_{ab}$ that allows direct comparison of the delocalization between related compounds can be

calculated using Eq. 1-5, where $r_{ab}$ is the distance between the two diabatic states. However Eq. 1-5 can only be applied to Gaussian shaped IVCT bands, a more rigorous formulation is given by Eq. 1-6. Where $e$ is the electron charge and $|\mu|$ is the transition dipole moment that can be calculated from the integration of the IVCT band with disregard of its shape.

$$H_{ab} = 2.05 \cdot 10^{-2} \, (\varepsilon_{max} \, \nu_{max} \, \Delta\nu_{1/2})^{1/2} / \, r_{ab} \qquad \text{Eq. 1-5}$$

$$H_{ab} = |\mu| \, \nu_{max} / \, e r_{ab} \qquad \text{Eq. 1-6}$$

In addition to the optically activated IVCT process, thermal activation and surface crossing can also trigger electron transfer (Figure 1-11). The energy barrier for the thermal electron transfer, $E_{th}$ can be calculated using Eq. 1-7.

$$E_{th} = (\lambda / 4) - H_{ab} + H_{ab}^{2} / \lambda \qquad \text{Eq. 1-7}$$

Despite the many examples of localised and delocalised systems that can be found in the literature, more recently, a number of studies have reported systems with an intermediate class-II/III behaviour. This is clearly a limitation of the Robin and Day classification system since in reality there are no abrupt boundaries between the three regimes. In addition, this theoretical treatment neglects any environmental effects[93] and fails to explain the unsymmetrically shaped IVCT bands and the presence of multiple IVCT bands experimentally observed.[94]

More recently, with the help of computational DFT calculations, rotamers have been proposed by our group as a crucial variable in the interpretation of the IVCT absorption bands.[95] This topic is addressed in more detail in Chapter 4, with the study of the spectroscopic features of several Ru mixed-valence species.

An alternative method to extract the coupling parameter from the spectral characteristic of the IVCT band was proposed by Creutz, Newton and Sutin. The so-called CNS model considers the coupling between centres to be facilitated by the bridge in a metal-to-ligand charge transfer (MLCT) and ligand-to-metal charge transfer (LMCT).[96] For a dinuclear system $M_1$-L-$M_2$ the coupling parameter $H_{M1M2}$ can be calculated as

$$H_{M1M2} = \frac{H_{M1L}H_{M2L}}{2\Delta E_{ML}} + \frac{H_{LM1}H_{LM2}}{2\Delta E_{LM}} \qquad \text{Eq. 1-8}$$

where $H_{M1}$L is the $M_1$-L coupling for the $M_1$ centre, $H_{M2}$L is the analogue for $M_2$, and the $\Delta E_{ML}$ is the effective M1-L energy gap calculated using Eq. 1-9.

$$\frac{1}{\Delta E_{ML}} = \frac{1}{2}\left(\frac{1}{\Delta E_{MLCT}} + \frac{1}{\Delta E_{IVCT}}\right) \qquad \text{Eq. 1-9}$$

Given the geometrical similarities between two redox sites, the Eq 1-8 can be further simplified by considering the subscripts $M_1$L and $LM_1$ are equivalent to $M_2$L and $LM_2$ respectively. The CNS model has been employed in the analysis of mixed valence complexes with results being in very close agreement with those obtained applying the Hush model.[94b, 96-97] However, the CNS method has been questioned due to the assumptions made for the charge transfer distance, a single orbital interaction along the wire bridge axis and the treatment of only one MLCT or LMCT excited states.[94b, 97] Detailed spectroscopic characterization of mixed-valence systems, supported by computational studies and theoretical models provides a solid platform from which to address charge transport in solid state single molecule studies.

Despite the great body of information gathered from the in-solution studies, no data is obtained regarding the metal|molecule interaction. However, the use of spectroscopic techniques in single molecule studies has been recently reported by Matsuhita *et al.*[98] In

their pioneering work, electrical performance and surface-enhanced Raman scattering (SERS) was employed to characterize the thiol-Au interaction in benzenedithiol molecules bridging the gap between the electrodes.

### *1.4.2. Charge transport in molecular junctions*

When a molecule is brought in contact with a metallic electrode, the molecular orbitals and the electrode states overlap to a certain extent to form a new hybrid electronic wavefunction. The degree of coupling may vary from conjugated states extending over the whole molecular junction, to the generation of orbital nodes along the junction acting as barriers to electronic transport between the electrodes. Despite the great progress made in this field, a full theoretical description of metal|molecule|metal junctions still remains a challenge. The most relevant parts influencing the conductance of a molecular junction are depicted in Figure 1-12.

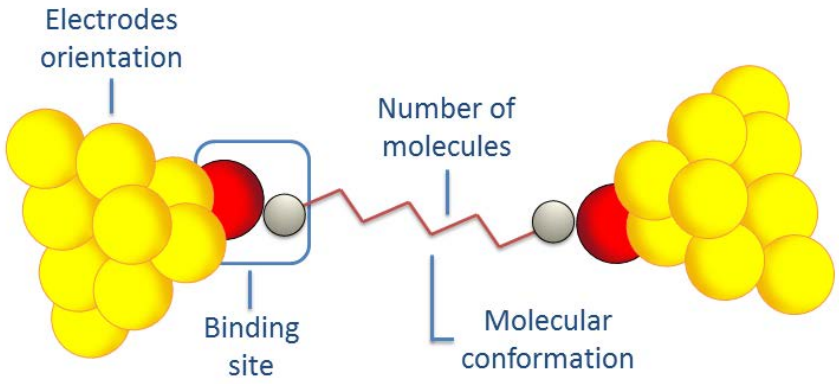


**Figure 1-12.** *Schematic representation of a fully characterized molecular junction with: binding sites; electrodes orientation; molecular conformation and number of molecules are accurately characterized.*

A simplified electronic description of a molecular junction involving two electrodes bridged by a molecule can be seen in Figure 1-13. Both electrodes are described as a

continuum of energy levels filled up to a given energy level (Fermi level), the energy symmetry between both electrodes is broken by the applied bias. On the other hand, the bridging molecule is characterized by discrete energy levels filled up to the HOMO. Importantly, the orbital alignment relative to the electrode Fermi level is directly characteristic of each molecular junction and dependant on several factors such as: the nature of the molecular bridge;[99] the nature of the metal-molecule interaction;[61c] the electronic and conformational changes induced by the charge transfer;[100] environmental effects[19b] and redox state. [19b, 101]

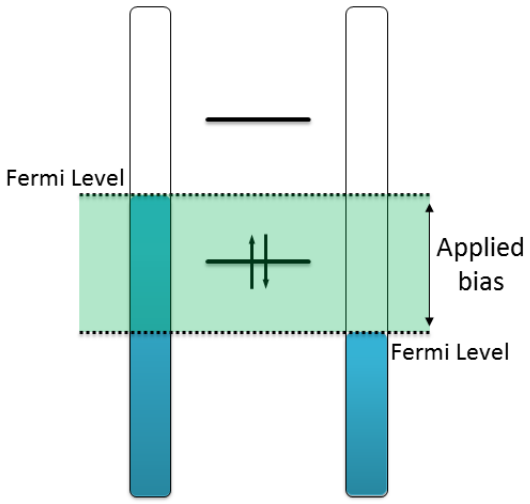


**Figure 1-13.** Simplified description of the electronic diagram of a molecular junction.

Charge transport in molecules contacted by macroscopic electrodes is best described by the Landauer formalism. In this description electrons are treated as waves that can be reflected or transmitted through the molecular bridge. According to the Landauer formalism the conductance *G* of a molecular junction can be calculated using Eq. 1-10.

$$G = \frac{2e^2}{h}\sum_n T_n \qquad \text{Eq 1-10}$$

where *e* is the electron charge, *h* is Planck's and $T_n$ are the transmission coefficients of the individual transport channels. According to this expression, the conductance of a system *G*, is the summation of all possible individual transmission channels. Perhaps the most

relevant implication of this equation is that conductance at the molecular level is quantized. For a perfect coupling *i.e.* ballistic conductors ($T_n = 1$), the conductance can only increase or decrease in units of the quantum of conductance $G_0 = 2e^2/h \sim 77480$ nS. It is important to clarify that the Landauer formalism does not imply that the conductance of any system must be an integer of $G_0$ however it defines the maximum conductance for a single transmission channel as the $G_0$. Transmission coefficients $T_n$ typically take values smaller than the unity and several transport channels coexist to give the system conductance. Conductance values for single molecules are orders of magnitude smaller than $G_0$ typically ranging from $(10^{-5} - 10^{-1})$ $G_0$.

Several theoretical models have been developed to describe the electron transport through molecular junctions, the temperature independent coherent tunnelling (superexchange) and Fowler-Nordheim tunnelling; and the temperature dependent thermionic (Schottky) emission and hopping conduction.[102] Despite the multiple models developed for temperature dependent and independent processes (mainly differing on their bias dependence), for simplicity in this work we will only differentiate between tunnelling (temperature independent) and hopping (temperature dependent) processes. A more complete description and discussion on this topic is available in several reviews.[103] Although, typically only one of these mechanisms dominates the charge transfer through the molecular junction, both tunnelling and hopping mechanisms can coexist.[104] Hence, the observed rate of electron transfer ($k_{et}$) results from the summation of the tunnelling ($k_{tunn}$) and hopping ($k_{hop}$) contributions. A schematic representation of both charge transport processes is shown in Figure 1-14.

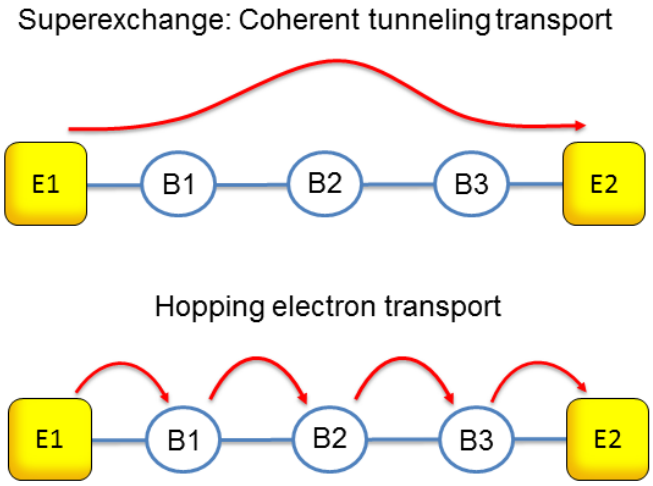


**Figure 1-14.** *Schematic representation of the superexchange and hopping mechanisms.*

*Superexchange: Coherent tunnelling transport*

The superexchange mechanism is based on the probability of an electron traversing an energy barrier coherently *i.e* in the absence of inelastic scattering events. In this case, the charge transfer takes place in one step through the molecular orbitals of the bridging molecule. Hence, the charge carrier is considered not to reside in the orbitals of the bridging molecular wire for a significant period of time. It is important to note that, the electron transference $k_{ET}$ is enhanced by the molecular orbitals increasing the probability of through-bond tunnelling over through-space tunnelling. In this scenario the energy barrier is set by the energetically higher electronic states of the bridge compared to those of the electron source. The electron transport rate $k_{ET}$ for the superexchange mechanism can be calculated using

$$k_{ET} = k_0\, e^{-\beta r} \qquad \text{Eq. 1-11}$$

where $k_0$ is a kinetic prefactor, $r$ is the distance between the two electrodes and $\beta$ ($nm^{-1}$) is the tunnelling attenuation factor. As it derives from Eq. 1-11 the superexchange mechanism is temperature independent and exponentially dependent on the electrode distance $r$. The attenuation factor $\beta$, represents the degree of electronic coupling present

along the molecular junction and enables direct comparison between single molecule studies. Typically the decay constant $\beta$ for π-conjugated molecules is an order of magnitude smaller (1 - 2 $nm^{-1}$) than that of the saturated σ-bonded chains *ca.* 10 $nm^{-1}$.[99, 105] Several distance dependence studies have reported $\beta$ values for a number of molecular systems: 3.4 $nm^{-1}$ for di-thiol terminated OPEs;[29b] 2.0 $nm^{-1}$ for amine terminated OPEs;[70e] 3.3 $nm^{-1}$ for pyridine terminated OPEs;[29c] 3.5 - 5 $nm^{-1}$ for di-thiol terminated oligophenylenes;[106] 1.8 $nm^{-1}$ for oligophenylene-vinylenes;[107] 1 $nm^{-1}$ for di-thiocyanate terminated oligothiophenes;[105] 0.6 $nm^{-1}$ for pyridine terminated oligoynes;[74c] as opposed to 9.4 $nm^{-1}$ for saturated di-thiol terminated alkyls[106a] and the 24-40 $nm^{-1}$ for vacuum.[87, 108] It is important to note that, the attenuation factor $\beta$ not only depends on the orbital delocalization of the molecular backbone but on the entire molecular junction, including the binding sites and the electrode shape and material (*i.e.* the measuring technique).[107a] However, due to the exponential distance dependence of the superexchange mechanism, coherent tunnelling is only effective for distances under 2.5 nm. The charge hopping mechanism is believed to dominate in those cases.

*Charge hopping*

Contrary to the superexchange mechanism, in this case the electron traversing the molecular wire is localized for a short time before moving to the next bridge site until it crosses through the molecular junction.[107b, 109] The hopping conduction mechanism is more likely to be present in molecular junctions where the Fermi levels of the metallic contacts lie close in energy to the molecular bridge frontier orbitals.[102] Importantly, significant nuclear motion is involved in this transport process as vibrational relaxation takes place at each bridge site. Contrary to the superexchange mechanism, charge hopping dependence on distance is less marked, *i.e.* inversely proportional to distance (Ohmic) (Eq. 1-12).[104] In

addition, due to the vibrational relaxation processes involved the hopping mechanism is temperature dependant.[102, 104]

$$k_{ET} = k_{hop} \propto 1/r \qquad \text{Eq. 1-12}$$

In order to experimentally determine the transport process ruling in a given molecular junction, two electrical measurements are typically performed: the length dependence of the molecular conductance and the temperature dependence of the *I-V* profile. These experiments also exclude the possibility of artefacts such as metallic filaments or interface effects being the source of the electrical properties registered. However, the determination of the charge transport mechanism can sometimes be difficult. For example, a pronounced temperature dependence was reported for the conductance of alkanedithiols attributed to changes in the distribution of the molecular conformers.[110]

The coexistence of both tunnelling and hopping mechanisms was first reported by Wasielewski and Ratner.[111] In their work, the recombination rate of several *p*-phenylene-vinylene oligomers (*n = 1 - 5*) performing as bridges for D-B-A in solution experiments was studied. Notably, a less marked distance dependence was found for those molecular bridges with sizes over 2.4 nm that was attributed to a change in the transport mechanism from superexchange (*n = 1 - 2*) to hopping (*n = 3 - 5*). More recently, Choi and co-workers reported a similar behaviour for phenyleneimine oligomers (*n = 1 – 10*) in solid state CP-AFM studies.[112] Those results confirmed the coexistence of both transport mechanisms in the solid state. In this case, transport mechanism was reported to change from tunnelling to hopping for molecular wires over 4 nm in size (*n = 6 - 10*). Despite the great experimental complexity of these experiments, a number of similar studies have been reported recently confirming the coexistence of both mechanisms.[29c, 70e, 113] Although in the first instance the charge hopping mechanism and its weaker distance dependence should allow long distance

charge transport, which makes it more attractive for potential electronic application, the tunnelling mechanism is still intriguing the scientific community. For instance, recent studies indicate that tunnelling-energy gap effects can differentiate the distance dependence of energy-storing charge-separation reactions from energy-wasting recombination processes.[87] Hence further understanding of the tunnelling mechanism may provide an additional way to obtain long-living charge-separated states.

*Electron transfer rates and molecular conductance, the relation*

As the number of single molecule studies increases, several theoretical studies have investigated the relation between the electron transfer rates ($k_{DA}$) obtained from the in-solution studies and the molecular conductance ($G$) obtained for molecular junctions.[114] Despite the fundamental differences behind the two physical systems both processes depend on quantum tunnelling to carry the charge through the molecular bridge.[103b, 115] Hence, the conduction profile of a given system and its electron transfer properties must be closely related.[114a] It is important to bear in mind that, because of the tunnelling regime there is always an Ohmic behaviour region near zero bias. On the basis of this similarity first noted by Nitzan,[114a, 116] the relation between the rate constant $k_{AD}$ and conductance $G$ is shown in Eq. 1-13,

$$G \approx \frac{e^2}{\Gamma_D \Gamma_A F} k_{DA} \qquad \text{Eq. 1-13}$$

where $e$ is the electron charge, and the $\Gamma$ factors are the inverse lifetimes of an electron on the donor and acceptor states once the molecular junction is formed, and $F$ is the Marcus thermally averaged Franck-Condon factor dependant of reorganization energy and temperature. However this relation is only applicable for the simple case of thermal, non-adiabatic electron transfer in those junctions where the molecular electronic structure is not

greatly affected by the metal-molecule interaction. A rough estimation of this relation for a junction with typical magnitudes of reorganization energy and metal-molecule coupling was done by Nitzan leading to $G(S) \sim 10^{-17}\ k_{DA}\ (s^{-1})$.[114a] Despite the fact that this theoretical model was first developed for the tunnelling mechanism, it was later extended to the hopping mechanism.[116] For those cases where the charge transfer takes place through a large number of bridge sites the relation between $G$ and $k_{DA}$ was found to be

$$G \approx \frac{e^2}{k_B T} e^{-\frac{\Delta E}{k_B T}} k_{DA} \qquad \text{Eq. 1-14}$$

where $k_B$ is the Boltzmann constant, $e$ is the electron charge and $\Delta E$ is the difference between the activation energies involved. Interestingly at $T = 300$ K, for those cases where $\Delta E \leq k_B T$, Eq 1-14 can be simplified as $G(S) \sim (5 \cdot 10^{-18})\ k_{DA}\ (s^{-1})$ remarkably similar to the numerical estimate obtained for the coherent tunnelling mechanism.

More recently, Wierzbinski and co-workers reported the first experimental study of this relationship.[113a] In their work, they evaluated the correlation between molecular conductance and electrochemical rate constants for alkanes and nucleic acid oligomers as a function of length, structure and charge transport. Interestingly, contrary to the linear correlation theoretically proposed by Nitzan a power law correlation was found between $G$ and $k_{DA}$ for each molecular bridge studied. The deviation from the linear relation was attributed to charge-transfer energy barriers and bridge dephasing. In situations where multiple mechanisms can coexist, these factors can lead to differences between the distance dependence of $k_{DA}$ and $G$. Generally speaking, these results show the relative propensity of different chemical species to transmit charge differently in electrochemical measurements as opposed to molecular junctions.

## 1.5. Challenges and future prospects in molecular electronics

As exposed along this Chapter, during the last 40 years since Aviram and Ratner proposed the idea of a molecular rectifier, the molecular electronics field is living a time of great activity and excitement. The great effort made by the scientific community during the last decades to address the unique and complex nature of charge transport at the molecular level has unlocked a bright future for the field. In fact, due to the wider access to the experimental tools that allow single molecule measurements many new charge transport phenomena have been characterized that go beyond the simple electronic transport. Amongst those phenomena, molecular rectifying (redox or thermal), wave-interference, spintronics and optoelectronics are of great interest nowadays.

This thesis represents a broad approach to the field encompassing the design and synthesis of the molecular candidates, the fabrication and characterization molecular devices (ensemble and single molecule) with the help of STM and AFM techniques. Special attention is paid to some of the field's hot topics such as: the importance of the linker on the molecular junction performance; the formation of the top electrode in sandwich-like molecular devices for improved reliability; and in-solution charge transfer studies, that together with a detailed theoretical description will lead to molecular behaviour prediction and ultimately to a more rational design of molecules.

In the words of Heath and Ratner,[117] on the molecular electronics horizon should be placed a very robust, energy-efficient, connected to the outside world, computational platform based on molecular electronics with a bit density of $10^{12}$ $cm^{-2}$. The great advances needed to accomplish that goal, would make it hard to believe that an electronic device will be the most significant result of such an effort.

## 1.6. References


1. Kwok, K. S.; Ellenbogen, J. C., *Mater. Today*, **2002**, *5*, 28-37.
2. Service, R. F., *Science*, **2001**, *294*, 2442-2443.
3. Khoo, I.-C.; Wiley, I., *Liquid crystals*. Wiley-Interscience: Hoboken, N.J., 2007.
4. (a) Kulkarni, A. P.; Tonzola, C. J.; Babel, A.; Jenekhe, S. A., *Chem. Mater.*, **2004**, *16*, 4556-4573; (b) Sasabe, H.; Kido, J., *Chem. Mater.*, **2010**, *23*, 621-630; (c) Zhong, C.; Duan, C.; Huang, F.; Wu, H.; Cao, Y., *Chem. Mater.*, **2010**, *23*, 326-340.
5. Hafez, W.; Feng, M., *Appl. Phys. Lett.*, **2005**, *86*, 152101.
6. Choi, H.; Mody, C. C. M., *Social Studies of Science*, **2009**, *39*, 11-50.
7. Moore, G. E., *Electronics Magazine*, **1965**, *38*, 8.
8. (a) Day, P., *Inorg. Chem.*, **1963**, *2*, 452-456; (b) Allen, G. C.; Hush, N. S., Intervalence-Transfer Absorption. Part 1. Qualitative Evidence for Intervalence-Transfer Absorption in Inorganic Systems in Solution and in the Solid State. In *Prog. Inorg. Chem.*, John Wiley & Sons, Inc.: 2007; pp 357-389; (c) Robin, M. B., *Inorg. Chem.*, **1962**, *1*, 337-342; (d) Culpin, D.; Day, P.; Edwards, P. R.; Williams, R. J. P., *Chem. Commun. (London)*, **1965**, 450-451.
9. Creutz, C.; Taube, H., *J. Am. Chem. Soc.*, **1969**, *91*, 3988-3989.
10. Day, P.; Hush, N. S.; Clark, R. J. H., *Philos. Trans. R. Soc. London, Ser. A*, **2008**, *366*, 5-14.
11. Launay, J.-P., *Coord. Chem. Rev.*, **2013**, *257*, 1544-1554.
12. Mann, B.; Kuhn, H., *J. Appl. Phys.*, **1971**, *42*, 4398-4405.
13. Aviram, A.; Ratner, M. A., *Chem. Phys. Lett.*, **1974**, *29*, 277-283.
14. Xia, Y.; Rogers, J. A.; Paul, K. E.; Whitesides, G. M., *Chem. Rev.*, **1999**, *99*, 1823-1848.
15. Hamers, R. J., *J. Phys. Chem.*, **1996**, *100*, 13103-13120.
16. Thompson, S. E.; Parthasarathy, S., *Mater. Today*, **2006**, *9*, 20-25.
17. (a) Wong, H.; Iwai, H., *Microelectron. Eng.*, **2006**, *83*, 1867-1904; (b) McCreery, R. L.; Yan, H.; Bergren, A. J., *Phys. Chem. Chem. Phys.*, **2013**, *15*, 1065-1081; (c) Manchanda, L.; Morris, M. D.; Green, M. L.; van Dover, R. B.; Klemens, F.; Sorsch, T. W.; Silverman, P. J.; Wilk, G.; Busch, B.; Aravamudhan, S., *Microelectron. Eng.*, **2001**, *59*, 351-359.
18. (a) Hylke, B. A.; Bert de, B., *J. Phys.: Condens. Matter*, **2008**, *20*, 013001; (b) Haick, H.; Cahen, D., *Acc. Chem. Res.*, **2008**, *41*, 359-366.
19. (a) McCreery, R. L.; Bergren, A. J., *Adv. Mater.*, **2009**, *21*, 4303-4322; (b) Nichols, R. J.; Haiss, W.; Higgins, S. J.; Leary, E.; Martin, S.; Bethell, D., *Phys. Chem. Chem. Phys.*, **2010**, *12*, 2801-2815.
20. Moreland, J.; Ekin, J. W., *J. Appl. Phys.*, **1985**, *58*, 3888-3895.
21. Muller, C. J.; van Ruitenbeek, J. M.; de Jongh, L. J., *Physica C: Superconductivity*, **1992**, *191*, 485-504.
22. (a) Agraït, N.; Yeyati, A. L.; van Ruitenbeek, J. M., *Physics Reports*, **2003**, *377*, 81-279; (b) Yexian, W.; Wenjing, H.; Terunobu, A.; Sebastian, G.; Viliam, K.; Thomas,

W.; Nico, F. d. R., *Nanotechnology*, **2013**, *24*, 235302; (c) Wu, Y.; Akiyama, T.; Gautsch, S.; de Rooij, N., *Procedia Engineering*, **2011**, *25*, 1661-1664.
23. Meded, V.; Bagrets, A.; Fink, K.; Chandrasekar, R.; Ruben, M.; Evers, F.; Bernand-Mantel, A.; Seldenthuis, J. S.; Beukman, A.; van der Zant, H. S. J., *Phys. Rev. B: Condens. Matter*, **2011**, *83*, 245415.
24. Rubio, G.; Agraït, N.; Vieira, S., *Phys. Rev. Lett.*, **1996**, *76*, 2302-2305.
25. van Wees, B. J.; van Houten, H.; Beenakker, C. W. J.; Williamson, J. G.; Kouwenhoven, L. P.; van der Marel, D.; Foxon, C. T., *Phys. Rev. Lett.*, **1988**, *60*, 848-850.
26. Agraït, N.; Rodrigo, J. G.; Vieira, S., *Phys. Rev. B: Condens. Matter*, **1993**, *47*, 12345-12348.
27. (a) Mehrez, H.; Ciraci, S.; Fong, C. Y.; Erkoç, S., *J. Phys.: Condens. Matter*, **1997**, *9*, 10843; (b) Mehrez, H.; Ciraci, S., *Phys. Rev. B: Condens. Matter*, **1997**, *56*, 12632-12642.
28. Reed, M. A.; Zhou, C.; Muller, C. J.; Burgin, T. P.; Tour, J. M., *Science*, **1997**, *278*, 252-254.
29. (a) Nakazumi, T.; Kaneko, S.; Matsushita, R.; Kiguchi, M., *J. Phys. Chem. C*, **2012**, *116*, 18250-18255; (b) Kaliginedi, V.; Moreno-García, P.; Valkenier, H.; Hong, W.; García-Suárez, V. M.; Buiter, P.; Otten, J. L. H.; Hummelen, J. C.; Lambert, C. J.; Wandlowski, T., *J. Am. Chem. Soc.*, **2012**, *134*, 5262-5275; (c) Zhao, X.; Huang, C.; Gulcur, M.; Batsanov, A. S.; Baghernejad, M.; Hong, W.; Bryce, M. R.; Wandlowski, T., *Chem. Mater.*, **2013**, *25*, 4340-4347; (d) González, M. T.; Wu, S.; Huber, R.; van der Molen, S. J.; Schönenberger, C.; Calame, M., *Nano Lett.*, **2006**, *6*, 2238-2242; (e) Kiguchi, M.; Murakoshi, K., *Thin Solid Films*, **2009**, *518*, 466-469; (f) Natelson, D., *ACS Nano*, **2012**, *6*, 2871-2876.
30. Makk, P.; Tomaszewski, D.; Martinek, J.; Balogh, Z.; Csonka, S.; Wawrzyniak, M.; Frei, M.; Venkataraman, L.; Halbritter, A., *ACS Nano*, **2012**, *6*, 3411-3423.
31. Xu, B.; Tao, N. J., *Science*, **2003**, *301*, 1221-1223.
32. (a) Haiss, W.; van Zalinge, H.; Higgins, S. J.; Bethell, D.; Höbenreich, H.; Schiffrin, D. J.; Nichols, R. J., *J. Am. Chem. Soc.*, **2003**, *125*, 15294-15295; (b) Haiss, W.; Nichols, R. J.; van Zalinge, H.; Higgins, S. J.; Bethell, D.; Schiffrin, D. J., *Phys. Chem. Chem. Phys.*, **2004**, *6*, 4330-4337.
33. Haiss, W.; Martín, S.; Leary, E.; Zalinge, H. v.; Higgins, S. J.; Bouffier, L.; Nichols, R. J., *J. Phys. Chem. C*, **2009**, *113*, 5823-5833.
34. Cui, X. D.; Primak, A.; Zarate, X.; Tomfohr, J.; Sankey, O. F.; Moore, A. L.; Moore, T. A.; Gust, D.; Harris, G.; Lindsay, S. M., *Science*, **2001**, *294*, 571-574.
35. (a) Morita, T.; Lindsay, S., *J. Am. Chem. Soc.*, **2007**, *129*, 7262-7263; (b) Cui, X. D.; Zarate, X.; Tomfohr, J.; Sankey, O. F.; Primak, A.; Moore, A. L.; Moore, T. A.; Gust, D.; Harris, G.; Lindsay, S. M., *Nanotechnology*, **2002**, *13*, 5.
36. (a) Shigeki, H.; Shinya, K.; Yasuo, A.; Daisuke, T.; Masanori, S.; Toshiharu, T.; Yutaka, M., *Nanotechnology*, **2012**, *23*, 185704; (b) Davidović, D.; Tinkham, M., *Appl. Phys. Lett.*, **1998**, *73*, 3959-3961.

37. (a) Xu, B.; Xiao, X.; Tao, N. J., *J. Am. Chem. Soc.*, **2003**, *125*, 16164-16165; (b) Ilya, V. P.; Gábor, M.; Koji, Y.; Artem, M.; Murat, G.; Martin, R. B.; Thomas, W., *J. Phys.: Condens. Matter*, **2012**, *24*, 164210.
38. (a) Heath, J. R., *Annual Review of Materials Research*, **2009**, *39*, 1-23; (b) Collier, C. P.; Jeppesen, J. O.; Luo, Y.; Perkins, J.; Wong, E. W.; Heath, J. R.; Stoddart, J. F., *J. Am. Chem. Soc.*, **2001**, *123*, 12632-12641.
39. Gates, B. D.; Xu, Q.; Stewart, M.; Ryan, D.; Willson, C. G.; Whitesides, G. M., *Chem. Rev.*, **2005**, *105*, 1171-1196.
40. (a) de Boer, B.; Frank, M. M.; Chabal, Y. J.; Jiang, W.; Garfunkel, E.; Bao, Z., *Langmuir*, **2004**, *20*, 1539-1542; (b) Haick, H.; Ghabboun, J.; Cahen, D., *Appl. Phys. Lett.*, **2005**, *86*, 042113; (c) Haynie, B. C.; Walker, A. V.; Tighe, T. B.; Allara, D. L.; Winograd, N., *Appl. Surf. Sci.*, **2003**, *203–204*, 433-436.
41. (a) Xu, T.; Morris, T. A.; Szulczewski, G. J.; Metzger, R. M.; Szablewski, M., *J. Mater. Chem.*, **2002**, *12*, 3167-3171; (b) Metzger, R. M.; Xu, T.; Peterson, I. R., *J. Phys. Chem. B*, **2001**, *105*, 7280-7290; (c) Xu, T.; Peterson, I. R.; Lakshmikantham, M. V.; Metzger, R. M., *Angew. Chem. Int. Ed.*, **2001**, *40*, 1749-1752; (d) Haick, H.; Niitsoo, O.; Ghabboun, J.; Cahen, D., *J. Phys. Chem. C*, **2007**, *111*, 2318-2329.
42. Zhou, C.; Deshpande, M. R.; Reed, M. A.; Jones, L.; Tour, J. M., *Appl. Phys. Lett.*, **1997**, *71*, 611-613.
43. Majumdar, N.; Gergel, N.; Routenberg, D.; Bean, J. C.; Harriott, L. R.; Li, B.; Pu, L.; Yao, Y.; Tour, J. M., *Journal of Vacuum Science & Technology B*, **2005**, *23*, 1417-1421.
44. (a) Magnussen, O. M.; Ocko, B. M.; Deutsch, M.; Regan, M. J.; Pershan, P. S.; Abernathy, D.; Grubel, G.; Legrand, J.-F., *Nature*, **1996**, *384*, 250-252; (b) Slowinski, K.; Fong, H. K. Y.; Majda, M., *J. Am. Chem. Soc.*, **1999**, *121*, 7257-7261; (c) Holmlin, R. E.; Haag, R.; Chabinyc, M. L.; Ismagilov, R. F.; Cohen, A. E.; Terfort, A.; Rampi, M. A.; Whitesides, G. M., *J. Am. Chem. Soc.*, **2001**, *123*, 5075-5085.
45. Becucci, L.; Rosa Moncelli, M.; Guidelli, R., *J. Electroanal. Chem.*, **1996**, *413*, 187-193.
46. Salomon, A.; Arad-Yellin, R.; Shanzer, A.; Karton, A.; Cahen, D., *J. Am. Chem. Soc.*, **2004**, *126*, 11648-11657.
47. (a) Haag, R.; Rampi, M. A.; Holmlin, R. E.; Whitesides, G. M., *J. Am. Chem. Soc.*, **1999**, *121*, 7895-7906; (b) Weiss, E. A.; Chiechi, R. C.; Kaufman, G. K.; Kriebel, J. K.; Li, Z.; Duati, M.; Rampi, M. A.; Whitesides, G. M., *J. Am. Chem. Soc.*, **2007**, *129*, 4336-4349.
48. (a) Watson, C. M.; Dwyer, D. J.; Andle, J. C.; Bruce, A. E.; Bruce, M. R. M., *Anal. Chem.*, **1999**, *71*, 3181-3186; (b) Li, J.; Abruña, H. D., *J. Phys. Chem. B*, **1997**, *101*, 2907-2916; (c) Vasjari, M.; Shirshov, Y. M.; Samoylov, A. V.; Mirsky, V. M., *J. Electroanal. Chem.*, **2007**, *605*, 73-76; (d) Li, J.; Abruña, H. D., *J. Phys. Chem. B*, **1997**, *101*, 244-252.
49. Akkerman, H. B.; Blom, P. W. M.; de Leeuw, D. M.; de Boer, B., *Nature*, **2006**, *441*, 69-72.

50. Tae-Wook, K.; Gunuk, W.; Hyoyoung, L.; Takhee, L., *Nanotechnology*, **2007**, *18*, 315204.
51. Kushmerick, J. G.; Holt, D. B.; Yang, J. C.; Naciri, J.; Moore, M. H.; Shashidhar, R., *Phys. Rev. Lett.*, **2002**, *89*, 086802.
52. (a) James, G. K.; Craig, M. W.; Steven, K. P.; Terence, L. S.; Ranganathan, S., *Nanotechnology*, **2004**, *15*, S489; (b) Kushmerick, J. G.; Holt, D. B.; Pollack, S. K.; Ratner, M. A.; Yang, J. C.; Schull, T. L.; Naciri, J.; Moore, M. H.; Shashidhar, R., *J. Am. Chem. Soc.*, **2002**, *124*, 10654-10655.
53. Chu, C.; Na, J.-S.; Parsons, G. N., *J. Am. Chem. Soc.*, **2007**, *129*, 2287-2296.
54. (a) Amlani, I.; Rawlett, A. M.; Nagahara, L. A.; Tsui, R. K., *Appl. Phys. Lett.*, **2002**, *80*, 2761-2763; (b) Long, D. P.; Patterson, C. H.; Moore, M. H.; Seferos, D. S.; Bazan, G. C.; Kushmerick, J. G., *Appl. Phys. Lett.*, **2005**, *86*,
55. Vilan, A.; Cahen, D., *Adv. Funct. Mater.*, **2002**, *12*, 795-807.
56. Shimizu, K. T.; Fabbri, J. D.; Jelincic, J. J.; Melosh, N. A., *Adv. Mater.*, **2006**, *18*, 1499-1504.
57. Loo, Y.-L.; Willett, R. L.; Baldwin, K. W.; Rogers, J. A., *Appl. Phys. Lett.*, **2002**, *81*, 562-564.
58. (a) Kumar, A.; Whitesides, G. M., *Appl. Phys. Lett.*, **1993**, *63*, 2002-2004; (b) Kumar, A.; Biebuyck, H. A.; Whitesides, G. M., *Langmuir*, **1994**, *10*, 1498-1511; (c) Balmer, T. E.; Schmid, H.; Stutz, R.; Delamarche, E.; Michel, B.; Spencer, N. D.; Wolf, H., *Langmuir*, **2004**, *21*, 622-632.
59. (a) Loo, Y.-L.; Lang, D. V.; Rogers, J. A.; Hsu, J. W. P., *Nano Lett.*, **2003**, *3*, 913-917; (b) Hsu, J. W. P.; Lang, D. V.; West, K. W.; Loo, Y.-L.; Halls, M. D.; Raghavachari, K., *J. Phys. Chem. B*, **2005**, *109*, 5719-5723; (c) Loo, Y.-L.; Willett, R. L.; Baldwin, K. W.; Rogers, J. A., *J. Am. Chem. Soc.*, **2002**, *124*, 7654-7655.
60. (a) Liu, K.; Wang, X.; Wang, F., *ACS Nano*, **2008**, *2*, 2315-2323; (b) Mayor, M.; von Hänisch, C.; Weber, H. B.; Reichert, J.; Beckmann, D., *Angew. Chem. Int. Ed.*, **2002**, *41*, 1183-1186.
61. (a) Cheng, Z. L.; Skouta, R.; H., V.; Widawsky, J. R.; Schneebeli, S.; Chen, W.; Hybertsen, M. S.; Breslow, R.; Venkataraman, L., *Nat. Nano*, **2011**, *6*, 353-357; (b) Su, T. A.; Widawsky, J. R.; Li, H.; Klausen, R. S.; Leighton, J. L.; Steigerwald, M. L.; Venkataraman, L.; Nuckolls, C., *J. Am. Chem. Soc.*, **2013**, *135*, 18331-18334; (c) Frei, M.; Aradhya, S. V.; Hybertsen, M. S.; Venkataraman, L., *J. Am. Chem. Soc.*, **2012**, *134*, 4003-4006; (d) Chen, F.; Li, X.; Hihath, J.; Huang, Z.; Tao, N., *J. Am. Chem. Soc.*, **2006**, *128*, 15874-15881; (e) Hong, S.; Reifenberger, R.; Tian, W.; Datta, S.; Henderson, J. I.; Kubiak, C. P., *Superlattices Microstruct.*, **2000**, *28*, 289-303; (f) Ke, S.-H.; Baranger, H. U.; Yang, W., *J. Am. Chem. Soc.*, **2004**, *126*, 15897-15904.
62. (a) Haiss, W.; Wang, C.; Jitchati, R.; Grace, I.; Martín, S.; Batsanov, A. S.; Higgins, S. J.; Bryce, M. R.; Lambert, C. J.; Jensen, P. S.; Nichols, R. J., *J. Phys.: Condens. Matter*, **2008**, *20*, 374119; (b) Haiss, W.; Wang, C.; Grace, I.; Batsanov, A. S.; Schiffrin, D. J.; Higgins, S. J.; Bryce, M. R.; Lambert, C. J.; Nichols, R. J., *Nat. Mater.*, **2006**, *5*, 995-1002.

63. (a) Li, Z.; Han, B.; Meszaros, G.; Pobelov, I.; Wandlowski, T.; Blaszczyk, A.; Mayor, M., *Faraday Discuss.*, **2006**, *131*, 121-143; (b) Quinn, J. R.; Foss, F. W.; Venkataraman, L.; Breslow, R., *J. Am. Chem. Soc.*, **2007**, *129*, 12376-12377.
64. Tour, J. M., *Molecular Electronics; Commercial Insights, Chemistry, Devices, Architecture and Programming*. World Scientific Publishing Co: Scientific, 2003.
65. Schwab, P. F. H.; Levin, M. D.; Michl, J., *Chem. Rev.*, **1999**, *99*, 1863-1934.
66. Stang, P. J.; Diederich, F., *Metal-Catalyzed Cross-Coupling Reactions, K. Sonogashira, in: pp. 203–229*. Wiley-VCH, Weinheim: 1998.
67. (a) Stephens, E. B.; Tour, J. M., *Adv. Mater.*, **1992**, *4*, 570-572; (b) Stephens, E. B.; Tour, J. M., *Macromolecules*, **1993**, *26*, 2420-2427; (c) Zawadzki, J., *Carbon*, **1988**, *26*, 619-625; (d) Wright, M. E., *Macromolecules*, **1989**, *22*, 3256-3259.
68. (a) Tanaka, T.; Sekine, C.; Ashida, T.; Ishitobi, M.; Konya, N.; Minai, M.; Fujisawa, K., *Mol. Cryst. Liq. Cryst. Sci. Technol., Sect. A*, **2000**, *346*, 209-216; (b) Lydon, D. P.; Albesa-Jové, D.; Shearman, G. C.; Seddon, J. M.; Howard, J. A. K.; Marder, T. B.; Low, P. J., *Liq. Cryst.*, **2008**, *35*, 119 - 132; (c) Vasconcelos, U. B.; Dalmolin, E.; Merlo, A. A., *Org. Lett.*, **2005**, *7*, 1027-1030.
69. (a) Sivakova, S.; Rowan, S. J., *Chem. Commun.*, **2003**, 2428-2429; (b) Janietz, D.; Ahuja, R. C.; Möbius, D., *Langmuir*, **1997**, *13*, 305-309; (c) Pera, G.; Martín, S.; Ballesteros, L. M.; Hope, A. J.; Low, P. J.; Nichols, R. J.; Cea, P., *Chem. Eur. J.*, **2010**, *16*, 13398-13405; (d) Villares, A.; Pera, G.; Lydon, D. P.; López, M. C.; Low, P. J.; Cea, P., *Colloids Surf., A*, **2009**, *346*, 170-176; (e) Arias-Marin, E.; Arnault, J. C.; Guillon, D.; Maillou, T.; Le Moigne, J.; Geffroy, B.; Nunzi, J. M., *Langmuir*, **2000**, *16*, 4309-4318; (f) Giménez, R.; Piñol, M.; Serrano, J. L., *Chem. Mater.*, **2004**, *16*, 1377-1383; (g) Pschirer, N. G.; Miteva, T.; Evans, U.; Roberts, R. S.; Marshall, A. R.; Neher, D.; Myrick, M. L.; Bunz, U. H. F., *Chem. Mater.*, **2001**, *13*, 2691-2696; (h) Schroeder, R.; Wilson, J. N.; Bunz, U. H. F.; Ullrich, B., *J. Phys. Chem. B*, **2003**, *107*, 11604-11607.
70. (a) Reed, M. A.; Chen, J.; Rawlett, A. M.; Price, D. W.; Tour, J. M., *Appl. Phys. Lett.*, **2001**, *78*, 3735-3737; (b) Fan, F.-R. F.; Lai, R. Y.; Cornil, J.; Karzazi, Y.; Brédas, J.-L.; Cai, L.; Cheng, L.; Yao, Y.; Price, D. W.; Dirk, S. M.; Tour, J. M.; Bard, A. J., *J. Am. Chem. Soc.*, **2004**, *126*, 2568-2573; (c) Xiao, X.; Nagahara, L. A.; Rawlett, A. M.; Tao, N., *J. Am. Chem. Soc.*, **2005**, *127*, 9235-9240; (d) Blum, A. S.; Kushmerick, J. G.; Long, D. P.; Patterson, C. H.; Yang, J. C.; Henderson, J. C.; Yao, Y.; Tour, J. M.; Shashidhar, R.; Ratna, B. R., *Nat. Mater.*, **2005**, *4*, 167-172; (e) Lu, Q.; Liu, K.; Zhang, H.; Du, Z.; Wang, X.; Wang, F., *ACS Nano*, **2009**, *3*, 3861-3868.
71. Häkkinen, H., *Nat. Chem*, **2012**, *4*, 443–455.
72. (a) Krüger, D.; Fuchs, H.; Rousseau, R.; Marx, D.; Parrinello, M., *Phys. Rev. Lett.*, **2002**, *89*, 186402; (b) Rubio-Bollinger, G.; Bahn, S. R.; Agraït, N.; Jacobsen, K. W.; Vieira, S., *Phys. Rev. Lett.*, **2001**, *87*, 026101; (c) Huang; Chen, F.; Bennett, P. A.; Tao, *J. Am. Chem. Soc.*, **2007**, *129*, 13225-13231; (d) Sondag-Huethorst, J. A. M.; Schonenberger, C.; Fokkink, L. G. J., *J. Phys. Chem.*, **1994**, *98*, 6826-6834.
73. (a) Ramachandran, G. K.; Hopson, T. J.; Rawlett, A. M.; Nagahara, L. A.; Primak, A.; Lindsay, S. M., *Science*, **2003**, *300*, 1413-1416; (b) Donhauser, Z. J.; Mantooth, B. A.; Kelly, K. F.; Bumm, L. A.; Monnell, J. D.; Stapleton, J. J.; Price, D. W.;

Rawlett, A. M.; Allara, D. L.; Tour, J. M.; Weiss, P. S., *Science*, **2001**, *292*, 2303-2307; (c) Yasuda, S.; Yoshida, S.; Sasaki, J.; Okutsu, Y.; Nakamura, T.; Taninaka, A.; Takeuchi, O.; Shigekawa, H., *J. Am. Chem. Soc.*, **2006**, *128*, 7746-7747.

74. (a) Ie, Y.; Hirose, T.; Nakamura, H.; Kiguchi, M.; Takagi, N.; Kawai, M.; Aso, Y., *J. Am. Chem. Soc.*, **2011**, *133*, 3014-3022; (b) Sedghi, G.; Garcia-Suarez, V. M.; Esdaile, L. J.; Anderson, H. L.; Lambert, C. J.; Martin, S.; Bethell, D.; Higgins, S. J.; Elliott, M.; Bennett, N.; Macdonald, J. E.; Nichols, R. J., *Nat. Nano*, **2011**, *6*, 517-523; (c) Wang, C.; Batsanov, A. S.; Bryce, M. R.; Martín, S.; Nichols, R. J.; Higgins, S. J.; García-Suárez, V. M.; Lambert, C. J., *J. Am. Chem. Soc.*, **2009**, *131*, 15647-15654.
75. (a) Venkataraman, L.; Park, Y. S.; Whalley, A. C.; Nuckolls, C.; Hybertsen, M. S.; Steigerwald, M. L., *Nano Lett.*, **2007**, *7*, 502-506; (b) Venkataraman, L.; Klare, J. E.; Tam, I. W.; Nuckolls, C.; Hybertsen, M. S.; Steigerwald, M. L., *Nano Lett.*, **2006**, *6*, 458-462.
76. Patrone, L.; Palacin, S.; Charlier, J.; Armand, F.; Bourgoin, J. P.; Tang, H.; Gauthier, S., *Phys. Rev. Lett.*, **2003**, *91*, 096802.
77. Moreno-García, P.; Gulcur, M.; Manrique, D. Z.; Pope, T.; Hong, W.; Kaliginedi, V.; Huang, C.; Batsanov, A. S.; Bryce, M. R.; Lambert, C.; Wandlowski, T., *J. Am. Chem. Soc.*, **2013**, *135*, 12228-12240.
78. Martin, S.; Haiss, W.; Higgins, S. J.; Nichols, R. J., *Nano Lett.*, **2010**, *10*, 2019-2023.
79. Kiguchi, M.; Miura, S.; Hara, K.; Sawamura, M.; Murakoshi, K., *Appl. Phys. Lett.*, **2006**, *89*, 213104.
80. (a) Chen, J.; Calvet, L. C.; Reed, M. A.; Carr, D. W.; Grubisha, D. S.; Bennett, D. W., *Chem. Phys. Lett.*, **1999**, *313*, 741-748; (b) Beebe, J. M.; Engelkes, V. B.; Miller, L. L.; Frisbie, C. D., *J. Am. Chem. Soc.*, **2002**, *124*, 11268-11269.
81. Fu, M.-D.; Chen, I. W. P.; Lu, H.-C.; Kuo, C.-T.; Tseng, W.-H.; Chen, C.-h., *J. Phys. Chem. C*, **2007**, *111*, 11450-11455.
82. Fukazawa, A.; Kiguchi, M.; Tange, S.; Ichihashi, Y.; Zhao, Q.; Takahashi, T.; Konishi, T.; Murakoshi, K.; Tsuji, Y.; Staykov, A.; Yoshizawa, K.; Yamaguchi, S., *Chem. Lett.*, **2011**, *40*, 174-176.
83. Komoto, Y.; Fujii, S.; Hara, K.; Kiguchi, M., *J. Phys. Chem. C*, **2013**, *117*, 24277-24282.
84. Hong, W.; Li, H.; Liu, S.-X.; Fu, Y.; Li, J.; Kaliginedi, V.; Decurtins, S.; Wandlowski, T., *J. Am. Chem. Soc.*, **2012**, *134*, 19425-19431.
85. Marques-Gonzalez, S.; Yufit, D. S.; Howard, J. A. K.; Martin, S.; Osorio, H. M.; Garcia-Suarez, V. M.; Nichols, R. J.; Higgins, S. J.; Cea, P.; Low, P. J., *Dalton Trans.*, **2013**, *42*, 338-341.
86. Ward, M. D., *Chem. Soc. Rev.*, **1995**, *24*, 121-134.
87. Wenger, O. S., *Acc. Chem. Res.*, **2010**, *44*, 25-35.
88. Nelsen, S. F.; Ismagilov, R. F.; Powell, D. R., *J. Am. Chem. Soc.*, **1997**, *119*, 10213-10222.
89. He, J.; Chen, F.; Li, J.; Sankey, O. F.; Terazono, Y.; Herrero, C.; Gust, D.; Moore, T. A.; Moore, A. L.; Lindsay, S. M., *J. Am. Chem. Soc.*, **2005**, *127*, 1384-1385.

90. (a) Arnold, D. P.; Heath, G. A.; James, D. A., *J. Porphyrins Phthalocyanines*, **1999**, *3*, 5-31; (b) Low, P.; Brown, N., *J. Cluster Sci.*, **2010**, *21*, 235-278; (c) D'Alessandro, D. M.; Keene, F. R., *Dalton Trans.*, **2004**, 3950-3954.
91. (a) Kalyanasundaram, K.; Nazeeruddin, M. K., *Inorg. Chim. Acta*, **1994**, *226*, 213-230; (b) Creutz, C., Mixed Valence Complexes of d5-d6 Metal Centers. In *Prog. Inorg. Chem.*, John Wiley & Sons, Inc.: 2007; pp 1-73.
92. Robin, M. B.; Day, P., Mixed Valence Chemistry-A Survey and Classification. In *Advances in Inorganic Chemistry and Radiochemistry*, Emeléus, H. J.; Sharpe, A. G., Eds. Academic Press: 1968; Vol. Volume 10, pp 247-422.
93. Chen, P.; Meyer, T. J., *Chem. Rev.*, **1998**, *98*, 1439-1478.
94. (a) Demadis, K. D.; Hartshorn, C. M.; Meyer, T. J., *Chem. Rev.*, **2001**, *101*, 2655-2686; (b) Nelsen, S. F., *Chem. Eur. J.*, **2000**, *6*, 581-588; (c) Brunschwig, B. S.; Creutz, C.; Sutin, N., *Chem. Soc. Rev.*, **2002**, *31*, 168-184.
95. Parthey, M.; Gluyas, J. B. G.; Schauer, P. A.; Yufit, D. S.; Howard, J. A. K.; Kaupp, M.; Low, P. J., *Chem. Eur. J.*, **2013**, *19*, 9780-9784.
96. (a) Creutz, C.; Newton, M. D.; Sutin, N., *J. Photochem. Photobiol., A*, **1994**, *82*, 47-59; (b) Brunschwig, B. S.; Sutin, N., *Coord. Chem. Rev.*, **1999**, *187*, 233-254.
97. Launay, J.-P., *Chem. Soc. Rev.*, **2001**, *30*, 386-397.
98. Matsuhita, R.; Horikawa, M.; Naitoh, Y.; Nakamura, H.; Kiguchi, M., *J. Phys. Chem. C*, **2013**, *117*, 1791-1795.
99. Huang, M. J.; Hsu, L. Y.; Fu, M. D.; Chuang, S. T.; Tien, F. W.; Chen, C. H., *J. Am. Chem. Soc.*, **2014**, *136*, 1832-1841.
100. Crispin, X.; Geskin, V.; Crispin, A.; Cornil, J.; Lazzaroni, R.; Salaneck, W. R.; Brédas, J.-L., *J. Am. Chem. Soc.*, **2002**, *124*, 8131-8141.
101. Tao, N. J., *Phys. Rev. Lett.*, **1996**, *76*, 4066-4069.
102. Wang, G.; Kim, T. W.; Lee, T.; Wang, W.; Reed, M. A., 4.16 - Electronic Properties of Alkanethiol Molecular Junctions: Conduction Mechanisms, Metal–Molecule Contacts, and Inelastic Transport. In *Comprehensive Nanoscience and Technology*, Andrews, D. L.; Scholes, G. D.; Wiederrecht, G. P., Eds. Academic Press: Amsterdam, 2011; pp 463-487.
103. (a) Malysheva, L.; Onipko, A., *physica status solidi (b)*, **2007**, *244*, 4244-4247; (b) Nitzan, A.; Ratner, M. A., *Science*, **2003**, *300*, 1384-1389; (c) Nitzan, A., *Annu. Rev. Phys. Chem.*, **2001**, *52*, 681-750; (d) Zimbovskaya, N. A.; Pederson, M. R., *Physics Reports*, **2011**, *509*, 1-87.
104. Adams, D. M.; Brus, L.; Chidsey, C. E. D.; Creager, S.; Creutz, C.; Kagan, C. R.; Kamat, P. V.; Lieberman, M.; Lindsay, S.; Marcus, R. A.; Metzger, R. M.; Michel-Beyerle, M. E.; Miller, J. R.; Newton, M. D.; Rolison, D. R.; Sankey, O.; Schanze, K. S.; Yardley, J.; Zhu, X., *J. Phys. Chem. B*, **2003**, *107*, 6668-6697.
105. Yamada, R.; Kumazawa, H.; Noutoshi, T.; Tanaka, S.; Tada, H., *Nano Lett.*, **2008**, *8*, 1237-1240.
106. (a) Wold, D. J.; Haag, R.; Rampi, M. A.; Frisbie, C. D., *J. Phys. Chem. B*, **2002**, *106*, 2813-2816; (b) Ishida, T.; Mizutani, W.; Aya, Y.; Ogiso, H.; Sasaki, S.; Tokumoto, H., *J. Phys. Chem. B*, **2002**, *106*, 5886-5892.

107. (a) Liu, H.; Wang, N.; Zhao, J.; Guo, Y.; Yin, X.; Boey, F. Y. C.; Zhang, H., *ChemPhysChem*, **2008**, *9*, 1416-1424; (b) Newton, M. D.; Smalley, J. F., *Phys. Chem. Chem. Phys.*, **2007**, *9*, 555-572.
108. Onuchic, J. N.; Beratan, D. N.; Winkler, J. R.; Gray, H. B., *Annu. Rev. Biophys. Biomol. Struct.*, **1992**, *21*, 349-377.
109. Joachim, C.; Ratner, M. A., *Nanotechnology*, **2004**, *15*, 1065.
110. Haiss, W.; van Zalinge, H.; Bethell, D.; Ulstrup, J.; Schiffrin, D. J.; Nichols, R. J., *Faraday Discuss.*, **2006**, *131*, 253-264.
111. Davis, W. B.; Svec, W. A.; Ratner, M. A.; Wasielewski, M. R., *Nature*, **1998**, *396*, 60-63.
112. Ho Choi, S.; Kim, B.; Frisbie, C. D., *Science*, **2008**, *320*, 1482-1486.
113. (a) Wierzbinski, E.; Venkatramani, R.; Davis, K. L.; Bezer, S.; Kong, J.; Xing, Y.; Borguet, E.; Achim, C.; Beratan, D. N.; Waldeck, D. H., *ACS Nano*, **2013**, *7*, 5391-5401; (b) Luo, L.; Choi, S. H.; Frisbie, C. D., *Chem. Mater.*, **2010**, *23*, 631-645; (c) Renaud, N.; Berlin, Y. A.; Lewis, F. D.; Ratner, M. A., *J. Am. Chem. Soc.*, **2013**, *135*, 3953-3963.
114. (a) Nitzan, A., *J. Phys. Chem. A*, **2001**, *105*, 2677-2679; (b) Berlin, Y. A.; Ratner, M. A., *Radiat. Phys. Chem.*, **2005**, *74*, 124-131; (c) Traub, M. C.; Brunschwig, B. S.; Lewis, N. S., *J. Phys. Chem. B*, **2007**, *111*, 6676-6683.
115. Bergfield, J. P.; Ratner, M. A., *physica status solidi (b)*, **2013**, *250*, 2249-2266.
116. Nitzan, A., *Isr. J. Chem.*, **2002**, *42*, 163-166.
117. Heath, J. R.; Ratner, M. A., *Physics Today*, **2003**, *56*, 43-49.

# 2. SYNTHESIS AND CHARACTERIZATION OF CARBOXY-SUBSTITUTED OPEs: A LB APPROACH TO MOLECULAR FILMS

## 2.1. Abstract

The synthesis, characterization and Langmuir-Blodgett (LB) surface studies of two carboxy-substituted oligo(phenylene-ethynylene) (OPE) derivatives are described (Chart 2-1). The available synthetic methodologies appropriate for the preparation of the highly conjugated OPE backbone are reviewed, and an optimized synthetic methodology developed to circumvent the solubility issues encountered for the synthesis of **6** and **15** is reported. In collaboration with Dr. Pilar Cea and her group in the University of Zaragoza, monolayers of both compounds were formed by means of the LB technique. The LB technique is briefly reviewed and the physical, optical and electrical properties of the monolayers prepared from **6** and **15** are discussed.

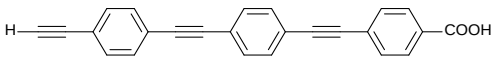


**6**

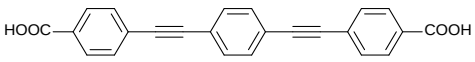


**15**

**Chart 2-1.** *Structures of OPEs **6** and **15**.*

## 2.2. Introduction

Highly conjugated derivatives such as OPEs are of great interest in many different fields of science due to their unique properties (*see* Chapter 1).[1] However in the context of this thesis, it is the extended, conjugated π-system and good single molecule conductance of the OPEs that merits particular attention.[2] In a study performed by Lu *et al.*[2f] to elucidate the charge transport mechanism(s) prevalent within an OPE molecular junction, the conductance of a series of different length amine terminated OPEs was determined, allowing the evaluation of the tunnelling attenuation factor $\beta$ for these compounds.

The STM-BJ studies performed on SAM in air, revealed a clear transition in the length dependence of the molecular conductance for OPEs for examples 3 nm in length. The electronic decay constant was found to drop from $\beta \sim 2$ nm$^{-1}$ for the shorter derivatives, to $\beta \sim 0.3$ nm$^{-1}$ for the longer members of the series. That sudden change in the conductance distance dependence was attributed to an intrinsic change in the charge transport mechanism from tunnelling (short OPEs less than 3 nm in length) to hopping (OPEs over 3 nm in length). More recently, in a parallel study by Zhao *et al.*[3] several pyridine terminated OPEs were subjects of similar studies but this time using the MCBJ method to form single molecule junctions. Despite the marked experimental differences, results revealed a similar transition in the attenuation constant for molecular lengths over 3 nm in good agreement with Lu's results. The distance dependence was again found to be less marked for the longer OPEs ($\beta \sim 0.1$ nm$^{-1}$) compared to that of the shorter analogues ($\beta \sim 3$ nm$^{-1}$).

However, the properties of the molecular backbone alone do not guarantee or directly map to electrical properties of a molecule when placed in a metal|molecule|metal junctions, and the nature of the metal-linker and linker-molecule is now being recognised as a critical element of the design of molecular components for electronic applications.[4] This has led us and many other groups to explore the use of different linkers groups to produce reliable and more transmissive molecular junctions.[4b, c, 5] Whilst self-assembly of thiols on gold has been a work-horse for the assembly of such junctions,[6] other substrates, surface contacts and deposition methods have also been explored (*see* Chapter 1).[7]

Compounds **6** and **15** bearing a hydrophilic carboxylic acid terminal group in addition to the hydrophobic OPE motif were designed for their use in the preparation of molecular films on a wide variety of substrates using the LB technique. In the case of **6** the acetylenic moiety was also introduced which, as will be shown, also provides a useful and

novel contact to gold.[8] The −C≡CH moiety carries a very rich surface chemistry allowing grafting of relatively complex molecular structures onto hydrogen passivated silicon surfaces via hydrosilylation[9] and facile derivative formation through click and cross-coupling chemistries.[10] Although to date, symmetrical compounds have been the most commonly studied molecular wire candidates, unsymmetrical compounds like **6** are of great interest as they can selectively contact different electrode materials.[11] Unsymmetrical molecular junctions showing preferential direction for charge transport can be seen as replacements for rectifiers or diodes, and hence introduction of electronic function beyond that of wire-like behaviour.[12]

## 2.3. Synthetic considerations

A plethora of reactions and functional group transformations are known that could in principle be used to develop an equally wide range of different strategies to the preparation of OPE derivatives.[13] Amongst the traditional, non-catalytic routes present in the literature, the synthesis of phenyl-ethynylenes by simple sequential addition of lithiated acetylide anions to benzoquinone prevails (Scheme 2-1).[14] After the initial nucleophilic attack the resulting di-en-diols are reduced typically using $SnCl_2$ in alcoholic mixtures, to yield the targeted ethynylbenzene in moderate yields *ca.* 30 - 60%. Despite the simplicity of this approach, the use of organolithium reagents narrows its applicability to molecules not containing base or nucleophile sensitive functional groups. Hence, a more convenient alternative requiring milder conditions is desirable.

A different approach proposed by Orita[15] consists of a multi-stepped double elimination of *β*-substituted sulfones (Scheme 2-1). The protocol comprises a succession of different reactions, namely aldol reaction, aldolate protection and final double elimination of the *β*-substituted sulfones. Despite the several steps, all operations can be carried out in

one pot and good overall yields *ca.* 75 %. However, rather than a substitute to the Pd/Cu catalysed chemistry, the procedure was proposed as an alternative towards the synthesis of dihalo-diphenylacetylenes (*see* Appendix B).

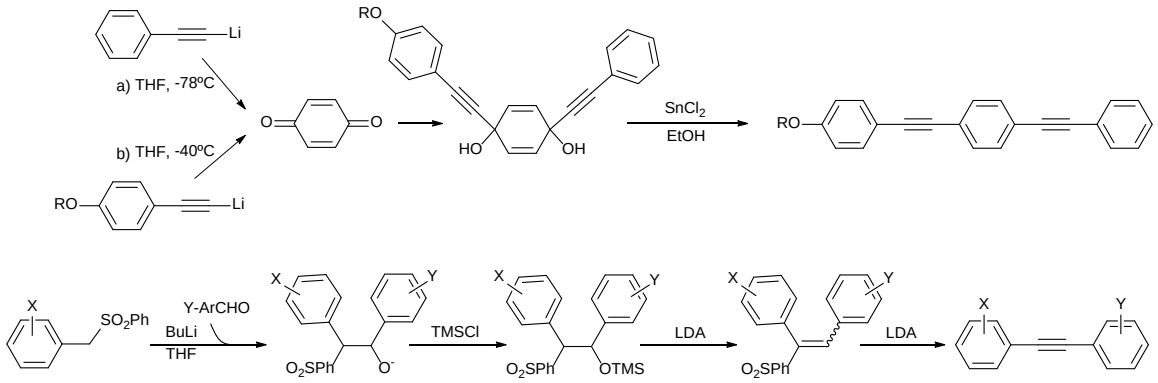


**Scheme 2-1.** *Alternatives to Sonogashira synthesis of conjugated OPEs by sequential addition of lithiated acetylide anions to benzoquinone (top) and double elimination of β-substituted sulfones (bottom).*

However the development of metal-catalysed cross-coupling reactions, recognised through the award of the 2010 Nobel Prize in Chemistry to Heck, Negishi, and Suzuki, has now led to these methods being adopted as principal tools in the preparation of $C_{sp}$−$C_{sp2}$ bonds.[16] Of the multitude of different metal-catalysed $C_{sp}$−$C_{sp2}$ cross-coupling reactions present in the literature, namely: Stephen-Castro;[13a] Cassar;[13b] Heck[13c] and Sonogashira[13d] the latter was chosen for the synthesis of OPEs **6** and **15** because of the mild conditions required, tolerance to a wide variety of functional groups and good yields (Scheme 2-1).[17]

In this context it is worth noting a very interesting variation on this approach the so-called sila-Sonogashira. Because of the nature of Sonogashira chemistry, ethynyl protecting group strategies are often required. The most common of the ethynyl protecting groups is trimethylsilane (-$SiMe_3$). The $C_{sp}$−Si bond is generally not affected by standard Sonogashira reaction conditions thereby the silyl group can be used as a protecting group

and later removed to furnish a structurally modified terminal ethynylene. Hence, the synthesis of extended OPEs following a Sonogashira protocol typically consists on a succession of cross-coupling followed by ethynyl deprotection reactions. The sila-Sonogashira protocol reported by Nishihara,[18] is capable of cross-coupling between aryl triflates or even chlorides with alkynylsilanes via Si-C bond activation (Scheme 2-2). The reaction is conducted under the standard Sonogashira conditions using a Pd/Cu co-catalyst system in DMF to prepare unsymmetrical diarylethynes in good yields *i.e.* 70 - 90%. It is worth noting that this reaction does not require the presence of any base or fluoride salt to take place, although in exchange large amounts of CuCl are required *i.e.* 50% mol. Despite effectively reducing the number of synthetic steps to a half, the large amounts of copper required renders the process ultimately inconvenient, especially for multi-gram synthesis.

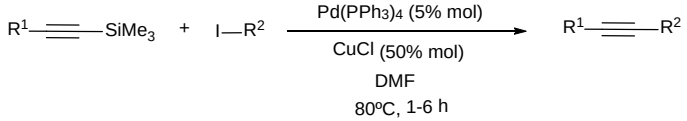


**Scheme 2-2.** *Optimized Nishihara sila-Sonogashira coupling conditions.*

Despite the many alternatives, all the OPEs included in this thesis were prepared under typical Sonogashira cross-coupling conditions *i.e.* 2 - 10% of $Pd(PPh_3)_4$ and CuI in amine solutions. Amongst the most commonly used amines are $NEt_3$ and $NHPr_2^i$ (Scheme 2-3). These amine bases can be used as the reaction primary solvent or in stoichiometric amounts in combination with an inert co-solvent for economical and solubility reasons.[19]

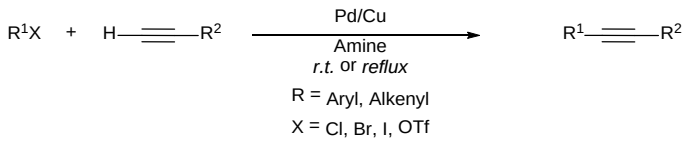


**Scheme 2-3.** *Standard conditions for the Pd/Cu catalysed Sonogashira cross-coupling.*

Scheme 2-4 describes the simplest, schematic representation of the catalytic mechanism that underpins the Sonogashira cross-coupling. The real cycle is believed to consist of two or three different cooperative catalytic processes that take place simultaneously.[17]

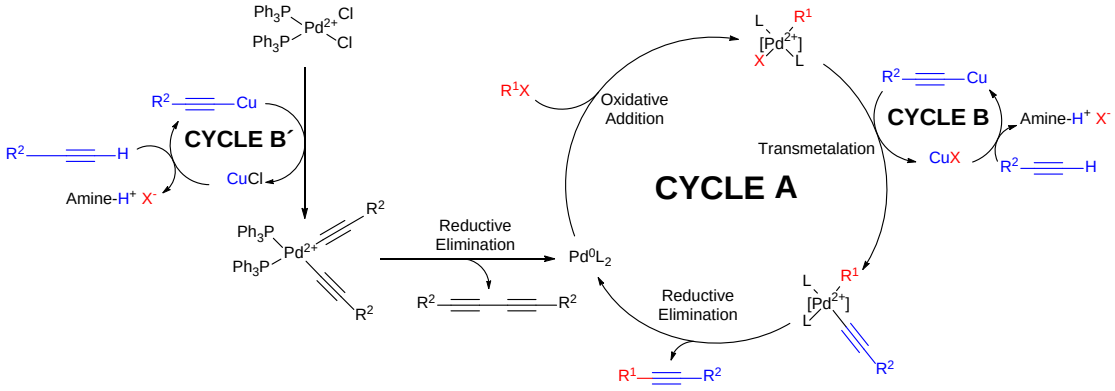


**Scheme 2-4.** *Sonogashira cross-coupling detailed mechanism.*

Despite the exact details of the reaction mechanism not being completely known and evidence for several subtle different mechanisms being presented, and likely the precise one in operation in any case being sensitive to the precise conditions employed, it is agreed that the Sonogashira reaction follows the common cross-coupling oxidative addition and reductive elimination process (Scheme 2-4, cycle A). It is generally assumed that neutral, coordinatively unsaturated $Pd^0$ species are the active catalytic agents in the cross-coupling cycle, although the role of anionic halide coordinated complexes has been discussed. [20] When the palladium catalyst employed is in an oxidation state other than neutral, the pre-catalyst must be reduced to its neutral active state prior to its entrance to the catalytic cycle. When $PdCl_2(PPh_3)_2$ is used, the pre-catalyst undergoes a copper mediated oxidative addition to yield the ethynyl-palladium species and further reductive elimination to generate the $14e^-$ active complex $Pd^0(PPh_3)_2$ (Scheme 2-4, cycle B´). The design and synthesis of exotic Pd catalysts based on novel ligands is a field of great activity nowadays.[21] The enhanced reactivity of those catalysts allow the use of less Pd and

open the door to cross-coupling on previously inert aryl chlorides. It should also be noted that over the last decades the number of catalytically active metals for $C_{sp}$–$C_{sp2}$ cross-couplings has dramatically increased.[22] To the best of our knowledge iron,[23] ruthenium,[24] cobalt,[25] rhodium,[26] nickel,[27] copper,[28] silver,[29] gold[30] and indium[31] have shown catalyst activity towards Sonogashira cross-couplings. In addition, the environmental impact of the reaction is being improved by catalyst immobilization[32] and the use of aqueous conditions.[33] However, most of the Sonogashira chemistry employed in modern context relies on the use of commercially available palladium catalysts such as: $Pd(OAc)_2$; $PdCl_2(PPh_3)_2$; $Pd_2(dba)_3{\cdot}CHCl_3$ and $Pd(PPh_3)_4$.

Despite $PdCl_2(PPh_3)_2$ being air-stable, $Pd(PPh_3)_4$ was the catalyst of choice for the preparation of OPEs in this thesis because of its sufficient catalytic activity and straightforward well-known synthesis.[34] The avoidance of the pre-catalyst reduction cycle to the active $Pd^0$ species also circumvents the generation of diyne by-products leading to easier reaction work-ups (*see experimental section*). The catalyst $Pd(PPh_3)_4$ is a bright light yellow coloured, oxygen, moisture sensitive and coordinatively saturated $Pd^0$complex that only requires the endergonic loss of triphenylphosphine to yield the catalytically active species $Pd^0(PPh_3)_2$. A widely used alternative to the preparation and storage of sensitive Pd catalysts is based on *in-situ* generation of the catalyst. That simple yet effective approach involves the addition of a readily available Pd salt such as $Pd(OAc)_2$ together with the ligand of choice to the reaction mixture. The $Pd^{2+}$ species undergo reduction and ligand substitution *in-situ* before getting involved in the cross-coupling cycle circumventing that way the delicate catalyst synthesis.

## 2.4. Synthesis of the OPE derivatives

Traditional Pd/Cu catalysed Sonogashira chemistry was employed to prepare compounds **6** and **15**. Despite the great similarity between both compounds, the symmetrical nature of **15** allows for a more direct convergent synthesis while a linear multi-stepped protocol was required for the synthesis of **6**. Despite its apparent simplicity, the synthesis of **6** resulted more challenging than initially expected due to severe solubility issues. Scheme 2-5 displays the coupling/deprotection reaction sequence initially followed for the synthesis of **6**.

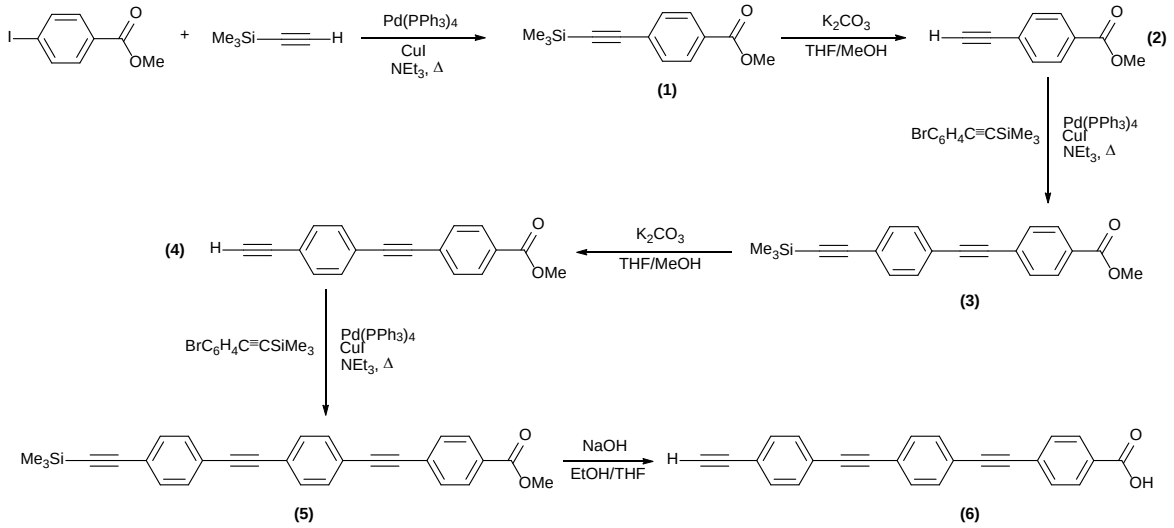


**Scheme 2-5.** *Methyl benzoate coupling/deprotection protocol for the synthesis **6**.*

In order to shorten the number of steps, a previously synthesized building block, $BrC_6H_4C{\equiv}CSiMe_3$ was employed (*see experimental section*). The first four steps of the synthetic route leading to isolation of **1**, **2**, **3** and **4** were performed without any remarkable problems. The Sonogashira coupling between methyl-4-iodobenzoate and trimethylsilylacetylene in the presence of Pd/Cu (5% mol) in $NEt_3$, at reflux temperature to yield **1** took place in excellent yield *ca.* 90%. The subsequent deprotection of the ethynyl moiety performed in the presence of excess $K_2CO_3$ in MeOH to prepare **2** took place in less acceptable, but functional yield of *ca.* 50%. The following coupling/deprotection steps

to prepare **3** and **4** ran smoothly but typically in slightly lower yields. Despite compound **4** started showing some evident solubility issues it was still soluble enough to allow characterization by $^{1}$H NMR spectroscopy (*see experimental section*). However, every attempt to synthesize **5** was in vain.

Despite the cross-coupling of **4** with $BrC_6H_4C{\equiv}CSiMe_3$ running smoothly, a statement supported by the smooth decay of the $^{1}$H NMR signal at δ 3.19 (s, 1H, $C_{sp}$−H), the poor solubility of **5** frustrated every attempt to purify and characterize the compound. After many unsuccessful attempts, a different approach was required in order to circumvent these solubility issues. To that end, a longer aliphatic chain ester was employed. The replacement of the methyl ester by a hexyl ester proved enough to improve the solubility throughout the synthetic route. In addition, to avoid transesterification of the hexyl ester under basic MeOH conditions the ethynyl deprotection steps were performed in the presence of tetra-n-butylammonium fluoride (TBAF) in THF. Scheme 2-6 presents the final synthetic route followed for the synthesis of **6**.

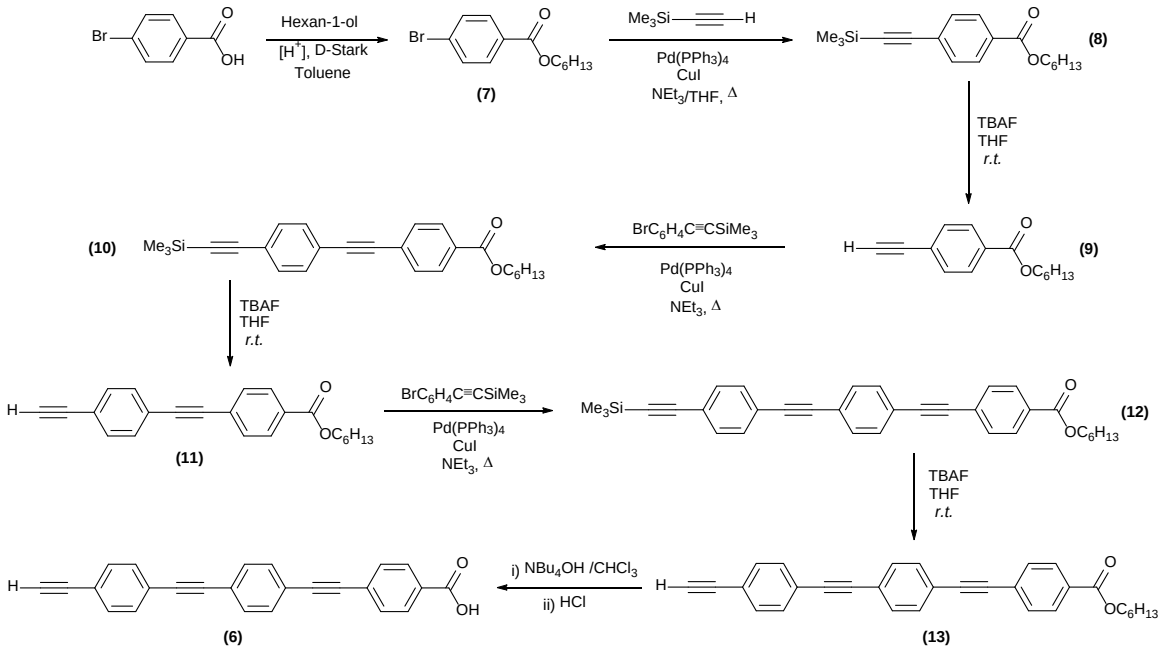


**Scheme 2-6.** *Hexyl benzoate synthetic route for the preparation of **6**.*

The acid catalysed esterification of 4-bromobenzoic acid in hexanol was performed in the presence of toluene as a supporting solvent to enhance solubility of the acid in the reaction mixture (Scheme 2-6). The reaction was conducted in a flask fitted with a Dean-Stark head to produce **7** in excellent yields of *ca.* 90%. The previously described sequential coupling/deprotection protocol was used over the next six steps to give **6** with Sonogashira couplings typically taking place in excellent yields of *ca.* 90 % and the $Si-C_{sp3}$ bond cleavage reactions with TBAF taking place in *ca.* 80% yields. Throughout these steps, the much improved solubility of the hexyl ester OPE precursors allowed easy chromatographic purification and full characterization of the products (*see experimental section*).

Despite the enhanced solubility of **13,** transesterification under basic NaOH/MeOH conditions led to the sodium salt of **6** as an extremely insoluble off-white precipitate that could not be appropriately characterized. Hence, in order to make the hydrolysis of **13** more evident, a more soluble ammonium salt of the carboxylate was prepared replacing the inorganic base NaOH by $NBu_4OH$. As a consequence, the formation of the carboxylate ammonium salt took place in $CHCl_3$ at room temperature. The solution was then acidified to pH 2 by addition of *conc.* HCl and the white precipitate of the desired acid, which was collected by filtration. Despite the poor solubility of **6**, it was possible to characterize the final product by $H^1$ NMR, $MS^+$ and IR (*see experimental section*). Interestingly, microanalysis performed on **6** showed a great deviation from the calculated values *i.e.* $C_{25}H_{14}O_2$ Calcd. C 86.69; H 4.07; Found C 45.69 H 3.03. To clarify this strong disagreement, a thermo gravimetric analysis was conducted on **6**. The TGA proved that only the 54.2 % of the sample weight was combusted at 1000 ºC. A deeper look into the literature revealed that thermal degradation of OPEs onto thermally robust by-products has been briefly reported previously.[35] The compound is also remarkably stable to chemical

attacks, as it was found when **6** was submitted for metal traces analysis by ICP or OES only for the digestion of the sample in $HNO_3$ or aqua regia to fail.

The experience gained during the synthesis of **6** cleared the path for the synthesis of **15** (Scheme 2-7). The symmetry of **14** allows a straightforward convergent synthesis by coupling **9** with 1,4-diiododbenzene under standard Sonogashira conditions. The reaction took place at room temperature in good yields *i.e.* 75%. In an analogue way to that employed for the synthesis of **6**, $NBu_4OH$ was used to generate a soluble ammonium carboxylate from **14**. Further acidification of the $CHCl_3$ mixture forced **15** to precipitate cleanly out of solution in good yield *ca.* 90%.

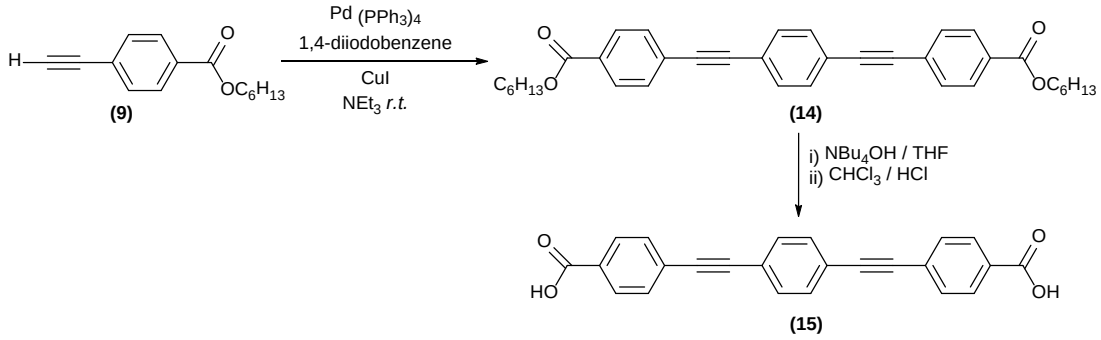


**Scheme 2-7.** *Synthetic steps for the synthesis of **15**.*

Despite its poor solubility, **15** was fully characterized by means of $^{1}H$ and $^{13}C$ NMR, MS and IR. Characterization by $^{13}C$ NMR was only possible thanks to the efforts of the staff in the Durham NMR Service, who collected NMR data from a DMSO-$d_6$ saturated solution of the compound during several hours at 50 ºC. Longer relaxation times were used to allow the $C_{sp}$ signals to acquire enough intensity to be assigned. TGA confirmed the thermal robustness previously reported for **6** and other OPEs showing incomplete combustion (90 %) at 1000 ºC.

## 2.5. Fabrication and characterization of Langmuir and Langmuir-Blodgett films

### *2.5.1. The Langmuir-Blodgett technique*

Despite their simplicity, the Langmuir and Langmuir-Blodgett techniques count as some of the few techniques able to handle matter at the molecular level.[36] A very simplified description of the technique consists on the dispersion of molecules on the surface of a liquid, so-called sub-phase, and compression of those molecules until a well-packed monolayer is formed. The molecular film (known as a Langmuir film, L) can be transferred from the sub-phase on to a variety of solid substrates for further characterization or applicability in a method known as the Langmuir-Blodgett (LB) technique. Despite the great capability of the LB technique, a good initial molecular design is crucial for the formation of well packed monolayers as it depends mostly on supramolecular interactions generated upon compression.

Figure 2-2 shows a scheme of the Langmuir trough utilised. The instrument is referred to as the Langmuir trough recognizing the great contribution of the Nobel Laureate Irving Langmuir to the field.[37] Despite not being the only sub-phase available,[38] all the Langmuir films presented in this Chapter were formed on water because of its high surface tension and availability.

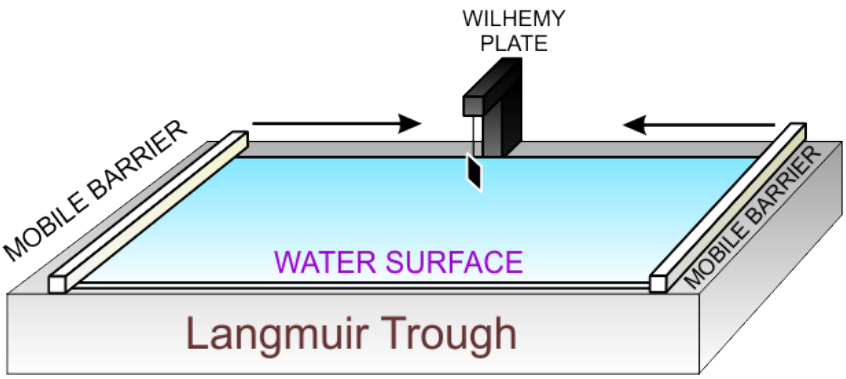


**Figure 2-2.** *Schematic representation of a Langmuir trough.*

Typically, a dilute solution (~$10^{-4}$ M) of the molecule of interest in a solvent immiscible with water is spread on the air-water interface by drop wise dissemination using a Hamilton micro-syringe. A fine spreading is crucial to achieve good reproducibility making this step the most problematic step of the experimental routine. After the organic solvent is allowed to evaporate, the compression process was initiated by slowly sweeping the water surface with two mobile barriers. The compression process was continuously monitored by registering the changes on the surface pressure π, using a Wilhemy plate. The surface pressure is defined as the difference between the surface tension of the clean water and the surface tension of the sub-phase covered with the molecules under study. When the surface pressure is plotted versus the area per molecule for a process recorded at constant temperature the curve obtained is referred to as the *π-A* isotherm. Figure 2-3 contains the different monolayer phases that can be found in a *π-A* isotherm upon compression.[39]

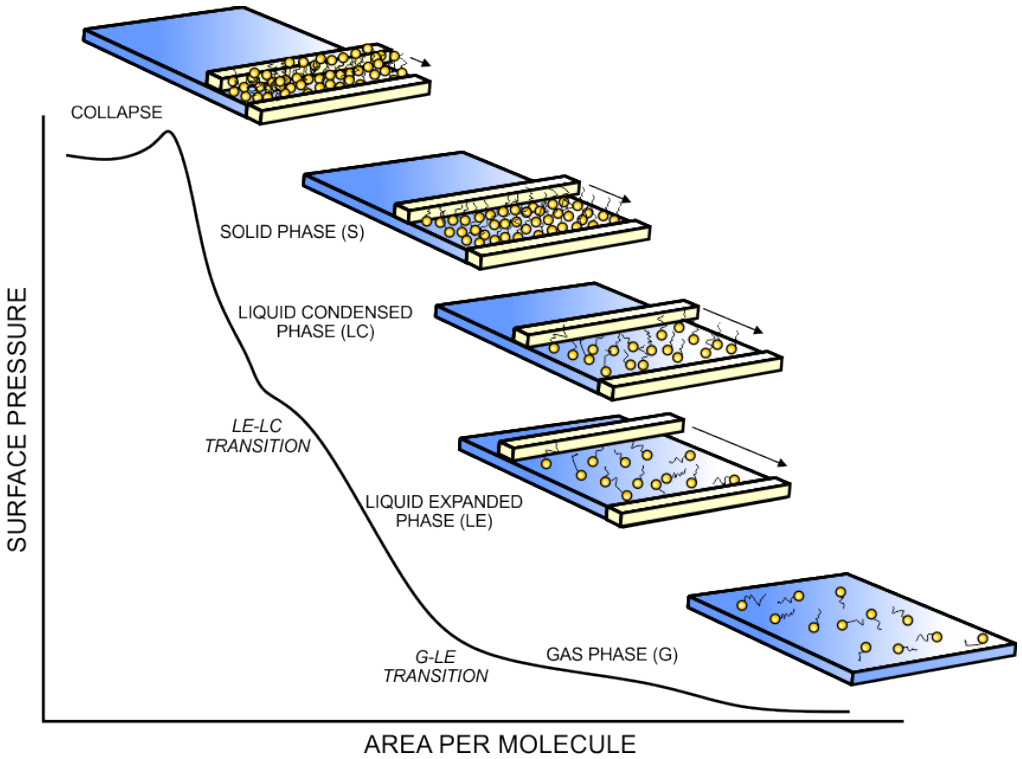


**Figure 2-3.** *General surface pressure-area per molecule isotherm showing all possible phase transitions of the film upon compression.*

The shape of the $\pi$-$A$ isotherms is extremely sensitive to slight changes in the experimental conditions, which can detrimentally affect reproducibility of results unless extreme care is exercised by the experimentalist. The compression process starts with the so called gas (G) phase, in which the surface pressure remains close to zero (Figure 2-3). The surface area available per molecule at this point is large enough to avoid intermolecular interactions. Then the compression begins and slowly the available surface area decreases while the surface pressure rises as consequence of repulsive interactions between the molecules at the interface and the water molecules below. The monolayer becomes more densely packed undergoing several phase changes until the available area per molecule is close to the cross-section of the molecule. At that point the monolayer is on its solid (S) phase (Figure 2-3). Further compression of the monolayer derives on a sudden drop of the surface pressure typically attributed to the collapse of the monolayer and the formation of 3D aggregates. Although surface pressure measurements give a good indication of the formation of, and transitions between, these various phases within the Langmuir film, in the work described in this thesis the Langmuir films were also monitored by means of the Brewster angle microscopy (BAM) and UV-Vis reflection spectroscopy by our collaborators.

Once the formation of solid Langmuir films is optimized, the monolayers can be transferred onto a variety solid substrates by driving a substrate in and out from the sub-phase to give Langmuir-Blodgett films, named after Langmuir and Katherine Blodgett. The different ways in which the molecules can be arranged on the substrates in response to multiple dipping cycles (denoted X, Y and Z by convention) are shown in Figure 2-4. To ensure the homogeneity of the film, the transference is carried out at a constant surface pressure. Once the monolayers are transferred onto a solid substrate several techniques become available for film characterization: UV-Vis and IR transmission spectroscopy on

quartz substrates; AFM analysis on silicon, mica or gold substrates; X-Ray Photoelectron Spectroscopy (XPS), Quartz Crystal Microbalance (QCM) and STM analysis on gold substrates; and electrode surface passivation experiments.

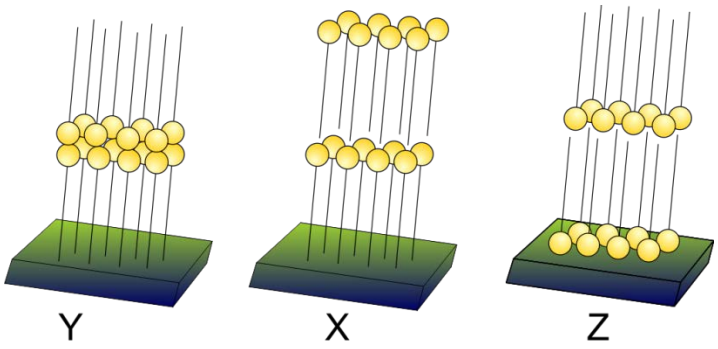


**Figure 2-4.** *LB deposition modes: Y (centro-symmetric film); X and Z.*

### *2.5.2. Molecular films preparation and characterization*

Molecular films of **6** and **15** were prepared and their physical, optical and electrical properties tested. Both compounds were initially designed with the preparation of LB films in mind. One of the main advantages the LB technique in comparison with SA is the wide variety terminal functional groups and substrates that can be combined. Amongst the most commonly used terminal polar heads are: −OH; −OR; −COOR; −CN; $-NH_2$; $-CONH_2$; $-NR_3^+$ and −COOH. Amongst the hydrophilic groups available, carboxylic acids were chosen because of their well-known strong affinity towards water.[37a]

Although it is not the only factor affecting the quality of the films produced, a strong interaction between the hydrophilic end of the molecule and the aqueous sub-phase is desirable for the formation of well-packed monolayers. In addition, the sensitivity of the carboxylic acid group to basic media allows modulation of the film morphology by changing the pH of the sub-phase.[40] Molecular films of **6** and **15**, were prepared and their physical, optical and electrical properties tested by our colleagues in the University of Zaragoza.

As it is common for polyaromatic derivatives, reproducible surface pressure-area per molecule isotherms were obtained for **6** and **15**.[41] The strong π-π intermolecular interactions drive the aggregates to form well-packed monolayers.[12d, 42] Langmuir films of **6** were prepared using a basic (pH 9, NaOH) aqueous sub-phase. The compression process was monitored *in-situ* by following the evolution of the surface pressure, surface potential, reflection UV-Vis spectroscopy and Brewster Angle Microscopy (BAM). The data gathered revealed that the optimum surface pressure for the formation of a defect-free monolayer was 18 mN/m. The monolayers were transferred (Z-type) on to mica and gold substrates with transfer ratios close to the unity as it was confirmed by QCM analysis. The surface coverage of the films was characterized by measuring the electrode passivation on cyclic voltammetry. The CV showed an almost complete electrode passivation after deposition of a single monolayer of **6** at the optimum surface pressure. AFM was used to characterize the physical properties of the film confirming its homogeneity and surface coverage. Attenuation of the Au*4f* signal in the XPS spectrum was used to determine the thickness of the monolayer (2.01 ± 0.05 nm).

The electrical performance of **6** and the ability of the −C≡CH moiety to act as a molecular linker within a metal|molecule|metal junction were evaluated with by STM based methods. These electrical measurements were performed in collaboration with Prof. Richard Nichols and his group in the University of Liverpool (UK). The films were deposited on Arrandee (111) gold-on-glass substrates and addressed from the top with the STM gold tip. To ensure reproducibility of the results, several current-voltage (*I*-*V*) curves were recorded and averaged from multiple scans from different locations on the substrate and different samples. In order to estimate the STM tip position with respect to the monolayer surface, the tip-substrate gap was calculated from experimental parameters set-point current ($I_0$) and working bias ($U$). To that end, several current-distance scans were

collected with the tip embedded within the monolayer showing a monotonic exponential decay of current as the tip is retracted. The exponential decay curves were averaged and plotted as ln(*I*) *vs.* distance (*s*), revealing a linear correlation where d ln(*I*)/d*s* = 5.46 ± 0.97 $nm^{-1}$. It is then assumed that the conductance at the point where the STM tip contacts the substrate is the conductance quantum ($G_0 = 2e^2h \sim 77480$ nS). The tip-substrate gap can be estimated using Eq. 2-1.

$$s = \frac{\ln(G_0 U_t / I_0)}{d\ln(I)/ds} \qquad \text{Eq. 2-1}$$

The tip-substrate gap (*s*) obtained from the experiments performed on monolayers of compound **6** at $U$ = 0.6 V and $I_0$ = 0.5, 0.8 and 1.1 nA was 2.09, 2.01 and 1.95 nm respectively. Since the monolayer thickness was calculated by XPS (2.01 ± 0.05 nm) the *I-V* profile obtained with $I_0$ = 0.8 nA corresponds to the situation where the STM tip in located right above the molecular film (Figure 2-5, red). On the other hand, the *I-V* curves collected with $I_0$ = 0.5 nA represent the electrical response of the film when the STM tip is laying far over the monolayer surface (lower conductance), and with $I_0$ = 1.1 nA the tip penetrates inside the monolayer (higher conductance) (Figure 2-5, black and blue).

The conductance value obtained from the Ohmic region (± 0.6 V) of the *I-V* curve ($I_0$ = 0.8 nA) for the monolayer of **6** ($1.48 \cdot 10^{-5}$ $G_0$) is of the same order of magnitude of other OPE derivatives bearing commonly used terminal groups (SH or $NH_2$).[2f, 43] Despite the known ability of −C≡CH group to chemisorb on gold surfaces,[8b] the nature of the interaction between the acetylenic moiety and the gold STM tip is not yet fully understood. However, the similarity between the conductance of **6** and that of the thiol and amine terminated analogues, provides evidence of an effective tip-molecule electronic coupling taking place between typically attributed to chemisorbed junctions.[44]

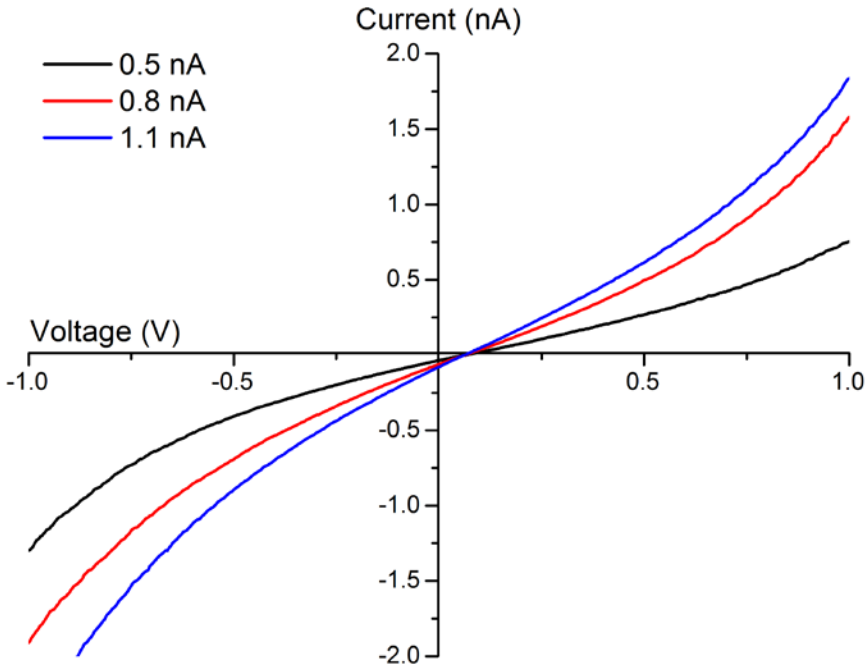


**Figure 2-5.** *Electrical response of an LB film of* ***6*** *(2.01 ± 0.05 nm) collected with an STM (U = 0.6 V) at* $I_0$ *= 0.5 nA (s = 2.09 nm) (black),* $I_0$ *= 0.8 nA (s = 2.01 nm) (red) and* $I_0$ *= 1.1 nA (s = 1.95 nm) (blue).*

The sigmoidal *I-V* curves with the absence of any additional spectroscopic peaks observed for the monolayer of **6**, are characteristic of the nonresonant tunnelling mechanism and typically described according to the Simmons model.[45] The model developed by John G. Simmons in 1963 is an excellent approximation of the Franz two-band model for those systems with a rectangular tunnelling barrier, where the Fermi level of an electrode is close in energy to one of the frontier orbitals of the molecular bridge so that the effect of the other energy distant molecular orbital is negligible.[45-46] According to the Simmons model, the current *I* can be calculated using Eq. 2-2;

$$I = \frac{Ae}{4\pi^2 \hbar d^2} \left\{ \begin{array}{l} \left(\phi - \frac{eU}{2}\right) exp\left[-\frac{2(2m)^{1/2}}{\hbar}\alpha\left(\phi - \frac{eU}{2}\right)^{1/2} d\right] - \\ \left(\phi + \frac{eU}{2}\right) exp\left[-\frac{2(2m)^{1/2}}{\hbar}\alpha\left(\phi + \frac{eU}{2}\right)^{1/2} d\right] \end{array} \right\} \qquad \text{Eq. 2-2}$$

where $U$ is the applied potential, $A$ is the contact area of the molecule with the tip, $d$ is the width of the tunnelling barrier, $\Phi$ is the effective tunnelling barrier height, $m$ is the mass of the tunnelling electron, $e$ is the electron charge and α is a unitless adjustable parameter introduced to either provide a way to apply this model to a non-rectangular barrier process or as an adjustment to account for the effective mass $(m)^*$, or both.[45, 47] In this model, $\alpha = 1$ corresponds to the case for a rectangular barrier and bare electron mass.

In order to characterize the tunnelling parameters ruling the charge transfer in the molecular assembly of **6**, the *I*-*V* profile was fitted to the Simmons model with $U$ = 0.6 V, $I_0$ = 0.8 nA, $A$ = 0.20 nm$^2$ estimated from the LB area per molecule at the transference surface pressure, $d$ = 2.12 nm calculated as through bond distance between the molecular end groups, leaving the effective tunnelling barrier height $\Phi$ and α as the fitting parameters. The best fit was obtained for values of $\Phi$ = 0.67 eV and α = 0.37 (Figure 2-6). Similar tunnelling barrier heights were previously reported for di-amine substituted OPEs ($\Phi$ ~ 0.6 eV)[2f] and di-thiol substituted OPEs ($\Phi$ = 0.77 eV)[2b] showing that the acetylene moiety can perform as a molecular linker that does not significantly alter the resistance of the molecular junction when compared against more commonly employed linkers. Due to the good agreement of the *I*-*V* curves with the Simmons model, it was concluded that the mechanism ruling the charge transfer on the metal-molecule-metal junction of **6** is coherent tunnelling. Interestingly, despite the unsymmetrical nature of the junction no current rectification was observed. Instead, a wire-like behaviour was observed throughout the whole bias window.

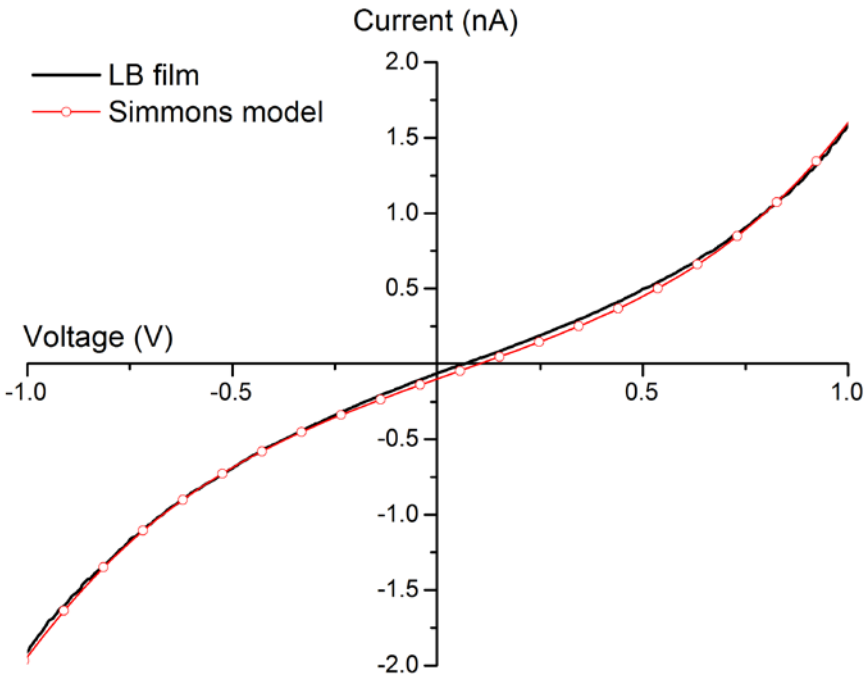


**Figure 2-6.** *I-V curve of a monomolecular film of* ***6*** *(black) and fitting according to the Simmons model with* $\Phi = 0.67$ *eV and* $\alpha = 0.37$ *(red).*

Driven by this encouraging results LB films of **15** were prepared. Langmuir films were prepared on aqueous sub-phases at pH neutral and basic (pH 11.4, NaOH). Although the preparation of well-packed monolayers was possible under both conditions, a more expanded isotherm was observed for the neutral sub-phase. *In-situ* UV-Vis reflection spectroscopy revealed that the tilt angle of the molecules on the neutral water surface remains unchanged upon compression at 60º, while on the basic sub-phase the tilt angle reached 67º.

In addition, the same UV-Vis studies revealed a bathochromic shift of **15** upon monolayer compression in neutral conditions. The opposite shift was observed upon compression when the basic conditions were employed. To our knowledge, this was the first example of an OPE not showing a hypsochromic shift characteristic of the formation of H-aggregates.[12g, 48]

In order to characterize this odd spectral shift in detail Langmuir films were transferred onto a variety of solid substrates. The ideal surface pressure for the transference was found to be 20 mN/m for both neutral and basic sub-phase. The formation of well-packed films was confirmed by QCM and electrode surface passivation experiments.

Three different causes for a red shift in the UV-Vis reflection spectra are commonly accepted: solvatochromic effect (increase in environment polarity); formation of J-aggregates (typically found for tilt angles <54º) or an increase of the conjugation length. Chemical reactivity of the coated substrates towards behenic acid monitored by QCM revealed that only the films prepared under basic conditions were active towards dimer formation (Figure 2-7).[41b]

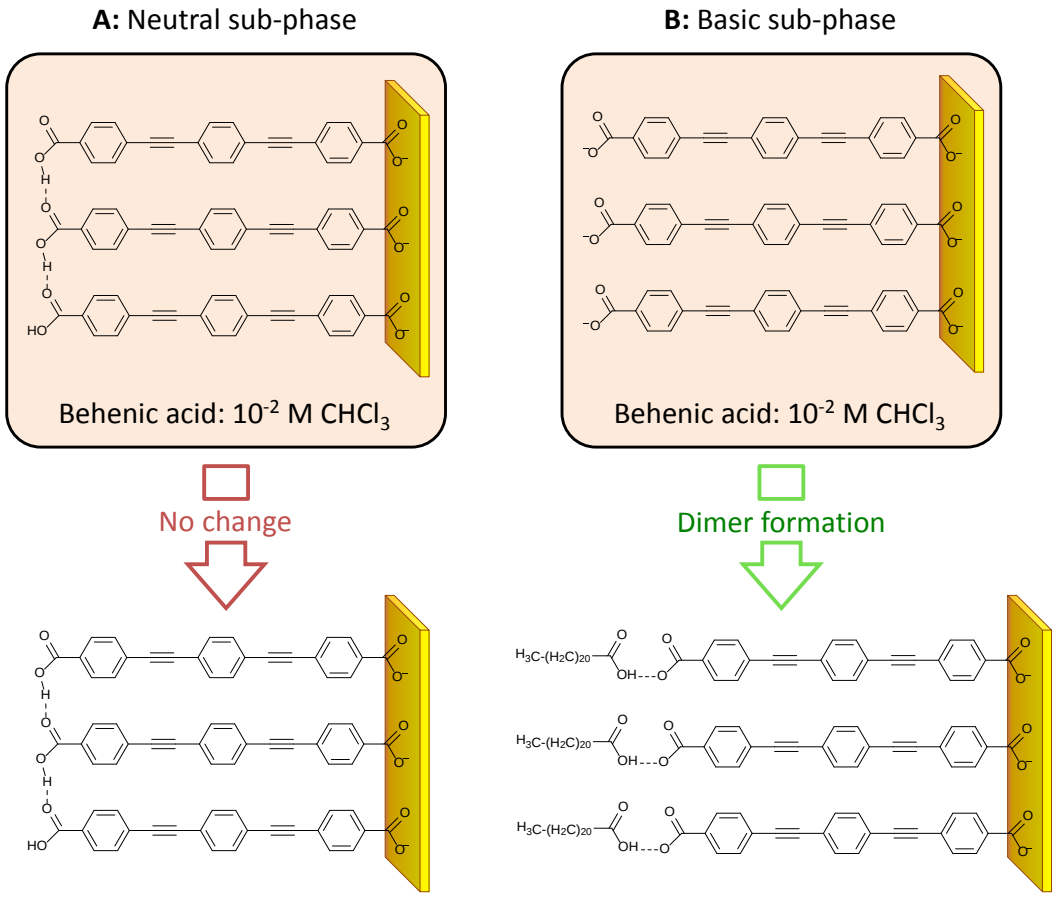


**Figure 2-7.** *Chemical reactivity of the LB films of **15** prepared under neutral (left) and basic (right) conditions monitored by QCM.*

One of the possible explanations to this lack of reactivity from the films prepared in neutral conditions is the formation of lateral H-bonds between the terminal –COOH groups of neighbouring molecules making them unreactive towards behenic acid. Angle resolved XPS (AR-XPS) experiments confirmed the protonated state of the terminal carbonyl group only for the films prepared under neutral conditions. Hence the bathochromic shift observed was attributed to the presence of intermolecular lateral H-bonds (Figure 2-7: A, bottom).

In order to characterize the electrical response of the LB films of **15** prepared under basic and neutral conditions the samples were tested with an STM in similar fashion to that employed for the study of **6**. In this case, the averaged d$\ln I$/d$s$ was found to be 6.91 ± 1.37 $nm^{-1}$ (neutral) and 5.48 ± 0.89 $nm^{-1}$ (basic).The tip-substrate distance was then calibrated using Eq. 2-1, to match the thickness of the transferred monolayers 1.81 ± 0.05 nm (neutral) and 1.95 ± 0.05 nm (basic) obtained from the XPS analysis. For the current-distance experiments performed with $U$ = 0.6 V, the calculated $I_0$ required to place the STM tip on the monolayer surface were 0.15 nA (neutral) and 1 nA (basic). In an analogous way to that done for films of **6**, to ensure reproducibility several *I-V* curves were recorded and averaged from different sample regions and different samples. The averaged *I-V* curves recorded under these conditions for samples prepared under neutral and basic conditions are shown in Figure 2-8. The conductance values obtained from the Ohmic region of the *I-V* curve (± 0.6 V), was found to be $1.75 \cdot 10^{-5}$ $G_0$ for the films prepared on a basic sub-phase (similar to conductance values of a single molecule), whilst the films prepared from a neutral sub-phase presented a conductance value seven times lower *i.e.* $0.26 \cdot 10^{-5}$ $G_0$.

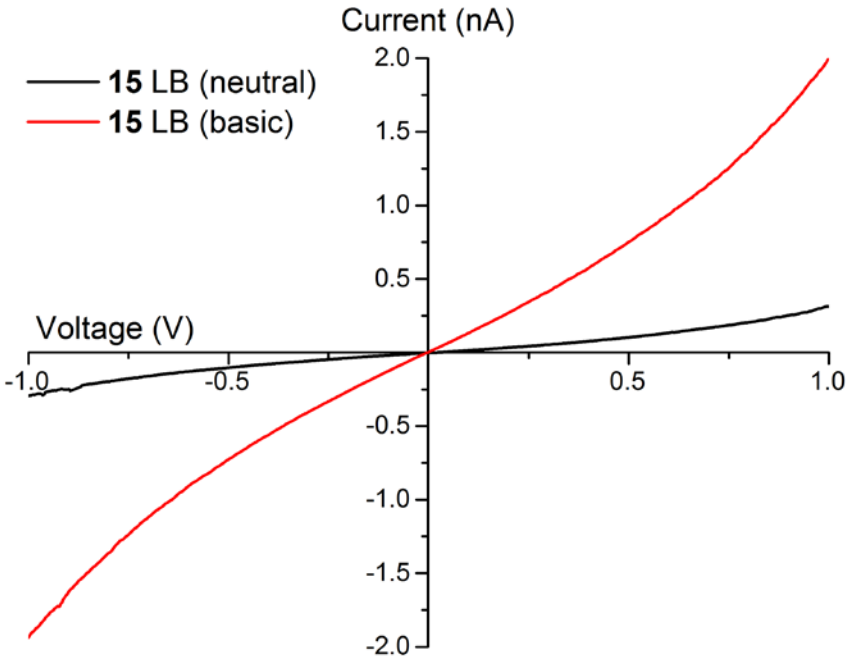


**Figure 2-8.** *Averaged I-V curves obtained employing the optimum current set-point for a monolayer of **15** prepared on a neutral (black) or basic (red) sub-phase.*

In addition, the Simmons model was fitted to the *I-V* curves obtained for films prepared under both neutral and basic conditions. In this case, *A* extracted from the LB isotherm was 0.31 $nm^2$ (neutral) and 0.25 $nm^2$ (basic), $d$ = 2.07 nm estimated as the distance between molecular end groups. Using Eq 2-2, good agreement between the experimental data and the theoretical model was obtained for $\Phi$ = 1.1 eV and $\alpha$ = 0.41 (neutral sub-phase) and $\Phi$ = 0.73 eV and $\alpha$ = 0.34 (basic sub-phase) (Figure 2-9). The differing tunnelling barrier heights $\Phi$ indicates an increased difficulty to transfer charge through a monolayer of **15** when prepared on a neutral sub-phase. Furthermore, the value of $\Phi$ obtained for the monolayer prepared under neutral conditions is remarkably high compared to values previously reported for parental compounds *ca.* 0.8-0.6 eV.[2f, 12g, 49] The lower conductance and higher tunnelling barrier found for the monolayers prepared under neutral conditions are in good agreement with the formation of a less effective electrical junction due to the presence of lateral H-bonds between the −COOH surface groups.

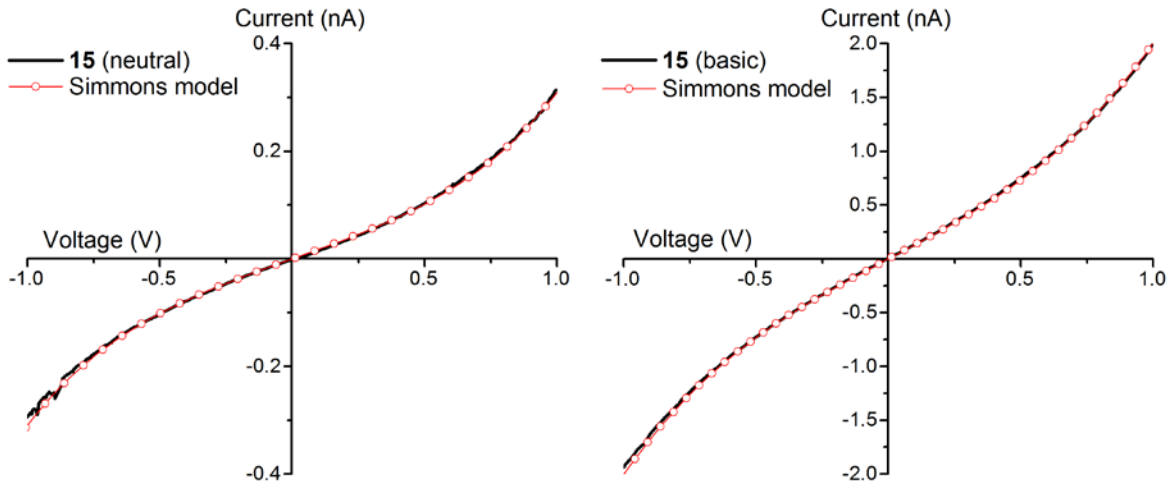


**Figure 2-9.** *Electrical response of a LB film of **15** (black) and Simmons model fitting (red scattered) prepared on a neutral (left) or basic (right) sub-phase*

## 2.6. Conclusions

Two carboxyl-terminated OPEs (**6** and **15**) have been synthesized and characterized. The strong interaction between the terminal –COOH group and the water surface allowed preparation of well-packed L and LB films. The monolayer formation process was optimized and fully characterized *in-situ*. Changes on the pH of the aqueous sub-phase were proven to result on film morphology modulation due to the linker pH sensitivity. The films were transferred onto a wide variety of substrates for further characterization. STM electronic characterization of the films revealed that the charge flow through monolayers of **6** and **15** takes place following a non-resonant tunnelling mechanism. In addition, modulation of conductance in monolayers of **15** was demonstrated. The conductance values for **6** and **15** were obtained and found to be similar to those reported previously for OPEs *ie.*$10^{-5}$ $G_0$. The use of −C≡CH as a novel molecular junction linker was demonstrated.

## 2.7. Experimental

### *2.7.1. General conditions*

All reactions were carried out in oven dried glassware under an oxygen-free nitrogen atmosphere using standard Schlenk techniques. Reaction solvents were dried over the appropriate drying agents: $NEt_3$ ($CaSO_4$); $NHPr^i_2$ (KOH) and distilled under nitrogen. Other reaction solvents were purified and dried using Innovative Technology SPS-400 and degassed before use. The catalyst $Pd(PPh_3)_4$ was prepared following literature methods.[34] Other reagents were purchased commercially and used as received. NMR spectra were recorded in deuterated solvent solutions on Varian Mercury 200 and 400, Bruker Avance 400, Varian Inova 500, and Varian VNMRS 600 and 700 spectrometers and referenced against solvent resonances ($^1H$, $^{13}C$) or external $H_3PO_4$ ($^{31}P$). ESI mass spectra were recorded using a TQD mass spectrometer (Waters Ltd, UK). Samples were (1 mg/mL) in analytical grade methanol. ASAP mass spectra were recorded from solid aliquots on an LCT Premier XE mass spectrometer (Waters Ltd, UK) or Xevo QToF mass spectrometer (Waters Ltd, UK) in which the aliquot is vaporized using hot $N_2$, ionized by a corona discharge and carried to the TOF detector (working range 100-1000 m/z). Matrix assisted-Laser Desorption/Ionisation (MALDI) mass spectra was obtained using an Autoflex II TOF/TOF mass spectrometer (Bruker Daltonik GmBH) using a trans-2-[3-(4-tert-butylphenyl)-2-methyl-2-propenylidene]malononitrile (DCTB) matrix. Infrared spectra were recorded from $CH_2Cl_2$ solutions or nujol mulls on $CaF_2$ plates using a Nicolet Thermo FT6700 or a Nicolet Avatar spectrometers. Thermal analyses were performed using a Perking Elmer Pyris thermo-gravimetric analyser (heating rate 10 ºC/min).

### *2.7.2. Synthesis and characterization*

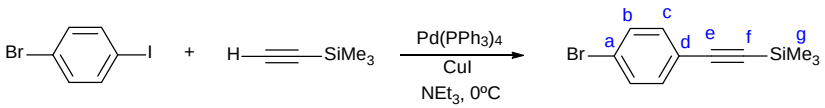


**Preparation of $BrC_6H_4C{\equiv}CSiMe_3$.**[50] To a 500 mL round Schlenk flask charged with $NEt_3$ (350 mL) immersed in ice, 4-iodo-bromobenzene (18.05 g, 63.80 mmol), $Pd(PPh_3)_4$ (1.85 g, 1.60 mmol) and CuI (0.30 g, 1.6 mmol) were added. To the cooled solution trimethylsilylacetylene (11.0 mL, 7.51 g, 76.5 mmol) was added drop wise. The mixture was stirred in an ice bath for 8 h. Upon completion of the reaction the brown suspension was taken to dryness under reduced pressure and the residue was purified by silica gel column chromatography (hexane). Removal of solvent from the main fraction yielded a colourless oil that crystallized on standing. Yield 15.9 g, 62.8 mmol, 99%. $^1$H NMR (400 MHz, $CDCl_3$) δ 7.43 (d, *J* = 9 Hz, 2H, *c*), 7.32 (d, *J* = 9 Hz, 2H, *b*), 0.24 (s, 9H, *g*). $^{13}C\{^1H\}$ NMR (101 MHz, $CDCl_3$) δ 133.5, 131.6 (*b*/*c*), 122.9, 122.3 (*a*/*d*), 104.0 (*f*), 95.7 (*e*), 0.0 (*g*). $MS^+$ (ASAP) *m/z* (%): 505.9 (100, $[2M\text{-}2H]^+$); 253.9 (41.8, $[M]^+$). IR (*nujol*) $cm^{-1}$: 2159 (*s*) ν(C≡C).

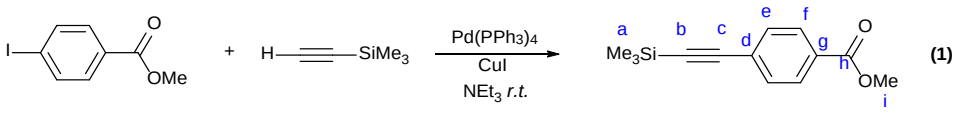


**(1)**

**Preparation of 1.**[51] To a 250 mL Schlenk flask charged with methyl 4-iodobenzoate (10.2 g, 38.9 mmol), $Pd(PPh_3)_4$ (2.24 g, 1.94 mmol) and CuI (0.369 g, 1.94 mmol) and $NEt_3$ (200 mL), trimethylsilylacetylene (7.0 mL, 4.8 g, 48.9 mmol) was added. The mixture was stirred at room temperature overnight. The mixture was taken to dryness under reduced pressure and the residue was purified through a silica gel column using hexane:$CH_2Cl_2$ (8:2) as the eluent. Removal of solvent from the main fraction yielded an off-white powder. Yield 8.01 g, 34.5 mmol, 89%. $^1$H NMR (400 MHz, $CDCl_3$) δ 7.89 (d, *J*

= 9 Hz, 2H, *f*), 7.47 (d, *J* = 9 Hz, 2H, *e*), 3.85 (s, 3H, *i*), 0.20 (s, 9H, *a*). $^{13}C\{^{1}H\}$ NMR (101 MHz, $CDCl_3$) δ 166.5 (*h*), 132.0, 129.5 (*e/f*), 129.8 (*g*), 127.9 (*d*), 104.2, 97.8 (*b/c*), 52.4 (*i*), 0.0 (*a*). $MS^+$ (ASAP) *m/z* (%): 464.19 (100, $[2M]^+$); 233.10 (70, $[M+H]^+$). IR (*nujol*) $cm^{-1}$: 2162 (m) *ν*(C≡C); 1732 (s) *ν*(C=O).

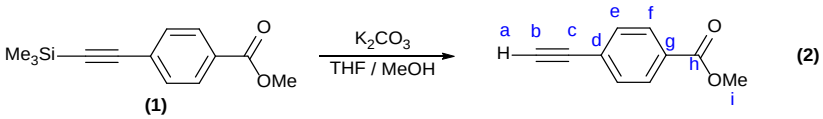


**Preparation of 2.**[52] To a solution of **1** (8.10 g, 34.9 mmol) in THF:MeOH (*1:1*, 150 mL), $K_2CO_3$ (5.1g, 36.9 mmol) was added and the mixture stirred at room temperature overnight. The mixture was then filtered and the filtrate taken to dryness. The solid residue redissolved in $CH_2Cl_2$ (100 mL), washed with water (2 × 100 mL) and brine (1 × 100 mL), and dried over $MgSO_4$. After taking the organic phase to dryness the pure product was obtained as an off-white powder. Yield 3.07 g, 19.20 mmol, 55%. $^{1}H$ NMR (400 MHz, $CDCl_3$) δ 7.99 (d, *J* = 9 Hz, 2H, *f*), 7.56 (d, *J* = 9 Hz, 2H, *e*), 3.92 (s, 3H, *i*), 3.23 (s, 1H, *a*). $^{13}C\{^{1}H\}$ NMR (101 MHz, $CDCl_3$) δ 166.5 (*h*), 132.2, 129.6 (*e/f*), 130.3 (*g*), 126.9 (*d*), 82.9, 80.2 (*b/c*), 52.4 (*i*). $MS^+$ (ASAP) *m/z* (%): 320.10 (68, $[2M]^+$); 161.05 (27, $[M+H]^+$). IR (*nujol*) $cm^{-1}$: 3244 (s) ($C_{sp}$–H); 2104 (w) ν(C≡C); 1700 (s) ν(C=O).

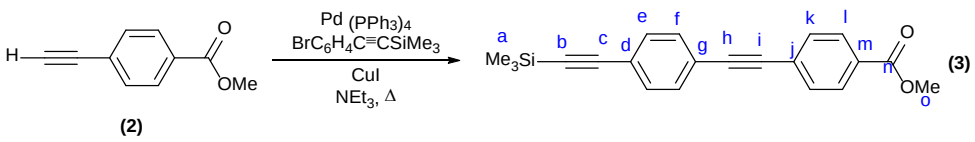


**Preparation of 3.** In an oven dried 250 mL Schlenk flask, **2** (4.01 g, 25.05 mmol), $BrC_6H_4C{\equiv}CSiMe_3$ (6.38 g, 25.20 mmol), $Pd(PPh_3)_4$ (0.30 g, 0.26 mmol) and CuI (0.05, 0.26 mmol) were dissolved in $NEt_3$ (150 mL) and the resulting solution was heated at reflux overnight. The black mixture was then taken to dryness under reduced pressure and the residue was purified through a silica gel column using hexane:$CH_2Cl_2$ (*7:3*) as the eluent system. The pure product was obtained as an off-white solid. Yield 6.86 g, 21.21

mmol, 85%.[1]H NMR (400 MHz, $CDCl_3$) δ 8.02 (d, *J* = 9 Hz, 2H, *l*), 7.58 (d, J = 9 Hz, 2H, *k*), 7.49 – 7.43 (m, 4H, *e-f*), 3.93 (s, 3H, *o*), 0.26 (m, 9H, *a*).

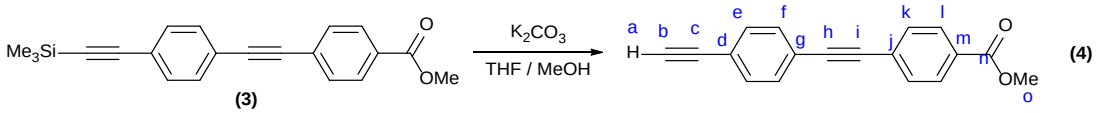


**Preparation of 4.** To a suspension of **3** (4.64 g, 14.34 mmol) in THF:MeOH (*1:1*, 150 mL), $K_2CO_3$(2.1 g, 15.2 mmol) was added and the mixture stirred at room temperature overnight. The mixture was then filtered, the filtrate taken to dryness and the solid residue redissolved in $CH_2Cl_2$ (100 mL). The organic phase was washed with water (2 × 100 mL), brine (1×100 mL) and dried over $MgSO_4$. After taking the organic phase to dryness the pure product was obtained as an off-white powder. Yield 1.98 g, 7.60 mmol, 53%. [1]H NMR (400 MHz, $CDCl_3$) δ 8.03 (d, *J* = 9 Hz, 2H, *l*), 7.59 (d, *J* = 9 Hz, 2H, *k*), 749 (s, 4H, *e-f*), 3.93 (s, 3H, *o*), 3.19 (s, 1H, *a*).

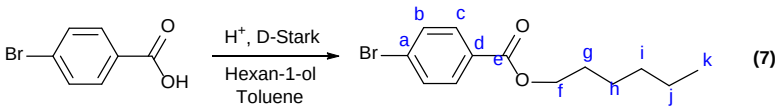


**Preparation of 7.** A 250 mL round bottom flask fitted with a Dean-Stark trap was charged with 4-bromobenzoic acid (8.94 g, 41.8 mmol) in hexan-1-ol (10 mL, 8.1 g, 80 mmol) toluene (150 mL) and catalytic amounts of $H_2SO_4$. The resulting emulsion was heated at reflux temperature overnight. Upon completion of the reaction, adjudged by TLC, the reaction mixture was poured into water and the organic phase was washed with water (2 × 150 mL) and once with brine (1 × 150 mL), and dried over $MgSO_4$. After removing the solvents under reduced pressure, the resulting dark-red oil was used in the next step without further purification. Yield 10.8 g, 38.0 mmol, 91%. [1]H NMR (400 MHz, $CDCl_3$) δ 7.87 (d, *J* = 8 Hz, 2H, *c*), 7.55 (d, *J* = 8 Hz, 2H, *b*), 4.28 (t, *J* = 7 Hz, 2H, *f*), 1.78 – 1.68 (m, 2H, *g*), 1.47 – 1.36 (m, 2H, *h*), 1.36 – 1.25 (m, 4H, *i-j*), 0.88 (t, *J* = 7 Hz, 3H, *k*).

$^{13}C\{^{1}H\}$ NMR (101 MHz, $CDCl_3$) δ 166.0 (*e*), 131.7 (*b*), 131.2 (*d*), 129.6 (*c*), 127.9 (*a*), 65.5 (*f*), 31.5 (*g*), 28.7 (*h*), 25.8 (*i*), 22.6 (*j*), 14.0 (*k*). $MS^+$ (ESI) *m/z* (%): 185.21 (100, $[M-OC_6H_{13}]^+$). IR (*cast*) $cm^{-1}$: 1723 (s) ν(C=O).

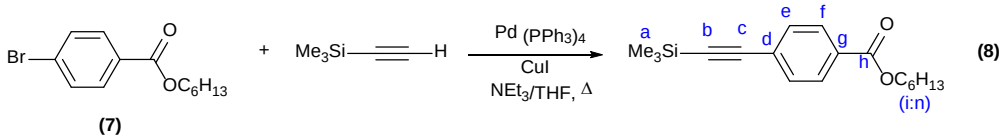


**Preparation of 8.** In a 250 mL Schlenk flask hexyl-4-bromobenzoate (10.03 g, 35.16 mmol), trimethylsilylacetylene (5.5 mL, 3.8 g, 39 mmol), $Pd(PPh_3)_4$ (1.210 g, 1.047 mmol) and CuI (0.335 g, 1.76 mmol) were dissolved in anhydrous degassed $NEt_3$:THF (*1:1*) (200 mL). The resulting solution was heated to reflux temperature overnight. Upon completion, the black mixture was taken to dryness under reduced pressure and the resulting oil was purified through a silica gel column using hexane:$CH_2Cl_2$ (*7:3*) as eluent system. The resulting red oil was sufficiently pure for use in the subsequent steps. Yield 9.81 g, 32.4 mmol, 92%. $^{1}H$ NMR (400 MHz, $CDCl_3$) δ 7.96 (d, *J* = 8.2 Hz, 2H, *f*), 7.51 (d, *J* = 8 Hz, 2H, *e*), 4.30 (t, *J* = 7 Hz, 2H, *i*), 1.80 – 1.70 (m, 2H, *j*), 1.49 – 1.38 (m, 2H, *k*), 1.37-1.31 (m, 4H, *l-m*), 0.90 (t, *J* = 7 Hz, 3H, *n*), 0.26 (s, 9H, *a*). $^{13}C\{^{1}H\}$ NMR (101 MHz, $CDCl_3$) δ 166.2 (*h*), 132.0 (*e*), 130.3 (*g*), 129.5 (*f*), 127.8 (*d*), 104.3 (*c*), 97.7 (*b*), 65.5 (*i*), 31.6 (*j*), 28.8 (*k*), 25.8 (*l*), 22.7 (*m*), 14.1 (*n*), 0.0 (*a*).$MS^+$ (ESI) *m/z* (%): 301.20 (100, $[M-H]^+$).

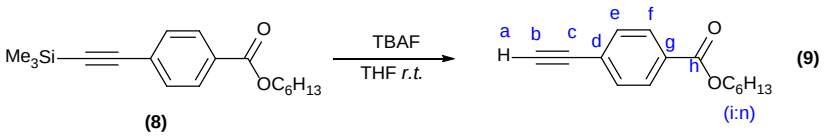


**Preparation of 9.** To a solution of **8** (9.310 g, 30.77 mmol) in THF (200 mL), TBAF (1 M in THF, 32.0 mL, 32.0 mmol) was added and the resulting black solution was stirred at room temperature overnight. The solution was then taken to dryness under reduced pressure and the resultant black oil was purified through a silica gel column using

hexane:$CH_2Cl_2$ (6:3) as the eluent system. Removal of solvent from the main fraction yielded the pure product as a white solid. Yield 5.81 g, 25.2 mmol, 82%. $^1$H NMR (400 MHz, $CDCl_3$) δ 7.99 (d, *J* = 8 Hz, 2H, *f*), 7.55 (d, *J* = 8 Hz, 2H, *e*), 4.31 (t, *J* = 7 Hz, 2H, *i*), 3.22 (s, 1H, *a*), 1.81 – 1.70 (m, 2H, *j*), 1.49 – 1.38 (m, 2H, *k*), 1.37 – 1.31 (m, 4H, *l*-*m*), 0.90 (t, *J* = 7 Hz, 3H, *n*). $^{13}$C{$^1$H} NMR (101 MHz, $CDCl_3$) δ 166.1 (*h*), 132.2 (*e*), 130.7 (*g*), 129.6 (*f*), 126.7 (*d*), 83.0 (*c*), 80.1 (*b*), 65.5 (*i*), 31.6 (*j*), 28.8 (*k*), 25.8 (*l*), 22.7 (*m*), 14.2 (*n*). MS$^+$ (ASAP) *m/z* (%): 147.04 (100.0, [M-$C_6H_{13}$]$^+$); 129.03 (40.4, [M-$OC_6H_{13}$]$^+$).

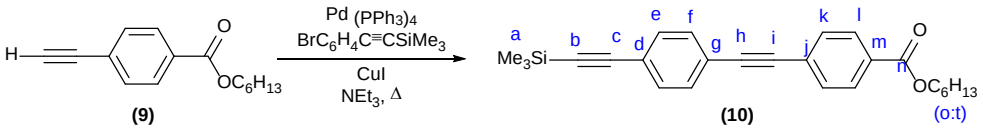


**Preparation of 10.** In an oven dried 250 mL Schlenk flask, **9** (5.51 g, 23.6 mmol), $BrC_6H_4C{\equiv}CSiMe_3$ (7.19 g, 28.4 mmol), $Pd(PPh_3)_4$ (1.641 g, 1.420 mmol) and CuI (0.273g, 1.43 mmol) were dissolved in $NEt_3$ (200 mL) and the resulting solution was heated at reflux overnight. The black mixture was then taken to dryness under reduced pressure and the residue was purified through a silica gel column using hexane:$CH_2Cl_2$ (*9:1*) as the eluent system. The pure product was obtained as an off-white solid. Yield 7.16 g, 17.8 mmol, 75%. $^1$H NMR (400 MHz, $CDCl_3$) δ 8.02 (d, *J* = 9 Hz, 2H, *l*), 7.57 (d, *J* = 9 Hz, 2H, *k*), 7.50 – 7.43 (m, 4H, *e*-*f*), 4.32 (t, *J* = 7 Hz, 2H, *o*), 1.82 – 1.72 (m, 2H, *p*), 1.49 – 1.41 (m, 2H, *q*), 1.39 – 1.30 (m, 4H, *r*-*s*), 0.91 (t, *J* = 7 Hz, 3H, *t*), 0.26 (s, 4H). $^{13}$C{$^1$H} NMR (101 MHz, $CDCl_3$) δ 166.2 (*n*), 132.1 (*k*), 131.7 (*e*), 131.6 (*f*), 130.3 (*m*), 129.6 (*l*), 127.7 (*j*), 123.6 (*g*), 122.9 (*d*), 104.7 (c), 96.8 (b), 92.0 (i), 90.7 (h), 65.5 (*o*), 31.6 (*p*), 28.8 (*q*), 25.9 (*r*), 22.7 (*s*), 14.1 (*t*), 0.1 (*a*). MS$^+$ (ASAP) *m/z* (%): 402.20 (100, [M]$^+$); 318.11 (6.8, [M-$C_6H_{13}$]$^+$). IR (*nujol*) cm$^{-1}$: 2157 (m) ν(C≡C); 1725 (s) ν(C=O).

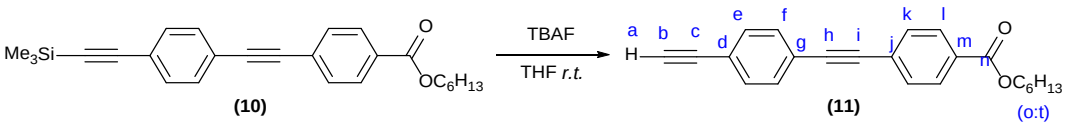


**Preparation of 11.** To a solution of **10** (6.87 g, 17.0 mol) in THF (150 mL), TBAF (1M in THF, 18 mL, 18 mmol) was added and the mixture stirred at room temperature overnight. The solution was then taken to dryness under reduced pressure and the resulting black oil was purified through a silica gel column using hexane:$CH_2Cl_2$ (8:2) as the eluent system. After taking the appropriate fractions to dryness the pure product was obtained as a white powder. Yield 4.79 g, 14.5 mmol, 85%. $^1$H NMR (400 MHz, $CDCl_3$) δ 8.03 (d, *J* = 8 Hz, 2H, *l*), 7.58 (d, *J* = 8 Hz, 2H, *k*), 7.53 – 7.47 (m, 4H, *e*-*f*), 4.32 (t, *J* = 6 Hz, 2H, *o*), 3.19 (s, 1H, *a*), 1.83 – 1.71 (m, 2H, *p*), 1.50 – 1.40 (m, 2H, *q*), 1.39 – 1.27 (m, 4H, *r*-*s*), 0.98 – 0.83 (m, 3H, *t*). $^{13}$C{$^1$H} NMR (101 MHz, $CDCl_3$) δ 166.2 (*n*), 132.3 (*k*), 131.7 (*e*), 131.7 (*f*), 130.3 (*m*), 129.7 (*l*), 127.6 (*j*), 123.3 (*g*), 122.5 (*d*), 91.7 (*i*), 90.7 (*h*), 83.3 (c), 79.3 (b), 65.5 (*o*), 31.6 (*p*), 28.8 (*q*), 25.8 (*r*), 22.7 (*s*), 14.2 (*t*). MS$^+$ (ASAP) *m/z* (%): 660.3 (100, $[2M]^+$); 246.0 (65.1, $[M\text{-}C_6H_{12}]^+$; 330. (7.4, $[M]^+$). IR (*nujol*) cm$^{-1}$: 3277 (m) ν($C_{sp}$–H); *not observed* ν(C≡C); 1717 (m) ν(C=O).

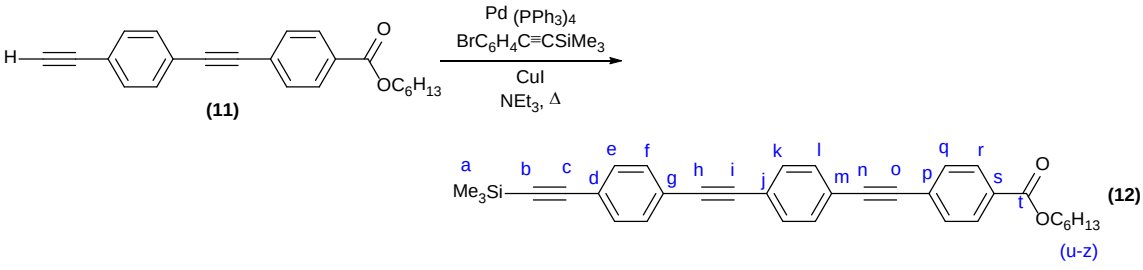


**Preparation of 12.** In an oven dried 250 mL round-bottom flask, **11** (4.59 g, 9.13 mmol), $BrC_6H_4C{\equiv}CSiMe_3$ (2.78 g, 10.9 mmol), $Pd(PPh_3)_4$ (0.528 g, 0.457 mmol) and CuI (0.092 g, 0.475 mmol) were dissolved in anhydrous degassed $NEt_3$ (250 mL). The resulting solution was heated at reflux overnight. Upon completion, adjudged by TLC, the reaction mixture was cooled in an ice bath and filtered. The brown filtrate was collected and

purified by passage through a silica gel column using hexane:$CH_2Cl_2$ (*8:2*) as eluent system. Removal of solvent from the appropriate fractions yielded the pure product as a white solid. Yield 2.46 g, 4.90 mmol, 54%. $^1$H NMR (400 MHz, $CDCl_3$) δ 8.03 (d, *J* = 8.5 Hz, 2H, *r*), 7.59 (d, *J* = 9 Hz, 2H, q), 7.53 – 7.49 (m, 4H, *k-l*), 7.46 (m, 4H, *e-f*), 4.33 (t, *J* = 7 Hz, 2H, *u*), 1.83 – 1.69 (m, 2H, *v*), 1.51 – 1.39 (m, 2H, *w*), 1.39 – 1.31 (m, 4H, *x-y*), 0.91 (t, *J* = 7 Hz, 3H, *z*), 0.26 (s, 9H, *a*). $^{13}$C{$^1$H} NMR (101 MHz, $CDCl_3$) δ 166.2 (*t*), 132.1 (*q*), 131.8, 131.8, 131.6, 131.6 (*e-f/k-l*), 130.2 (*s*), 129.7 (*r*), 127.7 (*p*), 123.5, 123.3, 123.1, 122.8 (*g, j, m, d*), 104.7 (*c*), 96.6 (*b*), 91.9 (*o*), 91.3 (*i*), 91.0 (*h*), 90.6 (*n*), 65.5 (*u*), 31.6 (*v*), 28.8 (*w*), 25.9 (*x*), 22.7 (*y*), 14.2 (*z*), 0.0 (*a*). MS$^+$ (ASAP) *m/z* (%): 502.2 (100, [M]$^+$); 419.1 (9, [M-$C_6H_{12}$]$^+$).

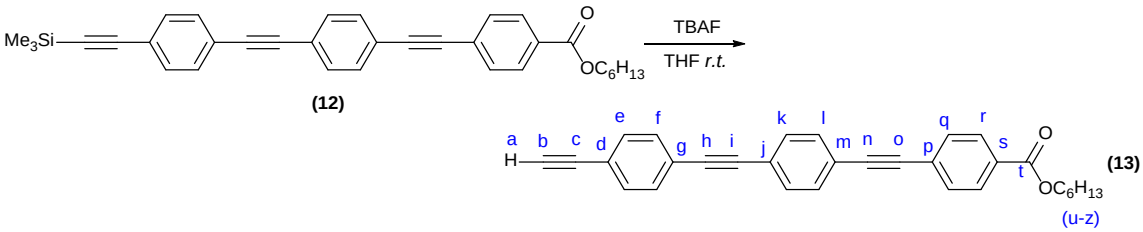


**Preparation of 13.** To a solution of **12** (1.821 g, 3.622 mmol) in THF (50 mL), TBAF (1M in THF, 3.7 mL, 3.7 mmol) was added and the resulting dark-red solution was stirred at room temperature overnight. After taking the solution to dryness, the resulting black oil was purified by chromatography on silica gel using hexane:$CH_2Cl_2$ (*6:4*) as eluent system. After solvent removal the pure product was obtained as a white powder. Yield 1.42 g, 3.30 mmol, 91% $^1$H NMR (400 MHz, $CDCl_3$) δ 8.03 (d, *J* = 8 Hz, 2H, *r*), 7.59 (d, *J* = 8 Hz, 2H, *q*), 7.53 (s, 4H, *k-l* ), 7.48 (s, 4H, *e- f*), 4.33 (t, *J* = 7 Hz, 2H, *u*), 3.19 (s, 1H, *a*), 1.86 – 1.71 (m, 2H, *v*), 1.51 – 1.41 (m, 2H, *w*), 1.40 – 1.29 (m, 4H, *x-y*), 0.91 (t, *J* = 7 Hz, 3H, *z*). $^{13}$C{$^1$H} NMR (176 MHz, $CDCl_3$) δ 166.23 (*t*), 132.26 (*q*), 131.85, 131.78, 131.65 (*e-f/k-l*), 130.26 (*s*), 129.67 (*r*), 127.69 (*p*), 123.58, 123.42, 122.96, 122.33 (*g, j, m, d*), 91.97 (*o*), 91.09 (*h/i*), 90.80 (*n*), 83.36 (*c*), 79.23 (*b*), 65.53 (*u*), 31.62 (*v*), 28.84

(*w*), 25.86 (*x*), 22.71 (*y*), 14.16 (*z*). $MS^+$ (ASAP) *m/z* (%): 430.2 (100, $[M]^+$); 406.2 (51.7, $[M\text{-}C_2H]^+$); 347.1 (16.8, $[M\text{-}C_6H_{13}]^+$); 861.31 (8.4, $[2M+H^+]$). IR (*nujol*) $cm^{-1}$: 3278 (s) $\nu(C_{sp}\text{–}H)$; *not observed* $\nu(C\equiv C)$; 1714 (s) $\nu(C=O)$.

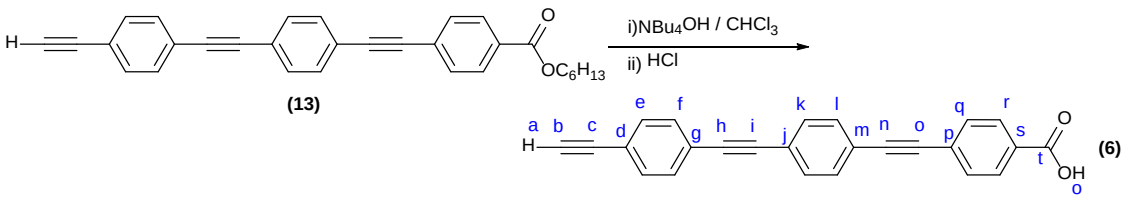


**Preparation of 6.** In a 50 mL round bottom flask, **13** (0.180 g, 0.36 mmol) and $(NBu)_4OH \cdot 30\ H_2O$ (0.784 g, 0.98 mmol) were dissolved in $CHCl_3$ (5 mL), and stirred for 3 h at room temperature. Upon formation of the ammonium carboxylate, (monitored by the shift in $\nu_{C=O}$ 1713 $cm^{-1}$ band), the solution was acidified to pH 2 upon addition of *conc.* HCl and the two phases were stirred vigorously for 2 h. The resulting white suspension was filtered, and the filtrate washed with water (3×10 mL) and acetone (3×10 mL) to yield the desired product as a white powder. Yield 0.094 g, 0.27 mmol, 75%. $^1H$ NMR (400 MHz, DMSO-$d_6$) δ 13.22 (*br*. s, 1H, *o*), 7.98 (d, *J* = 8 Hz, 2H, *r*), 7.69 (d, *J* = 8 Hz, 2H, *q*), 7.64 (d, *J* = 1 Hz, 4H, *k-l*), 7.57 (m, 4H, *e-f*), 4.41 (s, 1H, *a*). $MS^+$ (ASAP) *m/z* (%): 346.1 (100, $[M]^+$). TGA shows incomplete combustion (54%) at 1000 ºC.

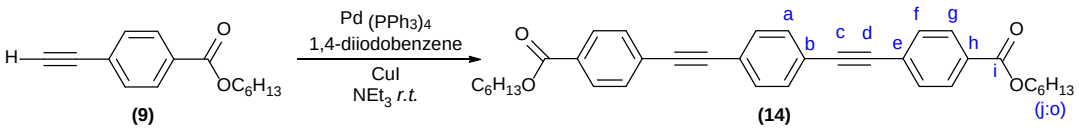


**Preparation of 14.** In a 50 mL round bottom flask, **9** (0.34 g, 1.5 mmol), 1,4-diiodobenzene (0.25 g, 0.76 mmol), $Pd(PPh_3)_4$ (0.045 g, 0.040 mmol) and CuI (0.007 g, 0.037 mmol) were added to $NEt_3$ (15 mL), and the resulting white suspension stirred at room temperature overnight. The precipitate was collected by filtration and washed thoroughly with hexane. The solids were dissolved in $CH_2Cl_2$ and filtered through silica gel. Solvent removal of the yellowish filtrate yielded the pure product as an off-white solid.

Yield 0.30 g, 0.56 mmol, 75%. $^{1}$H NMR (400 MHz, $CDCl_3$) δ 8.04 (d, *J* = 9 Hz, 4H, *g*), 7.59 (d, *J* = 9 Hz, 4H, *f*), 7.54 (s, 4H, *a*), 4.33 (t, *J* = 7 Hz, 2H, *j*), 1.82 – 1.72 (m, 4H, *k*), 1.49 – 1.40 (m, 4H, *l*), 1.39 – 1.29 (m, 8H, *m/n*), 0.92 (t, *J* = 7 Hz, 6H, *o*). $^{13}$C{$^{1}$H} NMR (101 MHz, $CDCl_3$) δ 166.2 (*i*), 131.9, 131.6 (f/*g*), 130.3 (*h*), 129.7 (*a*), 127.6, 123.2 (*b*/*e*), 91.9, 90.9 (*c*/*d*), 65.5 (*j*), 31.6 (*k*), 28.8 (*l*), 25.8 (*m*), 22.7 (*n*), 14.1 (*o*). MS$^{+}$ (ASAP) *m/z* (%): 451.19 (100, [M+H-$C_6H_{13}$]$^{+}$); 534.28 (53, [M]$^{+}$). IR (*nujol*) cm$^{-1}$: 1717 (m) ν(C=O).

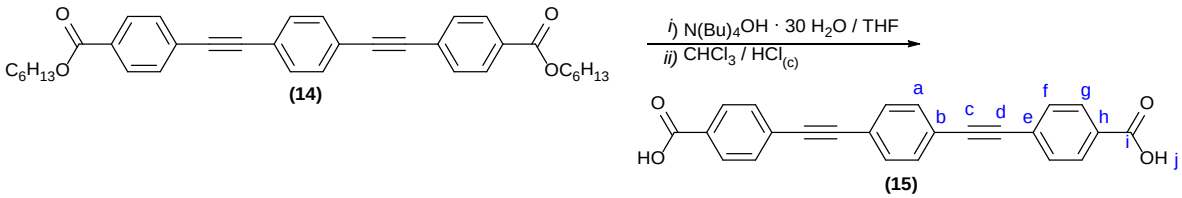


**Preparation of 15.** A solution of $N(Bu)_4OH \cdot 30\ H_2O$ (0.30 g, 0.38 mmol) in THF (3 mL) was added to solution of **14** (0.05 g, 0.09 mmol) in THF (3 mL). The resulting brown solution was stirred at room temperature for 30 minutes, taken to dryness and redissolved in $CHCl_3$ (2 mL). White solids precipitated upon addition of HCl and sonication of the two phases. The precipitate was collected by filtration and washed with water (2 × 5 mL), acetone (2 mL) and $Et_2O$ (5 mL) and dried in air. Yield 0.03 g, 0.08 mmol, 89%. $^{1}$H NMR (500 MHz, DMSO-$d_6$) δ 13.21 (*br.* s, 2H, *j*), 7.97 (d, *J* = 8 Hz, 4H, *g*), 7.67 (d, *J* = 8 Hz, 4H, *f*), 7.64 (s, 4H, *a*). $^{13}$C{$^{1}$H} NMR (126 MHz, DMSO-$d_6$, 50 ºC) δ 166.4 (*i*), 131.6, 131.4 (*f*/*g*), 130.8 (*h*), 129.3 (*a*), 126.0, 122.2 (*b*/*e*), 91.1, 90.6 (*c*/*d*). MS$^{-}$ (ESI) *m/z* (%): 183.3 (100, [M-2H]$^{2-}$); 365.5 (34, [M-H]$^{-}$). TGA shows incomplete combustion (91%) at 1000 ºC.

## 2.8. References


1. Tour, J. M., *Molecular Electronics; Commercial Insights, Chemistry, Devices, Architecture and Programming.* World Scientific Publishing Co: Scientific, 2003.
2. (a) Reed, M. A.; Chen, J.; Rawlett, A. M.; Price, D. W.; Tour, J. M., *Appl. Phys. Lett.*, **2001**, *78*, 3735-3737; (b) Liu, K.; Wang, X.; Wang, F., *ACS Nano*, **2008**, *2*, 2315-2323; (c) Fan, F.-R. F.; Lai, R. Y.; Cornil, J.; Karzazi, Y.; Brédas, J.-L.; Cai, L.; Cheng, L.; Yao, Y.; Price, D. W.; Dirk, S. M.; Tour, J. M.; Bard, A. J., *J. Am. Chem. Soc.*, **2004**, *126*, 2568-2573; (d) Xiao, X.; Nagahara, L. A.; Rawlett, A. M.; Tao, N., *J. Am. Chem. Soc.*, **2005**, *127*, 9235-9240; (e) Blum, A. S.; Kushmerick, J. G.; Long, D. P.; Patterson, C. H.; Yang, J. C.; Henderson, J. C.; Yao, Y.; Tour, J. M.; Shashidhar, R.; Ratna, B. R., *Nat. Mater.*, **2005**, *4*, 167-172; (f) Lu, Q.; Liu, K.; Zhang, H.; Du, Z.; Wang, X.; Wang, F., *ACS Nano*, **2009**, *3*, 3861-3868.
3. Zhao, X.; Huang, C.; Gulcur, M.; Batsanov, A. S.; Baghernejad, M.; Hong, W.; Bryce, M. R.; Wandlowski, T., *Chem. Mater.*, **2013**, *25*, 4340-4347.
4. (a) Hong, S.; Reifenberger, R.; Tian, W.; Datta, S.; Henderson, J. I.; Kubiak, C. P., *Superlattices Microstruct.*, **2000**, *28*, 289-303; (b) Frei, M.; Aradhya, S. V.; Hybertsen, M. S.; Venkataraman, L., *J. Am. Chem. Soc.*, **2012**, *134*, 4003-4006; (c) Beebe, J. M.; Engelkes, V. B.; Miller, L. L.; Frisbie, C. D., *J. Am. Chem. Soc.*, **2002**, *124*, 11268-11269.
5. (a) Park, Y. S.; Whalley, A. C.; Kamenetska, M.; Steigerwald, M. L.; Hybertsen, M. S.; Nuckolls, C.; Venkataraman, L., *J. Am. Chem. Soc.*, **2007**, *129*, 15768-15769; (b) Patrone, L.; Palacin, S.; Bourgoin, J. P., *Appl. Surf. Sci.*, **2003**, *212–213*, 446-451; (c) Chen, F.; Li, X.; Hihath, J.; Huang, Z.; Tao, N., *J. Am. Chem. Soc.*, **2006**, *128*, 15874-15881; (d) Fukazawa, A.; Kiguchi, M.; Tange, S.; Ichihashi, Y.; Zhao, Q.; Takahashi, T.; Konishi, T.; Murakoshi, K.; Tsuji, Y.; Staykov, A.; Yoshizawa, K.; Yamaguchi, S., *Chem. Lett.*, **2011**, *40*, 174-176; (e) Ie, Y.; Hirose, T.; Nakamura, H.; Kiguchi, M.; Takagi, N.; Kawai, M.; Aso, Y., *J. Am. Chem. Soc.*, **2011**, *133*, 3014-3022; (f) Kiguchi, M.; Takahashi, T.; Takahashi, Y.; Yamauchi, Y.; Murase, T.; Fujita, M.; Tada, T.; Watanabe, S., *Angew. Chem. Int. Ed.*, **2011**, *50*, 5708-5711; (g) Wang, C.; Batsanov, A. S.; Bryce, M. R.; Martín, S.; Nichols, R. J.; Higgins, S. J.; García-Suárez, V. M.; Lambert, C. J., *J. Am. Chem. Soc.*, **2009**, *131*, 15647-15654; (h) Cheng, Z. L.; Skouta, R.; H., V.; Widawsky, J. R.; Schneebeli, S.; Chen, W.; Hybertsen, M. S.; Breslow, R.; Venkataraman, L., *Nat. Nano*, **2011**, *6*, 353-357; (i) Kiguchi, M.; Murakoshi, K., *Thin Solid Films*, **2009**, *518*, 466-469.
6. Häkkinen, H., *Nat. Chem*, **2012**, *4*, 443–455.
7. (a) Haick, H.; Cahen, D., *Acc. Chem. Res.*, **2008**, *41*, 359-366; (b) Hylke, B. A.; Bert de, B., *J. Phys.: Condens. Matter*, **2008**, *20*, 013001; (c) Gyepi-Garbrah, S. H.; Silerova, R., *Phys. Chem. Chem. Phys.*, **2002**, *4*, 3436-3442.
8. (a) Ford, M. J.; Hoft, R. C.; McDonagh, A., *J. Phys. Chem. B*, **2005**, *109*, 20387-20392; (b) Maity, P.; Tsunoyama, H.; Yamauchi, M.; Xie, S.; Tsukuda, T., *J. Am. Chem. Soc.*, **2011**, *133*, 20123-20125.

9. (a) Stewart, M. P.; Buriak, J. M., *J. Am. Chem. Soc.*, **2001**, *123*, 7821-7830; (b) M. Buriak, J., *Chem. Commun.*, **1999**, 1051-1060.
10. Binder, W. H.; Sachsenhofer, R., *Macromol. Rapid Commun.*, **2007**, *28*, 15-54.
11. (a) Gimzewski, J. K.; Joachim, C., *Science*, **1999**, *283*, 1683-1688; (b) Collier, C. P.; Jeppesen, J. O.; Luo, Y.; Perkins, J.; Wong, E. W.; Heath, J. R.; Stoddart, J. F., *J. Am. Chem. Soc.*, **2001**, *123*, 12632-12641.
12. (a) Aviram, A.; Ratner, M. A., *Chem. Phys. Lett.*, **1974**, *29*, 277-283; (b) Dhirani, A.; Lin, P. H.; Guyot-Sionnest, P.; Zehner, R. W.; Sita, L. R., *J. Chem. Phys*, **1997**, *106*, 5249-5253; (c) Heath, J. R., *Annual Review of Materials Research*, **2009**, *39*, 1-23; (d) Kaliginedi, V.; Moreno-García, P.; Valkenier, H.; Hong, W.; García-Suárez, V. M.; Buiter, P.; Otten, J. L. H.; Hummelen, J. C.; Lambert, C. J.; Wandlowski, T., *J. Am. Chem. Soc.*, **2012**, *134*, 5262-5275; (e) Metzger, R. M.; Chen, B.; Höpfner, U.; Lakshmikantham, M. V.; Vuillaume, D.; Kawai, T.; Wu, X.; Tachibana, H.; Hughes, T. V.; Sakurai, H.; Baldwin, J. W.; Hosch, C.; Cava, M. P.; Brehmer, L.; Ashwell, G. J., *J. Am. Chem. Soc.*, **1997**, *119*, 10455-10466; (f) Metzger, R. M.; Xu, T.; Peterson, I. R., *J. Phys. Chem. B*, **2001**, *105*, 7280-7290; (g) Villares, A.; Lydon, D. P.; Low, P. J.; Robinson, B. J.; Ashwell, G. J.; Royo, F. M.; Cea, P., *Chem. Mater.*, **2007**, *20*, 258-264.
13. (a) Stephens, R. D.; Castro, C. E., *J. Org. Chem.*, **1963**, *28*, 3313-3315; (b) Cassar, L., *J. Organomet. Chem.*, **1975**, *93*, 253-257; (c) Dieck, H. A.; Heck, F. R., *J. Organomet. Chem.*, **1975**, *93*, 259-263; (d) Sonogashira, K.; Tohda, Y.; Hagihara, N., *Tetrahedron Lett.*, **1975**, *16*, 4467-4470; (e) Doucet, H.; Hierso, J.-C., *Angew. Chem. Int. Ed.*, **2007**, *46*, 834-871; (f) Bunz, U. H. F., *Acc. Chem. Res.*, **2001**, *34*, 998-1010.
14. Lydon, D. P.; Albesa-Jové, D.; Shearman, G. C.; Seddon, J. M.; Howard, J. A. K.; Marder, T. B.; Low, P. J., *Liq. Cryst.*, **2008**, *35*, 119 - 132.
15. Orita, A.; Miyamoto, K.; Nakashima, M.; Ye, F.; Otera, J., *Adv. Synth. Catal.*, **2004**, *346*, 767-776.
16. Marsden, J. A.; Haley, M. M., Cross-Coupling Reactions to sp Carbon Atoms. In *Metal-Catalyzed Cross-Coupling Reactions*, Wiley-VCH Verlag GmbH: 2008; pp 317-394.
17. (a) Stang, P. J.; Diederich, F., *Metal-Catalyzed Cross-Coupling Reactions, K. Sonogashira, in: pp. 203–229*. Wiley-VCH, Weinheim: 1998; (b) Hierso, J.-C.; Beaupérin, M.; Saleh, S.; Job, A.; Andrieu, J.; Picquet, M., *Comptes Rendus Chimie*, **2013**, *16*, 580-596.
18. (a) Nishihara, Y.; Inoue, E.; Ogawa, D.; Okada, Y.; Noyori, S.; Takagi, K., *Tetrahedron Lett.*, **2009**, *50*, 4643-4646; (b) Nishihara, Y.; Ikegashira, K.; Hirabayashi, K.; Ando, J.-i.; Mori, A.; Hiyama, T., *J. Org. Chem.*, **2000**, *65*, 1780-1787; (c) Nishihara, Y. I. K. M., A; Hiyama T., *Chem. Lett.*, **1997**, *26*, 1233-1234.
19. Sonogashira, K., *J. Organomet. Chem.*, **2002**, *653*, 46-49.
20. García-Melchor, M.; Braga, A. A. C.; Lledós, A.; Ujaque, G.; Maseras, F., *Acc. Chem. Res.*, **2013**, *46*, 2626-2634.
21. Chinchilla, R.; Nájera, C., *Chem. Rev.*, **2007**, *107*, 874-922.
22. Plenio, H., *Angew. Chem. Int. Ed.*, **2008**, *47*, 6954-6956.

23. Carril, M.; Correa, A.; Bolm, C., *Angew. Chem.*, **2008**, *120*, 4940-4943.
24. Park, S.; Kim, M.; Koo, D. H.; Chang, S., *Adv. Synth. Catal.*, **2004**, *346*, 1638-1640.
25. Feng, L.; Liu, F.; Sun, P.; Bao, J., *Synlett*, **2008**, *2008*, 1415-1417.
26. Kanuru, V. K.; Humphrey, S. M.; Kyffin, J. M. W.; Jefferson, D. A.; Burton, J. W.; Armbruster, M.; Lambert, R. M., *Dalton Trans.*, **2009**, 7602-7605.
27. Wang, L.; Li, P.; Zhang, Y., *Chem. Commun.*, **2004**, 514-515.
28. Li, J.-H.; Li, J.-L.; Wang, D.-P.; Pi, S.-F.; Xie, Y.-X.; Zhang, M.-B.; Hu, X.-C., *J. Org. Chem.*, **2007**, *72*, 2053-2057.
29. Li, P.; Wang, L., *Synlett*, **2006**, *2006*, 2261-2265.
30. (a) Hashmi, A. S. K., *Chem. Rev.*, **2007**, *107*, 3180-3211; (b) González-Arellano, C.; Abad, A.; Corma, A.; García, H.; Iglesias, M.; Sánchez, F., *Angew. Chem.*, **2007**, *119*, 1558-1560; (c) González-Arellano, C.; Abad, A.; Corma, A.; García, H.; Iglesias, M.; Sánchez, F., *Angew. Chem. Int. Ed.*, **2007**, *46*, 1536-1538.
31. Borah, H. N.; Prajapati, D.; Boruah, R. C., *Synlett*, **2005**, *2005*, 2823-2825.
32. (a) Dupont, J.; de Souza, R. F.; Suarez, P. A. Z., *Chem. Rev.*, **2002**, *102*, 3667-3692; (b) Lamblin, M.; Nassar-Hardy, L.; Hierso, J.-C.; Fouquet, E.; Felpin, F.-X., *Adv. Synth. Catal.*, **2010**, *352*, 33-79.
33. Bakherad, M., *Appl. Organomet. Chem.*, **2013**, *27*, 125-140.
34. Coulson, D. R.; Satek, L. C.; Grim, S. O., Tetrakis(Triphenylphosphine)Palladium(0). In *Inorg. Synth.*, John Wiley & Sons, Inc.: 2007; pp 107-109.
35. Stephens, E. B.; Tour, J. M., *Adv. Mater.*, **1992**, *4*, 570-572.
36. Ariga, K.; Mori, T.; Hill, J. P., *Langmuir*, **2013**, *29*, 8459-8471.
37. (a) Langmuir, I., *Proc. Natl. Acad. Sci. U.S.A.*, **1917**, *3*, 251-257; (b) Langmuir, I., *Nobel Lectures*, **1932**,
38. (a) Varaksa, N.; Pospíšil, L.; Janouêk, Z.; Grüner, B.; Wang, B.; Pecka, J.; Magnera, T.; Michl, J., *MRS Online Proceedings Library*, **2002**, *728*, null-null; (b) Magnera, T. F.; Peslherbe, L. M.; Körblová, E.; Michl, J., *J. Organomet. Chem.*, **1997**, *548*, 83-89; (c) Smith, T., *Adv. Colloid Interface Sci.*, **1972**, *3*, 161-221.
39. Martín, M. T.; Prieto, I.; Camacho, L.; Möbius, D., *Langmuir*, **1996**, *12*, 6554-6560.
40. Kundu, S.; Datta, A.; Hazra, S., *Chem. Phys. Lett.*, **2005**, *405*, 282-287.
41. (a) Ballesteros, L. M.; Martín, S.; Momblona, C.; Marqués-González, S.; López, M. C.; Nichols, R. J.; Low, P. J.; Cea, P., *J. Phys. Chem. C*, **2012**, *116*, 9142-9150; (b) Ballesteros , L. M.; Martín , S.; Cortés , J.; Marqués-González, S.; Higgins, S. J.; Nichols, R. J.; Low, P. J.; Cea , P., *Chem. Eur. J.*, **2013**, *19*, 5352-5363.
42. (a) Kim, B.; Choi, S. H.; Zhu, X. Y.; Frisbie, C. D., *J. Am. Chem. Soc.*, **2011**, *133*, 19864-19877; (b) Pera, G.; Villares, A.; López, M. C.; Cea, P.; Lydon, D. P.; Low, P. J., *Chem. Mater.*, **2007**, *19*, 857-864.
43. (a) Weibel, N.; Błaszczyk, A.; von Hänisch, C.; Mayor, M.; Pobelov, I.; Wandlowski, T.; Chen, F.; Tao, N., *Eur. J. Org. Chem.*, **2008**, *2008*, 136-149; (b) Haiss, W.; Wang, C.; Grace, I.; Batsanov, A. S.; Schiffrin, D. J.; Higgins, S. J.; Bryce, M. R.; Lambert, C. J.; Nichols, R. J., *Nat. Mater.*, **2006**, *5*, 995-1002.
44. (a) Salomon, A.; Cahen, D.; Lindsay, S.; Tomfohr, J.; Engelkes, V. B.; Frisbie, C. D., *Adv. Mater.*, **2003**, *15*, 1881-1890; (b) Cui, X. D.; Primak, A.; Zarate, X.; Tomfohr,

J.; Sankey, O. F.; Moore, A. L.; Moore, T. A.; Gust, D.; Harris, G.; Lindsay, S. M., *Science*, **2001**, *294*, 571-574; (c) Selzer, Y.; Salomon, A.; Cahen, D., *J. Am. Chem. Soc.*, **2002**, *124*, 2886-2887; (d) Seminario, J. M.; De La Cruz, C.; Derosa, P. A.; Yan, L., *J. Phys. Chem. B*, **2004**, *108*, 17879-17885.

45. Wang, G.; Kim, T. W.; Lee, T.; Wang, W.; Reed, M. A., 4.16 - Electronic Properties of Alkanethiol Molecular Junctions: Conduction Mechanisms, Metal–Molecule Contacts, and Inelastic Transport. In *Comprehensive Nanoscience and Technology*, Andrews, D. L.; Scholes, G. D.; Wiederrecht, G. P., Eds. Academic Press: Amsterdam, 2011; pp 463-487.
46. Simmons, J. G., *J. Appl. Phys.*, **1963**, *34*, 1793-1803.
47. (a) Holmlin, R. E.; Haag, R.; Chabinyc, M. L.; Ismagilov, R. F.; Cohen, A. E.; Terfort, A.; Rampi, M. A.; Whitesides, G. M., *J. Am. Chem. Soc.*, **2001**, *123*, 5075-5085; (b) Wang, W.; Lee, T.; Reed, M. A., *Phys. Rev. B: Condens. Matter*, **2003**, *68*, 035416; (c) Joachim, C.; Magoga, M., *Chem. Phys.*, **2002**, *281*, 347-352; (d) Simmons, J. G., *J. Phys. D: Appl. Phys.*, **1971**, *4*, 613.
48. (a) Villares, A.; Lydon, D. P.; Porrès, L.; Beeby, A.; Low, P. J.; Cea, P.; Royo, F. M., *J. Phys. Chem. B*, **2007**, *111*, 7201-7209; (b) Tang, Z.; Hicks, R. K.; Magyar, R. J.; Tretiak, S.; Gao, Y.; Wang, H.-L., *Langmuir*, **2006**, *22*, 8813-8820; (c) Villares, A.; Martin, S.; Giner, I.; Diaz, J.; Lydon, D. P.; Low, P. J.; Cea, P., *Soft Matter*, **2008**, *4*, 1508-1514; (d) Villares, A.; Pera, G.; Lydon, D. P.; López, M. C.; Low, P. J.; Cea, P., *Colloids Surf., A*, **2009**, *346*, 170-176.
49. (a) Liu, K.; Li, G.; Wang, X.; Wang, F., *J. Phys. Chem. C*, **2008**, *112*, 4342-4349; (b) Pera, G.; Martín, S.; Ballesteros, L. M.; Hope, A. J.; Low, P. J.; Nichols, R. J.; Cea, P., *Chem. Eur. J.*, **2010**, *16*, 13398-13405; (c) Ballesteros, L. M.; Martín, S.; Pera, G.; Schauer, P. A.; Kay, N. J.; López, M. a. C.; Low, P. J.; Nichols, R. J.; Cea, P., *Langmuir*, **2011**, *27*, 3600-3610.
50. Lydon, D. P.; Albesa-Jové, D.; Shearman, G. C.; Seddon, J. M.; Howard, J. A. K.; Marder, T. B.; Low, P. J., *Liq. Cryst.*, **2008**, *35*, 119-132.
51. Gottardo, C.; Aguirre, A., *Tetrahedron Lett.*, **2002**, *43*, 7091-7094.
52. Li, Q.; Rukavishnikov, A. V.; Petukhov, P. A.; Zaikova, T. O.; Jin, C.; Keana, J. F. W., *J. Org. Chem.*, **2003**, *68*, 4862-4869.

# 3. TOP ELECTRODE FORMATION: A NOVEL IN-SITU APPROACH

## 3.1. Abstract

Two novel approaches to the formation of the top electrode on molecular films to generate reliable molecular junctions are described (Figure 3-1). The synthetic methodologies appropriate for the preparation of gold ethynyl complexes Au(C≡CR)(L) (R = aryl, L= $PPh_3$ and CNR) that are critical to the thermal annealing route are also discussed.

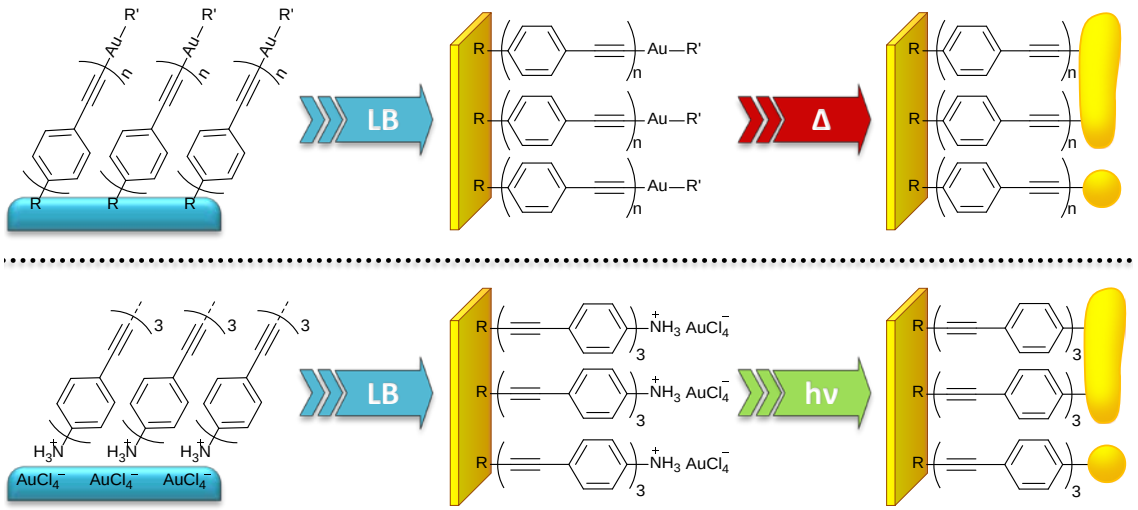


**Figure 3-1.** *Novel soft methods for top-electrode formation: thermally induced decomposition of an adsorbed gold complex (top) and photoreduction of aurate ions integrated on the molecular film by the LB technique (bottom).*

## 3.2. Introduction

The path towards further miniaturization of electronic devices has raised many scientific and technological challenges.[1] Nevertheless, the use of single molecules to perform as electronic components represents the ultimate miniaturization,[2] and therefore despite the difficulties associated with the construction of a molecular electronic device, the potential returns in terms of the capacity that such structures might offer to extend

Moore's Law are sufficiently compelling to drive a vast body of academic and increasingly industrial research in the field. Looking beyond the fundamental questions of molecular conductance and the development of both new molecular structures and metric methods appropriate for the investigation of even the most elementary of molecular junctions, the use of smaller components to allow for greater device density is accompanied by an increase on the difficulties to integrate them into a working device.[1a] In considering the challenges of fabricating a simple, two-electrode 'sandwich' device or scalable metal|molecule|metal junction, Langmuir-Blodgett or self-assembly are nowadays well developed techniques through which molecules can be orderly disposed on to a variety of *bottom* electrode surfaces. In many single molecule experiments the metallic tip of a scanning probe microscope serves as the top electrode and permits the formation of immensely useful molecular junctions for the assessment of molecular electronic properties and phenomena. However, the genuine technological application of molecule electronic science requires reliable methods to form the top electrode as a conducting film on top of a small bundle of molecules. Consequently, it is the preparation of the *top* electrode that completes metal|molecule|metal sandwich structure which has become key bottleneck in routes to fabricate a technologically viable molecular junction. Traditional methods to generate the top electrode contacts on sandwich-like devices are based on metal evaporation or sputtering atop a pre-formed molecular film. However, depositing a metallic electrode on top of a molecular film can, and often does, cause damage to the organic monolayer with penetration of the metallic layer through the organic film resulting on a short circuit that renders the device unusable. In order to avoid the problems found by the traditional methods to generate a defect-free molecular junction, two softer *in-situ* methods to generate the top electrode by thermal or photochemical means were designed. To these ends, compounds **16**, **20 - 22**, **25** and **[27H]Cl** were synthesized (Chart 3-1).

The first top electrode fabrication protocol involves the assembly of well-packed LB films of **20** and **22** on a metallic substrate. Decomposition of the assembled metallic complex is then thermally induced to produce nanometric gold particles that can act as the top electrode, although the fate of co-ligand has not been established. The second approach involves the preparation of a Langmuir film of the OPE ammonium salt **[27H]Cl** on an aqueous auric acid solution. The film is then transferred to a solid substrate leaving the gold ions adsorbed to the polar end of the molecule exposed on top of the molecular film. Photoreduction of the integrated aurate ions leads to the formation of metallic gold particles performing as the top electrode. Importantly, both processes are highly compatible with the prevailing lithographic routines employed to fabricate current electronic devices.

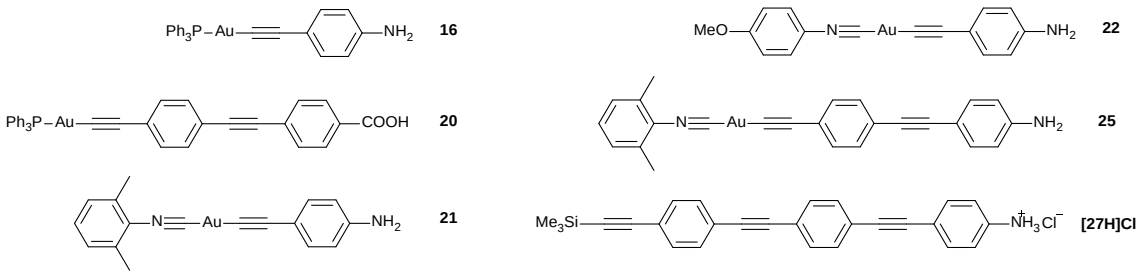


**Chart 3-1.** *Gold complexes and OPE derivatives prepared in this Chapter.*

## 3.3. Synthetic considerations: Au(C≡CR)(L) complexes

Despite having been studied for decades,[3] there is a renewed interest within the scientific community in ethynyl gold chemistry.[4] Their stability, linear rod-like structure and metallophilic interactions have made ethynyl gold complexes specially interesting in the fields of polymer and supramolecular chemistry.[5] In addition, these complexes are known to present remarkable photophysical properties such as luminescence[6] and non-linear optical behaviour.[7] Likewise, gold ethynyl complexes have been employed as synthetic intermediates taking the role of Cu in crosscoupling reactions of aryl halides with

cuprous ethynylenes.[8] As a result of these efforts, many examples of linear Au(C≡CR)(L) complexes can be found in the literature. A wide variety of co-ligands, L, have been successfully employed in stabilising these molecular rods over their homoleptic analogues[4b] including: tertiary phosphines;[9] arsines;[10] stibines;[11] isocyanides;[9, 12] pyridines[13] and amines.[14] A summary of the different routes found in the literature for the synthesis of Au(C≡CR)(L) is presented in Scheme 3-1. One of the most traditional methods consists in the treatment of AuClL with lithiated ethynylenes (Scheme 3-1, *a*).[15] Despite this method being successfully used in the synthesis of several ethynyl-gold complexes, the use of the highly reactive organolithium reagents restricts the applicability and convenience of this synthetic approach. A different approach (Scheme 3-1, *b*) consists on the formation of the polymeric precursors $[Au(C{\equiv}CR)]_n$ by treating AuCl(tht) (tht = tetrahydrothiophene) or $AuCl(SMe_2)$ with HC≡CR under basic conditions[4a, 9] which can be readily depolymerized through displacement of the network metal-alkyne π-interactions and aurophilic interactions by donor ligands L, to form the monomeric complexes Au(C≡CR)(L). The milder conditions required for this reaction allowed the synthesis of a much wider range of complexes. A related, but arguably less convenient approach (Scheme 3-1, *c*) involves the treatment of the polymeric $[Au(C{\equiv}CR)]_n$ first with $Cl^-$ to form anionic mononuclear complexes $[Au(C{\equiv}CR)Cl]^-$ and further treatment with L to displace the chloride.[16] A simpler higher yielding route (Scheme 3-1, *d*) involves the treatment of AuClL with a terminal alkyne and a base.[17] This approach can be seen as a milder variation of route (*a*) typically conducted in the presence of NaOEt or $KBu^tO$ in polar protic solvents such as EtOH. Despite its wider applicability, this reaction conditions may still be harsh enough to decompose the more sensitive ethynylgold complexes. A softer variation of route (*d*) involves the replacement of the strong inorganic bases for amines, typically $NEt_3$ or $NHPr^i_2$ together with organic aprotic solvents (Scheme 3-1, *e*).[18] However, these

changes typically lead to slower reaction kinetics that may require higher reaction temperatures. Milder conditions in the organic amine/solvent route can be achieved by addition of catalytic CuI which promotes formation of the desired Au(C≡CR)(L) complexes through a transmetallation reaction (Scheme 3-1, *f*).[18a, 19]

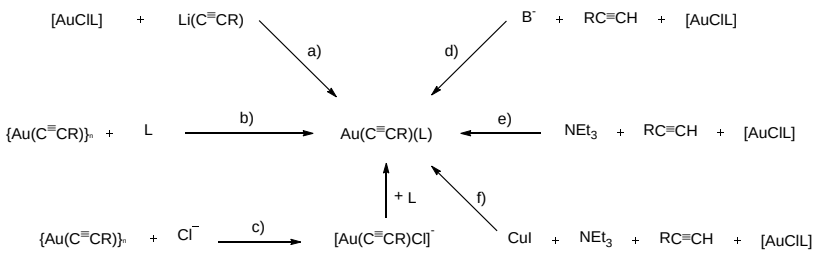


**Scheme 3-1.** *Summary of the available synthetic routes to ethynylgold (I) complexes. For details of reactions a - f see text.*

The first mention to the polymeric nature of ethynylgold complexes was made by Coates and Parkin who after preparing $[Au(C{\equiv}CBu^t)]_n$ suggested its polymeric structure purely from experimental observations without supporting structural data.[15] Three decades later X-ray crystallographic analysis on a sample prepared in the Mingos group demonstrated that the compound presented a novel catenane structure.[20] The structure presented two inter-locking six-membered rings in which three different coordination modes for the ethynyl ligand were present (one σ and two different π-coordination modes) confirming Coates prediction (Scheme 3-2).

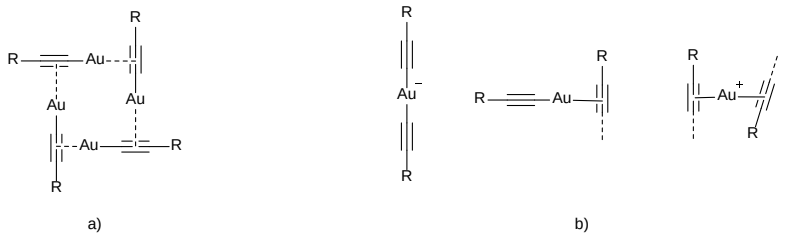


**Scheme 3-2.** *Alkyne coordination modes on ethynylgold complexes: a) Coates prediction; and b) found in Mingos catenane X-ray structure.*

However, the polymeric nature of the gold ethynylenes is still not completely understood. As an example of the wide variety of aurophilic interactions, Hogarth *et al.*[9] reported the synthesis and crystal structure of [Au(C≡C$C_6H_4NH_2$-4){P(3-tolyl)$_3$}] with molecules presenting N-H···Au supramolecular interactions. These various structural idiosyncrasies aside, it is simply pertinent to this discussion to note that there is ample synthetic precedence for the preparation of complexes Au(C≡CR)(L), with the wide range of different synthetic protocols that have already been described allowing preparation of a vast array of complexes with different R groups and supporting co-ligands L.

## 3.4. Synthesis

### *3.4.1. Synthesis of –AuPPh$_3$ complexes*

The stability of complexes **16** and **20** to reaction conditions involving polar protic solvents and strong bases, allowed for a straightforward synthetic approach. Both complexes were prepared by direct reaction of AuCl($PPh_3$) with the appropriate terminal alkyne under basic conditions (Scheme 3-3).

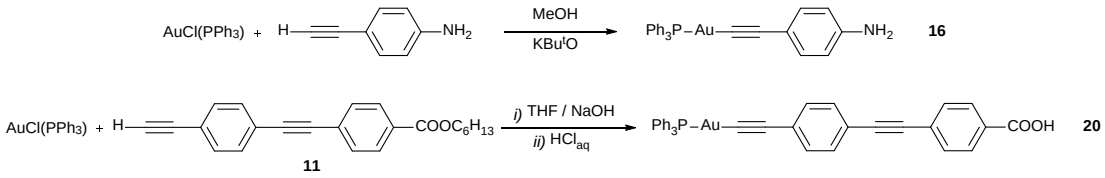


**Scheme 3-3.** *Synthesis of **16** and **20**.*

The gold precursor AuCl($PPh_3$) was prepared following well-established literature methods from AuCl(tht) in good yields.[21] Treatment of a suspension of AuCl($PPh_3$) in MeOH with potassium *tert*-butoxide ($KBu^tO$) and 4-ethynylaniline produced **16** as an orange precipitate in good yields (*ca.* 70%). The reaction, which took place at room temperature in under two hours could be easily monitored by IR spectroscopy.

Coordination of $AuCl(PPh_3)$ by ethynyl aniline leads to the reduction and ultimate consumption of the ν(C≡C-H) 3259 $cm^{-1}$ absorption band together with a marked shift in the ν(C≡C) vibration frequency from 2097 $cm^{-1}$ in the pro-ligand to 2213 $cm^{-1}$ in **16**.

However, contrary to the simple preparation of **16**, the synthesis of **20** was found to present several challenges that required an optimization process (Scheme 3-4). Although the amine mediated $Cu^+$ transmetallation route allowed the straightforward synthesis of **17** at room temperature, as deduced from the ν(C≡C) band shift and the $^{31}P\{^1H\}$ NMR which showed a singlet for $PPh_3$ that shifted from 57 ppm for $AuCl(PPh_3)$ to 39 ppm for **17**, the poor solubility of the product hindered chromatographic isolation of the reaction mixture. In order to circumvent the solubility issues encountered, a similar approach to that employed in Chapter 2 was adopted (Scheme 3-4, *b*). However, this synthetic route had to be reconsidered as treatment of **18** under basic aqueous MeOH conditions lead to transesterification and precipitation of the methyl ester made the formation of **20** uncertain. Hence, to avoid the transesterification reaction, the synthesis of **20** was conducted in THF and the mixture treated with aqueous $KBu^tO$ at reflux. However high temperatures induced decomposition of the gold derivative and a gold mirror was formed on the reaction flask (Scheme 3-4, *c*). Hence, a room temperature one-pot, two-step synthetic procedure was devised (Scheme 3-4, *d*). In a parallel manner analogous to that described for the synthesis of **18**, a suspension of $AuCl(PPh_3)$ and **11** (*see* Chapter 2) in THF was treated with an aqueous solution of NaOH (1M). The suspension was allowed to stir overnight to ensure coordination of the ethynylene to the gold atom with concomitant de-esterification and formation of the sodium carboxylate salt **19**. The reaction was monitored by IR spectroscopy, which allowed observation of the alkyne coordination to $AuCl(PPh_3)$ by following the decrease in intensity of the ν(C≡C-H) band at 3278 $cm^{-1}$ and the formation of the carboxylate anion by observation of the new ν($COO^-$) band at 1660 $cm^{-1}$. After

evaporation of the organic solvent, the remaining aqueous solution was acidified by addition of $HCl_{aq}$ (1M). Compound **20** was then easily collected from the aqueous mixture by centrifugation as an off-white solid in 70% yield. Despite the foreseen poor solubility of **20**, the compound could be fully characterized by IR, MS and $^{1}H$, $^{13}C$ and $^{31}P$ NMR (*see experimental section*).

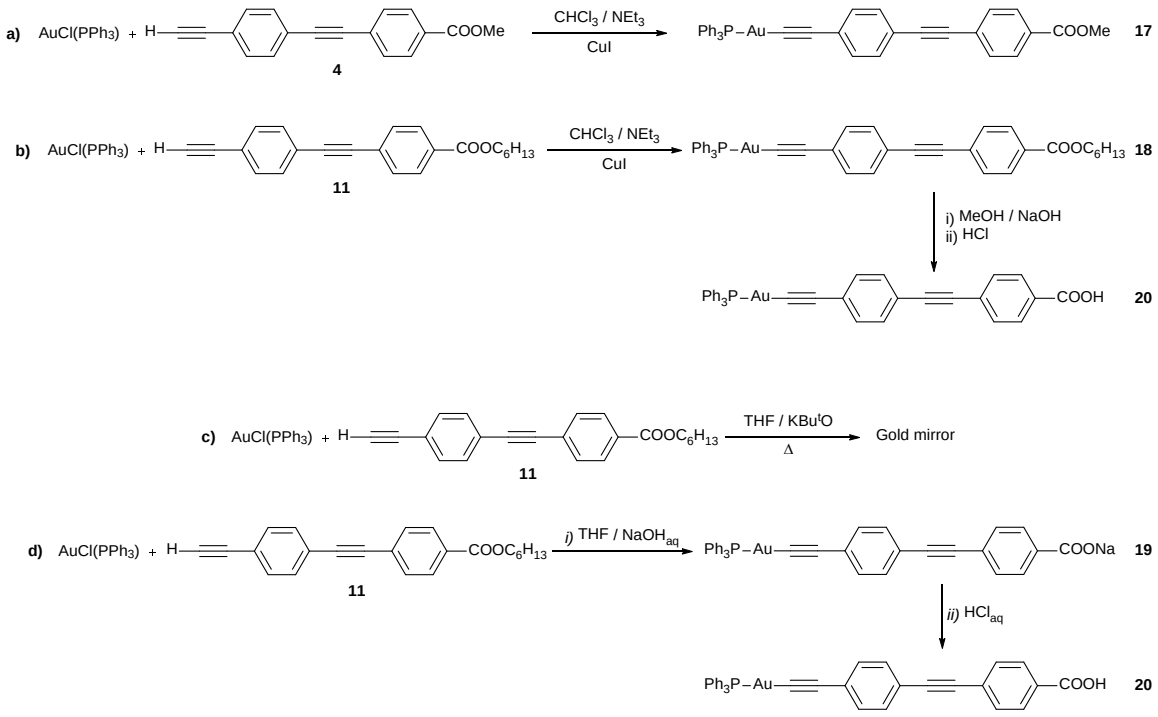


**Scheme 3-4.** *Attempted synthetic routes to **20**: a) Cu mediated transmetallation route on a methylester ligand; b) Cu mediated transmetallation route on a hexylester ligand; and c) Aqueous THF basic conditions at reflux; d) optimized two-stepped synthesis of **20**.*

### *3.4.2. Synthesis of –AuNCR complexes*

In initial survey and proof of principle work, the gold isocyanide complexes **21** and **22** were synthesized by drop wise addition of the appropriate isocyanide to a suspension of polymeric $[Au(C{\equiv}CC_6H_4NH_2\text{-}4)]_n$ in $CH_2Cl_2$ (Scheme 3-5). The preparation of the organogold polymer from AuCl(tht) ran smoothly following literature procedures.[9, 21a] The polymer $[Au(C{\equiv}CC_6H_4NH_2\text{-}4)]_n$ was characterized by IR spectroscopy with the formation

of a characteristic, broad ν(C≡C) band envelope spanning 2035 - 1910 $cm^{-1}$. The breadth and extraordinarily low frequency of the ν(C≡C) vibration is ascribed to the formation of a networked structure with alkyne-Au π bonds in addition to other supramolecular motifs.[15] Compounds **21** and **22** were obtained as a light-brown precipitate upon addition of hexane in good yields *ca.* 70%.

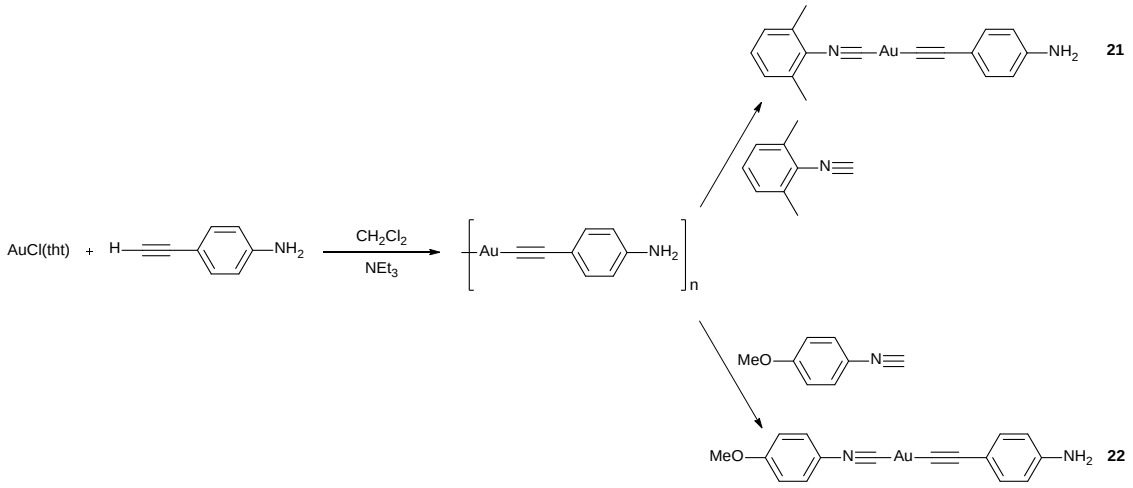


**Scheme 3-5.** *Synthesis of **21** and **22** through the polymeric route.*

However, a similar route based on polymeric precursors was found to be unsuitable for the preparation of the parent complex **25** (Scheme 3-6, *a*). Treatment of AuCl(tht) with **23** resulted on the instant formation of a dark precipitate that would develop an intense green colouration with time. The black precipitate **24**, which was poorly soluble in organic solvents was found to be unreactive towards the addition of 2,6-dimethylphenyl isocyanide. After several unsuccessful attempts to prepare **25**, an alternative route was designed. A two step one pot reaction (Scheme 3-6, *b*) was employed in which initially AuCl(tht) was treated with 2,6-dimethylphenyl isocyanide to form AuCl($CNC_5H_3Me_2$-2,6) overnight reaction. Subsequent addition of **23** and $NEt_3$, and further 24 hours reaction period at room temperature resulted in the formation of **25** in good yield *i.e.* 60%.

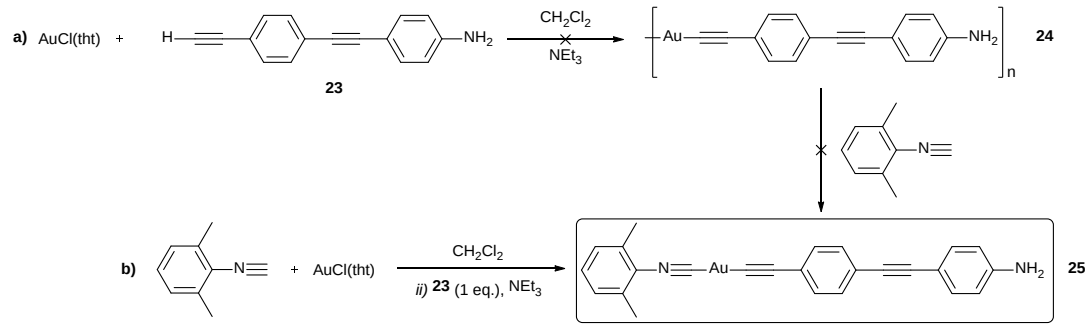


**Scheme 3-6.** *Synthesis of **25**: a) Unsuccessful polymeric route; and b) synthetic protocol based on in-situ formation of a gold isocyanide intermediate.*

### *3.4.3. Synthesis of OPE derivative [27H]Cl*

The synthesis of **[27H]Cl** was performed in a very similar manner to the carboxyl terminated OPEs **6** and **15** (*see* Chapter 2) taking advantage of the previously prepared building block $HC{\equiv}CC_6H_4C{\equiv}CSiMe_3$ (*see experimental section*).[22] Scheme 3-7 shows the one pot double-Sonogashira cross-coupling procedure used in the preparation of **[27H]Cl**. The first step involved selective crosscoupling of $HC{\equiv}CC_6H_4C{\equiv}CSiMe_3$ with 4-iodo-bromobenzene. In order for the oxidative addition to take place selectively on the iodine, the reaction was conducted in $NEt_3$ at 0 ºC for 5 h. When all the $HC{\equiv}CC_6H_4C{\equiv}CSiMe_3$ was consumed, 4-ethynylaniline was added and the reaction was stirred at reflux overnight. After chromatographic purification and crystallization from hot toluene **27** was obtained as orange crystals in acceptable yields *i.e.* 30%. For a fair yield comparison, the 30% yield obtained with the one-pot protocol should be compared with its equivalent coupling-deprotection-coupling procedure analogue to that employed in Chapter 2, with each of the reactions taking place in 67% yields. More importantly the one-pot synthetic route takes place in 24 hours and only one work-up is required. Finally a solution of **27** in $CH_2Cl_2$ was exposed to $HCl_{(g)}$ generating **[27H]Cl** as a brown precipitate that was collected by filtration.

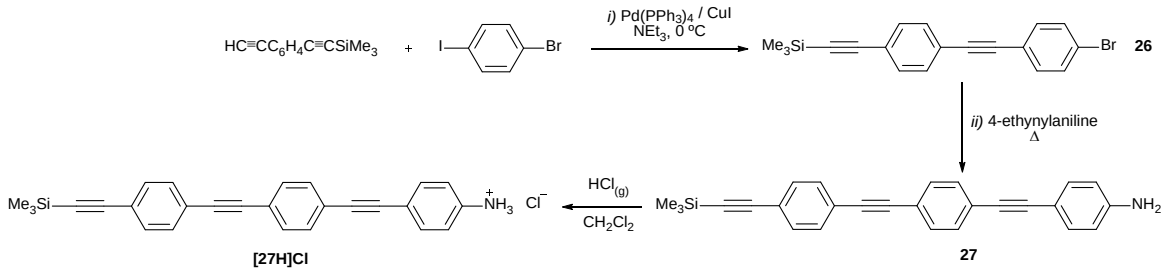


**Scheme 3-7.** *One-pot double-Sonogashira protocol to prepare* ***[27H]Cl****.*

## 3.5. Film and junction formation and characterization

### *3.5.1. Thermally induced decomposition of monolayers of 20 and 22*

In order to produce Langmuir monolayers free of 3D aggregates, exceptionally diluted solutions of **20** and **22** (~$10^{-5}$ M) had to be spread over the water surface. The tendency of ethynyl gold complexes to generate supramolecular aggregates is well known and typically attributed to strong aurophilic interactions between neighbouring metallic centres.[23] After the Langmuir film preparation was optimized, the films were transferred onto solid substrates at surface pressures of 10 mN/m (*ca.* 0.35 $nm^2$/molecule) for **20** and 16 mN/m (*ca.*0.2 $nm^2$/molecule) for the comparatively less bulky isocyanide complex **22**. The good quality of the LB films prepared was confirmed by QCM and electrode passivation experiments. Thermal treatment of the LB films of **20** and **22** was found to cause significant changes to the sample appearance and composition of the film surface. These results being consistent with the previously discussed thermal decomposition of **20** (formation of a gold mirror) when reflux conditions were employed (Scheme 3-4, *c*). In order to optimize the thermal treatment of both systems, Langmuir films of **20** and **22** were deposited on QCM substrates and changes in frequency were monitored upon time at temperatures ranging from 75 to 200 ºC.

The optimum annealing conditions for LB films of **20** was found for samples treated at 150ºC for 2 hours. After the thermal treatment and rinsing with $CHCl_3$ a change of 14Hz in the QCM frequency was found, consistent with the calculated loss of the $PPh_3$ ligand (262 amu). Further characterization of the effects of the thermal process on the monolayers of **20** was possible by means of XPS. Figure 3-2 shows the evolution of the characteristic phosphorus 2p photoelectron signal (~131 eV) associated with the $PPh_3$ moiety before (*top*) and after (*bottom*) the sample thermal treatment and rinsing. As it is clear from the XPS spectra, no phosphorus signal is observed for the thermally annealed films which fits with the hypothesised loss of the $–PPh_3$ moiety upon thermal treatment. In addition, the XPS signals attributable to $Au^+$ (85.04 and 88.74 eV) at the Au*4f* region were found to disappear upon annealing indicating the possible reduction of the $Au^+$ atom and the formation of $Au^0$.[24]

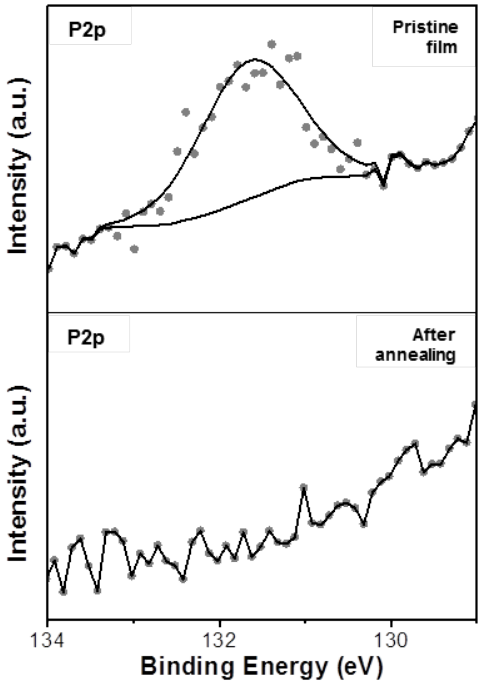


**Figure 3-2.** *XPS spectra of $P_{2p}$ photoelectron signal obtained for a monolayer of **20** before (top) and after thermal treatment at 150 ºC for 2 hours (bottom).*

These results, together with the formation of a gold mirror when **20** was prepared at reflux temperatures (*vide supra*), lead us to believe that thermal treatment of the samples induced the reduction of **20** resulting on the formation of gold nanoparticles (GNPs) on the film surface. The electrical response of the metal|molecule|GNP structures generated after thermal treatment was tested with a CP-AFM. Figure 3-3 shows the averaged *I-V* profile obtained for the GNPs when contacted with the AFM tip employing a force set-point of 26 nN. The conductance value obtained from the Ohmic region of the *I-V* curve (± 0.3 V) revealed an average conductance of $4.65 \cdot 10^{-5}$ $G_0$ similar to that of other phenyl ethynylene molecular ensembles previously reported.[25] Importantly, no low resistance *I-V* curves were observed indicating the lack of metallic filaments diffusing through the organic monolayer.

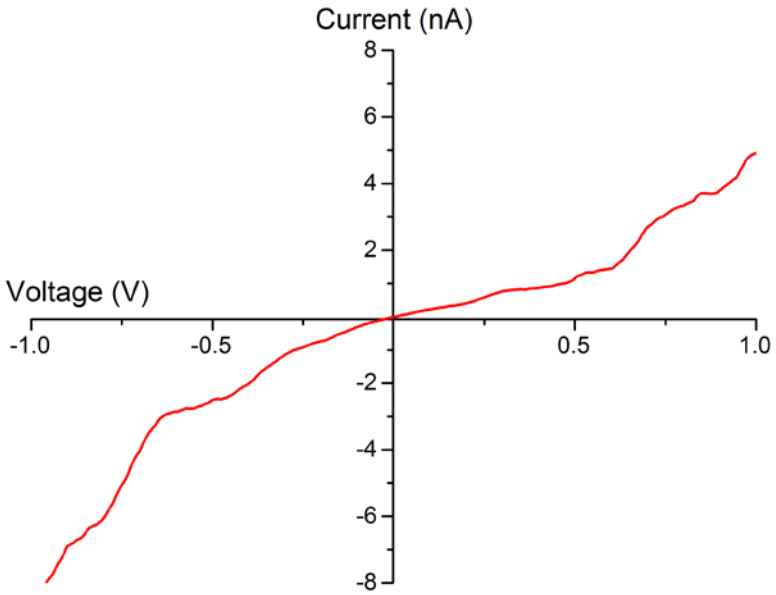


**Figure 3-3.** *Averaged electrical response obtained for metal|**20**|GNP junctions when addressed by the CP-AFM tip.*

In the case of LB films of **22**, the optimum thermal treatment was found for samples that were heated at 100 ºC for 2 hours. The sample surface transformation was evidenced by the different contact angle results for the sample before and after being annealed. The results showed a contact angle of 67º for the pristine LB film, compared to

the 42º of the more hydrophilic annealed sample. The samples surface was further characterized by AFM imaging, showing the characteristic appearance of nanometric sized particles on the annealed samples surface (Figure 3-4). That is clearly evidenced by the dramatic increase of the root mean square (RMS) roughness from 0.2 to 0.9 nm for the thermally treated samples.

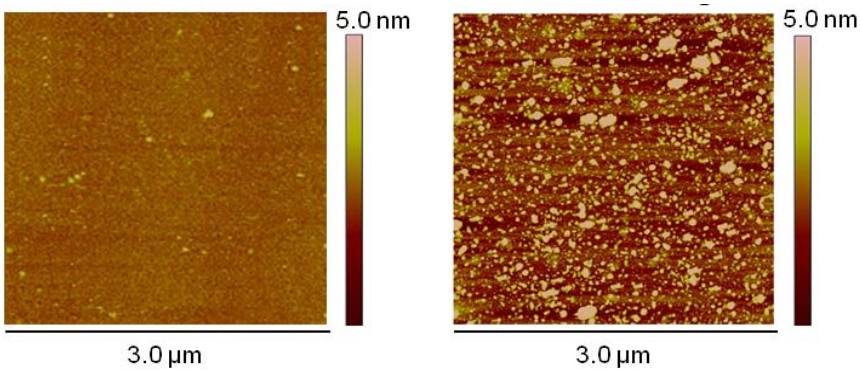


**Figure 3-4.** *AFM images of a pristine molecular film of **22** (left), and the same film after thermal annealing (right) showing the formation of gold nanoparticles (GNPs).*

The Au*4f* region of the XPS spectra for the annealed samples revealed the same features previously observed for annealed films of **20** ascribed to the formation of $Au^0$ superficial particles as a result of $Au^+$ reduction. In addition, QCM experiments revealed a weight loss on the annealed samples consistent with the loss of the $C{\equiv}NC_6H_4OMe$-4 moiety (133 amu). Following the protocol employed for **20**, the electrical properties of the sandwich like structures generated after thermal treatment of LB films of **22** were evaluated with a CP-AFM employing a force set-point of 35nN. The *I-V* curves collected by addressing several different particles found along the surface revealed an averaged conductance of $1.35 \cdot 10^{-4}$ $G_0$ (Figure 3-5). The comparatively higher conductance value obtained for **22**, around three times that observed for **20** ($4.65 \cdot 10^{-5}$ $G_0$) was ascribed to the narrower tunnelling barrier provided by the shorter derivative **20**. In addition, none of the GNP addressed by the AFM tip presented a metallic electrical response ruling out the presence of filaments diffusing through the organic monolayer.

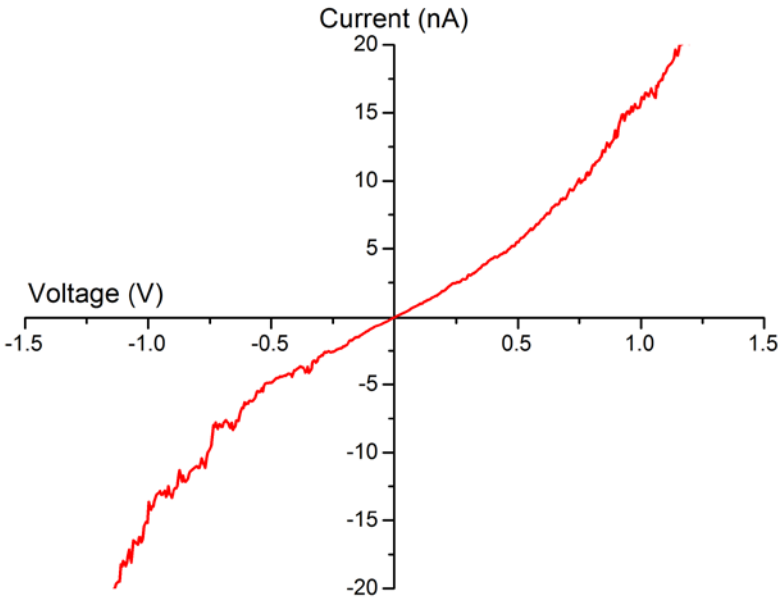


**Figure 3-5.** *Averaged electrical response obtained for metal|**22**|GNP junctions when the gold particles were addressed employing the CP-AFM.*

### *3.5.2. Photoreduction of auric ions on molecular films of [27H]$AuCl_4$*

The hydrophilic ammonium chloride head of **[27H]Cl** facilitates the formation of dense well-ordered monolayers on the water surface. In addition, the $Cl^-$ can be readily displaced by different anions when those are introduced into the aqueous phase. Thus, $HAuCl_4$ was added to the sub-phase in order to conveniently exchange $Cl^-$ for $AuCl_4^-$ forming **[27H]$AuCl_4$**. The preparation of Langmuir films of **[27H]Cl** on an aqueous auric acid sub-phase ($2 \cdot 10^{-5}$ M) was optimized using similar methods to those described above by our collaborators in Zaragoza. The molecular films were transferred from the water onto a variety of solid substrates that were initially held outside of the sub-phase by the vertical dipping method. The transference was performed at a constant surface pressure of 20 mN/m (*ca.* 0.5 $nm^2$/molecule). Under these conditions the trimethylsilyl group was chemisorbed to the substrate (as it was confirmed by XPS) leaving the aurate anions exposed on the top surface of the molecular film. Irradiation of the samples with UV light (254 nm) resulted on the formation of metallic nanoparticles on the film surface.

The formation of metallic gold particles was possible by tracking the development of a gold plasmon band on the UV-Vis spectra (550 nm) of the irradiated film. The formation of metallic gold on the monolayer surface was confirmed by XPS. In order to investigate the distribution of the photochemically produced gold nanoparticles, SEM images of the LB films were taken before and after irradiation (Figure 3-6). The original samples showed a homogeneous surface very different to the several circular spots (5-20 nm diameter size) found on the irradiated films.

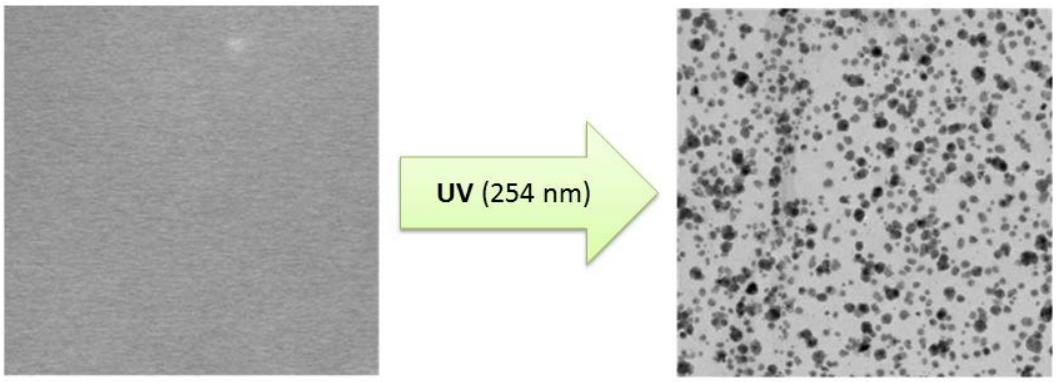


**Figure 3-6.** *SEM image (500×500) nm$^2$, molecular film of* ***[27H]AuCl$_4$*** *on glass before (left) and after (right) UV (254 nm) irradiation.*

In order to characterize the physical and electrical properties of the irradiated films AFM was employed. The AFM topographic images confirmed the presence of round nanometric size particles on the surface of the organic monolayer. In addition a conductive AFM tip was employed to address the superficial gold particles allowing electrical *I-V* characterization of the metal|molecule|GNP sandwich device. The *I-V* curves were averaged from multiple scans to ensure reproducibility and reliability (Figure 3-7). The electric response observed is nearly symmetric with a marked sigmoidal shape over the studied voltage range. The conductance value obtained from the Ohmic region (± 0.5 V) of the averaged *I-V* trace is $7.86 \cdot 10^{-5}$ $G_0$. Importantly, none of the curves collected presented the low resistance profile characteristic of metallic short circuits.

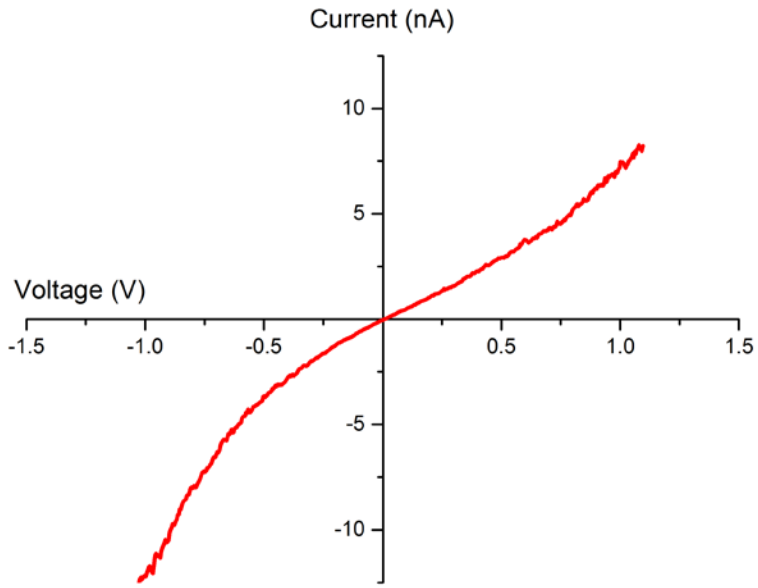


**Figure 3-7.** *Averaged I-V curve obtained from the gold particles on the surface of the irradiated* ***[27H]AuCl$_4$*** *film when addressed with the CP-AFM.*

## 3.6. Conclusions

Compounds **16**, **20 - 22**, **25** and **[27H]Cl** were synthesized and preparative routes optimised. In addition a more rapid synthetic procedure to prepare unsymmetrically substituted OPEs was described. Two novel top-electrode fabrication methods were developed based on thermal and photochemical decomposition of gold containing precursors. Monolayers of **20** and **22** were assembled and transferred on to gold substrates by the LB technique. Thermal treatment of the monolayers for 2 hours at 150 ºC induced decomposition of the ethynylgold complexes leading to the formation of gold nano-particles atop the molecular films. A second approach, towards the soft formation of the top electrode employing the purely organic **[27H]Cl** was described. By preparing the Langmuir films of **[27H]Cl** on an aqueous auric acid sub-phase metathesis of the $Cl^-$ by $AuCl_4^-$ takes place. After film transference, photoreduction of the exposed aurate anions on the film surface lead to the formation of nanometric gold particles distributed along the film surface. In both cases, the gold nano-particles performed as defect free top-electrodes

allowing electrical characterization of the molecular junction. Encouraged by these first results, further research is being conducted on parent compounds **16**, **21** and **25** in an attempt to improve electrode coverage and to obtain further information on the metallization process.

## 3.7. Experimental

### *3.7.1. General conditions*

General experimental conditions were reported in Chapter 2. The organometallic precursors AuCl(tht),[21a] AuCl($PPh_3$)[21b] and [AuC≡C$C_6H_4NH_2$-4]$_n$[9] were prepared by literature methods. The synthesis of **11** (Chapter 2) was reported in previous experimental sections of this thesis. Other reagents were purchased commercially and used as received.

### *3.7.2. Synthesis and characterization*

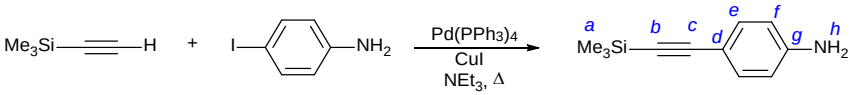


**Preparation of 4-(trimethylsilylethynyl)aniline.**[26] In a 100 mL Schlenk flask 4-iodoaniline (4.2 g, 20 mmol), trimethylsilylacetylene (3.5 mL, 2.4 g, 25 mmol), $Pd(PPh_3)_4$ (1.184 g, 1.025 mmol) and CuI (0.239 g, 1.256 mmol) were dissolved in anhydrous degassed $NEt_3$ (100 mL). The resulting solution was heated at reflux temperature overnight. Upon completion of the reaction, the black mixture was taken to dryness under reduced pressure and the residue was purified by silica gel column chromatography (hexane:$CH_2Cl_2$) (*1:1*). Removal of solvent from the main fraction yielded a colourless oil that crystallized on standing. Yield 2.2 g, 12 mmol, 60%.$^1$H NMR (400 MHz, $CDCl_3$) δ 7.27 (d, *J* = 9 Hz, 2H, *e*), 6.57 (d, *J* = 9 Hz, 2H, *f*), 3.79 (s *br*., 2H, *h*), 0.22 (s, 9H, *a*).

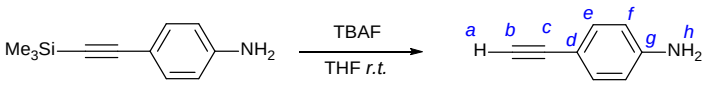


**Preparation of 4-ethynylaniline.**[26] To a solution of 4-(trimethylsilylethynyl) aniline (2.12 g, 11.2 mmol) in THF (50 mL), TBAF (1M in THF, 12 mL ~12 mmol) was added and the resulting black solution stirred at room temperature overnight. The solution was then taken to dryness under reduced pressure and the remaining black oil was re-dissolved in $CH_2Cl_2$ (50 mL). The organic phase was washed with water (2×50 mL), brine (1×50 mL) and dried over $MgSO_4$. Removal of solvent of the organic phase yielded the pure product as a light-brown solid. Yield 1.3 g, 11.1 mmol, 99%. $^1$H NMR (400 MHz, $CDCl_3$) δ 7.29 (d, *J* = 9 Hz, 2H, *e*), 6.59 (d, *J* = 9 Hz, 2H, *f*), 3.82 (s, 2H, *h*), 2.95 (s, 1H, *a*). $^{13}$C{$^1$H} NMR (101 MHz, $CDCl_3$) δ 147.2 (*g*), 133.8 (*e*), 114.7 (*f*), 111.4 (*d*), 84.5, 75.0 (*b/c*). IR (*nujol*) cm$^{-1}$: 3485, 3388 (m) ν($NH_2$); 3259 (m) ν($C_{sp}$–H); 2097 (w) ν(C≡C).

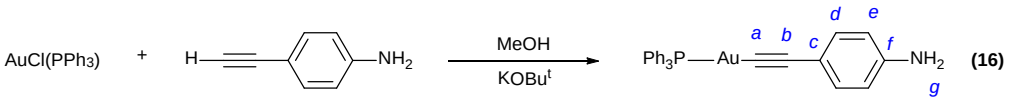


**Preparation of 16.** To a Schlenk flask charged with KOBu$^t$ (0.030 g, 0.26 mmol), 4-ethynylaniline (0.024 g, 0.20 mmol) and 5 mL of MeOH, $AuCl(PPh_3)$ (0.10 g, 0.21 mmol) was added. The orange suspension was stirred in the absence of light at room temperature for 2 hours. The precipitate was collected by filtration and washed thoroughly with hexane. The solids were extracted with $Et_2O$ (2 × 5 mL). The white precipitate formed upon addition of hexane to the combined ether extracts was collected by filtration, washed with hexane (5 mL) and dried in air (0.080 g, 0.14 mmol, 70%). $^1$H NMR (400 MHz, $CDCl_3$) δ 7.47 (m, 15H, *PPh*$_3$), 7.33 (d, *J* = 9 Hz, 2H, *d*), 6.56 (d, *J* = 9 Hz, 2H, *e*), 3.68 (br. s, 2H, *g*). $^{31}$P{$^1$H} NMR (162 MHz, $CDCl_3$) δ 41.6 (s, *PPh*$_3$). MS (ESI)$^+$ *m/z* (%) 576.0 (10, $[M+H]^+$), 1033.8 (100, $[2M\text{-}C_2PhNH_2]^+$). IR (*nujol*) cm$^{-1}$: 3439, 3349 ν($NH_2$); 2213 ν(C≡C).

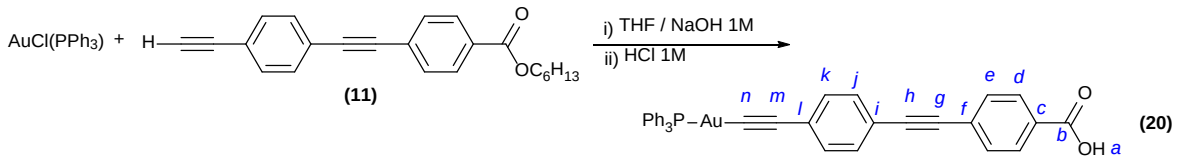


**Preparation of 20.** In a 25 mL round bottom flask, chloro(triphenylphosphine) gold (I) (0.102 g, 0.206 mmol) and **11** (0.069 g, 0.209 mmol) were dissolved in THF (10 mL). To that solution, NaOH (1M, 5 mL) was added. The mixture was allowed to stir overnight at room temperature. The organic solvent was removed under vacuum and the remaining aqueous solution was acidified to pH ~2 by addition of HCl (1M). The off-white precipitate was isolated by centrifugation, washed with acetone (10 mL), and dried under vacuum. Yield 0.098 g, 0.139 mmol, 68%. $^{1}$H NMR (600 MHz, DMSO-d$_6$) δ 13.17 (*br.* s, 1H, *a*), 7.95 (d, *J* = 8 Hz, 2H, *d*), 7.62 (d, *J* = 8 Hz, 2H, *e*), 7.63-7.51 (m, 15H, *PPh$_3$*), 7.48 (d, *J* = 8 Hz, 2H, *k/j*), 7.37 (d, *J* = 8 Hz, 2H, *k/j*). $^{13}$C{$^{1}$H} NMR (151 MHz, DMSO-d$_6$) δ 167.12 (*b*), 134.35 (d, *J* = 14 Hz, *PPh$_3$*), 132.43 (*br.* s, *PPh$_3$*), 132.12 (*k/j*), 132.02 (*k/j*), 131.92 (*e*), 131.06 (*c/f/g*), 130.08 (d, *J* = 11 Hz, *PPh$_3$*), 130.00 (*d*), 129.62 (d, *J* = 56 Hz, *PPh$_3$*), 126.98 (*c/f/g*), 126.46, 120.20, 102.98, 92.39 (*m/l/i/h*), 90.30 (*c/f/g*), (*n*, not observed). $^{31}$P{$^{1}$H} NMR (243 MHz, DMSO-d$_6$) δ 41.5 (s, *PPh$_3$*). MS$^{+}$ (ASAP) *m/z* (%) 705.1 (4, [M+H]$^{+}$), 263.1 (100, [M−AuPPh$_3$+O]$^{+}$). IR (*nujol*) cm$^{-1}$: 3391 (br. s) ν(COO−H); 2216 (w); 2108 (w) ν(C≡C); 1682 (s) ν(C=O).

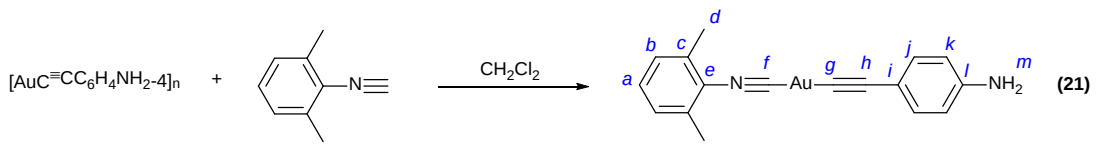


**Preparation of 21.** To a suspension of [AuC≡CC$_6$H$_4$NH$_2$-4]$_n$ (0.075 g, 0.24 mmol), in $CH_2Cl_2$ (10 mL) 2,6-dimethylphenyl isocyanide (0.030 g, 0.25 mmol) was added. The mixture was stirred at room temperature for 30 minutes. Upon complete dissolution of the solids suspended, the mixture was concentrated by solvent evaporation (~ 2 mL) and the

desired product precipitated upon hexane addition. The light-brown powder was collected by filtration, washed thoroughly with hexane and ether (2 mL) and dried in air (0.075 g, 0.17 mmol, 70%). $^{1}$H NMR (400 MHz, $CDCl_3$) δ 7.35 – 7.27 (m, 3H, *a-b*), 7.16 (d, *J* = 8 Hz, 2H, *j*), 6.56 (d, *J* = 8 Hz, 2H, *k*), 3.70 (s, 2H, *m*), 2.43 (s, 6H, *d*). $MS^{+}$ (ESI) *m/z* (%): 445.6 (100, $[M+H]^{+}$). IR (*nujol*) $cm^{-1}$: 3453, 3352 (*m*) ν($NH_2$); 2196 (*s*) ν(N≡C); 2109 (*w*) ν(C≡C).

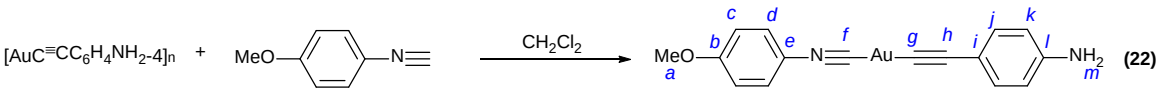

(22)

**Preparation of 22.** To a suspension of $[AuC{\equiv}CC_6H_4NH_2\text{-}4]_n$ (0.051 g, 0.16 mmol), in $CH_2Cl_2$ (10 mL) 4-methoxyphenyl isocyanide (0.024 g, 0.18 mmol) was added. The mixture was stirred at room temperature for 30 minutes. Upon complete dissolution of the solids suspended, the mixture was concentrated by solvent evaporation (~2 mL) and the desired product was precipitated upon addition of hexane. The light-brown powder was collected by filtration, washed thoroughly with hexane and ether (2 mL) and dried in air (0.049 g, 0.11 mmol, 69%). $^{1}$H NMR (600 MHz, $CDCl_3$) δ 7.45 (d, J = 9 Hz, 2H, *d*), 7.29 (d, J = 9 Hz, 2H, *k*), 6.94 (d, J = 9 Hz, 2H, *c*), 6.56 (d, J = 9 Hz, 2H, *j*), 3.85 (s, 3H, *a*), 3.70 (s, 2H, *m*). $^{13}C\{^{1}H\}$ NMR (151 MHz, $CDCl_3$) δ 161.52 (*b*), 145.50 (*g/h/i/l*), 133.73 (*k*), 128.48 (*d*), 119.03 (*g/h/i/l*), 116.91 (*e*), 115.19 (*c*), 114.58 (*j*), 114.21 (*g/h/i/l*), 104.52 (*g/h/i/l*), 55.78 (*a*). MS $(ESI)^{+}$ *m/z* (%) 447.6 (100, $[M+H]^{+}$). IR (*nujol*) $cm^{-1}$: 3439, 3354 ν($NH_2$) (*m*); 2214 ν(N≡C) (*s*); 2210 ν(C≡C) (*w*). Elemental analysis % calcd. (found): C 43.06 (42.92); H 2.94 (2.94); N 6.28 (6.39).

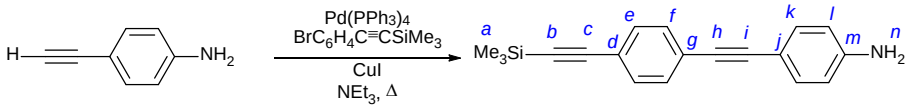


**Preparation of $Me_3SiC{\equiv}CC_6H_4C{\equiv}CC_6H_4NH_2$.**[26] To a 50 mL Schlenk flask charged with $NEt_3$ (40 mL), 4-ethynylaniline (1.25 g, 10.7 mmol), $BrC_6H_4C{\equiv}CSiMe_3$ (2.71 g, 10.7 mmol), $Pd(PPh_3)_4$ (0.610 g, 0.528 mmol) and CuI (0.118 g, 0.621 mmol) were added. The resulting suspension was heated at reflux overnight. The black mixture was taken to dryness under reduced pressure and the residue purified by silica gel column chromatography (hexane:$CH_2Cl_2$) (*1:1*). Yield 2.5 g, 8.6 mmol, 80%. $^1$H NMR (400 MHz, $CDCl_3$) δ 7.41 (s, 4H, *e/f*), 7.32 (d, *J* = 9 Hz, 4H, *k*), 6.63 (d, *J* = 9 Hz, 4H, *l*), 3.83 (br.s, 2H, *n*), 0.25 (s, 9H, *a*). IR (*nujol*) cm$^{-1}$: 3483, 3395 (m) ν($NH_2$); 2153, 2144 (w) ν(C≡C).

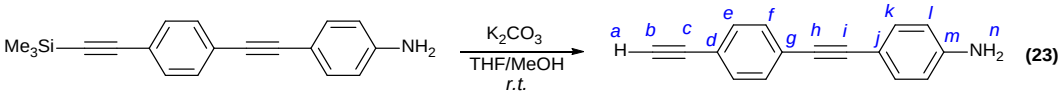


**(23)**

**Preparation of 23.**[26] The base, $K_2CO_3$ (3.0 g, 21.7 mmol) was added to a solution of $Me_3SiC{\equiv}CC_6H_4C{\equiv}CC_6H_4NH_2$ (2.41 g, 7.14 mmol) in THF:MeOH (1:1) (50 mL) in a 100 mL round bottomed flask. The mixture was stirred at room temperature overnight. The orange precipitate was collected by filtration and washed thoroughly with water and acetone. The orange product was used in subsequent reactions without further purification. Yield 1.4 g, 6.4 mmol, 90%. $^1$H NMR (400 MHz, $CDCl_3$) δ 7.52 – 7.42 (m, 4H, *e/f*), 7.33 (d, *J* = 9 Hz, 2H, *k*), 6.64 (d, *J* = 9 Hz, 2H, *l*), 3.85 (s, 2H, *n*), 3.15 (s, 1H, *a*). IR (*nujol*) cm$^{-1}$: 3482 (w), 3389 (m) ν($NH_2$); 3249 (m) ν($C_{sp}$–H); *not observed* ν(C≡C).

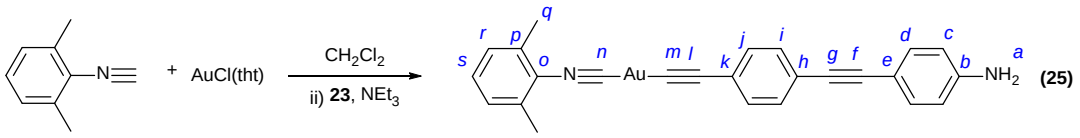


**(25)**

**Preparation of 25.** To a Schlenk flask charged with a solution of AuCl(tht) (0.20 g, 0.62 mmol) in $CH_2Cl_2$ (10 mL), 2,6-dimethylphenyl isocyanide (0.08 g, 0.62 mmol) was added. The clear solution was allowed to stir at room temperature overnight. To the

reaction mixture $NEt_3$ (0.5 mL) and **23** (0.14 g, 0.64 mmol) were added and allowed to react overnight. The precipitate was removed by filtration and the filtrate taken to dryness under reduced pressure. The orange residue was purified by silica gel column chromatography using hexane:$CH_2Cl_2$ (1:1) as the eluent. Removal of solvent from the main fraction yielded the pure product as an orange solid. Yield 0.20 g, 0.37 mmol, 60%. $^1$H NMR (400 MHz, $CDCl_3$) δ 7.41 (d, *J* = 9 Hz, 2H, *i*/*j*), 7.36 (d, *J* = 9 Hz, 2H, *i*/*j*), 7.34-7.31 (m, 3H, *d*/*s*), 7.16 (br. d, *J* = 8 Hz, 2H, *r*), 6.63 (d, *J* = 9 Hz, 2H, *c*), 3.82 (br. s, 2H, *a*), 2.44 (s, 6H, *q*) $^{13}$C{$^1$H} NMR (126 MHz, $CDCl_3$) δ 160.1 (t, *J* = 24 Hz, *n*), 136.4 (*p*), 133.1, 132.5, 131.1 (*d*/*i*/*j*), 131.00 (*s*), 128.6 (*r*), 124.5 (t, *J* = 13 Hz, *o*), 124.3 (*m*/*l*), 124.0, 122.5 (*h*/*k*), 114.9 (*c*), 112.8 (s), 104.1 (*m*/*l*), 91.6, 87.6 (*g*/*f*), 18.8 (*q*). MS (ESI)$^+$ *m*/*z* (%): 586.2 (100, [M+H+MeCN]$^+$). IR ($CH_2Cl_2$) cm$^{-1}$: 3485, 3394 (br. w) ν($NH_2$); 2208 (*s*) ν(N≡C).

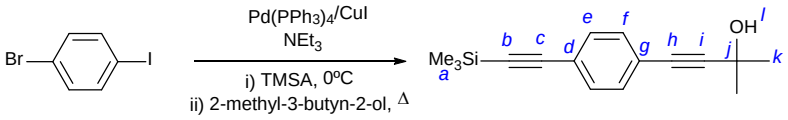


**Preparation of $Me_3SiC{\equiv}CC_6H_4C{\equiv}CC(Me)_2OH$.**[22] To a 500 mL Schlenk flask immersed in an ice bath and charged with $NEt_3$ (450 mL), 1-bromo-4-iodobenzene (30.01 g, 106.1 mmol), $Pd(PPh_3)_4$ (6.12 g, 5.30 mmol) and CuI (1.01 g, 5.30 mmol) were added. To the cooled suspension, trimethylsilylacetylene (16.5 mL, 11.4 g, 116 mmol) was added in small portions over an hour. After stirring the solution at 0 ºC for 6 h, trimethylsilylacetylene excess was removed under reduced pressure keeping the reaction vessel in the ice bath. After refilling the vessel with $N_2$, 2-methyl-3-butyn-2-ol (11.3 mL, 9.81 g, 116 mmol) was added and the reaction mixture was taken out of the ice bath and heated at reflux overnight. The reaction mixture was then taken to dryness under reduced pressure, and the resulting black residue was re-dissolved in $CH_2Cl_2$ and adsorbed onto

silica for further silica gel column chromatography (hexane). The pure product was collected upon solvent evaporation of the main fraction as a yellow powder. Yield 21 g, 83 mmol, 78%. $^{1}$H NMR (400 MHz, $CDCl_3$) δ 7.37 (d, *J* = 9 Hz, 2H, *e*), 7.31 (d, *J* = 9 Hz, 2H, *f*), 1.32 (s, 6H, *k*), 2.01 (s, 1H, *l*), 0.25 (s, 9H, *a*). $^{13}$C{$^{1}$H} NMR (101 MHz, $CDCl_3$) δ 131.8, 131.5 (*e/f*), 123.0, 122.9 (*d/g*), 104.7 (*b*), 96.2, 95.8, 81.8 (*c/h/i*), 65.7 (*j*), 31.51 (*k*), 0.0 (*a*). MS$^{+}$ (ASAP) *m/z* (%): 241.10 (100, [M-OH]$^{+}$).

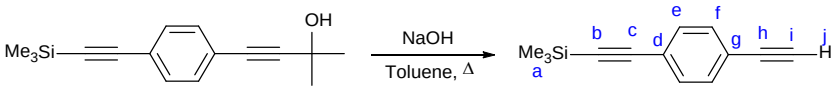


**Preparation of $Me_3SiC{\equiv}CC_6H_4C{\equiv}CH$.**[22] A 250 mL round bottom flask, fitted with a nitrogen purge, reflux condenser and bubbler was charged with sodium hydroxide (0.63 g, 0.16 mmol), Me3SiC≡CC6H4C≡CC(Me)$_2$OH (3.25 g, 12.6 mmol) and anhydrous toluene (150 mL). The solution was heated at reflux for 30 min whilst nitrogen was bubbled through it. Upon completion of the reaction, the red solution was poured into water, and the organic phase was washed with water (2 × 150 mL) and brine (1 × 150 mL), and dried over $MgSO_4$. The solvent was removed under reduced pressure and the residue was purified by silica gel column chromatography using hexane:$CH_2Cl_2$ (9:1) as the eluent. Removal of solvent from the main fraction yielded the pure product as a white solid. Yield 1.83 g, 9.23 mmol, 73%. $^{1}$H NMR (400 MHz, $CDCl_3$) δ 7.41 (s, 4H, *e/f*), 3.16 (s, 1H, *j*), 0.25 (s, 9H, *a*). $^{13}$C{$^{1}$H} NMR (101 MHz, $CDCl_3$) δ 132.1, 132.0 (*e/f*), 123.7, 122.2 (*d/g*), 104.5 (*b*), 96.6 (*c*), 83.3 (*h*), 79.1 (*i*), 0.0 (*a*). MS$^{+}$ (ASAP) *m/z* (%): 183.05 (100, [M-$CH_3$]$^{+}$), 198.07 (24.4, [M]$^{+}$). IR (*nujol*) cm$^{-1}$: 3311 (m) ($C_{sp}$–H); 2159 (m) ν(C≡C).

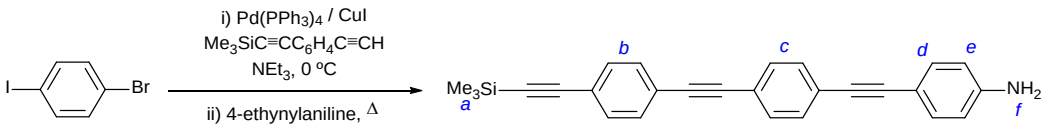


**Preparation of 27.**[26] To a 100 mL Schlenk flask charged with $NEt_3$ (70 mL), immersed in an ice bath, $Me_3SiC{\equiv}CC_6H_4C{\equiv}CH$ (0.15 g, 0.76 mmol), $Pd(PPh_3)_4$ (0.04 g, 0.04 mmol) and CuI (0.01 g, 0.05 mmol) were added. To the cooled mixture, 1-bromo-4-iodobenzene (0.22 g, 0.78 mmol) was added. After stirring the solution at 0 ºC for 5 h, 4-ethynylaniline (0.09 g, 0.77 mmol) was added and the reaction mixture was taken out of the ice bath and heated at reflux overnight. Upon completion of the reaction, the precipitate was removed by filtration and the yellow filtrate taken to dryness under reduced pressure. The resulting yellow residue was then purified by column chromatography in neutral alumina (hexane:EtOAc) (6:4). The orange solid obtained from taking the appropriate fraction to dryness was crystallised from hot toluene giving the pure product as a yellow powder. Yield 0.09 g, 0.23 mmol, 30%. $^1$H NMR (400 MHz, $CDCl_3$) δ 7.46 (s, 4H, *b*), 7.44 (s, 4H, *c*), 7.34 (d, *J* = 9 Hz, 2H, *d*), 6.64 (d, *J* = 9 Hz, 2H, *e*), 3.85 (s *br.*, 2H, *f*), 0.25 (s, 9H, *a*). IR (*nujol*) cm$^{-1}$: 3449 (w), 3366 (m) *ν*(N−H); 2201 (m), 2140 (s) *ν*(C≡C). MS$^+$ (ASAP) *m/z* (%): 389.2 (100, $[M]^+$).

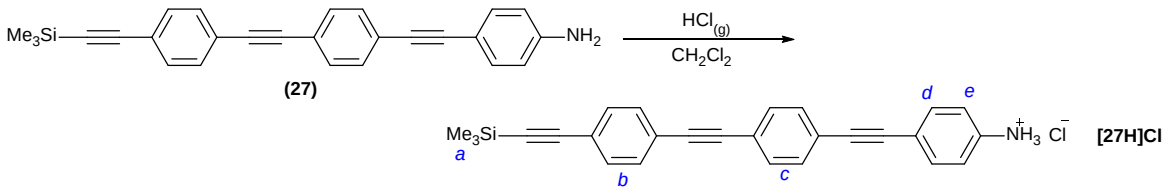


**Preparation of [27H]Cl.** In 25 mL Schlenk flask charged with $CH_2Cl_2$ (20 mL), **27** (0.026 g, 0.067 mmol) was added. The yellow suspension was then stirred vigorously for 3 hours under an $HCl_{(g)}$ atmosphere (generated by drop wise addition of $H_2SO_4$ to NaCl and passed through the reaction vessel by connecting it to the $HCl_{(g)}$ reactor with PVC tubing) at room temperature. The precipitate was collected by filtration and the brown precipitate

was washed with $CH_2Cl_2$ (2 × 5 mL), $Et_2O$ (2 × 5 mL), and dried in air. The pure product was collected as a brown powder. Yield 0.024 g, 0.056 mmol, 84 %. $^1$H NMR (400 MHz, $CD_3OD$) δ 7.67 (d, *J* = 8 Hz, 2H, *e*), 7.54 (s, 4H, *b*), 7.49 (d, *J* = 8 Hz, 2H, *c*), 7.44 (d, *J* = 8 Hz, 2H, *c*), 7.38 (d, *J* = 8 Hz, 2H, *d*), 0.23 (s, 9H, *a*). IR (*nujol*) cm$^{-1}$: 2650-2400 (s) *v*(N−H); 2207 (w), 2153 (m) *v*(C≡C). MS$^+$ (ASAP) *m/z* (%): 389.1 (100, [M-H]$^+$); 390.1 (81.6, [M]$^+$).

## 3.8. References


1. (a) McCreery, R. L.; Bergren, A. J., *Adv. Mater.*, **2009**, *21*, 4303-4322; (b) Nichols, R. J.; Haiss, W.; Higgins, S. J.; Leary, E.; Martin, S.; Bethell, D., *Phys. Chem. Chem. Phys.*, **2010**, *12*, ; (c) Joachim, C.; Ratner, M. A., *Proc. Natl. Acad. Sci. U.S.A.*, **2005**, *102*, 8801-8808; (d) Nitzan, A.; Ratner, M. A., *Science*, **2003**, *300*, 1384-1389; (e) Joachim, C.; Gimzewski, J. K.; Aviram, A., *Nature*, **2000**, *408*, 541-548.
2. (a) Moore, G. E., *Electronics Magazine*, **1965**, *38*, 8; (b) Aviram, A.; Ratner, M. A., *Chem. Phys. Lett.*, **1974**, *29*, 277-283.
3. Uson, R., *Synth. React. Inorg. Met.-Org. Chem.*, **1978**, *8*, 503-504.
4. (a) Mingos, D. M. P.; Vilar, R.; Rais, D., *J. Organomet. Chem.*, **2002**, *641*, 126-133; (b) Buschbeck, R.; Low, P. J.; Lang, H., *Coord. Chem. Rev.*, **2011**, *255*, 241-272.
5. (a) Vicente, J.; Chicote, M.-T.; Alvarez-Falcón, M. M.; Fox, M. A.; Bautista, D., *Organometallics*, **2003**, *22*, 4792-4797; (b) Koshevoy, I. O.; Karttunen, A. J.; Tunik, S. P.; Haukka, M.; Selivanov, S. I.; Melnikov, A. S.; Serdobintsev, P. Y.; Khodorkovskiy, M. A.; Pakkanen, T. A., *Inorg. Chem.*, **2008**, *47*, 9478-9488; (c) Koshevoy, I. O.; Karttunen, A. J.; Tunik, S. P.; Haukka, M.; Selivanov, S. I.; Melnikov, A. S.; Serdobintsev, P. Y.; Pakkanen, T. A., *Organometallics*, **2009**, *28*, 1369-1376.
6. (a) Yam, V. W.-W.; Kam-Wing Lo, K.; Man-Chung Wong, K., *J. Organomet. Chem.*, **1999**, *578*, 3-30; (b) Che, C.-M.; Chao, H.-Y.; Miskowski, V. M.; Li, Y.; Cheung, K.-K., *J. Am. Chem. Soc.*, **2001**, *123*, 4985-4991; (c) Chao, H.-Y.; Lu, W.; Li, Y.; Chan, M. C. W.; Che, C.-M.; Cheung, K.-K.; Zhu, N., *J. Am. Chem. Soc.*, **2002**, *124*, 14696-14706; (d) Shakirova, J. R.; Grachova, E. V.; Gurzhiy, V. V.; Koshevoy, I. O.; Melnikov, A. S.; Sizova, O. V.; Tunik, S. P.; Laguna, A., *Dalton Trans.*, **2012**, *41*, 2941-2949; (e) Camara, J.; Crespo, O.; Gimeno, M. C.; Koshevoy, I. O.; Laguna, A.; Ospino, I.; Smirnova, E. S.; Tunik, S. P., *Dalton Trans.*, **2012**, *41*, 13891-13898.
7. (a) Hurst, S. K.; Lucas, N. T.; Cifuentes, M. P.; Humphrey, M. G.; Samoc, M.; Luther-Davies, B.; Asselberghs, I.; Van Boxel, R.; Persoons, A., *J. Organomet. Chem.*, **2001**, *633*, 114-124; (b) McDonagh, A. M.; Lucas, N. T.; Cifuentes, M. P.; Humphrey, M. G.; Houbrechts, S.; Persoons, A., *J. Organomet. Chem.*, **2000**, *605*,

193-201; (c) Hurst, S. K.; Cifuentes, M. P.; McDonagh, A. M.; Humphrey, M. G.; Samoc, M.; Luther-Davies, B.; Asselberghs, I.; Persoons, A., *J. Organomet. Chem.*, **2002**, *642*, 259-267.

8. (a) Man, W. Y.; Bock, S.; Zaitseva, N. N.; Bruce, M. I.; Low, P. J., *J. Organomet. Chem.*, **2011**, *696*, 2172-2176; (b) Hashmi, A. S. K., *Chem. Rev.*, **2007**, *107*, 3180-3211; (c) Panda, B.; Sarkar, T. K., *Synthesis*, **2013**, *45*, 817-829; (d) González-Arellano, C.; Abad, A.; Corma, A.; García, H.; Iglesias, M.; Sánchez, F., *Angew. Chem.*, **2007**, *119*, 1558-1560.
9. Hogarth, G.; Álvarez-Falcón, M. M., *Inorg. Chim. Acta*, **2005**, *358*, 1386-1392.
10. Bhargava, S. K.; Kitadai, K.; Mirzadeh, N.; Privér, S. H.; Takahashi, M.; Wagler, J., *J. Organomet. Chem.*, **2010**, *695*, 1787-1793.
11. (a) Vicente, J.; Arcas, A.; Mora, M.; Solans, X.; Font-Altaba, M., *J. Organomet. Chem.*, **1986**, *309*, 369-378; (b) Levason, W.; Matthews, M. L.; Reid, G.; Webster, M., *Dalton Trans.*, **2004**, 554-561; (c) Bojan, V. R.; Fernández, E. J.; Laguna, A.; López-de-Luzuriaga, J. M.; Monge, M.; Olmos, M. E.; Puelles, R. C.; Silvestru, C., *Inorg. Chem.*, **2010**, *49*, 5530-5541.
12. (a) Ferrer, M.; Mounir, M.; Rodríguez, L.; Rossell, O.; Coco, S.; Gómez-Sal, P.; Martín, A., *J. Organomet. Chem.*, **2005**, *690*, 2200-2208; (b) Hashmi, A. S. K.; Hengst, T.; Lothschütz, C.; Rominger, F., *Adv. Synth. Catal.*, **2010**, *352*, 1315-1337; (c) Chico, R.; Castillejos, E.; Serp, P.; Coco, S.; Espinet, P., *Inorg. Chem.*, **2011**, *50*, 8654-8662.
13. Kilpin, K. J.; Horvath, R.; Jameson, G. B.; Telfer, S. G.; Gordon, K. C.; Crowley, J. D., *Organometallics*, **2010**, *29*, 6186-6195.
14. Vicente, J.; Chicote, M.-T.; Alvarez-Falcón, M. M.; Jones, P. G., *Organometallics*, **2005**, *24*, 5956-5963.
15. Coates, G. E.; Parkin, C., *J. Chem. Soc*, **1962**, 3220-3226.
16. Abu-Salah, O. M.; Al-Ohaly, A. R., *Inorg. Chim. Acta*, **1983**, *77*, L159-L160.
17. (a) Cross, R. J.; Davidson, M. F., *J. Chem. Soc., Dalton Trans.*, **1986**, 411-414; (b) Bruce, M.; Horn, E.; Matisons, J.; Snow, M., *Aust. J. Chem.*, **1984**, *37*, 1163-1170.
18. (a) Packheiser, R.; Lang, H., *Inorg. Chim. Acta*, **2011**, *366*, 177-183; (b) Kuchison, A. M.; Wolf, M. O.; Patrick, B. O., *Inorg. Chem.*, **2010**, *49*, 8802-8812.
19. (a) Wang, N.; Ko, S.-B.; Lu, J.-S.; Chen, L. D.; Wang, S., *Chem. Eur. J.*, **2013**, *19*, 5314-5323; (b) Packheiser, R.; Rüffer, T.; Ecorchard, P.; Lang, H., *Z. Anorg. Allg. Chem.*, **2010**, *636*, 2607-2616.
20. Mingos, D. M. P.; Yau, J.; Menzer, S.; Williams, D. J., *Angew. Chem. Int. Ed. (English)*, **1995**, *34*, 1894-1895.
21. (a) Uson, R.; Laguna, A.; Laguna, M.; Briggs, D. A.; Murray, H. H.; Fackler., J. P., (Tetrahydrothiophene)gold (I) or gold (III) complexes. In *Inorg. Synth.*, 2007; Vol. 26, pp 85-91; (b) Bruce, M. I.; Nicholson, B. K.; Shawkataly, O. B.; Shapley, J. R.; Henly, T., Synthesis of Gold-Containing Mixed-Metal Cluster Complexes. In *Inorg. Synth.*, John Wiley & Sons, Inc.: 2007; pp 324-328.
22. Nguyen, P.; Yuan, Z.; Agocs, L.; Lesley, G.; Marder, T. B., *Inorg. Chim. Acta*, **1994**, *220*, 289-296.

23. (a) Schmidbaur, H.; Schier, A., *Chem. Soc. Rev.*, **2008**, *37*, 1931-1951; (b) Liang, T.-C.; Lin, H.-C., *J. Mater. Chem.*, **2009**, *19*, 4753-4763.
24. (a) Boyen, H.-G.; Kästle, G.; Weigl, F.; Koslowski, B.; Dietrich, C.; Ziemann, P.; Spatz, J. P.; Riethmüller, S.; Hartmann, C.; Möller, M.; Schmid, G.; Garnier, M. G.; Oelhafen, P., *Science*, **2002**, *297*, 1533-1536; (b) Liu, G.; Luais, E.; Gooding, J. J., *Langmuir*, **2011**, *27*, 4176-4183; (c) Fratoddi, I.; Venditti, I.; Battocchio, C.; Polzonetti, G.; Cametti, C.; Russo, M. V., *Nanoscale Res. Lett.*, **2011**, *6*, 98.
25. (a) Ballesteros, L. M.; Martín, S.; Pera, G.; Schauer, P. A.; Kay, N. J.; López, M. a. C.; Low, P. J.; Nichols, R. J.; Cea, P., *Langmuir*, **2011**, *27*, 3600-3610; (b) Pera, G.; Martín, S.; Ballesteros, L. M.; Hope, A. J.; Low, P. J.; Nichols, R. J.; Cea, P., *Chem. Eur. J.*, **2010**, *16*, 13398-13405.
26. Lu, Q.; Liu, K.; Zhang, H.; Du, Z.; Wang, X.; Wang, F., *ACS Nano*, **2009**, *3*, 3861-3868.

# 4. SYNTHESIS AND CHARACTERIZATION OF ETHYNYL-RUTHENIUM COMPLEXES

## 4.1. Abstract

A novel and convenient route towards the synthesis bis(ethynyl) complexes *trans*-$Ru(C{\equiv}CR)_2(dppe)_2$ [**30**, R = $C_6H_4Me$ (**a**), $C_6H_4C_5H_{11}$ (**b**), $C_6H_4OMe$ (**c**), $C_6H_4CO_2Me$ (**d**), $C_6H_4NO_2$ (**e**), $C_6H_4C{\equiv}CSiMe_3$ (**f**), $C_6H_4C{\equiv}CBu^t$ (**g**), $C_6H_4NH_2$ (**h**), $C{\equiv}CSiMe_3$ (**j**)] and unsymmetrically substituted *trans*-$Ru(C{\equiv}CR^1)(C{\equiv}CR^2)(dppe)_2$ (**31**: $R^1$ = $C_6H_4C{\equiv}CSiMe_3$, $R^2$ = $C_6H_4NH_2$; **32**: $R^1$ = $C_6H_4CO_2Me$, $R^2$ = $C_6H_4NH_2$; **33**: $R^1$ = $C_6H_4CO_2Me$, $R^2$ = $C_6H_4OMe$) prepared from reactions of *trans*-$RuCl(C{\equiv}CR^1)(dppe)_2$ **29 (a - h, j)** with terminal alkynes in $CH_2Cl_2$ solutions containing 1,8-diazabicycloundec-7-ene (DBU) and $TlBF_4$ is described. Desilylation of **29f** and **30f** afford **29i** and **30i** ($R^1$ = $C_6H_4C{\equiv}CH$-4) respectively. In addition, the synthesis of the mono-ethynyl complex **29k** *trans*-$RuCl(C{\equiv}CPy\text{-}4)(dppe)_2$ (Py = pyridine), is reported.

The molecular structures of **30a**, **30b**, **30c**, **30d, 30f**, **30g, 30h** and **30i** have been determined and are reported here together with the structures of the mono ethynyl complexes **29f**, **29g**, **29i**, **29j** and **29k** and compared with related compounds from the literature. Complexes **30(a - j)**, **31**, **32** and **33** undergo one reversible electrochemical oxidation process, which can be attributed to depopulation of an orbital with significant ethynyl ligand character. The one-electron oxidation products $[\mathbf{30f}]^{\bullet+}$, $[\mathbf{30h}]^{\bullet+}$, $[\mathbf{31}]^{\bullet+}$ and $[\mathbf{32}]^{\bullet+}$ exhibit a series of NIR absorption between 15000-5000 $cm^{-1}$ which on the basis of TD-DFT calculations cannot be attributed to a single, static lowest energy molecular structure. Rather, the transitions that are responsible for the absorption band envelope have varying degrees of LMCT, ethynyl-ligand IVCT or MLCT character that depends not only

on the nature of the $R^n$ groups but also on the ensemble of thermally populated molecular conformers in solution with various relative orientations of the metal fragment and arylethynyl moieties.

## 4.2. Introduction

Complexes of the general form *trans*-$Ru(C{\equiv}CR)_2(dppe)_2$ and unsymmetrically substituted derivatives *trans*-$Ru(C{\equiv}CR^1)(C{\equiv}CR^2)(dppe)_2$ are emerging as important structural and electronic moieties in a range of molecular electronic[1] (*see* Chapter 5) and electro-optic[2] applications. These materials properties arise due in no small part to the efficient mixing of the organic ethynyl π-electron system with the central metal *d*-orbitals, which leads polymetallic systems with highly delocalized electronic structures.[3] One-pot methods for the preparation of complexes *trans*-$Ru(C{\equiv}CR)_2(dppe)_2$ are often based on activation of *cis*-$RuCl_2(dppe)_2$ with $NaPF_6$ in the presence of the precursor alkyne and a suitable base, usually $NEt_3$, over reaction periods that can extend for several days (Scheme 4-1).[4] Bis(ethynyl) complexes *trans*-$Ru(C{\equiv}CR)_2(dppe)_2$ may also be prepared in a two-step method via intermediate mono-ethynyl *trans*-$RuCl(C{\equiv}CR)(dppe)_2$ or vinylidene $[RuCl(C{=}CHR)(dppe)_2]^+$ complexes through a sequence of deprotonation (in the case of vinylidenes), halide abstraction, alkyne coordination, rearrangement and deprotonation (Scheme 4-1, *a*).[4a, 5]

Alternatively, ammine complex intermediates, $[Ru(C{\equiv}CR)(NH_3)(dppe)_2]^+$, which can be prepared from either *trans*-$RuCl(C{\equiv}CR)(dppe)_2$, $NH_4PF_6$ and $NEt_3$ (Scheme 4-1, *b*)[6] or *trans*-$Ru(C{\equiv}CR)_2(dppe)_2$ and $NH_4PF_6$ (Scheme 4-1, *c*)[5c] may be employed as precursors to *trans*-bis(ethynyl) complexes. The latter procedures are useful alternatives to the preparation of unsymmetrically substituted derivatives generally prepared from the

appropriate vinylidenes (Scheme 4-1, *d*)[7] and similar strategies have been employed with good effect for the preparation of Os analogues.[6]

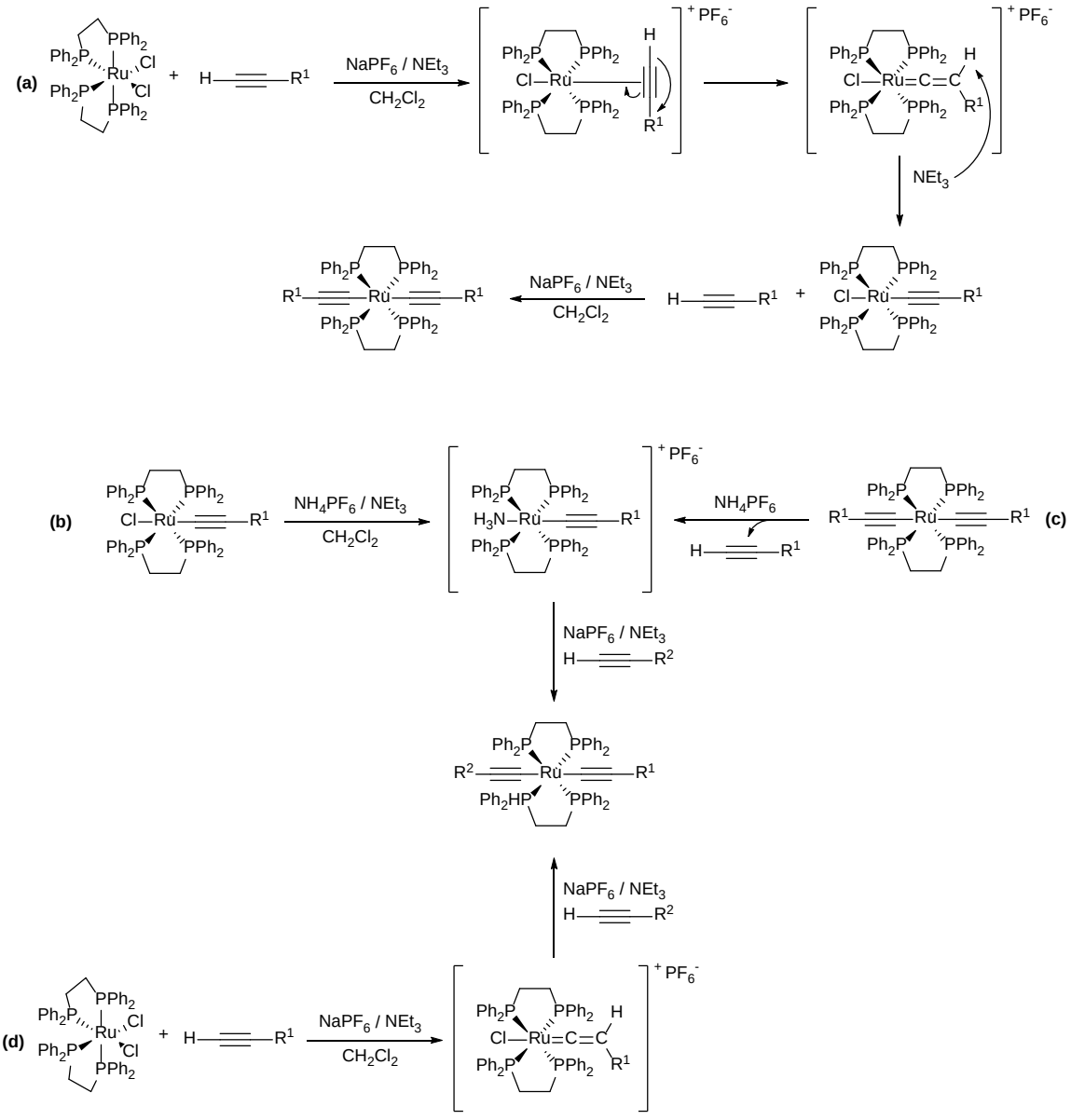


**Scheme 4-1.** *The conceptual steps in the preparation of: a) trans-Ru(C≡CR$^1$)$_2$(dppe)$_2$ from cis-RuCl$_2$(dppe)$_2$; b) trans-Ru(C≡CR$^1$)(C≡CR$^2$)(dppe)$_2$ from trans-RuCl(C≡R$^1$)(dppe)$_2$ via intermediate ammine complexes; c) trans-Ru(C≡CR$^1$)(C≡CR$^2$)(dppe)$_2$ from trans-Ru(C≡CR$^1$)$_2$(dppe)$_2$ via intermediate ammine complexes; d) trans-Ru(C≡CR$^1$)(C≡CR$^2$)(dppe)$_2$ via intermediate vinylidene complexes [RuCl(C=CHR)(dppe)$_2$]PF$_6$.*

Here were report some further explorations of the synthetic routes to complexes *trans*-Ru(C≡CR$^1$)$_2$(dppe)$_2$ and *trans*-Ru(C≡CR$^1$)(C≡CR$^2$)(dppe)$_2$. A combination of spectroelectrochemical (UV-Vis-NIR) and computational (DFT/TDDFT) methods have been used to explore the electronic structure of these species, with the oxidation leading to more or less highly delocalized radical cations, the precise distribution of spin density within which is highly dependent on the relative conformation of the metal centre and ethynyl ligand substituents.

## 4.3. Synthetic considerations

The complex *trans*-RuCl$_2$(dppe)$_2$ is relatively inert to substitution reactions due to the limited lability of the chloride ligands,[8] and efficient preparations of *trans*-Ru(C≡CR)$_2$(dppe)$_2$ complexes from this precursor are generally restricted to transmetallation strategies using trimethyltin alkynes and CuI catalysts.[9] In contrast, one chloride ligand in *cis*-RuCl$_2$(dppe)$_2$ is more labile due to the stronger *trans*-effect of the phosphine ligands. Thus, in the presence of a suitable halide abstracting agent, such as $NaPF_6$, reactions of *cis*-RuCl$_2$(dppe)$_2$ with 1-alkynes, HC≡CR, proceed to give the corresponding vinylidene *trans*-[RuCl(C=CHR)(dppe)$_2$]$^+$ (Scheme 4-1, *a*).[5c] The strongly electron-withdrawing nature of the vinylidene ligand decreases the lability of the remaining chloride, allowing ready isolation of the mono-vinylidene compounds, which can be readily deprotonated to give the analogous ethynyl complexes *trans*-RuCl(C≡CR(dppe)$_2$. The reaction of the five-coordinate complex [RuCl(dppe)$_2$]OTf (**28**) with 1-alkynes, HC≡CR, is now also well known to rapidly give the corresponding vinylidene complexes *trans*-[RuCl(C=CHR)(dppe)$_2$]$^+$.[5b, 10] Thus treatment of a $CH_2Cl_2$ solution of [RuCl(dppe)$_2$]OTf (**28**) with an excess of the appropriate ethynyl ligand and

1,8-diazabicycloundec-7-ene (DBU) gives yellow solutions of ethynyl complexes *trans*-$RuCl(C{\equiv}CR)(dppe)_2$, with the stronger *trans*-effect of the ethynyl ligand leading to an increase in lability of the chloride ligand and permitting access to bis(ethynyl) complexes.[11] The formation of mono- and bis(ethynyl) complexes can be easily monitored by $^{31}P\{^1H\}$ NMR. Typically, the singlet corresponding to the dppe ligands can be observed at under 50 ppm for mono(ethynyl) complexes, and over 50 ppm for the bis(ethynyl) complexes generally shifted downfield by 2-3 ppm with respect to the mono(ethynyl) signal. By way of example, the $^{31}P\{^1H\}$ NMR obtained from the reaction of **28**, with 2 equivalents of electron-withdrawing ligand 1-ethynyl-4-nitrobenzene (**29e**) and electron-donating ligand 4-ethynylaniline (**29h**), in the presence of DBU excess are shown in Figure 4-1. After 30 minutes, in the absence of any halide abstracting agent the reaction with 1-ethynyl-4-nitrobenzene (Figure 4-1, *top*) presents a singlet at ~49 ppm corresponding to the formation of mono-substituted (**29e**), while the reaction with the electron-donating ligand 4-ethynylaniline (Figure 4-1, *bottom*) progressed further yielding a mixture of mono- (**29h**, ~53 ppm) and bis-substituted complexes (**30h**, ~57 ppm).

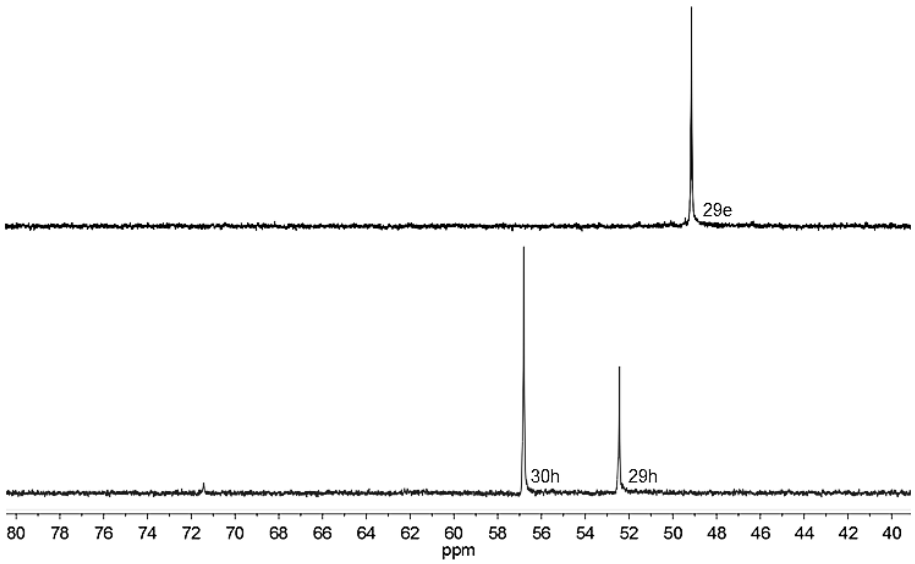


**Figure 4-1.** *$^{31}P\{^1H\}$ NMR spectra obtained from the reaction of **28** with 1-ethynyl-4-nitrobenzene (top) and 4-ethynylaniline (bottom) in the presence of DBU (t =30 min).*

Hence, the relatively kinetically inert complex featuring electron-withdrawing ligands provides an opportunity to prepare $RuCl(C{\equiv}CR)(dppe)_2$ complexes in an expeditious manner, by treatment of **28** with the appropriate ethynyl ligand and DBU for 15 - 30 minutes at room temperature until the reaction mixture turns yellow. The mono(ethynyl) complexes present in the mixture, can then be precipitated upon addition of the appropriate solvent (*see experimental section*) and collected by simple filtration (Scheme 4-2). This synthetic protocol was successfully employed to synthesize mono(ethynyl) complexes **29 (d - g, j, k)**. However, this strategy was found to be impractical for the preparation of mono(ethynyl) complexes bearing electron-donating substituents [R = Me (**29a**), $C_5H_{11}$ (**29b**), OMe (**29c**), $NH_2$ (**29h**)]. Due to the increased ionization of the Ru-Cl bond, slow conversion of these complexes to the generation of bis(ethynyl) complexes takes place, deriving in the generation of mixtures of mono- and bis(ethynyl) complexes. In many cases, the chromatographic purification required to isolate the pure compounds led to decomposition of the product. However, the natural tendency of the ligands bearing strong electron-donating substituents, namely [R = OMe, $NH_2$] allowed for the generation of bis(ethynyl) complexes **30c** and **30h** in the absence of a halide abstracting agent by treatment of **28** with DBU and 4-ethynyl aniline and 4-ethynyl anisole respectively. Over the course of 7 days, the greenish reaction mixtures slowly deposited an off-white precipitate of pure bis(ethynyl) complexes **30c** and **30h** in ca. 45% isolated yield.

By way of a rapid and versatile synthetic approach to bis(ethynyl) complexes, thallium salts proved to be extremely efficient, albeit toxic, halide abstracting agents allowing access to a wide range of the desired compounds. In a manner entirely analogous to that described above, treatment of a $CH_2Cl_2$ solution of **28** with an excess of DBU and the appropriate alkyne ligand gave yellow solutions of the mono- and bis(ethynyl)

complexes. Subsequent addition of halide abstracting agent $TlBF_4$ resulted in the immediate precipitation of TlCl and formation of the symmetrically substituted complexes **30 (a - g, j)** (Scheme 4-2). After careful filtration of the TlCl precipitate, the pure bis(ethynyl) complexes were precipitated from the filtrate by addition of the appropriate solvent (*see experimental section).*

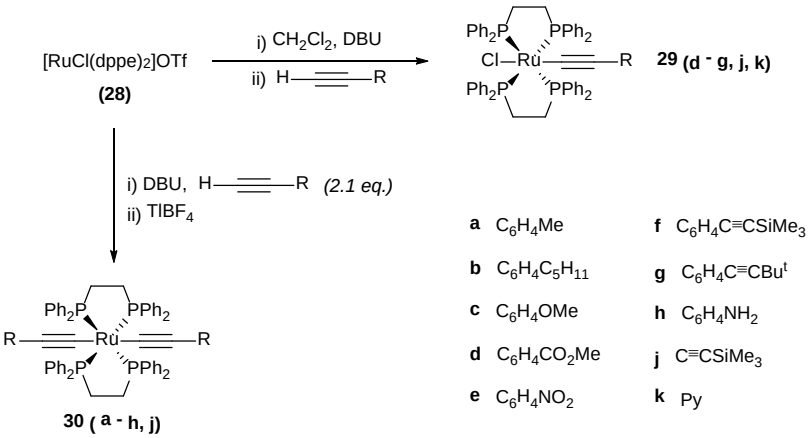


**Scheme 4-2.** *Synthesis of mono(ethynyl) complexes **29 (d – g, j, k)** and one-pot $Tl^+$ mediated synthetic route to symmetrically substituted complexes **30 (a – h, j)**.*

However, despite the broad scope of this procedure, a few exceptions were encountered. Thus, whilst the addition of $TlBF_4$ to a mixture of **29h**, DBU and $HC{\equiv}CC_6H_4NH_2$ was found to produce the desired *trans*-$Ru(C{\equiv}CC_6H_4NH_2\text{-}4)_2(dppe)_2$ (**30h**) any attempt to purify the final product from the reaction mixture lead to decomposition. A second exception regards the synthesis of *trans*-$Ru(C{\equiv}CC_6H_4NO_2\text{-}4)_2(dppe)_2$ (**30e**). The addition of $Tl^+$ salts was found insufficient to drive the reaction of **28** with two equivalents of 1-ethynyl-4-nitrobenzene to completion, yielding instead a mixture of mono- (**29e**) and bis(ethynyl) (**30e**) complexes over 48 hours. Whilst the use of $NaPF_6$ in the presence of $NEt_3$ allows further substitution of the chloride ligand in **29c**,[2b] in our hands the $Tl^+$ salts proved less effective in this context. In addition, the poor solubility of **30e** hindered further chromatographic purification reducing the final yield *ca.* 15%.

The last exception regards the preparation of *trans*-Ru(C≡CPy-4)$_2$(dppe)$_2$ (**30k**). Addition of $TlBF_4$ to a mixture of **29k**, DBU and HC≡CPy·HCl was found to produce a mixture of several unknown compounds that frustrated every attempt to synthesize **30k**. The formation of these unknown compounds can be clearly observed in the $^{31}P\{^1H\}$ NMR collected before (*top*) and after (*bottom*) the addition of $Tl^+$ salts (Figure 4-2).

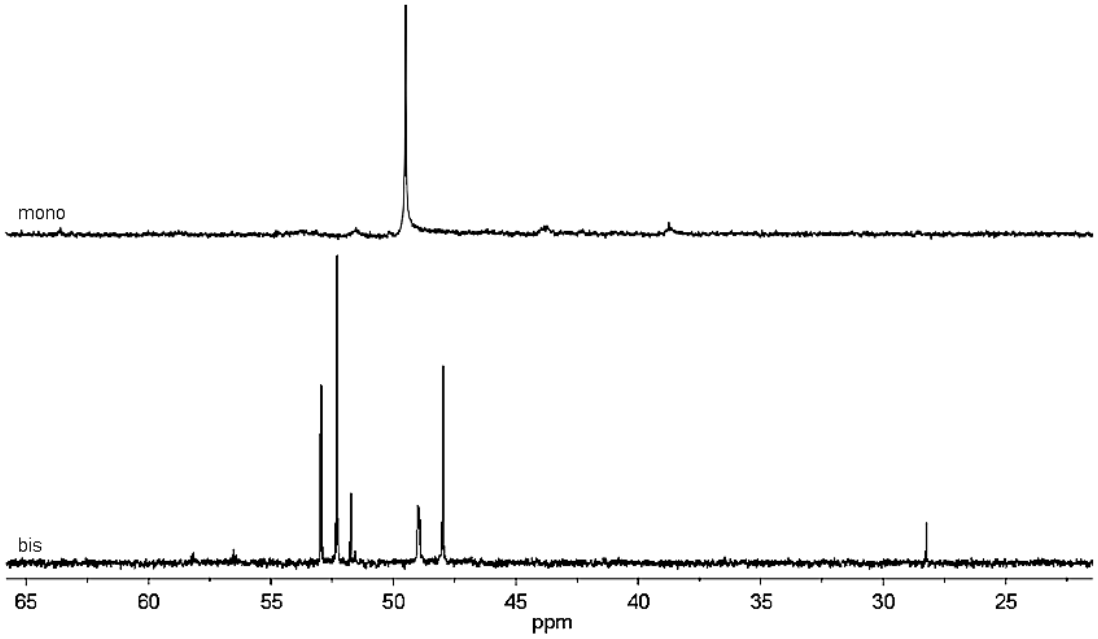


**Figure 4-2.** *Selected $^{31}P\{^1H\}$ NMR spectra obtained from a mixture of **29k**, DBU and HC≡CPy·HCl, before (top) and after the addition of $Tl^+$ salts (bottom).*

In spite of these exceptions, the reaction sequence described above can be adapted to permit the rapid and convenient formation of unsymmetrically substituted complexes *trans*-Ru(C≡CR$^1$)(C≡CR$^2$)(dppe)$_2$ (Scheme 4-3). In our hands, the preparation of unsymmetrical substituted complexes *trans*-[Ru(C≡CR$^1$)(C≡CR$^2$)(dppe)$_2$] from *trans*-RuCl(C≡CR$^1$)(dppe)$_2$ by activation with $NaPF_6$ proved problematic, with ligand scrambling leading to mixtures of symmetric and unsymmetric products. Similar difficulties have been noted in analogous dppm systems.[12] Ligand scrambling is perhaps unsurprising given the acid-base relationship that exists between ethynyl and vinylidene complexes and the reversibility of the sequence of reactions shown in Scheme 4-1 (*d*) and

might account for the modest yields of the unsymmetrical complexes often reported.[11] These complications can be avoided to some extent through the use of transmetallation based synthetic strategies,[9] or through the use of activated ethynyl-amine complexes[7] and reaction media containing a strong, non-nucleophilic base to minimize the accumulation of vinylidene intermediates.[5b] However the selective formation unsymmetrically substituted complexes **31 - 33** is achieved upon drop wise addition of a terminal alkyne HC≡CR$^2$ (30 minutes) to a $CH_2Cl_2$ solution of the appropriate mono(ethynyl) complex (**30d** and **30f**), excess DBU and one equivalent of $TlBF_4$. After careful filtration of TlCl precipitate, the unsymmetric products **31 - 33** were obtained as pure precipitates in moderate to good yield upon addition of hexane.

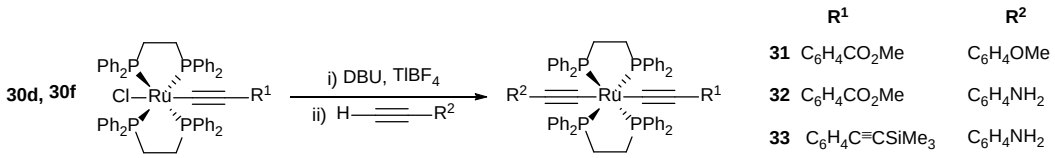


**Scheme 4-3.** *Synthesis of unsymmetrically substituted complexes **31 – 33** using $TlBF_4$.*

## 4.4. Crystallographic studies

The structures of the bis(ethynyl) complexes **30a**, **30b**, **30c**, **30d**, **30f**, **30g**, **30h** and **30i** together with those of the mono(ethynyl) species **29f, 29g, 29i, 29j** and **29k** were determined by Dr. Dmitry Yufit employing single-crystal X-ray diffraction at Durham University. Single crystals of the unsymmetrically substituted complexes **31 - 33** were found to be disordered impeding conclusive identification of the ethynyl substituents. Representative molecular plots for compounds **29f** and **30h** with representative atom labelling schemes are given in Figures 4-3 and 4-4 respectively. Key bond lengths (Å) and angles (°) for these complexes and related systems reported elsewhere are given together in Tables 4-1 and 4-2 for comparison. The crystallographic information files of these complexes can be found in the associated electronic content that accompanies this thesis.

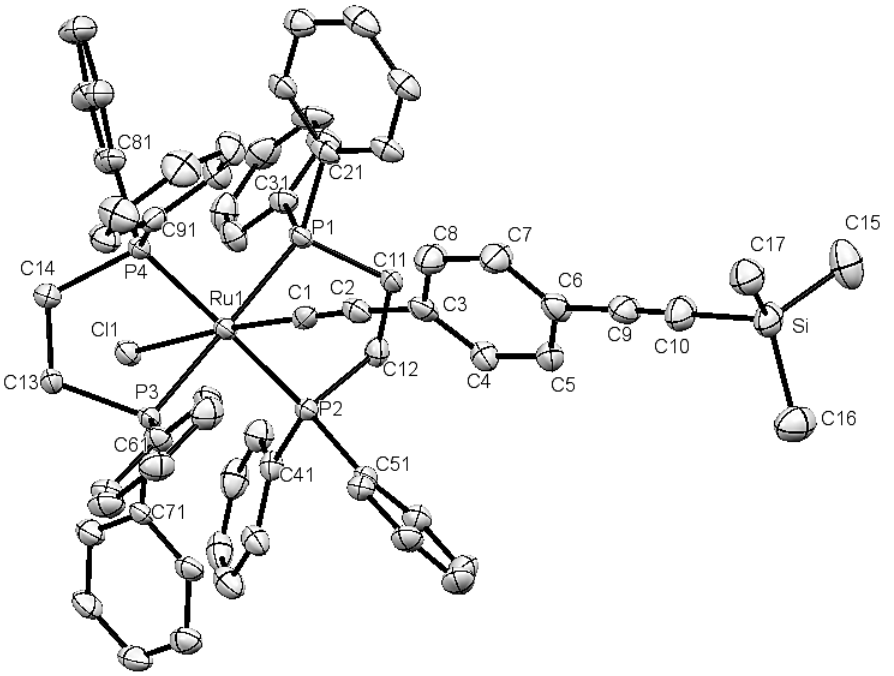


**Figure 4-3.** *trans-RuCl(C≡CC$_6$H$_4$C≡CSiMe$_3$)$_2$(dppe)$_2$ (**29f**) molecular structure (thermal ellipsoids at 50%). Solvent molecules and hydrogen atoms have been omitted for clarity.*

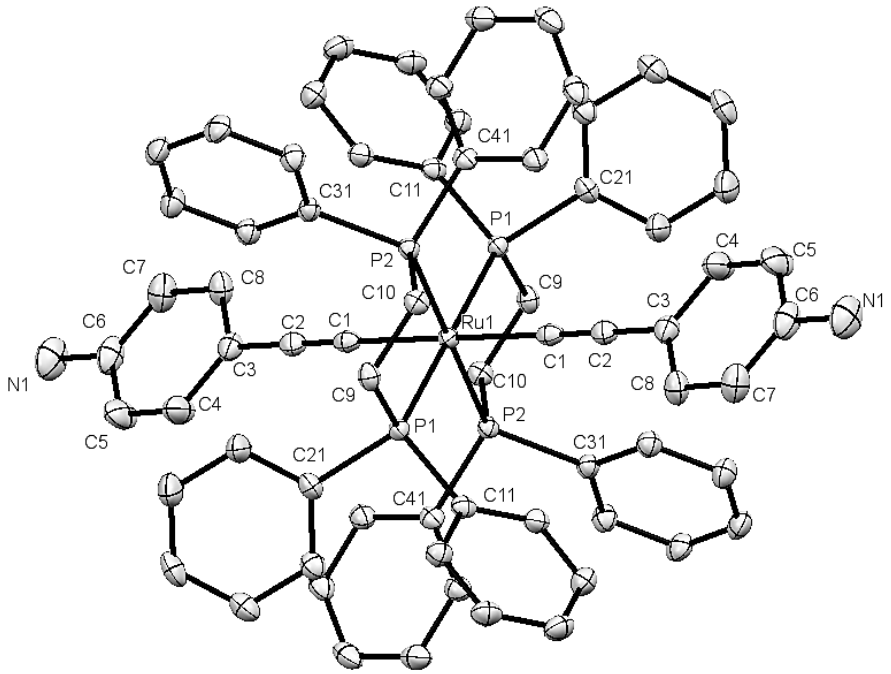


**Figure 4-4.** *Plot of a molecule of trans-Ru(C≡CC$_6$H$_4$NH$_2$)$_2$(dppe)$_2$ (**30h**) with thermal ellipsoids at 50%. Hydrogen atoms have been omitted for clarity.*

All the studied complexes were found to adopt an approximately octahedral environment at the Ru centre, with small distortions arising from the constrained bite angle of the dppe ligands. Although the experimental evidence show that chloride substitution in *trans*-RuCl(C≡CR)$(dppe)_2$ is clearly influenced by the electronic character of the ethynyl ligand, there is little evidence for a closely correlated structural *trans*-effect (Table 4-1). At first inspection, complexes such as *trans*-RuCl(C≡C$C_6H_4NPh_2$)$(dppe)_2$ and **29c** bearing electron donating groups display elongated Ru-Cl bond lengths, consistent with the electron donating ability of the ethynyl ligand located *trans* to chloride. Similarly, at the opposite end of the table, shorter Ru-Cl bond lengths can be found associated with complexes featuring *trans* ethynyl ligands bearing electron withdrawing substituents such as *trans*-RuCl{C≡C$C_6H_3$(Me-2)$NO_2$-4}$(dppe)_2$ and **29d**. These structural features, which reflect the π-donor properties of the chloride ligand and π-donor/weak π-acceptor character of the ethynyl ligand, are in agreement with the synthetic observations, where electron donating ligands favour the substitution of the *trans*-disposed chloride.

However, Table 4-1 also contains several examples of mono(ethynyl) complexes for which the structural data is in disagreement with the experimental observations. For example, the complex *trans*-RuCl(C≡C$C_6H_5$)$(dppe)_2$ presents a Ru-Cl bond length (2.4786(13) Å), which is unexpectedly shorter than that of the most unreactive complex of the series *trans*-RuCl(C≡C$C_6H_4NO_2$-4)$(dppe)_2$ (**29e**, 2.500(1) Å). On the other hand, the complex *trans*-RuCl{C≡C$C_6H_3$(Me-2)$NO_2$-4}$(dppe)_2$, which is closely related to **29e**, presents the shortest of the Ru-Cl bond lengths observed in Table 4-1 (2.473(3) Å). A further remarkable exception concerns complex *trans*-RuCl(C≡C$C_6H_4$Me)$(dppe)_2$ (**29a**) which presents two substantially different Ru-Cl bond lengths depending on the nature of the solvate in the unit cell: 0.5THF 2.4907(12) Å; 2$CH_2Cl_2$ 2.5096(8) Å.[10a]

**Table 4-1.** *Selected bond lengths (Å) from crystallographically characterized complexes trans-RuCl(C≡CR)(dppe)$_2$.*

| R | Ru-Cl | Ru-C≡C | C≡C | Ru-$P_{avg}$ | $\theta$ (º) | Ref |
|---|---|---|---|---|---|---|
| $C_6H_3$(Me-2)$NO_2$-4 | 2.473(3) | 2.013(11) | 1.189(14) | 2.386 | 2 | 8 |
| C≡CPy-4 | 2.4749(9) | 1.986(4) | 1.211(5) | 2.373 | 78 | **(29k)** |
| $C_6H_5$ | 2.4786(13) | 2.007(5) | 1.198(7) | 2.371 | 7 | 4d |
| $C_6H_4C{\equiv}CBu^t$ | 2.4799(11) | 1.997(4) | 1.234(5) | 2.369 | 75 | **(29g)** |
| $C_6H_4CO_2Me$ | 2.4806(13) | 1.998(5) | 1.195(8) | 2.368 | 92 | 10a |
| $C_6H_4$-$C_3N_3$(NHCOEt)$_2$ | 2.4811(10) | 1.988(4) | 1.221(5) | 2.372 | 74 | 13 |
| $C_6H_4C$(=O)Me-4 | 2.4831(11) | 1.989(4) | 1.212(6) | 2.3685 | 92 | 14 |
| $C_6H_4$-$C_3N_3$(NHCO$Bu^t$)$_2$ | 2.4832(9) | 1.996(4) | 1.204(5) | 2.362 | 72 | 13 |
| $C_5H_3NC_5H_4N$ | 2.4871(15) | 2.007(6) | 1.183(8) | 2.367 | 88 | 12 |
| $C_6H_4CH{=}CHC_6H_4NO_2$ | 2.489(1) | 1.996(4) | 1.205(7) | 2.368 | 26 | 15 |
| $C_6H_4Me{\cdot}0.5THF$ | 2.4907(12) | 2.009(5) | 1.196(6) | 2.360 | 12 | 10a |
| $C_5H_3NC_5H_4N.PdCl_2$ | 2.4988(13) | 1.969(5) | 1.235(7) | 2.368 | 6 | 12 |
| $C_6H_4NO_2$-4 | 2.500(1) | 1.986(5) | 1.206(7) | 2.366 | 66 | 8 |
| $C_6H_4C{\equiv}CH$ | 2.50030(6) | 2.027(2) | 1.190(3) | 2.3879 | 59 | **(29i)** |
| $C_6H_4C{\equiv}CSiMe_3$ | 2.5041(11) | 2.005(5) | 1.196(6) | 2.359 | 4 | **(29f)** |
| $C_6H_4C$(=O)H | 2.507(1) | 2.012(4) | 1.158(5) | 2.377 | 65 | 15 |
| $C_6H_4Me{\cdot}2CH_2Cl_2$ | 2.5096(8) | 2.007(4) | 1.202(5) | 2.369 | 64 | 10a |
| $C_4H_2SCH{=}CHC_4H_2SC$(=O)H | 2.5099(10) | 1.990(4) | 1.197(5) | 2.379 | 78 | 16 |
| $C_6H_4OMe$ | 2.5118(9) | 2.018(4) | 1.188(5) | 2.369 | 65 | 10a |
| $C_6H_4F$-4 | 2.5149(10) | 2.013(4) | 1.197(5) | 2.371 | 51 | 17 |
| $C{\equiv}CSiMe_3$ | 2.5233(9) | 1.978(4) | 1.205(5) | 2.368 | --- | **(29j)** |
| $C_6H_4NPh_2$ | 2.5349(7) | 1.997(3) | 1.215(4) | 2.366 | 90 | 18 |
| $C_6H_4F$-3 (poor data set) | 2.5370(18) | 2.043(8) | 1.096(9) | 2.376 | 14 | 5a |
| H (CCH/Cl disorder 50:50 occupancy) | 2.5838(14) | 1.936(5) | 1.190(5) | 2.367 | --- | 19 |

A closer analysis of the structural details of these complexes revealed that for complex *trans*-RuCl(C≡C$C_6H_4$Me)(dppe)$_2$·0.5THF (**29a**·0.5THF), the torsion angle between the plane of the arylethynyl ligand and the plane bisecting the dppe ligands, $\theta$ depicted in Figure 4-5, is 12º while for *trans*-RuCl(C≡C$C_6H_4$Me)(dppe)$_2$·2$CH_2Cl_2$ $\theta$ = 64º. Previous computational studies revealed that the Ru-based $d_{xz}$ and $d_{yz}$ orbitals are involved in the HOMO of *trans*-RuCl(C≡C$C_6H_4$R)(dppe)$_2$ complexes[14] (taking the axial Ru-ethynyl

vector as the *z*-direction, and *x* and *y* in the plane of the equatorial dppe ligands). Thus, a $\theta$ = 90º or 0º configuration of the aromatic portion of the ethynyl ligand (shaded entries in Table 4-1) provides better overlap of the arylethynyl ligand π and π* orbitals with respect to the metal centre, enhancing the electronic influence of the ligand on the Ru-Cl bond length and giving rise to a consistent structure-property relationship. The structural parameters of complexes which offer $\theta$ values substantially removed from the optimal 0° or 90° conformations are less well correlated with the simple ideas of the structural *trans*-effect based on the donor or acceptor properties of the ethynyl ligand substituent, due to the lack of extended conjugation between the substituent and the metal centre.

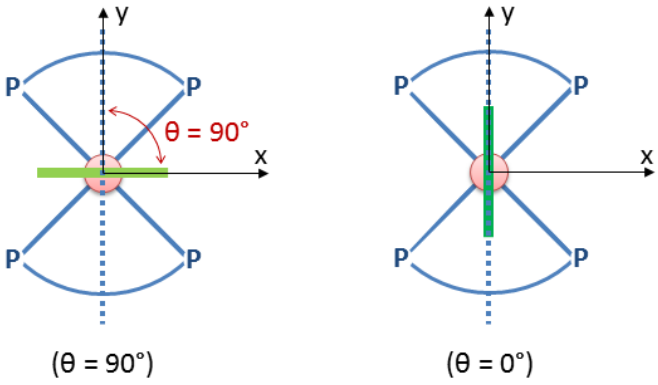


**Figure 4-5.** *Representation of angle θ in trans-RuCl(C≡CC$_6$H$_4$R)(dppe)$_2$.*

The importance of the ligand orientation (expressed as the angle $\theta$) is clearly illustrated by the contrasting molecular structures of the closely related complexes *trans*-RuCl(C≡CC$_6$H$_4$NO$_2$-4)(dppe)$_2$ (**29e**) and *trans*-RuCl{C≡CC$_6$H$_3$(Me-2)NO$_2$-4}(dppe)$_2$. Despite the electronic properties of the ligands 4-nitrophenyl ethynyl and 4-nitro-2-methyl ethynyl being very similar, the latter complex presents a much shorter Ru-Cl bond length (Table 4-1, 2.473(3) *vs* 2.500(1) Å). It appears from inspection of a space filling model that the methyl group present in *trans*-RuCl{C≡CC$_6$H$_3$(Me-2)NO$_2$-4}(dppe)$_2$ locks into a groove formed by the dppe phenyl rings and forces the nitroaromatic moiety to adopt a $\theta$ = 2° configuration, enhancing drastically the *trans*-effect. On the other hand, the non-

sterically hindered C≡C$C_6H_4NO_2$-4 adopts a configuration in the crystal ($\theta$ = 66º) which reduces the electronic influence of the ligand on the *trans*-disposed chloride. The importance of ligand orientation and molecular conformation on molecular electronic and spectroscopic properties is becoming increasingly recognized as a contributing factor to solution-based spectroscopic properties (*vide infra*),[20] and these observations are supported by the solid-state structure-property relationships summarized in Table 4-1.

The bis(ethynyl) complexes **30a**, **30b**, **30c**, **30d**, **30f**, **30g**, **30h** and **30i** complexes and other examples in Table 4-2 present a linear rod-like structure with angles along the -C≡C-Ru-C≡C- fragment close to 180º and the aryl rings of both ethynyl ligands lying in a common plane. Compared to their mono-substituted counterparts (**29**), the bis(ethynyl) complexes (**30**) generally exhibit longer Ru-C≡C bonds and correspondingly shorter Ru-P bond lengths (Table 4-2). In a manner similar to that described for the mono(ethynyl) complexes, a variety of $\theta$ angles from 0 - 90° can be found across the data set, but few near the critical angles of 0 and 90°. Due to the importance of orbital overlap on the propagation of electronic effects through the molecular backbone, a systematic relationship between the electronic properties of the ethynyl ligand substituent and bond lengths cannot be found for these complexes with $\theta$ angles that deviate from the optimal 0 and 90° positions. However, it appears that the greater σ- and π-donor properties of the additional ethynyl ligand in bis(ethynyl) complexes (**30**) vs the inductive electron withdrawing and π-donor properties of the chloride ligand in complexes (**29**) leads to an increased amount of electron density at the metal centre, and a greater degree of π- back donation to the phosphine ligands. This in turn leads to shorter Ru-P distances in the bis(ethynyl) complexes than in the mono(ethynyl) analogues.

**Table 4-2.** *Selected bond lengths (Å) from crystallographically characterised complexes trans-Ru(C≡CR$^1$)(C≡CR$^2$)(dppe)$_2$.*

| $R_1$ | $R_2$ | Ru-C≡C*R*$^1$ | Ru-C≡C*R*$^2$ | C≡C | Ru-$P_{avg}$ | $\theta$ (º) | REF |
|---|---|---|---|---|---|---|---|
| C{CH=C(CN)$_2$}=C(CN)$_2$ | C{CH=C(CN)$_2$}=C(CN)$_2$ | 2.007(7) | | 1.231(9) | 2.389 | --- | [21] |
| $C_6H_2(OMe)_2C{\equiv}CH$ | $C_6H_2(OMe)_2C{\equiv}CH$ | 2.047(5) | | 1.223(6) | 2.352 | 2 | [22] |
| C≡CH | C≡CH | 2.050(4) | | 1.198(5) | 2.369 | --- | [23] |
| $C_6H_4C{\equiv}CBu^t$ | $C_6H_4C{\equiv}CBu^t$ | 2.057(2) | | 1.211(3) | 2.358 | 65 | **(30g)** |
| $C_6H_2(OMe)_2C{\equiv}CSiMe_3$ | $C_6H_2(OMe)_2C{\equiv}CSiMe_3$ | 2.0583(17) | | 1.218(2) | 2.357 | 17 | [22] |
| $C_6H_4C{\equiv}CH$ (mol A) | $C_6H_4C{\equiv}CH$ | 2.061(3) | | 1.212(4) | 2.357 | 55 | **(30i)** |
| $C_6H_5$ | $C_6H_5$ | 2.061(5) | 2.064(5) | 1.207(7)<br>1.194(7) | 2.360 | 0/58 | [9] |
| $C_6H_5$ | $C_6H_4C(=O)H$ (disordered) | 2.0619(19) | | 1.213(3) | 2.363 | 75 | [24] |
| $C_6H_4C{\equiv}CH$ (mol B) | $C_6H_4C{\equiv}CH$ | 2.062(3) | | 1.209(4) | 2.354 | 82 | **(30i)** |
| $C_6H_5$ | $C_6H_4C{\equiv}C\{Fe(dppe)Cp^*\}^+$ | 2.063(5) | 2.062(5) | 1.209(6) / 1.201(6) | 2.369 | 60/60 | [25] |
| $C_6H_4OMe$ | $C_6H_4OMe$ | 2.0648(16) | | 1.217(2) | 2.358 | 70 | **(30c)** |
| $C_6H_4Me$-4 | $C_6H_4Me$-4 | 2.065(2) | | 1.210(3) | 2.349 | 68 | **(30a)** |
| $C_6H_4C{\equiv}CSiMe_3$ | $C_6H_4C{\equiv}CSiMe_3$ | 2.066(3) | | 1.204(4) | 2.358 | 68 | **(30f)**[26] |
| $C_6H_5C_5H_{11}$-4 | $C_6H_5C_5H_{11}$-4 | 2.0666(16) | | 1.206(2) | 2.355 | 59 | **(30b)** |
| $C_6H_4CO_2Me$ | $C_6H_4CO_2Me$ | 2.0687(18) | | 1.197(2) | 2.357 | 64 | **(30d)** |
| $TTFMe_3$ | $TTFMe_3$ | 2.0691(18) | | 1.203(3) | 2.373 | 13 | [27] |
| $C_6H_4NH_2$ | $C_6H_4NH_2$ | 2.074(2) | | 1.197(3) | 2.349 | 64 | **(30h)** |
| Fc | Fc | 2.075(3) | | 1.212(5) | 2.358 | --- | [28] |
| Fc | $C_6H_4NPh_2$ | 2.082(3) | 2.061(3) | C≡CR$^1$: 1.213(4)<br>C≡CR$^2$: 1.213(4) | 2.356 | ---/86 | [18] |
| $C{\equiv}CSiMe_3$ | $C{\equiv}CSiMe_3$ | 2.095(14) | | 1.099(17) | 2.360 | --- | [23] |
| $C_6H_5$ | $C_5H_3NC_5H_4N$.Dyhfacac | 2.105(7) | 2.049(6) | 1.118(9)<br>1.210(7) | 2.350 | 5/45 | [29] |

## 4.5. Electrochemistry

The availability of a substantial number of mono and bis(ethynyl) complexes provided an opportunity to explore trends in the electrochemical response of *trans*-$RuX(C{\equiv}CR)(dppe)_2$ (X = Cl, C≡CR) complexes. Results are summarized in Table 4-3, although comparisons with data reported elsewhere is made somewhat more difficult by the various combinations of solvent, electrolyte, and reference potential employed in these earlier works. However, several consistencies can be identified as discussed below.

**Table 4-3.** *Electrochemical data from* ***29(a - g, i - k)***, ***30(a - j)***, *and* ***31 - 33***.[a]

| Complex | $^1E_{1/2}{}^o$ (V) | $^2E_{1/2}{}^o$ (V) | $^3E_{1/2}{}^o$ (V) | $E^{ox}$ (V) |
|---|---|---|---|---|
| **29a**[10a] | -0.03 | --- | --- | 0.85 |
| **29b**[10a] | -0.04 | --- | --- | 0.83 |
| **29c**[10a] | -0.10 | --- | --- | 0.69 |
| **29d** | 0.10 | --- | --- | 0.98 |
| **29e** | 0.20 | --- | --- | 1.10 |
| **29f** | 0.04 | --- | --- | 0.98 |
| **29g** | -0.01 | --- | --- | 0.85 |
| **29i** | 0.06 | --- | --- | 0.90 |
| **29f** | 0.14 | --- | --- | 1.12 |
| **29k** | 0.20 | --- | --- | --- |
| **30a** | -0.06 | --- | --- | 0.85 |
| **30b** | -0.09 | --- | --- | 0.80 |
| **30c** | -0.15 | --- | --- | 0.65 |
| **30d** | 0.12 | --- | --- | 0.90 |
| **30e** | 0.26 | --- | --- | --- |
| **30f** | 0.05 | --- | --- | 0.90 |
| **30g** | 0.00 | --- | --- | 0.85 |
| **30h** | -0.29 | 0.10 | 0.46 | --- |
| **30i** | 0.05 | --- | --- | 0.90 |
| **30j** | 0.16 | --- | --- | --- |
| **31** | -0.21 | 0.2 | --- | --- |
| **32** | -0.19 | 0.22 | --- | 0.61 |
| **33** | -0.04 | --- | --- | 0.76 |

[a] $E_{1/2}$ *vs* ferrocene/ferrocenium ($FeCp_2/[FeCp_2]^+$) ($CH_2Cl_2$, 0.1 M $NBu_4BF_4$, Pt dot working electrode). Under these conditions, internal reference decamethylferrocene/ decamethylferrocenium ($FeCp^*_2/[FeCp^*_2]^+$) = -0.53 V *vs* $FeCp_2/[FeCp_2]^+$.

As previously reported in earlier studies of similar complexes, a reversible first oxidation process $^{1}E_{1/2}^{o}$ was present in almost every case,[4a, 5b, 6, 8, 10a, 22] although the poor solubility of **30e** prevented the recording of accurate voltammetric data in $CH_2Cl_2$. One or two additional oxidation processes ($^{2}E_{1/2}^{o}$, $^{3}E_{1/2}^{o}$) were found for amino-substituted complexes **30h, 4** and **5**. The low oxidation potential of **30h** provides a reasonable explanation to the experimental difficulties found during work-up. In most cases an irreversible, multi-electron oxidation wave $E^{ox}$ was also present close to the anodic solvent limit.

The range of potentials $E_1^{o}$ recorded for compounds **29 (a - g, i - k)** and **30 (a - j)** span 300 mV to over 500 mV, respectively. The correlation of the electronic character of the remote substituents on the redox properties of the complexes is consistent with a strong aryl-ethynyl character of the HOMO[3, 30] and the greater conformational freedom offered by the solution medium as opposed to the solid state that permits better π-conjugation in the molecular backbone. Complexes **29c**, **30h** and **30c** bearing the most electron-donating aryl substituents were more easily oxidized in the thermodynamic sense than other members of the series, while oxidation of **29d**, **30d** and **30e** bearing electron withdrawing substituents, took place at more positive potentials. According to Lever's early model, the influence of different ligands on the electronic properties of a coordination complex is frequently found to be additive.[31] However, Heath and Humphrey reported an attenuation of those additive effects for complexes bearing *trans*-disposed π-accepting ligands.[32] Lever's model is able to accurately predict the influence of a ligand on the electronic properties of a coordination complex when the oxidation process is located on the metal centre. Hence, ethynyl complexes of Os and Ru, which present a characteristic and pronounced ligand contribution to the HOMO (*vide infra*), often deviate from the predictions of the Lever model.[33] This becomes especially relevant for complexes bearing redox active ligands in which the metallic nature of the redox processes is not clearly established.

## 4.6. Spectroelectrochemistry and quantum chemical calculations

Although various examples of the complexes *trans*-RuX(C≡CR)(dppe)$_2$ have been the subject of UV-Vis-NIR spectroelectrochemical studies,[2b, 14, 34] curiously the use of IR spectroelectrochemical methods to study this class of compounds is rare,[22, 35] despite the considerable amount of complementary electronic and chemical structural detail contained in the IR spectroelectrochemical response of ethynyl complexes.[36] To further explore the effects of oxidation on the molecular and electronic structure of this class of complex an IR spectroelectrochemical study of compounds **30c**, **30f**, **30h**, **31**, **32** and **33**, together with comparable UV-Vis-NIR spectroelectrochemical studies of compounds the unsymmetrically substituted complexes **31** and **32** with reference data from **30f** and **30h** was undertaken. These complexes were selected because of their demonstrated (**30f**), or potential (**30h**, **31**), capacity to perform as wires during single molecule conductance measurements,[26] or to serve as reference compounds with different electron-donating groups (**30c**) or vibrational probes (**32**, **33**). To gain further insight into the electronic structure, density functional theory (DFT) calculations on [**30f**]$^{n+}$, [**30h**]$^{n+}$, [**31**]$^{n+}$ and [**32**]$^{n+}$ (n = 0, 1) were performed in collaboration with Prof. Dr. Martin Kaupp group at the Technische Universität Berlin. The BLYP35 functional[37] in combination with suitable solvent models, COSMO[38] as implemented in the TURBOMOLE 6.4 code[39] and C-PCM[40] as implemented in the Gaussian09 code,[41] was employed. The BLYP35 functional has proven to reliably reproduce and more importantly predict the ground-state charge distribution and spectra including excitations involving charge transfer for organic[37, 42] and transition-metal [43] mixed-valence systems.

Molecular and electronic structural changes upon oxidation were conveniently followed by monitoring the key IR vibrational modes, such as $\nu$(Ru-C≡C) and the non-coordinated $\nu$(C≡C), together with $\nu$(C=O) and $\nu$(N−H) bands when present (Figure 4-6).

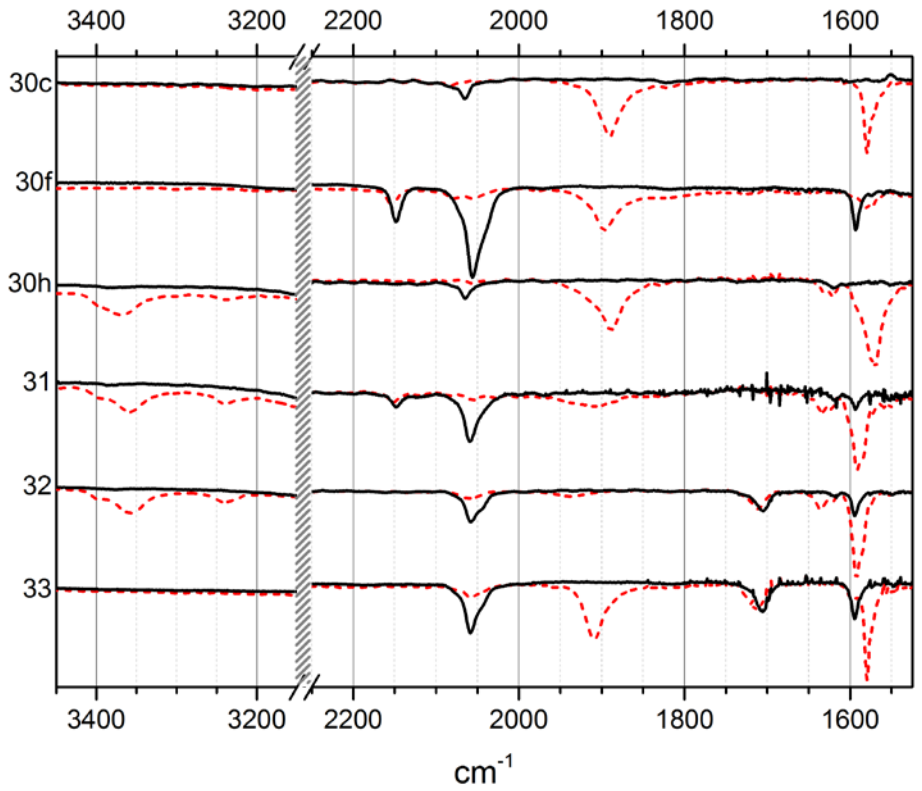


**Figure 4-6.** *IR spectra of complexes [trans-Ru(C≡CR$^1$-4)$_2$(dppe)$_2$]$^{n+}$ [R$^1$ = C$_6$H$_4$OMe (**30c**), C$_6$H$_4$C≡CSiMe$_3$ (**30f**), C$_6$H$_4$NH$_2$ (**30h**)] and [trans-Ru(C≡CR$^1$-4)(C≡CR$^2$-4)(dppe)$_2$]$^{n+}$ [R$^1$ = C$_6$H$_4$NH$_2$, R$^2$ = C$_6$H$_4$C≡CSiMe$_3$ (**31**); R$^1$ = C$_6$H$_4$NH$_2$, R$^2$ = C$_6$H$_4$CO$_2$Me (**32**); R$^1$ = C$_6$H$_4$OMe, R$^2$ = C$_6$H$_4$CO$_2$Me (**33**)] (n = 0, black solid line; n = 1 red dotted line).*

The *ν*(Ru-C≡C) metal coordinated ethynyl bands were present between 2054-2066 cm$^{-1}$ for all complexes in the closed shell, 18 e$^-$ configuration, whilst the 17 e$^-$ Ru ethynyl complexes derived by oxidation were characterized by the appearance of a broad and asymmetric *ν*(Ru-C≡C) band at 1900 cm$^{-1}$.[22, 44] The aryl ring breathing mode gains in intensity on oxidation and appears as an intense band between 1568-1592 cm$^{-1}$ for all complexes except **30f**, where upon oxidation to [**30f**]$^{\bullet+}$ the ν(C=C) mode decreases in intensity and shifts to lower wavenumbers. The less intense *ν*(C≡C) from the non-coordinated C≡C moiety in **30f** and **31** present at 2148 cm$^{-1}$, shifted towards slightly higher wavenumbers (2153 cm$^{-1}$) and lost intensity on oxidation. Vibrational frequencies computed within the

harmonic approach at the optimized structures are fully consistent with the recorded spectra of [**30f**]$^{n+}$, [**30h**]$^{n+}$, [**31**]$^{n+}$ and [**32**]$^{n+}$ (n = 0, 1; Table 4-4).[45] The oxidized species **[30h]**$^{\bullet+}$, **[31]**$^{\bullet+}$ and **[32]**$^{\bullet+}$ were also characterized by two sharp low-intensity bands between 3400-3200 cm$^{-1}$, attributed to the $\nu$(N−H) mode. Frequency calculations with computational models of **30h** and **31** confirm the extremely weak oscillator strength of the $\nu$(N−H) band for these systems (*vide infra*). The calculations also predict a marked increase in the intensity of the N-H bands on oxidation, in good agreement with the spectroscopic data recorded. Overall, the IR studies strongly suggest a great degree of ligand redox activity in these complexes.

**Table 4-4.** *Experimental and calculated (shaded entries) vibrational frequencies of [**30f**]*$^{\bullet+}$*, [**30h**]*$^{\bullet+}$*, [**31**]*$^{\bullet+}$ *and [**32**]*$^{\bullet+}$*.*

| Complex | $\nu$ (Ru-C≡C) | $\nu$ (C=C$_{aryl}$) | $\nu$ (C≡C) | $\nu$ (N−H) | $\nu$ (C=O) |
|---|---|---|---|---|---|
| **[30f]**$^{\bullet+}$ | 1899(m) | 1580(w) | 2155(w) | --- | --- |
| | *1981(s)* | *1484(w)* | *2180(w), 2177(w) 2034 (w)* | --- | --- |
| **[30h]**$^{\bullet+}$ | 1890(s) | 1574(s) | --- | 3370(m), 3235(w) | --- |
| | *1942(s)* | *1583(m), 1581(m), 1578(m)* | --- | *3458(w), 3446(w)* | --- |
| **[31]**$^{\bullet+}$ | 1912(m) | 1592(s) | 2153(w) | 3360(m), 3235(w) | --- |
| | *1964(m)* | *1587(s) 1582 (w)* | *2179(w) 2078(w)* | *3460(w)* | --- |
| **[32]**$^{\bullet+}$ | 1933(w) | 1593(s) | --- | 3361(m), 3242(w) | 1712(m) |
| | *1934(s)* | *1576(s) 1559 (m)* | --- | *3464(m)* | *1735(w)* |

The concept of ligand redox activity (or non-innocence) in these complexes is supported by the spin densities obtained from the DFT structure optimizations of **[30f]**$^{\bullet+}$, **[30h]**$^{\bullet+}$, **[31]**$^{\bullet+}$ and **[32]**$^{\bullet+}$ (Table 4-5).[46]

The optimized structures, derived from $C_i$-symmetric starting geometries, have the ethynylaromatic moiety bisecting the dppe ligands ($\theta$ ~ 0º, Figure 4-5) and the two aryl moieties in the same plane (torsion angle Ω = 0º, Figure 4-8). For convenience and clarity the complexes with this geometry are now defined here as ***in-plane*-[30f]**$^{\bullet+}$, ***in-plane*-[30h]**$^{\bullet+}$, ***in-plane*-[31]**$^{\bullet+}$ and ***in-plane*-[32]**$^{\bullet+}$**.**

**Table 4-5.** *Mulliken fragment spin-density contributions (%) for the in-plane conformations of* ***[30f]***$^{\bullet+}$, ***[30h]***$^{\bullet+}$, ***[31]***$^{\bullet+}$, ***[32]***$^{\bullet+}$.

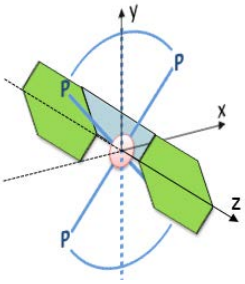


| Complex | Spin density contribution (%) | | | | |
|---|---|---|---|---|---|
| | ***R*$^1$*C*$_6$*H*$_4$** | ***C*≡*C*** | ***[Ru]*** | ***C*≡*C*** | ***C*$_6$*H*$_4$*R*$^2$** |
| ***in-plane*-[30f]**$^{\bullet+}$ | *7* | *11* | *71* | *6* | *5* |
| ***in-plane*-[30h]**$^{\bullet+}$ | *18* | *18* | *54* | *6* | *7* |
| ***in-plane*-[31]**$^{\bullet+}$ | ($NH_2$) *30* | *27* | *43* | *1* | *2* |
| ***in-plane*-[32]**$^{\bullet+}$ | ($NH_2$) *22* | *18* | *57* | *4* | *3* |

While the Ru(dppe)$_2$ fragment contributes significantly in all cases (***in-plane structures* [30f]**$^{\bullet+}$: 71%; **[30h]**$^{\bullet+}$: 54%; **[31]**$^{\bullet+}$: 43%; **[32]**$^{\bullet+}$: 57%), the ligand involvement in supporting the unpaired spin density depends strongly on the substitution of the aromatic unit, and for ***in-plane*-[30f]**$^{\bullet+}$ the outer-most parts of the ethynyl ligands barely contribute (12% of the total). Thus, whilst the spin density is high on the C≡C$_6$H$_4$NH$_2$-4 ligands in ***in-plane*-[31]**$^{\bullet+}$ (57%) and ***in-plane*-[32]**$^{\bullet+}$ (40%), the alkyne ligand bearing the less electron donating substituent is largely redox-inactive or -innocent (***in-plane*-[31]**$^{\bullet+}$: C≡C$_6$H$_4$C≡CSiMe$_3$-4: 3%; (***in-plane*-[32]**$^{\bullet+}$: C≡C$_6$H$_4$CO$_2$Me-4: 7%). It is also noteworthy that in these lowest-energy conformations, for ***in-plane*-[30h]**$^{\bullet+}$ the spin density is partly

localized on one ligand and the ruthenium unit, but little on the other ethynyl ligand. The DFT calculations therefore suggest that, for the *in-plane* conformations of **[30h]**$^{\bullet+}$, **[31]**$^{\bullet+}$, **[32]**$^{\bullet+}$ might be considered as further examples of metal-bridged organic mixed-valence systems.[47] With this notion of metal-bridged, organic mixed-valence character in mind, the observation of the low-energy tail of a NIR electronic transition band in the IR spectra of **[30h]**$^{\bullet+}$ and **[31]**$^{\bullet+}$ between 7000-5500 cm$^{-1}$ is intriguing, with similar low-energy bands having been observed in closely related complexes by Rigaut, Winter and colleagues,[22] prompting further consideration of the underlying electronic transitions here.

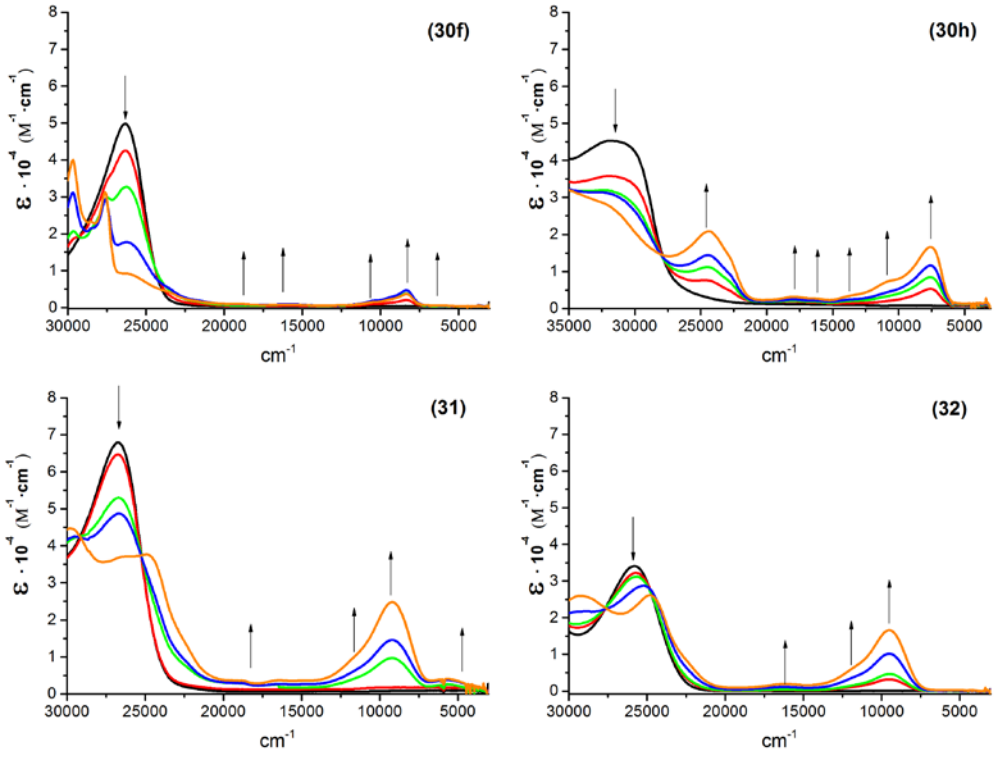


**Figure 4-7.** *UV-Vis-NIR spectral changes of **30f**, **30h**, **31** and **32** resulting from the first oxidation process.*

A series of UV-Vis-NIR spectroelectrochemical experiments (Figure 4-7), supported by time-dependent DFT (TDDFT) studies, was performed on **30f**, **30h**, **31** and **32** as representative examples by Matthias Parthey of the Kaupp group. The results are reproduced here for completeness and illustration of the critical points underlying the conformational

effects on the appearance of the electronic spectra. For each complex **30f**, **30h**, **31** and **32** a well-defined UV absorption band was observed in the electronic spectrum, at 26667 $cm^{-1}$ (**30f**), 31847 $cm^{-1}$ (**30h**), 26316 $cm^{-1}$ (**31**) or 25839 $cm^{-1}$ (**32**), respectively. Upon oxidation in the OTTLE cell, the main absorption band of four complexes undergoes a marked intensity loss and several new features develop in the NIR region of the spectra. The spectroscopic details of **[30f]**$^{\bullet+}$, **[30h]**$^{\bullet+}$, **[31]**$^{\bullet+}$ and **[32]**$^{\bullet+}$ are summarized in Table 4-6**.**

**Table 4-6.** *UV-Vis-NIR spectral data of [**30f**]*$^{\bullet+}$*, [**30h**]*$^{\bullet+}$*, [**31**]*$^{\bullet+}$ *and [**32**]*$^{\bullet+}$ *obtained upon oxidation of **30i**, **30f**, **31** and **32**.*

| **Complex** | $\nu_{max}$ ($cm^{-1}$) [$\varepsilon$ / $10^4 \cdot M^{-1} \cdot cm^{-1}$] |
|---|---|
| **[30f]**$^{\bullet+}$ | 23640 **[0.4]**, 18761 **[0.1]**, 15625 **[0.1]**, 10417 **[0.2]**, 9328 **[0.3]**, 8333 **[0.5]**, 6131 **[0.1]** |
| **[30h]**$^{\bullet+}$ | 24331 **[2.1]**, 22779 **[1.4]**, 18214 **[0.3]**, 16339 **[0.3]**, 13679 **[0.3]**, 10822 **[0.7]**, 7662 **[1.6]** |
| **[31]**$^{\bullet+}$ | 24814 **[3.7]**, 22522 **[1.4]**, 18727 **[0.4]**, 16474 **[0.4]**, 11507 **[1.0]**, 9191 **[2.5]**, 5695 **[0.4]** |
| **[32]**$^{\bullet+}$ | 24691 **[2.6]**, 22573 **[0.9]**, 16155 **[0.2]**, 12062 **[0.6]**, 9551 **[1.6]** |

For the symmetrically substituted complexes (**30f** and **30h)**, Gaussian09 TDDFT calculations at the fully optimized structures give only one intense ($\mu_{trans}$ > 1.0 D) transition at 11316 $cm^{-1}$ ($\mu_{trans}$ = 9.7 D) for ***in-plane*-[30f]**$^{\bullet+}$ and at 7778 $cm^{-1}$ ($\mu_{trans}$ = 11.7 D) for ***in-plane*-[30h]**$^{\bullet+}$ arising from a β-HOMO - β-SOMO excitation (Table 4-7). While for both complexes the β-HOMO features significant contributions from both ethynyl ligands (***in-plane*-[30f]**$^{\bullet+}$: 85% and for ***in-plane*-[30h]**$^{\bullet+}$: 91%), the β-SOMO is mainly C≡CRu(dppe)$_2$C≡C centred for ***in-plane*-[30f]**$^{\bullet+}$ (75%) while for for ***in-plane*-[30h]**$^{\bullet+}$ it is localized at one C≡C$C_6H_4NH_2$-4 ligand (40%) and the Ru(dppe)$_2$ moiety (39%). Hence the main NIR transition in symmetrical complexes **[30f]**$^{\bullet+}$and **[30h]**$^{\bullet+}$ for the in-plane conformations has appreciable ligand-metal CT (LMCT) character, being more pronounced for **[30f]**$^{\bullet+}$ while some interligand IVCT character is present in **[30h]**$^{\bullet+}$.

Similarly, TDDFT calculations performed in complexes **[31]**$^{\bullet+}$ and **[32]**$^{\bullet+}$ gave each one intense transition below 15000 cm$^{-1}$. For ***in-plane*-[31]**$^{\bullet+}$ the computed transition energy 8999 cm$^{-1}$ ($\mu_{trans}$ = 11.2 D) is in good agreement with the experimentally obtained band at 9191 cm$^{-1}$. This transition arises from β-HOMO - β-SOMO excitation. Analogously to ***in-plane*-[30f]**$^{\bullet+}$ and ***in-plane*-[30h]**$^{\bullet+}$, the β-HOMO of ***in-plane*-[31]**$^{\bullet+}$ is effectively delocalized over the molecular backbone while the β-SOMO is essentially localized on the 4-$NH_2C_6H_4C{\equiv}C$ ligand and the $Ru(dppe)_2$ moiety while the $C{\equiv}CC_6H_4C{\equiv}CSiMe_3$-4 ligand barely contributes (Table 4-7). This principal contribution to the NIR spectrum can therefore be approximated better as an IVCT transition between the arylethynyl ligand moieties linked by the *trans*-{$Ru(dppe)_2$} bridge with even more IVCT character than in ***in-plane*-[30h]**$^{\bullet+}$. For ***in-plane*-[32]**$^{\bullet+}$ the β-HOMO - β-SOMO transition at 9286 cm$^{-1}$ ($\mu_{trans}$ = 11.1 D) is also the only excitation for which appreciable intensity is computed, and it is of similar mixed LMCT and inter-ligand IVCT character as the transition calculated for ***in-plane*-[30h]**$^{\bullet+}$ (Table 4-7).

**Table 4-7.** *Summary of the main electronic transitions calculated for the in-plane conformations of* ***[30f]***$^{\bullet+}$, ***[30h]***$^{\bullet+}$, ***[31]***$^{\bullet+}$, ***[32]***$^{\bullet+}$.

| Complex | Calc. transition $\mu_{trans}$ (D) | Orbitals | Spin density contribution (%) | | | | |
|---|---|---|---|---|---|---|---|
| | | | $R^1C_6H_4$ | C≡C | [Ru] | C≡C | $C_6H_4R^2$ |
| ***in-plane*-[30f]**$^{\bullet+}$ | 11316 cm$^{-1}$ | β-SOMO | 11 | 15 | 50 | 10 | 8 |
| | (9.7) | β-HOMO | 25 | 19 | 8 | 18 | 23 |
| ***in-plane*- [30h]**$^{\bullet+}$ | 7778 cm$^{-1}$ | β-SOMO | 19 | 21 | 39 | 9 | 6 |
| | (11.7) | β-HOMO | 25 | 12 | 4 | 19 | 35 |
| ***in-plane*- [31]**$^{\bullet+}$ | 8999 cm$^{-1}$ | β-SOMO | *($NH_2$)* 31 | 29 | 29 | 4 | 1 |
| | (11.2) | β-HOMO | *($NH_2$)* 24 | 7 | 17 | 22 | 20 |
| ***in-plane*-[32]**$^{\bullet+}$ | 9286 cm$^{-1}$ | β-SOMO | *($NH_2$)* 23 | 22 | 39 | 6 | 4 |
| | (11.1) | β-HOMO | *($NH_2$)* 35 | 11 | 12 | 22 | 12 |

However, in addition to the main NIR transitions several additional low-energy absorption features can be found for all complexes (Figure 4-7). Recently the appearance of additional features, such as shoulders in the NIR bands, in mixed-valence complexes was assigned on the basis of quantum-chemical calculations to the presence of different thermally accessible conformational structures[43a] and synthetic restriction to a small conformational subspace led to an appreciable decrease of intensity of the shoulder in experiment.[43a]

Different twisted configurations of the C≡C$C_6H_4$R-4 ligands found in the crystal structures (Table 4-2) point towards a conformational distribution in solution being a possible explanation for these additional spectral features. Hence, the influence of different conformational forms on the appearance of the UV-Vis-NIR spectrum was investigated quantum-chemically. Due to the particularly good agreement with experiment, **[30h]**$^{\bullet+}$ was chosen by way of example. The influence of the orientation of the aryl portion of the C≡C$C_6H_4NH_2$-4 ligand relative to the ruthenium moiety in [**30h**]$^{\bullet+}$ was examined by varying the previously described torsion angle θ in a range from 0° to 90° (Figure 4-5). Additionally the conformation of the two C≡C$C_6H_4NH_2$-4 aryl moieties relative to each other was explored by varying the torsion angle Ω from 0° to 90° (Figure 4-8).

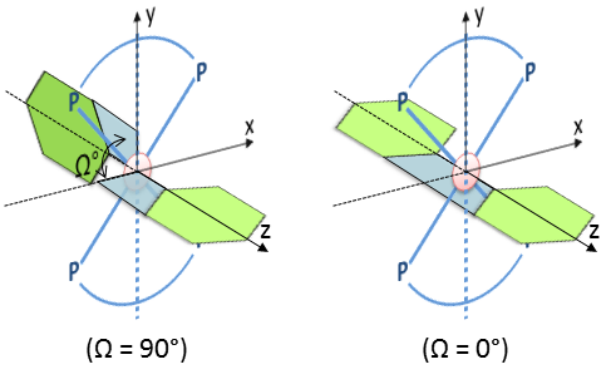


**Figure 4-8.** *Representation of the torsion angle Ω in trans-Ru(C≡C$C_6H_4R^1$)$_2$(dppe)$_2$.*

The resulting potential-energy surface (PES) is shown in Figure 4-9. The energy difference between the minimum on the PES ($\theta \approx 0°$, $\Omega = 20°$) and the maximum ($\theta \approx 90°$, $\Omega = 30°$) is computed to be only 16.6 kJ/mol higher in energy (Figure 4-9). When varying $\Omega$ with one ligand being fixed at $\theta \approx 0°$ the rotational barrier was found to be 3.2 kJ/mol between the minimum ($\Omega = 20°$) and the maximum energy conformers ($\Omega = 60°$) .

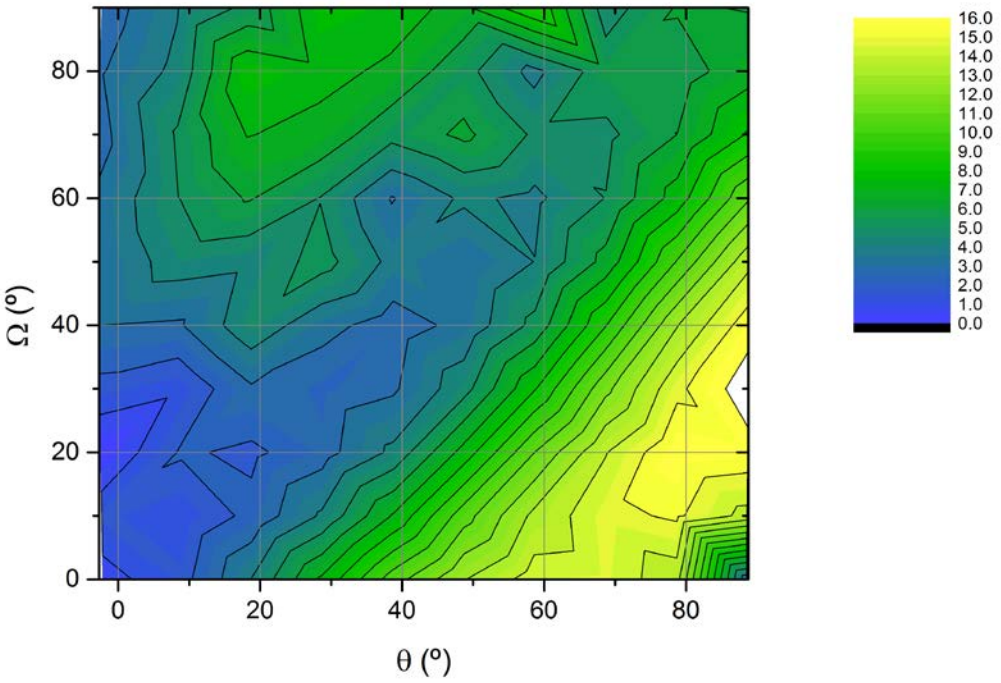


**Figure 4-9.** *Computed potential energy surface for complex* ***[30h]***$^{\bullet+}$ *for the range* $\theta = 0 - 90°$, *and* $\Omega = 0 - 90°$ *{in kJ/mol; BLYP35/COSMO* ($CH_2Cl_2$) *level}.*

As the spin density obtained from the full optimization (Table 4-7) already exhibits slight symmetry-breaking, this low barrier can be explained by the tendency of **[30h]**$^{\bullet+}$ towards charge localization onto one $C{\equiv}CC_6H_4NH_2$-4 ligand and the metal centre. Hence the $C{\equiv}CC_6H_4NH_2$-4 unit not involved in the charge delocalization can rotate almost freely. As $\Omega$ goes to 90° the spin density becomes steadily more localized onto one ligand and the ruthenium centre, resulting in a clearly symmetry-broken structure for $\Omega = 90°$, which is only 2.5 kJ/mol higher in energy than the minimum. For this structure the frontier orbitals are centred on the $Ru(dppe)_2$ unit and one ligand. In this conformation, the main electronic

excitations at 9900 $cm^{-1}$ ($\mu_{trans}$ = 10.0 D) arise from the β-HOMO-1 - β-SOMO transition. Both these orbitals are located at the same aniline unit, the phenyl plane of which bisects the dppe ligands, (β-HOMO-1: 42%; β-SOMO: 24%) and the C≡CRu(dppe)$_2$C≡C (β-HOMO-1: 49%; β-SOMO: 70%). They are of π-, π*-character, respectively. Thus only little charge is transferred upon excitation. Obviously, although the experimental excitation energy of 10822 $cm^{-1}$ is underestimated, this transition can be assigned to the high-energy shoulder obtained in the UV-Vis-NIR spectrum. The rotation of both C≡C$C_6H_4NH_2$-4 ligands out of the plane bisecting the dppe ligands by increasing θ from 0°, while keeping the relative conformation of the ligands at Ω = 0°, is associated with a more sizeable barrier than the rotation of only one ligand (*vide supra*). Interestingly, a minimum is found at $\theta \approx 90°$, which is disfavoured by only 3.2 kJ/mol compared to the minimum of the relaxed scan and by 2.6 kJ/mol compared to the lowest-energy structure at $\theta \approx 0°$ of the PES cut at Ω = 0°. Hence the spectral features of this local minimum are also likely to contribute to the overall spectral profile. TDDFT calculations using this local minimum (θ ≈ 90°, Ω = 0°) give two excitations below 15000 $cm^{-1}$ with $\mu_{trans}$ > 1.0 D. The more intense excitation at 7849 $cm^{-1}$ ($\mu_{trans}$ = 12.1 D) arises from the β-HOMO - β-SOMO transition and appears at very similar energy as for ***in-plane*-[30h]$^{\bullet+}$**. Indeed the orbital distribution is comparable to the fully optimized structure ($NH_2C_6H_4$C≡C/Ru(dppe)$_2$/C≡C$C_6H_4NH_2$, β-HOMO: 34%/2%/58% β-SOMO: 45%/34%/17%). At 11959 $cm^{-1}$ ($\mu_{trans}$ = 1.5 D) a second, less intense excitation arises from the β-HOMO-5 to the β-SOMO, corresponding to a metal-ligand CT (the β-HOMO-5 exhibits almost exclusively metal character, 83%).

To perform vibrational analyses within the harmonic framework, selected points on the PES were re-optimized without constraints. The minima, indicated by the absence of imaginary frequencies, gave computed frequencies very similar to the lowest energy structure ***in-plane*-[30h]$^{\bullet+}$** (ν(RuC≡C) = 1942 $cm^{-1}$). Optimizations starting from the two points **[30h]**

$^{\bullet+}$ ($\theta \approx 0°$, $\Omega = 90°$) and **[30h]**$^{\bullet+}$ ($\theta \approx 90°$, $\Omega = 0°$) gave two minima ***perp*-[30h]**$^{\bullet+}$ and ***out-of-plane*-[30h]**$^{\bullet+}$ (*see* Table 4-8). TDDFT calculations give the same main spectral features for the minima ***perp*-[30h]**$^{\bullet+}$ at 8268 cm$^{-1}$ ($\mu_{trans}$ = 11.6 D) and for ***out-of-plane*-[30h]**$^{\bullet+}$ at 9295 cm$^{-1}$ ($\mu_{trans}$ = 10.7 D) as observed for the corresponding relaxed-scan structures.

In addition, the previously discussed low-intensity MLCT excitation is computed at 11558 cm$^{-1}$ ($\mu_{trans}$ = 1.2 D) and 11526 cm$^{-1}$ ($\mu_{trans}$ = 1.3 D). However, fully optimized structures ***perp*-[30h]**$^{\bullet+}$ and ***out-of-plane*-[30h]**$^{\bullet+}$ are slightly favored energetically (by 2.7 kJ/mol and 0.7 kJ/mol, respectively). Hence, within the accuracy of the method all three structures can be considered isoenergetic and all would contribute significantly to the observed spectroscopic profile. Vibrational analysis gave ν(RuC≡C) at 1930 cm$^{-1}$ for ***perp*-[30h]**$^{\bullet+}$ and 1915 cm$^{-1}$ for ***out-of-plane*-[30h]**$^{\bullet+}$, which is in good agreement with the slightly broadened ν(RuC≡C) peak found experimentally for **[30h]**$^{\bullet+}$ (Figure 4-6). Hence the finding of different rotameric forms contributing to the UV-Vis-NIR spectrum is fully consistent with the experimentally observed IR signature.

Table 4-8 presents the results obtained from extending this method of analysis to complexes **[30f]**$^{\bullet+}$, **[31]**$^{\bullet+}$ and **[32]**$^{\bullet+}$ starting from inputs, in which one ($\theta \approx 0°$, $\Omega = 90°$) or both ligands ($\theta \approx 90°$, $\Omega = 0°$) are perpendicular to the plane bisecting the dppe ligands and optimized without constraints. A complete list of calculated electronic transitions and IR frequencies for the different conformers of **[30f]**$^{\bullet+}$, **[30h]**$^{\bullet+}$, **[31]**$^{\bullet+}$ and **[32]**$^{\bullet+}$ can be found in the associated electronic content that accompanies this thesis.

**Table 4-8.** *Main electronic transitions calculated for the out-of-plane conformers of* ***[30f]***$^{\bullet+}$, ***[30h]***$^{\bullet+}$, ***[31]***$^{\bullet+}$ *and* ***[32]***$^{\bullet+}$.

| Conformer | Angles (º) | Complex | Main calculated transition ($\mu_{trans}$ D) | Orbitals | Spin density contribution (%) $R^1C_6H_4$ | C≡C | [Ru] | C≡C | $C_6H_4R^2$ |
|---|---|---|---|---|---|---|---|---|---|
| 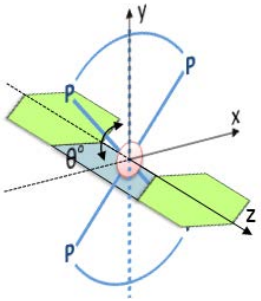 | θ = 90<br>Ω = 0 | *Out-of-plane* [30f]$^{\bullet+}$ | 10860cm$^{-1}$, (10.3) | β-SOMO | 0 | 15 | 65 | 12 | 0 |
| | | | | β-HOMO | 27 | 21 | 18 | 13 | 15 |
| | | *Out-of-plane* [30h]$^{\bullet+}$ | 8268 cm$^{-1}$, (11.6) | β-SOMO | 16 | 19 | 38 | 12 | 8 |
| | | | | β-HOMO | 29 | 14 | 5 | 17 | 32 |
| | | *Out-of-plane* [31]$^{\bullet+}$ | 9198 cm$^{-1}$, (11.1) | β-SOMO | *($NH_2$)* 36 | 31 | 23 | 3 | 0 |
| | | | | β-HOMO | *($NH_2$)* 18 | 5 | 13 | 27 | 29 |
| | | *Out-of-plane* [32]$^{\bullet+}$ | 9024 cm$^{-1}$, (11.6) | β-SOMO | *($NH_2$)* 31 | 26 | 30 | 5 | 1 |
| | | | | β-HOMO | *($NH_2$)* 27 | 8 | 12 | 28 | 17 |
| 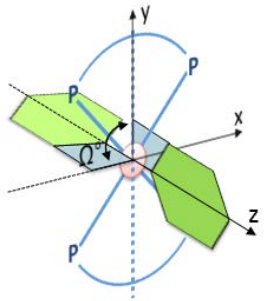 | θ = 0<br>Ω = 90 | *perp*-[30f]$^{\bullet+}$ | 12287 cm$^{-1}$, (8.1) | β-SOMO | 13 | 18 | 54 | 9 | 0 |
| | | | | β-HOMO-1 | 0 | 7 | 19 | 28 | 41 |
| | | *perp*-[30h]$^{\bullet+}$ | 9295 cm$^{-1}$, (10.7) | β-SOMO | 2 | 9 | 40 | 21 | 21 |
| | | | | β-HOMO | 46 | 24 | 7 | 8 | 11 |
| | | *perp*-[31]$^{\bullet+}$ | 9555 cm$^{-1}$, (10.2) | β-SOMO | *($NH_2$)* 33 | 30 | 29 | 4 | 0 |
| | | | | β-HOMO-1 | *($NH_2$)* 36 | 7 | 31 | 18 | 0 |
| | | *perp*-[32]$^{\bullet+}$ | 9709 cm$^{-1}$, (10.4) | β-SOMO | *($NH_2$)* 28 | 27 | 35 | 5 | 0 |
| | | | | β-HOMO-1 | *($NH_2$)* 38 | 10 | 23 | 20 | 0 |
| 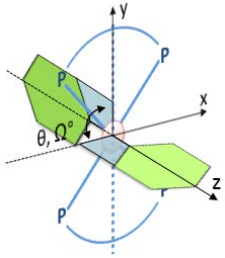 | θ = 90<br>Ω = 90 | *perp*-[31]$^{\bullet+}$ | 10072 cm$^{-1}$, (10.0) | β-SOMO | *($NH_2$)* 38 | 32 | 23 | 3 | 0 |
| | | | | β-HOMO-1 | *($NH_2$)* 31 | 6 | 31 | 23 | 0 |
| | | *perp*-[32]$^{\bullet+}$ | 9381 cm$^{-1}$, (9.9) | β-SOMO | *($NH_2$)* 0 | 12 | 57 | 15 | 9 |
| | | | | β-HOMO-1 | 0 | 19 | 19 | 26 | 19 |

In addition to the main electronic transitions present in Table 4-8, both ***in-plane*-[30f]$^{\bullet+}$** and ***perp*-[30f]$^{\bullet+}$** exhibit an additional low-intensity transition ($\mu_{trans} < 0.5$ D) at 8825 cm$^{-1}$, and 8517 cm$^{-1}$ respectively, arising from metal-centred orbitals. These two excitations may exhibit or even gain intensity for other rotameric forms and thus they may offer a possible explanation for the weak low-energy band in the experimental spectrum (Table 4-6). As expected for **[31]$^{\bullet+}$** and **[32]$^{\bullet+}$**, the structures with $\theta \approx 0°$, $\Omega \approx 90°$ exhibit similar spectral features as the minimum energy structure. For these unsymmetrically substituted compounds, θ is defined as the angle between the C≡C$C_6H_4NH_2$-4 ligand and the plane bisecting the dppe ligands. TDDFT calculations yield an intense β-HOMO-1 - β-SOMO excitation at 9555 cm$^{-1}$ ($\mu_{trans}$ = 10.2 D) for **[31]$^{\bullet+}$** and at 9709 cm$^{-1}$ ($\mu_{trans}$ = 10.2 D) for **[32]$^{\bullet+}$**. While the contributions to the β-SOMO stay nearly unchanged compared to the minimum structures (*see associated electronic content*), the β-HOMO-1 is localized on the $C_6H_4NH_2$-4 ligand (**[31]$^{\bullet+}$**: 36%; **[32]$^{\bullet+}$**: 38%) and the C≡CRu(dppe)$_2$C≡C unit (**[31]$^{\bullet+}$**: 56%; (**[32]$^{\bullet+}$**: 53%). Hence these transitions have substantial π-π* character.

In the case of **[31]$^{\bullet+}$** with $\theta \approx 90°$, $\Omega \approx 90°$ the dominant feature is again the β-HOMO-1 - β-SOMO transition, which is computed at 10072 cm$^{-1}$ ($\mu_{trans}$ = 10.0 D). This excitation exhibits ligand π-π* character accompanied by small LMCT contributions and is probably responsible for the high-energy shoulder observed in the experimental spectrum (Figure 4-7). A second low-intensity excitation from the lower-lying orbitals β-HOMO-5 and β-HOMO-4, which are metal centred (*see associated electronic content*), to the β-SOMO is computed at 13613 cm$^{-1}$ ($\mu_{trans}$ = 1.2 D). For **[32]$^{\bullet+}$** this structure likely makes only a relatively minor contribution to the UV-Vis-NIR spectrum, as it is disfavoured by 16.4 kJ/mol. For the asymmetric complexes **[31]$^{\bullet+}$** and **[32]$^{\bullet+}$** the computed excitations for the ***out-of-plane*** structures (Table 4-8) are very similar to those of the ***in-plane*** structures (Table 4-7). The β-HOMO - β-SOMO transition appears slightly blue-shifted at 9198 cm$^{-1}$

($\mu_{trans}$ = 11.1 D) for ***out-of-plane*-[31]$^{\bullet+}$** and slightly red-shifted at 9024 cm$^{-1}$ ($\mu_{trans}$ = 11.6 D) for ***out-of-plane*-[5]$^{\bullet+}$**. For ***out-of-plane*-[31]$^{\bullet+}$** the previously discussed low-intensity LMCT excitation from the lower-lying orbitals β-HOMO-5 and β-HOMO-4 is also found at 13461 cm$^{-1}$ ($\mu_{trans}$ = 1.0 D). Again low-intensity transitions of mixed LMCT/ IVCT character are found for the different conformers of **[31]$^{\bullet+}$** between 3740 cm$^{-1}$ ($\mu_{trans}$ = 0.9 D, $\theta \approx 90°$, $\Omega \approx 90°$) and 5037 cm$^{-1}$ ($\mu_{trans}$ = 0.1 D, ***in-plane*-[31]$^{\bullet+}$**), which may explain the lowest energy band envelope in the experimental spectrum (Table 4-6).

## 4.7. Conclusions

The *trans*-effects of ethynyl ligands bearing substituents, $R^1$, on the reactions of *trans*-RuCl(C≡C$R^1$-4)(dppe)$_2$ with terminal alkynes were examined. Whilst strongly electron-donating $R^1$ groups (e.g. $C_6H_4NH_2$, $C_6H_4OMe$) labilize the *trans*-chloride ligand sufficiently to promote the slow formation of bis(ethynyl) complexes, precursors bearing more modestly donating groups ($R^1$ = $C_6H_4Me$) or withdrawing groups ($R^1$ = $C_6H_4NO_2$, $C_6H_4CO_2Me$) are largely inert to further reaction in the absence of a suitable halide abstracting agent. In the presence of $Tl^+$ salts and the non-coordinating base 1,8-diazabicycloundec-7-ene (DBU), conversion of mono(ethynyl) complexes to symmetrically or unsymmetrically substituted bis(ethynyl) complexes can be achieved in high yields in a matter of minutes as pure precipitates which can be isolated from the reaction mixtures by simple filtration. These complexes undergo one or more electrochemical oxidations, which are shown by IR spectroelectrochemical methods to be substantially ethynyl ligand in character.

Quantum-chemical calculations carried out by our collaborators in Berlin at DFT and TDDFT levels on the monooxidized complexes using the BLYP35 functional and continuum solvent models indicate: a) substantial delocalization of spin density between metal centres

and the ethynyl ligand framework; b) ligand-based mixed-valence character in some of the symmetrical diethynyl complexes; and c) substantial importance of the relative conformational arrangement of the aromatic rings of the ethynyl ligands for both electronic and vibrational spectra. That is, the PES of the complexes [*trans*-Ru(C≡CR$^{n}$-4)$_2$(dppe)$_2$]$^{\bullet+}$ feature several minima which differ in the relative orientation of the ligands and metal centre. These are close in energy with small barriers between them, and many are likely to be thermally populated in solution at RT. These conformations offer electronic transitions that differ in energy and character depending on both conformation and nature of the aryl ligand substituent. In general, the lowest-energy transitions are associated with LMCT (symmetrically substituted complexes such as **[30f]**$^{\bullet+}$) or inter-aryl ligand IVCT (complexes with redox active ligands such as [**30h**]$^{\bullet+}$ and related asymmetric complexes [**31**]$^{\bullet+}$ and [**32]**$^{\bullet+}$) character. The higher-energy shoulders observed in the experimental spectra arise from the slightly higher-energy conformations in which one or more of the arylethynyl moieties has partially lost conjugation with the other side of the complex. The excitations of these conformers have more MLCT and ligand π-π* character. These studies have shown that the NIR absorption band envelopes observed for symmetrically and unsymmetrically substituted complexes [*trans*-Ru(C≡CR$^{n}$-4)$_2$(dppe)$_2$]$^{\bullet+}$ are not accurately described in terms of transitions of one specific character (MLCT, LMCT, IVCT etc). Rather, the conformational ensembles present in solution mean that these complex band envelopes arise from transitions with distinct electronic origin, a finding that should be of importance in interpreting the optical and electronic behavior of compounds and materials based on this motif.

## 4.8. Experimental

### *4.8.1 General conditions*

General experimental conditions were reported in Chapter 2. No special precautions were taken to exclude air during the workup. Preparative TLC was carried out of 20 × 20 cm glass plates coated with silica gel (GF254, 500 μm thick). The metallic salts $[RuCl(dppe)_2]OTf$ (**28**)[10a] and $TlBF_4$[48] were prepared by literature methods. *Warning: $TlBF_4$ should always be handled in a well-ventilated fume hood and personal protective equipment should be worn throughout.* The synthesis of **2** (Chapter 2), $HC{\equiv}CC_6H_4NH_2$ and $HC{\equiv}CC_6H_4C{\equiv}CSiMe_3$ (Chapter 3) were reported in previous experimental sections of this thesis. Other reagents were purchased commercially and used as received.

### *4.8.2 Synthesis and characterization*

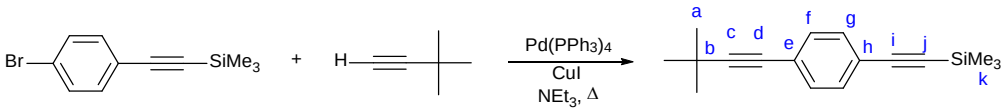


**Preparation of $Me_3SiC{\equiv}CC_6H_4C{\equiv}CBu^t$.** To a 100 mL oven-dried Schlenk flask charged with $BrC_6H_4C{\equiv}CSiMe_3$ (2.53 g, 9.99 mmol), $Pd(PPh_3)_4$ (0.60 g, 0.52 mmol) and CuI ( 0.30 g, 0.52 mmol) in $NEt_3$ (100 mL), 3,3-dimethylbut-1-yne (1.53 mL, 1.02 g, 12.4 mmol) was added. The mixture was stirred at reflux overnight. The brown suspension was filtered and the red filtrate taken to dryness under reduced pressure. The residue was purified through a silica gel column using hexane as eluent. The pure product was obtained as an off-white powder upon solvent evaporation of the main fraction. Yield 2.16 g, 8.49 mmol, 85%. $^1$H NMR (400 MHz, $CDCl_3$) δ 7.37 (d, *J* = 9 Hz, 2H, *g*), 7.31 (d, *J* = 9 Hz, 2H, *f*), 1.32 (s, 9H, *a*), 0.25 (s, 9H, *k*). $^{13}C\{^1H\}$ NMR (101 MHz, $CDCl_3$) δ 133.8, 131.5 (*e*/*h*), 122.4, 122.1 (*i*/*j*), 105.0, 100.7, 95.6 (*d*/*i*/*j*), 79.0 (*c*), 31.1 (*a*), 28.2 (b) 0.1 (*k*).

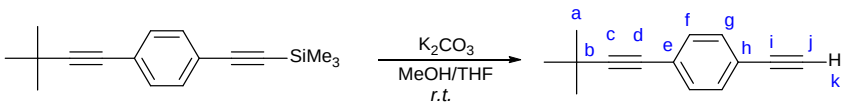


**Preparation of HC≡CC$_6$H$_4$C≡CBu$^t$.** To a 250 mL round bottomed flask charged with a solution of Me$_3$SiC≡CC$_6$H$_4$C≡CBu$^t$ (1.5 g, 5.9 mmol) in MeOH/THF (1:1) (100 mL), $K_2CO_3$ (0.83 g, 6.0 mmol) and the suspension was stirred at room temperature overnight. The solution was then filtered and the filtrate taken to dryness under reduced pressure. The resultant black oil was re-dissolved in $Et_2O$ (50 mL) and washed with water (2×50 mL) and brine (1×50 mL) and dried over $MgSO_4$. Removal of solvent yielded the pure product as a yellowish oil. Yield 1.0 g, 5.5 mmol, 93%. $^1$H NMR (400 MHz, $CDCl_3$) δ 7.39 (d, *J* = 9 Hz, 2H, *g*), 7.56 (d, *J* = 9 Hz, 2H, *f*), 3.13 (s, 1H, *k*), 1.31 (s, 9H, *a*). $^{13}$C{$^1$H} NMR (101 MHz, $CDCl_3$) δ 132.0, 131.6 (*f/g*), 124.9, 121.1 (*e/h*), 100.9, 83.6, 78.9, 78.4 (*c/d/i/j*), 31.1 (*a*), 28.2 (b). IR (*cast*) cm$^{-1}$: 3291 (m) *ν*(C≡C-H); 2236, 2192 (w) *ν*(C≡C).

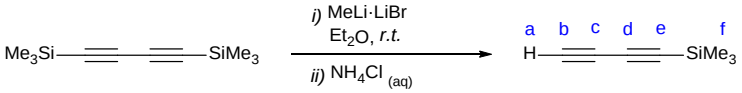


**Preparation of HC≡CC≡CSiMe$_3$.**[49] To a 100 mL oven-dried Schlenk flask charged with a solution of 1,4-bis(trimethylsilyl)buta-1,3-diyne (3.20 g, 16.46 mmol) in dry $Et_2O$ (70 mL), MeLi·LiBr (1.5M in $Et_2O$) (11.0 mL, 16.5 mmol) was added. The mixture develops a red colour that gets darker with time. The solution is stirred at room temperature overnight yielding a black solution. The reaction mixture is then poured onto an $NH_4Cl$ saturated aqueous solution (100 mL). The two phases were then separated and the aqueous phase extracted with $Et_2O$ (2×100 mL). The combined organic phases were washed with brine (1×150 mL), dried over $MgSO_4$ and the solvent was carefully removed yielding a dark oil. The pure product was obtained as a yellowish oil by distillation of the crude oil (~19 mbar, 45 ºC). Yield 1.52 g (~1.9 mL), 12.43 mmol, 81%. $^1$H NMR (400 MHz, $CDCl_3$) δ 2.11 (s, 1H, *a*), 0.20 (s, 9H, *f*). $^{13}$C{$^1$H} NMR (101 MHz, $CDCl_3$) δ 87.5, 84.8 (*d/e*), 68.4, 66.8 (*b/c*), 0.41 (*f*). IR (*cast*) cm$^{-1}$: 3311 *ν*(C≡C-H); 2189, 2069 *ν*(C≡C).

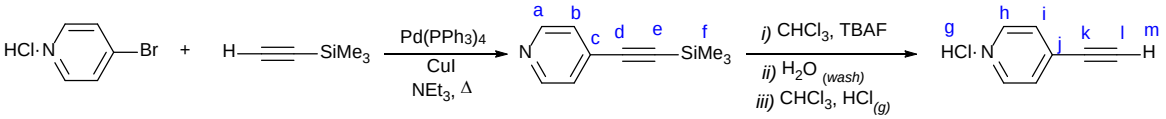


**Preparation of HC≡CPy·HCl.** To 50 mL round bottom flask charged with 4-bromopyridine (0.50 g, 2.57 mmol), $Pd(PPh_3)_4$ (0.15 g, 0.13 mmol) and CuI ( 0.02 g, 0.11 mmol), $NEt_3$ (15 mL) and THF (15 mL), trimethylsilylacetylene (0.37 mL, 2.58 mmol) was added and the mixture was stirred at reflux overnight in the dark. The reaction mixture was then taken to dryness and the black residue was purified through a silica gel column using hexane:EtOAc (90:10) as the eluent. Removal of solvent from the main fraction yielded an orange oil that tends to crystallize on standing. The product, $Me_3SiC{\equiv}CPy$ was *in-situ* deprotected for further reaction with $[RuCl(dppe)_2]OTf$ without further purification. Yield 0.40 g, 2.80 mmol, 89%. $^1H$ NMR (400 MHz, $CDCl_3$) δ 7.56 (d, *J* = 6 Hz, 2H, *a*), 7.30 (d, *J* = 6 Hz, 2H, *b*), 0.26 (s, 9H, *f*).

The oil can be dissolved in $CHCl_3$ (50 mL) under inert atmosphere yielding an orange solution that turned black upon drop wise addition of TBAF (1M in THF) (2.9 mL, 2.9 mmol). The mixture was stirred at room temperature in the dark for further 15 minutes and poured into water. The organic red phase was washed with water (2×50 mL), brine (1×50 mL) and dried over $MgSO_4$. The bright red solution was stirred vigorously under an $HCl_{(g)}$ atmosphere for 20 minutes at room temperature, upon that time, the solution turned yellow and a brown precipitate was formed. The precipitate was filtered and the yellow filtrate purged with $N_2$. The off-white solids precipitated out of solution upon solvent evaporation. The precipitate was filtered, washed with $Et_2O$ and dried in air before storage under inert atmosphere at -24 ºC. Yield 0.253 g, 0.056 mmol, 65%. $^1H$ NMR (400 MHz, DMSO-$d_6$) δ 11.25 (s *br*., 1H, *g*), 8.86 (d, *J* = 6 Hz, 2H, *h*), 7.97 (d, *J* = 6, 2H, *i*), 5.20 (s, 1H, *m*). $^{13}C\{^1H\}$ NMR (101 MHz, $CDCl_3$) δ 144.1, 128.5 (*h/i*), 136.5 (*j*) 91.4, 79.9 (*k/l*). $MS^+$ (ASAP) *m/z* (%): 279.09 (100, $[2M]^+$). IR (*nujol*) $cm^{-1}$: 3132 $\nu(C_{sp}{-}H)$; 2100 $\nu(C{\equiv}C)$.

*Synthesis of trans-RuCl(C≡CR)(dppe)$_2$* **29 (d – g, j, k):**

To a solution of **1** (0.100 g, 0.092 mmol) and 1, 8-diazabicyclo[5.4.0]undec-7-ene (DBU) (*excess*) in $CH_2Cl_2$ (4 mL), the appropriate arylethynyl ligand (0.10 mmol) was added. The red solution typically turned yellow (with the exception of **29e**) after stirring at room temperature for 1h. The final products were obtained from the reaction mixture after the appropriate purification (*vide infra*).

**(29d) *trans*-RuCl(C≡CC$_6$H$_4$CO$_2$Me-4)(dppe)$_2$.** The yellow solution was filtered through neutral alumina (Brockmann I). Addition of hexane to the filtrate yielded a pale-yellow precipitate that was collected by filtration, washed with hexane and dried in air (97 mg, 97%). $^1$H δ 7.76 (d, *J* = 8 Hz, 2H, *o*-Ph-CO$_2$Me), 7.45–7.39 (m, 8H, *o*-PPh$_2$), 7.36–7.30 (m, 8H, *o*-PPh$_2$), 7.23–7.14 (m, 8H, *p*-PPh$_2$), 7.05–6.98 (m, 8H, *m*-PPh$_2$), 6.98–6.90 (m, 8H, *m*-PPh$_2$), 6.57 (d, *J* = 8 Hz, 2H, *m*-Ph-CO$_2$Me), 3.89 (s, 3H, COO-Me), 2.77–2.59 (m, 8H, dppe). $^{31}$P{$^1$H} δ 48.2 (s, *dppe*). IR (*nujol)* cm$^{-1}$: 2064 (m) *ν*(Ru-C≡C); 1716 (m) *ν*(C=O).

**(29e) *trans*-RuCl(C≡CC$_6$H$_4$NO$_2$-4)(dppe)$_2$.** The bright orange solution was filtered through neutral alumina (Brockmann I). Addition of hexane to the filtrate yielded an orange precipitate that was collected by filtration, washed with MeOH and dried in air (93 mg, 94%). $^1$H δ 7.94 (d, *J* = 8 Hz, 2H, *o*-Ph-NO$_2$), 7.41–7.30 (m, 16H, *o*-PPh$_2$), 7.24–7.17 (m,8H, *p*-PPh$_2$), 7.06–6.99 (m, 8H, *m*-PPh$_2$), 6.98–6.91 (m, 8H, *m*-PPh$_2$), 6.44 (d, *J* = 8 Hz, 2H, *m*-Ph-NO$_2$), 2.81–2.58 (m, 8H, dppe). $^{31}$P{$^1$H} δ 47.7 (s, *dppe*). IR (*nujol)* cm$^{-1}$: 2052 (m) *ν*(Ru-C≡C).

**(29f) *trans*-RuCl(C≡CC$_6$H$_4$C≡CSiMe$_3$-4)(dppe)$_2$.** The yellow solution was filtered through neutral alumina (Brockmann I). Addition of hexane to the yellow filtrate yielded the pure product as a yellow precipitate (96 mg, 92%). Single crystals suitable for X-ray diffraction were obtained from $CH_2Cl_2$/hexane. $^1$H δ 7.44–7.38 (m, 8H, *o*-PPh$_2$), 7.37–7.30

(m, 8H, *o*-$PPh_2$), 7.23–7.12 (m, 10H, $C_2$-Ph-$C_2$/ *p*-$PPh_2$), 7.05–6.97 (m, 8H, *m*-$PPh_2$), 6.95–6.88 (m, 8H, *m*-$PPh_2$), 6.49 (d, *J* = 8 Hz, 2H, $C_2$-Ph-$C_2$), 2.75–2.61 (m, 8H, dppe), 0.26 (s, 9H, $SiMe_3$). $^{31}P\{^1H\}$ δ 50.1 (s, *dppe*). IR (*nujol)* $cm^{-1}$: 2150 (m) *ν*(C≡C); 2068 (s) *ν*(Ru-C≡C).

**(29g) *trans*-RuCl(C≡C$C_6H_4$C≡C$Bu^t$-4)$(dppe)_2$.** The yellow solution was filtered through neutral alumina (Brockmann I). Addition of $Et_2O$ to the yellow filtrate yielded the pure product as a yellow precipitate (74 mg, 72%). Single crystals suitable for X-ray diffraction were obtained from $CDCl_3/Et_2O$. $^1H$ δ 7.46–7.41 (m, 8H, *o*-$PPh_2$), 7.36–7.30 (m, 8H, *o*-$PPh_2$), 7.22–7.12 (m, 10H $C_2$-Ph-$C_2$/ *p*-$PPh_2$), 7.04–6.98 (m, 8H *m*-$PPh_2$), 6.95–6.89 (m, 8H, *m*-$PPh_2$), 6.50 (d, *J* = 8 Hz, 2H, $C_2$-Ph-$C_2$), 1.33 (s, 9H, $CMe_3$). $^{31}P\{^1H\}$ δ 49.2 (s, *dppe*). IR (*nujol)* $cm^{-1}$: 2183 (w) ν(C≡C); 2068 (s) *ν*(Ru-C≡C).

**(29i) *trans*-RuCl(C≡C$C_6H_4$C≡CH-4)$(dppe)_2$.** Reaction of **(29f)** (50 mg, 0.044 mmol) with TBAF (1M in THF, 50 µL, 0.050 mmol) in $CH_2Cl_2$ at room temperature overnight. The orange solution was filtered through basic alumina (Brockmann III) and the filtrate taken to dryness to obtain the pure product as an orange powder (41 mg, 88%). Single crystals suitable for X-ray diffraction were obtained from $CH_2Cl_2/Et_2O$. $^1H$ δ 7.50–7.42 (m, 8H, *o*-$PPh_2$), 7.35-7.28 (m, 8H, *o*-$PPh_2$), 7.25–7.14 (m, 10H, C≡C-Ph-C≡C/*p*-$PPh_2$), 7.05–6.98 (m, 8H, *m*-$PPh_2$), 6.98–6.92 (m, 8H, *m*-$PPh_2$), 6.52 (d, *J* = 8Hz, 2H, C≡C-Ph-C≡C), 3.11 (s, 1H, C≡C-H), 2.78–2.59 (m, 8H, dppe). $^{31}P\{^1H\}$ δ 50.3 (s, *dppe*). IR (*nujol)* $cm^{-1}$: 3270 (s) *ν*(C≡C-H); 2050 (m) *ν*(Ru-C≡C).

**(29j) *trans*-RuCl(C≡CC≡C$SiMe_3$)$(dppe)_2$.** The off-white precipitate generated upon addition of hexane was collected by filtration, washed with MeOH and dried in air (86 mg, 89%). Single crystals suitable for X-ray diffraction were obtained from $CH_2Cl_2$/hexane. $^1H$ NMR (400 MHz, $CDCl_3$) δ 7.49–7.41 (m, 8H, *o*-$PPh_2$), 7.25–7.18 (m, 8H, *p*-$PPh_2$), 7.18–7.11

(m, 8H, *o*-$PPh_2$), 7.09–6.96 (m, 16H, *m*-$PPh_2$), 2.70–2.61 (m, 8H, dppe), 0.21 (s, 9H, $SiMe_3$). $^{31}P\{^1H\}$ NMR (162 MHz, $CDCl_3$) δ 47.7 (s, *dppe*). IR (*nujol)* $cm^{-1}$: 2169 (w) *v*(C≡C); 2064 (m) *v*(Ru-C≡C)

**(29k) *trans*-RuCl(C≡CPy)(dppe)$_2$.** In our hands, the use of HC≡CPy resulted problematic. Hence, HC≡CPy was generated in-situ by deprotection of the more stable $Me_3SiC$≡CPy employing 1eq. TBAF (1M in THF). The yellow precipitate generated upon addition of MeOH was collected by filtration and dried in air (67 mg, 70%). Single crystals suitable for X-ray diffraction were obtained from $CH_2Cl_2/Et_2O$. $^1H$ NMR (400 MHz, $CDCl_3$) δ 8.22 (d, *J* = 6 Hz, 2H, *Py*), 7.41 – 7.31 (m, 16H, *o*-$PPh_2$), 7.24 – 7.15 (m, 8H, *p*-$PPh_2$), 7.06 – 6.99 (m, 8H, *m*-$PPh_2$), 6.98 – 6.91 (m, 8H, *m*-$PPh_2$), 6.35 (d, *J* = 6 Hz, 2H, *Py*), 2.79 – 2.58 (s, 8H, *dppe*). $^{31}P\{^1H\}$ δ 49.4 (s, *dppe*). IR (*nujol)* $cm^{-1}$: 2068 (m) *v*(Ru-C≡C).

*Synthesis of trans-Ru(C≡CR)$_2$(dppe)$_2$* **30 (a - h, j)**:

To a solution of [RuCl(dppe)$_2$]OTf (**28**) (0.100 g, 0.092 mmol) and 1,8-diazabicyclo[5.4.0]undec-7-ene (DBU) (*excess*) in $CH_2Cl_2$ (4 mL), slight excess of the appropriate alkyne (0.20 mmol) was added. The resulting red solution typically turned yellow after stirring at room temperature for 20 minutes. To the yellow solution, one equivalent of $TlBF_4$ (0.027 g, 0.092 mmol) was added and the off-white precipitate (TlCl) was carefully removed by filtration. The final products were obtained from the filtrate after the appropriate purification (*vide infra*).

**(30a) *trans*-Ru(C≡CC$_6$H$_4$Me-4)$_2$(dppe)$_2$.** The TlCl precipitate was removed by filtration through neutral alumina (Brockmann I). Addition of hexane to the yellow filtrate yielded the pure product as a pale-yellow precipitate (72 mg, 69%). Single crystals suitable for X-ray diffraction were obtained from hot toluene. $^1H$ δ 7.56–7.48 (m, 16H, *o*-$PPh_2$), 7.20–7.12 (m, 8H, *p*-$PPh_2$), 7.05–6.85 (m, 20H, Ph-Me/*o*-$PPh_2$), 6.67 (d, *J* = 8 Hz, 4H, Ph-Me),

2.65–2.56 (m, 8H, *dppe*), 2.31(s, 6H, OMe). $^{31}P\{^{1}H\}$ δ 53.2 (s, *dppe*). IR (*nujol)* $cm^{-1}$: 2069 (m) *ν*(Ru-C≡C).

**(30b) *trans*-Ru(C≡C$C_6H_4C_5H_{11}$-4)$_2$(dppe)$_2$.** The TlCl precipitate was removed by filtration through neutral alumina (Brockmann I). The pure product precipitated out of the filtrate as pale-yellow solids upon addition of MeOH (59 mg, 52%). Crystals suitable for X-ray diffraction were obtained from $CHCl_3$/MeOH. $^{1}H$ δ 7.58–7.47 (m, 16H, *o*-$PPh_2$), 7.20–7.15 (m, 8H, *p*-$PPh_2$), 7.00–6.92 (m, 20H, Ph-$C_5H_{11}$/*m*-$PPh_2$), 6.70 (d, *J* = 8 Hz, 4H, Ph-$C_5H_{11}$), 2.65–2.52 (m, 12H dppe/*α*-$CH_2$), 1.63 (q, *J* = 7 Hz, 4H, *β*-$CH_2$), 1.40-1.34 (m, 8H, *γ,δ*-$CH_2$), 0.93 (t, *J* = 7 Hz, 6H, *ε*-$CH_2$). $^{31}P\{^{1}H\}$ δ 55.0 (s, *dppe*). IR (*nujol)* $cm^{-1}$: 2065 (m) *ν*(Ru-C≡C).

**(30c) *trans*-Ru(C≡C$C_6H_4$OMe-4)$_2$(dppe)$_2$.** The TlCl precipitate was removed by filtration through neutral alumina (Brockmann I). The pure product was obtained from the filtrate as a yellow precipitate upon addition of $Et_2O$ (67 mg, 63%). Single crystals suitable for X-ray diffraction were obtained from hot toluene. $^{1}H$ δ 7.56–7.50 (m, 16H, *o*-$PPh_2$), 7.19–7.12 (m, 8H, *p*-$PPh_2$), 6.97–691 (m, 16H, *m*-$PPh_2$), 6.79 (s, 8H, $C_2$-Ph-OMe), 3.80 (s, 6H, OMe), 2.65–2.56 (m, 8H, dppe), $^{31}P\{^{1}H\}$ δ 54.1 (s, *dppe*). IR (*nujol)* $cm^{-1}$: 2069 (m) *ν*(Ru-C≡C).

**(30d) *trans*-Ru(C≡C$C_6H_4CO_2$Me-4)$_2$(dppe)$_2$.** The TlCl precipitate was removed by filtration through neutral alumina (Brockmann I). The pure product precipitated from the filtrate as pale-yellow solids upon addition of $Et_2O$ (67 mg, 60%). Crystals suitable for X-ray diffraction were obtained from $CH_2Cl_2$/$Et_2O$. $^{1}H$ δ 7.81 (d, *J* = 8 Hz, 4H, *o*-Ph-$CO_2$Me), 7.51–7.44 (m, 16H, *o*-$PPh_2$), 7.20–7.14 (m, 8H, *p*-$PPh_2$), 6.98–6.90 (m, 16H, *m*-$PPh_2$), 6.71 (d, *J* = 8 Hz, 4H, *m*-Ph-$CO_2$Me), 3.90 (s, 6H, COO-Me), 2.68–2.57 (m, 8H, dppe). $^{31}P\{^{1}H\}$ δ 54.4 (s, *dppe*). IR (*nujol)* $cm^{-1}$: 2058 (s) *ν*(Ru-C≡C); 1722 (m) *ν*(C=O).

**(30e) *trans*-Ru(C≡CC$_6$H$_4$NO$_2$-4)$_2$(dppe)$_2$.** The TlCl precipitate was removed from the red mixture upon filtration through neutral alumina (Brockmann I). The red solids precipitated from the filtrate upon addition of $Et_2O$ were collected by filtration and purified further by preparatory silica TLC using hexane:$CH_2Cl_2$ (2:3) as the eluent. The pure product was obtained as a red powder from the top red band (15 mg, 14%). $^1$H δ 7.94 (d, *J* = 8 Hz, 4H, , *o*-Ph-NO$_2$), 7.47–7.40 (m, 16H, *o*-PPh$_2$), 7.25–7.16 (m, 8H, *p*-PPh$_2$), 7.00–6.93 (m, 16H, *m*-PPh$_2$), 6.65 (d, *J* = 8 Hz, 4H, *m*-Ph-NO$_2$), 2.62 (t, *J* = 8 Hz, 8H, dppe). $^{31}$P{$^1$H} δ 52.0 (s). IR (*nujol)* cm$^{-1}$: 2047 (m) *v*(Ru-C≡C).

**(30f) *trans*-Ru(C≡CC$_6$H$_4$C≡CSiMe$_3$-4)$_2$(dppe)$_2$.** The TlCl precipitate was removed by filtration through neutral alumina (Brockmann I). The pure product was obtained from the filtrate as a pale-yellow precipitate upon addition of $Et_2O$ (96 mg, 81%). Single crystals suitable for X-ray diffraction were obtained from $CH_2Cl_2$/hexane. $^1$H δ 7.52–7.43 (m, 16H, *o*-PPh$_2$), 7.25 (d, *J* = 8 Hz, 4H, C$_2$-Ph-C$_2$), 7.18–7.11 (m, 8H, *p*-PPh$_2$), 6.97–689 (m, 16H, *m*-PPh$_2$), 6.62 (d, *J* = 8 Hz, 4H, C$_2$-Ph-C$_2$), 2.66–2.58 (m, 8H, dppe), 0.26 (s, 9H, SiMe$_3$). $^{31}$P{$^1$H} δ 53.4 (s, *dppe*). IR (*nujol)* cm$^{-1}$: 2153 (m) *v*(C≡C); 2065 (s) *v*(Ru-C≡C).

**(30g) *trans*-Ru(C≡CC$_6$H$_4$C≡CBu$^t$-4)$_2$(dppe)$_2$.** The TlCl precipitate was removed by filtration through neutral alumina (Brockmann I). The pure product precipitated from the filtrate as pale-yellow solids upon addition of $Et_2O$ (96 mg, 83%). Single crystals suitable for X-ray diffraction were obtained from $CHCl_3$/MeOH. $^1$H δ 7.52–7.43 (m, 16H, *o*-PPh$_2$), 7.20–7.10 (m, 12H, C$_2$-Ph-C$_2$/*p*-PPh$_2$), 6.96–6.88 (m, 16H, *m*-PPh$_2$), 6.63 (d, *J* = 8 Hz, 4H, C$_2$-Ph-C$_2$), 2.68–2.56 (m, 8H, dppe), 1.33 (s, 18H, CMe$_3$). $^{31}$P{$^1$H} δ 52.5 (s, *dppe*). IR (*nujol)* cm$^{-1}$: 2177 (w) *v*(C≡C); 2069 (s) *v*(Ru-C≡C).

**(30i) *trans*-Ru(C≡CC$_6$H$_4$C≡CH-4)$_2$(dppe)$_2$.** Reaction of **(30f)** (30 mg, 0.023 mmol) with TBAF (1M in THF, 46 µL, 0.046 mmol) in $CH_2Cl_2$ at room temperature overnight. The orange solution was filtered through neutral alumina (Brockmann I) and the filtrate taken to dryness to obtain the pure product as an orange powder (24 mg, 91%). Single crystals suitable for X-ray diffraction were obtained from $CH_2Cl_2$/hexane. $^1$H δ 7.53–7.43 (m, 16H, *o*-$PPh_2$), 7.26 (d, *J* = 8Hz, 4H, $C_2$-Ph-$C_2$), 7.20–7.13 (m, 8H, *p*-$PPh_2$), 6.99–6.89 (m, 16H, *m*-$PPh_2$), 6.64 (d, *J* = 8Hz, 4H, $C_2$-Ph-$C_2$), 3.11 (s, 2H, C≡C-H), 2.66–2.56 (m, 8H, dppe). $^{31}$P{$^1$H} δ 52.6 (s, *dppe*). IR (*nujol)* cm$^{-1}$: 3276 (s) *ν*(C≡C-H); 2054 (w) *ν*(Ru-C≡C).

**(30j) *trans*-Ru(C≡CC≡CSiMe$_3$)$_2$(dppe)$_2$.** The TlCl precipitate was removed by filtration through a PTFE filter (0.2 µm pore size). The off-white precipitate generated upon addition of hexane was collected by filtration and rinsed with MeOH (89 mg, 85%). Single crystals suitable for X-ray diffraction were obtained from $CHCl_3$/MeOH. $^1$H NMR (400 MHz, $CDCl_3$) δ 7.33–7.27 (m, 16H, *o*-$PPh_2$), 7.24–7.17 (m, 12H, *p*-$PPh_2$), 7.05–6.99 (m, 16H, *o*-$PPh_2$), 2.65–7.50 (m, 8H, dppe), 0.22 (s, 18H, $SiMe_3$). $^{31}$P{$^1$H} NMR (162 MHz, $CDCl_3$) δ 52.5 (s, *dppe*). IR (*nujol)* cm$^{-1}$: 2168 (w) *ν*(C≡C); 2062 (m) *ν*(Ru-C≡C).

*Halide abstractor-free synthesis of trans-Ru(C≡CR)$_2$(dppe)$_2$* **(30c, 30h)**:

To a solution of **28** (0.100 g, 0.092 mmol) and DBU (*excess*) in $CH_2Cl_2$ (4 mL), the appropriate alkyne (0.20 mmol) was added. The resulting solution was stirred at room temperature for 7 days. The yellow precipitate was removed by filtration and washed thoroughly with hexane. Product **30c** was obtained as a yellow solid (47 mg, 44%), **30h** was obtained as an off-white powder (51 mg, 48%) Single crystals suitable for X-ray diffraction were obtained from $CH_2Cl_2$/hexane. $^1$H δ 7.64–7.57 (m, 16H, *o*-$PPh_2$), 7.25–7.19 (m, 8H, *p*-$PPh_2$), 7.04 – 6.99 (m, 16H, *m*-$PPh_2$), 6.68 (d, *J* = 8 Hz, 4H, Ph-$NH_2$), 6.59 (d, *J* = 8 Hz, 4H, Ph-$NH_2$), 3.56 (s, 4H, $NH_2$), 2.73–2.61 (m, 8H, dppe). $^{31}$P{$^1$H} δ 53.2 (s, *dppe*). IR (*nujol)* cm$^{-1}$: 3351 (m) *ν*($NH_2$); 2073 cm$^{-1}$ *ν*(C≡C).

*Synthesis of trans-Ru(C≡CR)(C≡CR')(dppe)$_2$* **(31 - 33)**:

To a solution of the appropriate *trans*-RuCl(C≡CR)(dppe)$_2$ (0.10 g) and DBU (*excess*) in $CH_2Cl_2$ (4 mL), TlBF4 (1 eq.) was added. Subsequent drop wise addition of HC≡CR' (1.1 eq.) dissolved in $CH_2Cl_2$ (~3 mL) over 30 minutes generated an off-white precipitate (TlCl) that was removed by filtration. The final products were isolated from the filtrate (*vide infra*).

**(31) *trans*-Ru(C≡CC$_6$H$_4$C≡CSiMe$_3$-4)(C≡CC$_6$H$_4$NH$_2$-4)(dppe)$_2$.** To a solution of **29f** (0.100 g, 0.083 mmol), 4-ethynylaniline (0.012 g, 0.10 mmol) was added according to the general procedure. The TlCl precipitate was removed by filtration through basic alumina (Brockmann III). The pure product precipitated from the filtrate as orange solids upon addition of hexane (61 mg, 0.050 mmol, 60%). $^1$H δ 7.67–7.60 (m, 8H, *o*-PPh$_2$), 7.39–7.34 (m, 8H, *o*-PPh$_2$), 7.23 (d, J = 8 Hz, 2H, *o*-Ph-TMSA), 7.20–7.09 (m, 8H, *p*-PPh$_2$), 7.20–7.09 (m, 8H, *m*-PPh$_2$), 7.00–6.93 (m, 8H, *m*-PPh$_2$), 6.68 (d, J = 8 Hz, 2H, Ph-NH$_2$), 6.56 (m, 2H, *m*-Ph-TMSA), 6.53 (d, J = 8 Hz, 2H, Ph-NH$_2$) 3.51 (s, 2H, NH$_2$), 2.65–2.58 (m, 8H, dppe), 0.26 (s, 9H, Si-Me$_3$). $^{31}$P{$^1$H} δ 52.8 (s, *dppe*). IR (*nujol)* cm$^{-1}$: *not observed v*(NH$_2$); 2151 (w) *v*(C≡C); 2062 (s) *v*(Ru-C≡C).

**(32) *trans*-Ru(C≡CC$_6$H$_4$CO$_2$Me-4)(C≡CC$_6$H$_4$NH$_2$-4)(dppe)$_2$.** To a solution of **29d** (0.100 g, 0.092 mmol), 4-ethynylaniline (0.012 g, 0.10 mmol) was added following the general procedure. The TlCl precipitate was removed by filtration through basic alumina (Brockmann III). The pure product precipitated from the filtrate as yellow solids upon addition of hexane washed with Et$_2$O (50 mg, 0.043 mmol, 47%). $^1$H δ 7.79 (d, *J* = 8 Hz, 2H, *o*-Ph-CO$_2$Me), 7.70–7.58 (m, 8H, *o*-PPh$_2$), 7.41–7.32 (m, 8H, *o*-PPh$_2$), 7.16 (m, 8H, *p*-PPh$_2$), 7.01–6.95 (m, 8H, *m*-PPh$_2$), 6.95–6.88 (m, 8H, *m*-PPh$_2$), 6.69 (d, *J* = 8 Hz, 2H, Ph-NH$_2$), 6.64 (d, *J* = 8 Hz, 2H, *m*-Ph-CO$_2$Me), 6.54 (d, *J* = 8 Hz, 2H, Ph-NH$_2$), 3.90 (s, 3H, COO-Me), 3.52 (s br., 2H, NH$_2$), 2.66 – 2.58 (m, 8H, dppe). $^{31}$P{$^1$H} δ 52.8 (s, *dppe*). IR (*nujol)* cm$^{-1}$: *not observed v*(NH$_2$); 2058 *v*(Ru-C≡C).

**(33) *trans*-Ru(C≡CC$_6$H$_4$CO$_2$Me-4)(C≡CC$_6$H$_4$OMe-4)(dppe)$_2$.** To a solution of **29d** (0.100 g, 0.092 mmol), 1-ethynyl-4-methoxybenzene (0.013 g, 0.10 mmol) was added following the general procedure previously described. The TlCl precipitate was removed by filtration through basic alumina (Brockmann III). The pure product precipitated from the filtrate as bright yellow solids upon addition of hexane (95 mg, 0.080 mmol, 87%). $^1$H δ 7.79 (d, *J* = 8 Hz, 2H, *o*-Ph-CO$_2$Me), 7.65–7.59 (m, 8H, *o*-PPh$_2$), 7.41–7.35 (m, 8H, *o*-PPh$_2$), 7.21–7.12 (m, 8H, *p*-PPh$_2$), 7.01–6.95 (m, 8H, *m*-PPh$_2$), 6.95–6.89 (m, 8H, *m*-PPh$_2$), 6.79–6.71 (m, 4H, *o/m*-Ph-OMe), 6.65 (d, *J* = 8 Hz, 2H, *m*-Ph-CO$_2$Me), 3.90 (s, 4H, COO-Me), 3.81 (s, 4H, O-Me), 2.66-2.58 (t, *J* = 7 Hz, 8H, dppe). $^{31}$P{$^1$H} δ 52.8 (s, *dppe*). IR (*nujol)* cm$^{-1}$: 2060 *v*(Ru-C≡C); 1704 *v*(C=O).

## 4.9. References


1. (a) Meng, F.; Hervault, Y.-M.; Norel, L.; Costuas, K.; Van Dyck, C.; Geskin, V.; Cornil, J.; Hng, H. H.; Rigaut, S.; Chen, X., *Chem. Sci.*, **2012**, *3*, 3113-3118; (b) Kim, B. S.; Beebe, J. M.; Olivier, C.; Rigaut, S.; Touchard, D.; Kushmerick, J. G.; Zhu, X. Y.; Frisbie, C. D., *J. Phys. Chem. C*, **2007**, *111*, 7521-7526; (c) Rigaut, S., *Dalton Trans.*, **2013**, *42*, 15859-15863.
2. (a) Powell, C. E.; Humphrey, M. G., *Coord. Chem. Rev.*, **2004**, *248*, 725-756; (b) Dalton, G. T.; Cifuentes, M. P.; Watson, L. A.; Petrie, S.; Stranger, R.; Samoc, M.; Humphrey, M. G., *Inorg. Chem.*, **2009**, *48*, 6534-6547.
3. Costuas, K.; Rigaut, S., *Dalton Trans.*, **2011**, *40*, 5643-5658.
4. (a) Benameur, A.; Brignou, P.; Di Piazza, E.; Hervault, Y.-M.; Norel, L.; Rigaut, S., *New J. Chem.*, **2011**, *35*, 2105-2113; (b) Rigaut, S.; Perruchon, J.; Le Pichon, L.; Touchard, D.; Dixneuf, P. H., *J. Organomet. Chem.*, **2003**, *670*, 37-44; (c) McDonagh, A. M.; Powell, C. E.; Morrall, J. P.; Cifuentes, M. P.; Humphrey, M. G., *Organometallics*, **2003**, *22*, 1402-1413; (d) Faulkner, C. W.; Ingham, S. L.; Khan, M. S.; Lewis, J.; Long, N. J.; Raithby, P. R., *J. Organomet. Chem.*, **1994**, *482*, 139-145.
5. (a) Gauthier, N.; Olivier, C.; Rigaut, S.; Touchard, D.; Roisnel, T.; Humphrey, M. G.; Paul, F., *Organometallics*, **2008**, *27*, 1063-1072; (b) Olivier, C.; Kim, B.; Touchard, D.; Rigaut, S., *Organometallics*, **2008**, *27*, 509-518; (c) Touchard, D.; Haquette, P.; Guesmi, S.; Le Pichon, L.; Daridor, A.; Toupet, L.; Dixneuf, P. H., *Organometallics*, **1997**, *16*, 3640-3648.

6. West, P. J.; Cifuentes, M. P.; Schwich, T.; Randles, M. D.; Morrall, J. P.; Kulasekera, E.; Petrie, S.; Stranger, R.; Humphrey, M. G., *Inorg. Chem.*, **2012**, *51*, 10495-10502.
7. Touchard, D.; Guesmi, S.; Le Pichon, L.; Daridor, A.; Dixneuf, P. H., *Inorg. Chim. Acta*, **1998**, *280*, 118-124.
8. Younus, M.; Long, N. J.; Raithby, P. R.; Lewis, J.; Page, N. A.; White, A. J. P.; Williams, D. J.; Colbert, M. C. B.; Hodge, A. J.; Khan, M. S.; Parker, D. G., *J. Organomet. Chem.*, **1999**, *578*, 198-209.
9. Atherton, Z.; Faulkner, C. W.; Ingham, S. L.; Kakkar, A. K.; Khan, M. S.; Lewis, J.; Long, N. J.; Raithby, P. R., *J. Organomet. Chem.*, **1993**, *462*, 265-270.
10. (a) Fox, M. A.; Harris, J. E.; Heider, S.; Pérez-Gregorio, V.; Zakrzewska, M. E.; Farmer, J. D.; Yufit, D. S.; Howard, J. A. K.; Low, P. J., *J. Organomet. Chem.*, **2009**, *694*, 2350-2358; (b) Fillaut, J.-L.; Andriès, J.; Marwaha, R. D.; Lanoë, P.-H.; Lohio, O.; Toupet, L.; Gareth Williams, J. A., *J. Organomet. Chem.*, **2008**, *693*, 228-234.
11. Powell, C. E.; Hurst, S. K.; Morrall, J. P.; Cifuentes, M. P.; Roberts, R. L.; Samoc, M.; Humphrey, M. G., *Organometallics*, **2007**, *26*, 4456-4463.
12. Koutsantonis, G. A.; Jenkins, G. I.; Schauer, P. A.; Szczepaniak, B.; Skelton, B. W.; Tan, C.; White, A. H., *Organometallics*, **2009**, *28*, 2195-2205.
13. Ouerfelli, I.; Gatri, R.; Lotfi Efrit, M.; Dua, N.; Perruchon, J.; Golhen, S.; Toupet, L.; Fillaut, J.-L., *J. Organomet. Chem.*, **2011**, *696*, 670-675.
14. Gauthier, N.; Tchouar, N.; Justaud, F.; Argouarch, G.; Cifuentes, M. P.; Toupet, L.; Touchard, D.; Halet, J. F.; Rigaut, S.; Humphrey, M. G.; Costuas, K.; Paul, F., *Organometallics*, **2009**, *28*, 2253-2266.
15. Hurst, S. K.; Cifuentes, M. P.; Morrall, J. P. L.; Lucas, N. T.; Whittall, I. R.; Humphrey, M. G.; Asselberghs, I.; Persoons, A.; Samoc, M.; Luther-Davies, B.; Willis, A. C., *Organometallics*, **2001**, *20*, 4664-4675.
16. Fillaut, J.-L.; Perruchon, J.; Blanchard, P.; Roncali, J.; Golhen, S.; Allain, M.; Migalsaka-Zalas, A.; Kityk, I. V.; Sahraoui, B., *Organometallics*, **2005**, *24*, 687-695.
17. Morrall, J. P. L.; Cifuentes, M. P.; Humphrey, M. G.; Kellens, R.; Robijns, E.; Asselberghs, I.; Clays, K.; Persoons, A.; Samoc, M.; Willis, A. C., *Inorg. Chim. Acta*, **2006**, *359*, 998-1005.
18. Grelaud, G.; Cifuentes, M. P.; Schwich, T.; Argouarch, G.; Petrie, S.; Stranger, R.; Paul, F.; Humphrey, M. G., *Eur. J. Inorg. Chem.*, **2012**, *2012*, 65-75.
19. Trujillo, A.; Fuentealba, M.; Arratia-Perez, R.; Howard, J. A. K., *Acta Crystallogr. Sect. E*, **2012**, *68*, m1445.
20. Low, P. J., *Coord. Chem. Rev.*, **2013**, *257*, 1507-1532.
21. Bruce, M. I.; Büschel, S.; Cole, M. L.; Scoleri, N.; Skelton, B. W.; White, A. H.; Zaitseva, N. N., *Inorg. Chim. Acta*, **2012**, *382*, 6-12.
22. Wuttke, E.; Pevny, F.; Hervault, Y.-M.; Norel, L.; Drescher, M.; Winter, R. F.; Rigaut, S., *Inorg. Chem.*, **2012**, *51*, 1902-1915.
23. Anderson, J. N.; Brookes, N. J.; Coe, B. J.; Coles, S. J.; Light, M. E.; Hursthouse, M. B., *Acta Crystallogr. Sect. C: Cryst. Struct. Commun.*, **2003**, *59*, m215-m217.
24. Jeffery, C. J.; Cifuentes, M. P.; Dalton, G. T.; Corkery, T. C.; Randles, M. D.; Willis, A. C.; Samoc, M.; Humphrey, M. G., *Macromol. Rapid Commun.*, **2010**, *31*, 846-849.

25. Gauthier, N.; Argouarch, G.; Paul, F.; Toupet, L.; Ladjarafi, A.; Costuas, K.; Halet, J.-F.; Samoc, M.; Cifuentes, M. P.; Corkery, T. C.; Humphrey, M. G., *Chem. Eur. J.*, **2011**, *17*, 5561-5577.
26. Marques-Gonzalez, S.; Yufit, D. S.; Howard, J. A. K.; Martin, S.; Osorio, H. M.; Garcia-Suarez, V. M.; Nichols, R. J.; Higgins, S. J.; Cea, P.; Low, P. J., *Dalton Trans.*, **2013**, *42*, 338-341.
27. Vacher, A.; Barrière, F. d. r.; Roisnel, T.; Piekara-Sady, L.; Lorcy, D., *Organometallics*, **2011**, *30*, 3570-3578.
28. Lebreton, C.; Touchard, D.; Pichon, L. L.; Daridor, A.; Toupet, L.; Dixneuf, P. H., *Inorg. Chim. Acta*, **1998**, *272*, 188-196.
29. Norel, L.; Bernot, K.; Feng, M.; Roisnel, T.; Caneschi, A.; Sessoli, R.; Rigaut, S., *Chem. Commun.*, **2012**, *48*, 3948-3950.
30. McGrady, J. E.; Lovell, T.; Stranger, R.; Humphrey, M. G., *Organometallics*, **1997**, *16*, 4004-4011.
31. Lever, A. B. P., *Inorg. Chem.*, **1990**, *29*, 1271-1285.
32. (a) Heath, G. A.; Humphrey, D. G., *J. Chem. Soc., Chem. Commun.*, **1991**, 1668-1671; (b) McDonagh, A. M.; Whittall, I. R.; Humphrey, M. G.; Hockless, D. C. R.; Skelton, B. W.; White, A. H., *J. Organomet. Chem.*, **1996**, *523*, 33-40.
33. Pombeiro, A. J. L., *J. Organomet. Chem.*, **2005**, *690*, 6021-6040.
34. (a) Powell, C. E.; Cifuentes, M. P.; Morrall, J. P.; Stranger, R.; Humphrey, M. G.; Samoc, M.; Luther-Davies, B.; Heath, G. A., *J. Am. Chem. Soc.*, **2002**, *125*, 602-610; (b) Pevny, F.; Di Piazza, E.; Norel, L.; Drescher, M.; Winter, R. F.; Rigaut, S. p., *Organometallics*, **2010**, *29*, 5912-5918.
35. Wuttke, E.; Hervault, Y.-M.; Polit, W.; Linseis, M.; Erler, P.; Rigaut, S.; Winter, R. F., *Organometallics*, **2014**,
36. Low, P. J.; Bock, S., *Electrochim. Acta*, **2013**, *110*, 681-692.
37. Renz, M.; Theilacker, K.; Lambert, C.; Kaupp, M., *J. Am. Chem. Soc.*, **2009**, *131*, 16292-16302.
38. Klamt, A.; Schuurmann, G., *J. Chem. Soc. Perk. Trans. 2*, **1993**, 799-805.
39. TURBOMOLE, *( V6.4 2012) a development of University of Karlsruhe and Forschungszentrum Karlsruhe GmbH, 1989-2007, TURBOMOLE GmbH, since 2007*,
40. (a) Cossi, M.; Rega, N.; Scalmani, G.; Barone, V., *J. Comput. Chem.*, **2003**, *24*, 669-681; (b) Barone, V.; Cossi, M., *J. Phys. Chem. A*, **1998**, *102*, 1995-2001.
41. Frisch, M. J., *Gaussian 09; Revision A.02 ed.; Gaussian, Inc.: Wallingford, CT*, **2009**,
42. Kaupp, M.; Renz, M.; Parthey, M.; Stolte, M.; Wurthner, F.; Lambert, C., *Phys. Chem. Chem. Phys.*, **2011**, *13*, 16973-16986.
43. (a) Parthey, M.; Gluyas, J. B. G.; Schauer, P. A.; Yufit, D. S.; Howard, J. A. K.; Kaupp, M.; Low, P. J., *Chem. Eur. J.*, **2013**, *19*, 9780-9784; (b) Vincent, K. B.; Zeng, Q.; Parthey, M.; Yufit, D. S.; Howard, J. A. K.; Hartl, F.; Kaupp, M.; Low, P. J., *Organometallics*, **2013**, *32*, 6022-6032.
44. Fox, M. A.; Roberts, R. L.; Khairul, W. M.; Hartl, F.; Low, P. J., *J. Organomet. Chem.*, **2007**, *692*, 3277-3290.

45. (a) Röder, J. C.; Meyer, F.; Hyla-Kryspin, I.; Winter, R. F.; Kaifer, E., *Chem. Eur. J.*, **2003**, *9*, 2636-2648; (b) Scott, A. P.; Radom, L., *J. Phys. Chem.*, **1996**, *100*, 16502-16513.
46. *The contributions for 31 and 32 sum up to more than 100%, which is due to rounding of contributions and negative contributions to the spin-density due tospin polarization.*,
47. (a) Jones, S. C.; Coropceanu, V.; Barlow, S.; Kinnibrugh, T.; Timofeeva, T.; Brédas, J.-L.; Marder, S. R., *J. Am. Chem. Soc.*, **2004**, *126*, 11782-11783; (b) Parthey, M.; Vincent, K. B.; Renz, M.; Schauer, P. A.; Yufit, D. S.; Howard, J. A. K.; Kaupp, M.; Low, P. J., *Inorg. Chem.*, **2014**, DOI http://dx.doi.org/10.1021/ic402538e.
48. Pascal, P., Nouveau Traité de Chimie Minérale. Masson-Paris, Ed. 1961; Vol. VI, p 92.
49. Doak, B. C.; Scanlon, M. J.; Simpson, J. S., *Org. Lett.*, **2011**, *13*, 537-539.

# 5. SINGLE MOLECULE CONDUCTANCE STUDIES ON PHENYLETHYNYL DERIVATIVES

## 5.1. Abstract

In this Chapter the single molecule conductance studies of phenylethynyl derivatives **27**, **30f**, **30h** and **34 – 38** are presented (Chart 5-1). The STM conductance measurements were performed in collaboration with Prof. Richard Nichols and his group at the University of Liverpool. A novel molecular junction linker $-C\equiv CSiMe_3$ is introduced and its electrical properties benchmarked against the $-NH_2$ moiety, the latter being a well-known and characterised contact group in the formation and study of metal|molecule|metal junctions. In addition, the electrical properties of **35** and the organometallic analogue **30f** (*see* Chapter 4) are compared. Differences in the electronic properties of these compounds are interpreted in terms of the influence of the ruthenium core on the electronic structure of **30f**. In addition, preliminary electrochemical STM (EC-STM) studies performed on the organometallic complex **30f** are presented. The transistor-like behaviour observed is explained in terms of molecular orbital alignment with the electrode Fermi levels according to the Kuznetsov-Ulstrup two-step electron transfer model.

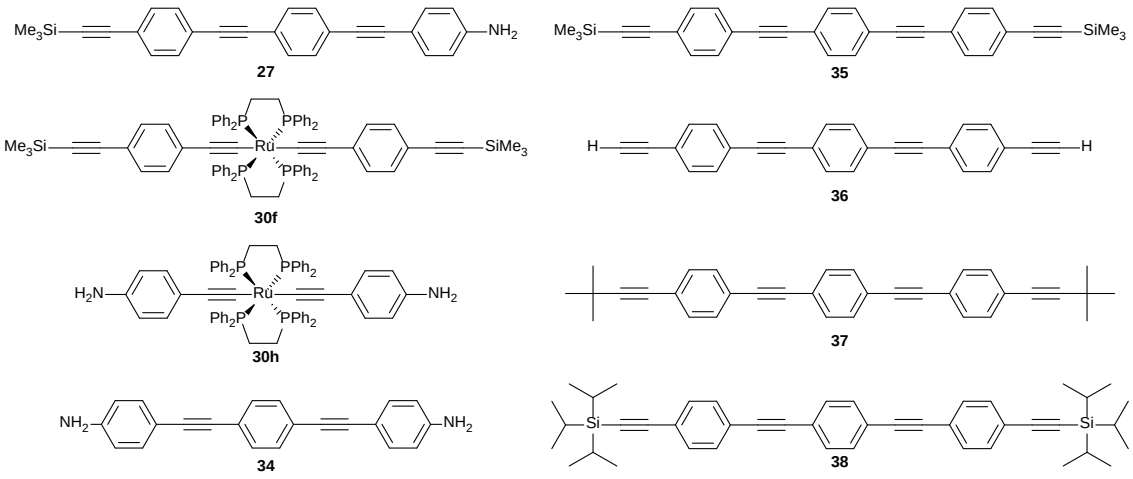


**Chart 5-1.** *Compounds subject of single molecule conductance studies in this Chapter.*

## 5.2. Introduction

The integration of molecular junctions on working electronic devices requires the formation of stable reproducible self-assembled electrode-molecule contacts,[1] and it is now agreed that the conductance across a metal|molecule|metal junction is strongly influenced by the nature of the anchoring groups.[2] The difference between a chemisorbed and a physisorbed system in terms of conductance can be up to three orders of magnitude[1b, 3] with the functional groups that serve as molecular linkers not only affecting the molecular frontier orbitals but also the alignment of these orbitals energies relative to the electrode Fermi levels.[1b] However, whilst the great influence of the contacting group on junction behaviour is widely recognised, very little is known about the processes that take place at the metal-molecule interface when the junction is formed. Furthermore, single molecule studies tend to be strictly focused on the electrical properties of the junction without explicit consideration of the electrode shape or the molecular geometry within the device, or variations in these between individual devices or junctions.[4] Indeed, typically, multiple conductance values can be observed for a single molecule in single molecule studies and this variability is commonly ascribed to differences in the structure of the individual junctions used to construct the overall measurement.[2b, 5] Amongst the different linkers found in the literature, thiols (SH) are the prevailing anchoring groups for single molecule studies.[6] The thiolate-gold bond has a strength close to that of the gold-gold bond[7] and consequently the adhesion of thiols is known to lead to modification of the gold surface adding uncertainty about the junction geometry.[8] It is surprising that, despite the wide use of the gold-sulfur couple, structural details of that interface have been largely neglected in analyses of results of molecular conductance studies.[9] As a consequence, several research groups are now exploring new molecular linkers in order to improve the reliability and stability of the junctions. Amongst the most relevant alternatives to thiols as molecular

linkers on gold are: pyridine;[10] amines;[11] selenides;[12] dihydrobenzo[*b*] thiophene;[13] carboxylic acids;[14] cyanides;[15] isocyanides;[15-16] isothiocyanides;[17] phosphines;[11c] phosphine sulphides;[18] or more recently halides;[19] direct C-Au bonding[20] and silicon.[21] Following previous reports on the ability of aliphatic compounds containing the $-C\equiv CSiMe_3$ moiety to self-assemble on to gold surfaces,[22] our contribution takes advantage of the geometrical constraints introduced by this silyl linker[23] to simplify the conductance fingerprint of molecular junctions. In a parallel way, single molecule conductance studies on organometallic complexes are becoming more frequent nowadays.[10b, 24] Organometallic derivatives have captured the attention of the scientific community because of their enhanced conductance and added structural, chemical and electronic functionality. The introduction of electronic function beyond a simple wire-like behaviour takes the field a step closer to the future preparation of molecular devices.[25]

## 5.3. Results and discussion

An Agilent STM controlled using Picoscan 4.19 software was used to collect all the measurements. The STM tips were freshly prepared for each experiment by etching a Au wire (99.99%) in a HCl:EtOH (50 v/v) at 2.4V. The gold-on-glass substrates employed were purchased from Arrandee, Schroeer, Germany. The substrates were flame annealed with a butane flame immediately before use. This thermal treatment is known to generate atomically flat terraces on the Au(111) substrate.[26] The substrates were immersed in low concentration solutions ($\sim 10^{-5}$ M, $CHCl_3$) of the targeted molecule for 40 seconds. The low concentrations and short immersion times were chosen to favour a low surface coverage of the gold substrate, consequently promoting single molecule events instead of molecular aggregates. After adsorption, the sample was rinsed thoroughly with $CHCl_3$ and blown dry in a stream of $N_2$ gas.

### *5.3.1. Linker influence in the molecular conductance fingerprint*

As discussed in previous sections of this Chapter, the conductance across a molecular junction is strongly influenced by the nature of the anchoring groups. Typically, several conductance values can be observed in the conductance histograms of a single molecule. It is now generally accepted that the different conductance values arise from differences on the junction formation, commonly ascribed to different linker-surface interactions. The different conductance values have been found to be strongly related to the surface roughness and the STM experimental conditions.[2b, 5a] From lower to higher conductance the different conductance values are typically referred to as A, B and C (Figure 5-1). Low conductance (type A) contacts are due to molecular binding at low coordination surface sites. On the other hand the higher conductance modes B and C are believed to arise from molecular contacts at one (B type) or two (C type) defect coordination sites (Figure 5-1). This hypothesis is in good agreement with the higher conductance values typically observed for MCBJ or STM-BJ studies.[27] As these techniques involve surface reforming, a greater number of defect coordination sites become available hence the higher conductance binding mode (C type) prevails. The use of STM-BJ typically shows a broader distribution of conductance values attributed to a single molecule and relatively higher conductance values.[10c, 28] Conversely, "softer" STM methods such as the $I(s)$ or $I(t)$ typically register lower conductance (A type) values due to a lower number defect of coordination sites present. This variability is one of the biggest challenges towards the integration of molecules in working devices, as was discussed in detail in Chapter 3.

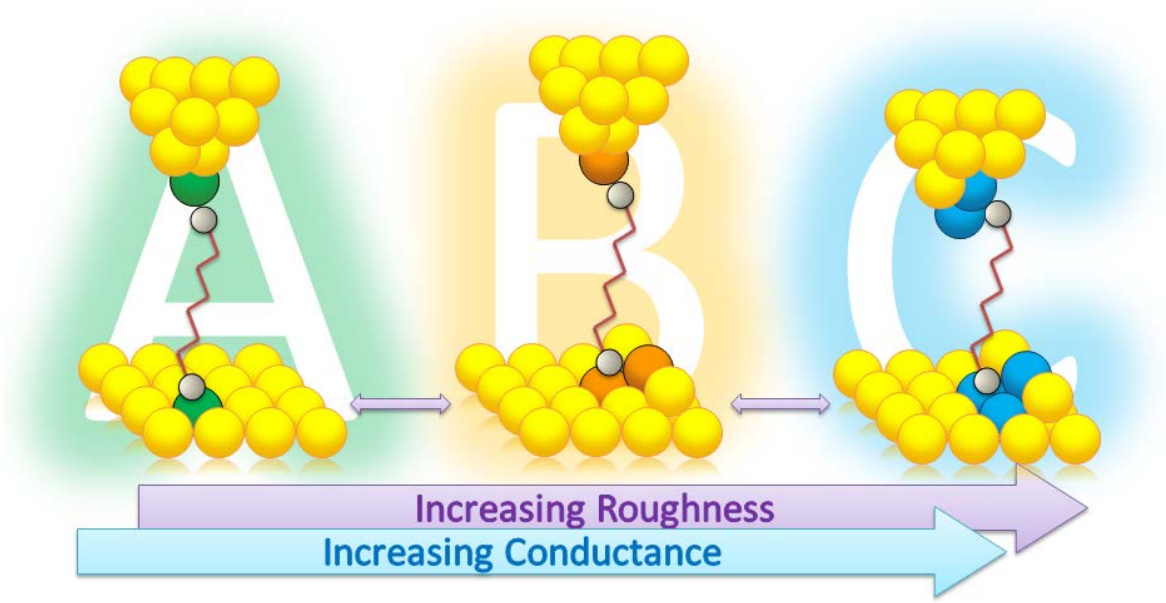


**Figure 5-1.** Schematic representation of *A, B and C contact modes.*

Recently the −C≡CSiMe$_3$ group has emerged as a promising molecular linker. The ability of the ethynyl(trimethyl)silyl linker to form well-ordered self-assembled monolayers on Au(111) surfaces has been demonstrated elsewhere.[22-23] STM images of the self-assembled monolayers of the silyl-terminated molecules studied showed the vertical alignment of the molecules relative to the substrate. In addition, atom-step etch-pits were occasionally found on the treated gold substrates,[22a] providing evidence for chemisorption in a manner entirely consistent with observations made from thiol-contacted monolayer on gold substrates.[9] In order to evaluate the performance of the −C≡CSiMe$_3$ group in molecular junctions, the electrical properties of ethynyl(trimethyl)silyl terminated OPE **35** were benchmarked against –NH$_2$ terminated parent compounds **27** and **34**.

The *I*(*s*) STM experiments performed on the diamino substituted OPE **34** led to two different conductance values (Figure 5-2) by slightly changing the STM experimental parameters. STM measurements on **34** were performed at 600 mV with current setpoints 10 nA (*green*) and 20 nA (*orange*) respectively. The lowest conductance value of (3.20 ±

0.83)·$10^{-5}$ $G_0$ was assigned to the "flat" contact without the presence of any adatoms (A type). By increasing the current setpoint to 20 nA a second conductance value was distinguishable (14.4 ± 2.78)·$10^{-5}$ $G_0$ (B type) in good agreement with previously reported data from STM-BJ measurements.[29] The use of higher set-points at a constant sample bias results in a closer tip-substrate gap that results in an increased probability of higher conductance junctions (B or C type) being formed.

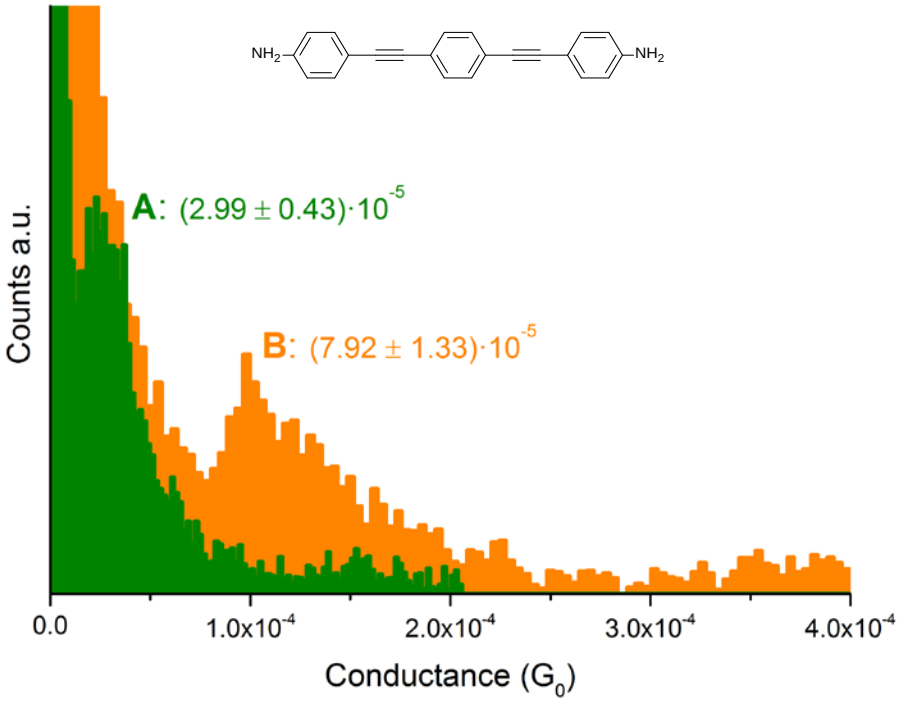


**Figure 5-2.** *Conductance histogram of **34** obtained by the I(s) method at 600mV with setpoint currents 10 nA (A type, green) and 20 nA (B type, orange).*

To our initial surprise, similar STM *I*(*s*) studies performed on **35** gave rise to a single low conductance value *ca.* 3·$10^{-5}$ $G_0$ for all setpoints explored ascribed to an A-type contact mode. These preliminary results, together with a low hit ratio (*ca.* 10%) led us to believe that the −C≡CSiMe$_3$ group may introduce some geometrical constraints to the junction preventing the contact at defect sites and leading to a simplified conductance profile. To confirm this hypothesis, the STM-BJ method was employed in order to

encourage the formation of higher conductance junctions (B or C type). Interestingly, the STM-BJ conductance histogram of the bis(trimethylsilyl)ethynyl derivative **35** (Figure 5-3) shows a single well-defined, conductance peak at $(2.75 \pm 0.56)\cdot10^{-5}$ $G_0$ indicating the exclusive formation of defect free A type junctions despite the extensive surface restructuring associated with the STM-BJ method.

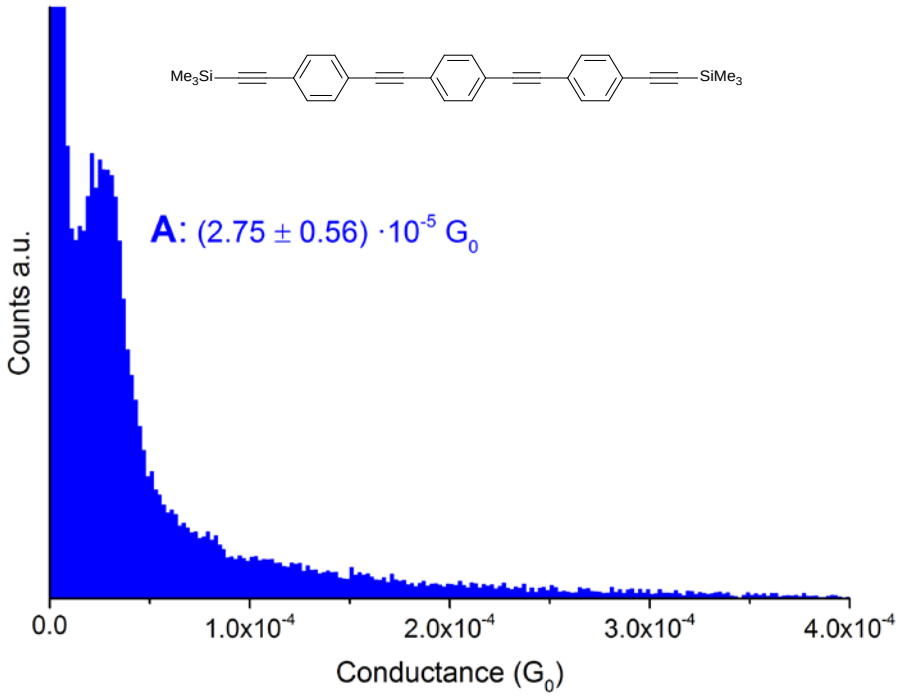


**Figure 5-3.** *Conductance histogram of **35** obtained employing the STM-BJ method at 600mV showing the formation of a single low conductance value (A type).*

Interestingly, replacement of one $-C\equiv CSiMe_3$ contact for $-NH_2$ in the unsymmetrically substituted derivative **27**, resulted in two different conductance values being observed: $(2.99 \pm 0.43)\cdot10^{-5}$ $G_0$ (A type) and $(7.92 \pm 1.33)\cdot10^{-5}$ $G_0$ (B type). The great similarity between the A-type conductance values obtained for the trimethylsilyl terminated **27** and **34** (*ca.* $3\cdot10^{-5}$ $G_0$) prove the similar electronic performance of the $-C\equiv CSiMe_3$ linker compared to that of the $-NH_2$ on gold. In addition the A-type conductance value is of the same order of magnitude as that obtained for the A-type

contact of the equivalent bis(thiol) terminated compound (HS-OPE-SH) of $1.8 \cdot 10^{-5}$ $G_0$.[30] The observation of an additional B type contact in **27** not observable for **35** is consistent with the presence of a single $-NH_2$ contact, which can bind in defect sites on the gold substrate or STM tip.

The nature of the $-C{\equiv}CSiMe_3$ interaction with the gold electrode implicit in these single molecule conductance measurements of **27** and **35** is far from well understood, and merits further discussion here. In a recent study, the formation of highly transmissive C-Au contacts has been reported by using a related Group 14 derived $-SnMe_3$ linker.[20a] In this work, the conductance of molecular junctions derived from $Me_3Sn\text{-}CH_2\text{-}C_6H_4\text{-}CH_2\text{-}SnMe_3$ was studied using STM-BJ methods. The observation of a high molecular conductance approaching 0.1 $G_0$ suggests a radically different mechanism for molecule-surface contact than in virtually all other molecular junctions. Organotin reagents are well known for their high reactivity and despite their toxicity are widely used as carbon transfer reagents in the Stille cross-coupling chemistry, in which Sn-Pd transmetallation processes play a critical role. Transmetallation/oxidative addition reactions between bis(alkyltin) molecule to the gold substrate and electrode STM tip therefore seems feasible.

Given the evidence for $SnMe_3$ moieties adsorbed on the surface, the working hypothesis, which is supported by transport calculations, involves cleavage of the Sn-methylene bond, transfer of the tin moiety to the surface, and formation of a direct Au-C bond to the *para*-xylene fragment which forms the junctions. Coupling of the surface orbitals with the xylyl-methylene σ*-orbitals (i.e. hyperconjugation) and hence into the phenylene π (or π*) systems leads to the high conductance observed. The implication of this model and the dramatically higher conductance measured, is that the π-system of other molecules studied in molecular junctions do not couple effectively to the metal electrodes. There are many similarities in the structural and reaction chemistry of trialkyl-Sn and -Si

compounds, so it is pertinent to consider if related Si-C bond cleavage processes are involved in the formation of molecular junctions from $-C\equiv CSiMe_3$ derivatives. The trimethylsilyl group is readily cleaved on reactions with nucleophiles, although it is less prone to transmetallation processes.

In order to assess the influence of the $-C\equiv CSiMe_3$ moiety on the conductance of **35**, a series of experiments were performed in which the STM gold substrate was incubated in a diluted solution of **35** (~$10^{-5}$ M, $CHCl_3$) in the presence of the TBAF (2 eq.). Under these conditions, the trimethylsilyl capping group in **35** reacts with $F^-$ ions to form the insoluble $SiMe_3F$ leaving the highly reactive $-C\equiv C^-$ moiety as a potential surface linker. The absence of the capping silyl group can theoretically enable direct C≡C-Au interaction in an analogue way to that reported for the Sn reagents. The assembly of **35** on a gold substrate under these conditions was confirmed by QCM experiments, and preliminary STM-BJ conductance studies on samples prepared following this protocol, show a noticeable increase in conductance *ca.* (7.0 ± 2.1 ·$10^{-5}$) $G_0$ with respect to the silyl terminated **35** (*ca.* 3·$10^{-5}$ $G_0$) (Figure 5-4).

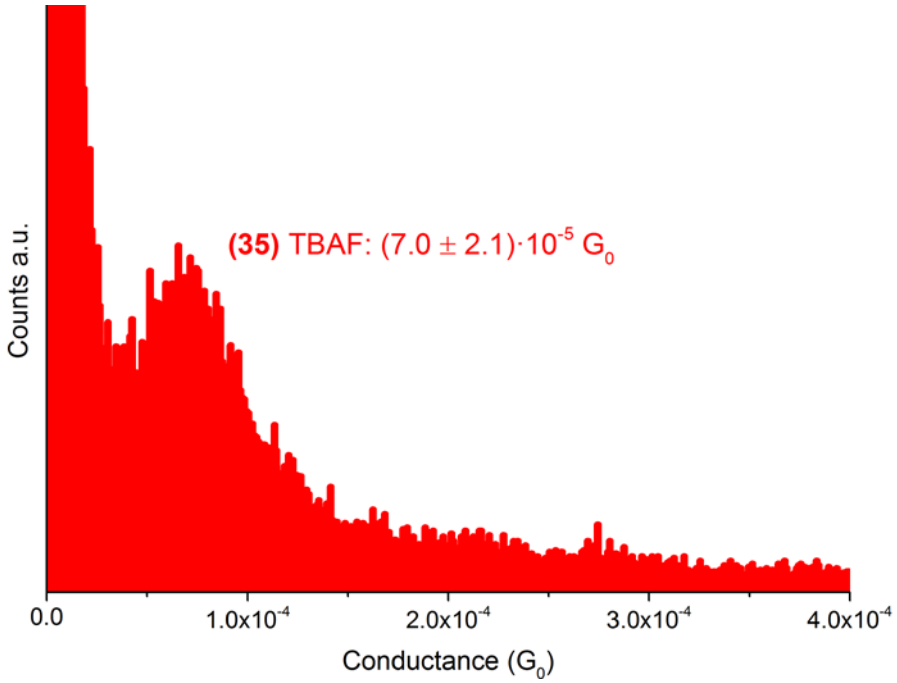


**Figure 5-4.** *STM-BJ (600 mV) for samples of **35** incubated in the presence of TBAF.*

Interestingly, the conductance histogram obtained for those samples prepared in the presence of fluoride ions shows a much broader conductance profile consistent with the lack of geometrical constraints imposed by the trimethylsilyl linker. However further studies are required in order to determine the influence of the sample preparation in the junction conductance.

In order to shed further light on the nature of the metal|molecule interaction in the silyl-based molecular junctions, a series of QCM and XPS were performed on compounds **27**, **36 - 38**. QCM studies performed at the University of Zaragoza by the group of Dr. Pilar Cea confirmed the chemisorption of **35** (−C≡CSiMe$_3$) and **36** (−C≡CH) onto gold substrates. On the other hand, no weight change was observed for their carbon counterpart **37** (−C≡CCMe$_3$) and the sterically hindered triisopropylsilyl terminated **38** (−C≡CSiPr$_3^i$), indicating that these do not adsorb. Interestingly, when the QCM experiments for the silyl terminated OPEs **35** and **38** were conducted in the presence of TBAF, both compounds were found to produce molecular assemblies on the QCM substrates. In addition XPS measurements performed on **35** as powder and SAMs confirmed the presence of the -SiMe$_3$ moiety in both cases, although a slight shift observed for the 2s peak of the SAMs could indicate a change in the hybridization of the Si atom.

Preliminary STM-BJ conductance studies on OPE **38** for samples prepared by *in-situ* deprotection of the terminal triisopropyl moiety revealed a conductance value similar to that obtained for samples of **35** prepared following the same protocol (*ca.* $7 \cdot 10^{-5}$ $G_0$). However, further studies are required in order to fully characterize the electrical properties of the *in-situ* deprotected samples of **35** and **38** and the influence of preparation and experimental conditions on the junction formation.

In the light of these results, it has been proposed that given the capacity of $Si^{4+}$ to adopt coordination numbers greater than four the $-C{\equiv}CSiMe_3$ linker could adopt a five-coordinate trigonal bipyramidal geometry at the silicon with a Si-Au bond, aided by the presence of the electron-withdrawing ethynyl substituent.[22-23, 31] This linker geometry would imply the three silicon methyl groups distorting from the idealised tetrahedral geometry and approaching a plane parallel to the Au surface, thereby sterically hindering the formation of junctions adjacent to defect sites (Figure 5-5). The geometrical constraints imposed by the $-C{\equiv}CSiMe_3$ linker results on the simplification of the conductance fingerprint of the molecule by preventing contact at under-coordinated surface defect sites such as step edges and adjacent surface adatoms. On the other hand, its carbon counterpart $-C{\equiv}CCMe_3$ and the sterically hindered $-C{\equiv}CSiPr^i_3$ can only interact with the gold surface by weaker van der Waals interactions that lead to insufficient molecule-surface coupling.

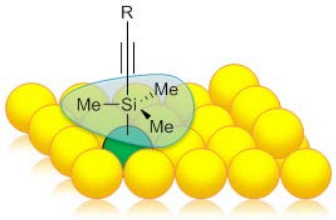


**Figure 5-5.** *Schematic representation of the proposed five-coordinate trigonal bipyramidal geometry of the ethynyl(trimethylsilyl) linker on gold.*

### *5.3.2. Ruthenium molecular wires*

Taking advantage of the $-C{\equiv}CSiMe_3$ ability to generate simplified conductance histograms, a comparative STM study between compounds **30f** and **35** was performed. Both compounds offer a rod-like geometry with estimated Si···Si distances of 24.49 and 23.97 Å. The conductance histograms built from the current traces of **30f** and **35** reveal single conductance values of $(2.75 \pm 0.56) \cdot 10^{-5}$ $G_0$ and $(5.10 \pm 0.99) \cdot 10^{-5}$ $G_0$ respectively (Figure 5-6). These results confirm the ability of $-C{\equiv}CSiMe_3$ to exclusively generate A-

type junctions, in good agreement with low number of traces showing plateaus (14 - 16% of the scans). The higher conductance of the organometallic junction is consistent with the shorter molecular length but also with a better alignment of the HOMO with the electrodes Fermi levels.[24c, 32]

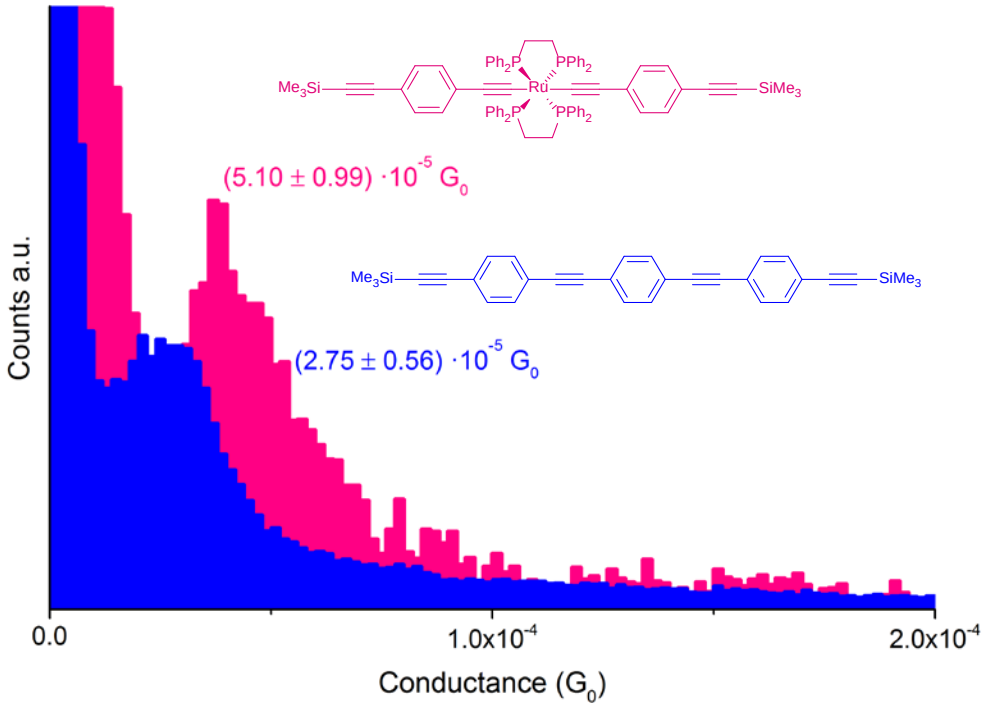


**Figure 5-6.** *Conductance histograms of **35** (blue) and the organometallic **30f** (pink).*

Previous studies by Liu *et al.*[24c] report similar results for thiol terminated analogues of **35** and **30f** (**39** and **40**, Chart 5-2) using the STM-BJ method. In those studies, the thiol terminated OPE showed a conductance value four times smaller ($4.6 \cdot 10^{-5}$ $G_0$) than that of the $Ru(dppm)_2$ analogue ($2.45 \cdot 10^{-4}$ $G_0$). However, in a parallel study performed by Mayor *et al.*[33] on thiol terminated platinum complexes (**41** and **42**, Chart 5-2) using the MCBJ method the insulating properties of the platinum core are described. In their work, a dramatic increase in resistance was found for the platinum complex **42** (5 – 50 GΩ ~ $10^{-7}$ $G_0$) about three orders of magnitude larger than that observed for the purely organic wire **41**. It is generally accepted that the difference in conductance between the Pt and Ru

complexes is due to the highly delocalized π−d−π nature of the $Ru(C{\equiv}CR)_2(dppm)_2$ systems which spans the length of the molecular backbone (*see* Chapter 4)[34] whilst the analogous $d_{xz}$ and $d_{yz}$ orbitals on square planar Pt are not available to promote extended delocalised electronic structures.

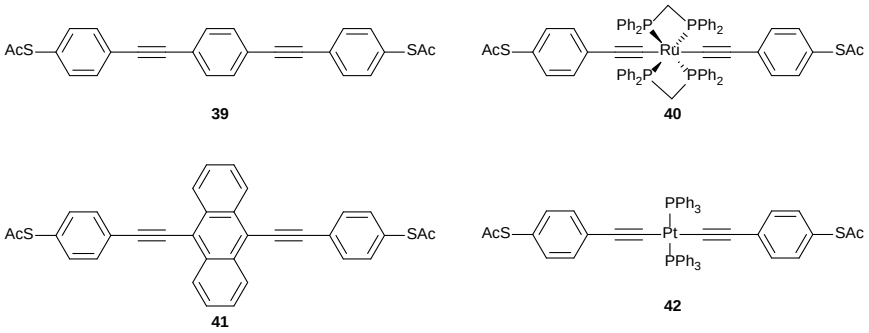


**Chart 5-2.** *Thiol terminated derivatives **39** and **40** studied by Liu et al.[24c] and compounds **41** and **42** studied by Mayor et al.[33] assessing the influence of the metallic core on the junction electric performance.*

### *5.3.3. Electrochemical gating in an STM*

As it has been briefly discussed in previous sections of this Chapter, the use of conjugated organometallic derivatives is not only interesting because of their enhanced conductance, but also because of their accessible redox states. In the last decade, several redox active organic [24d, 28, 35] and organometallic [36] derivatives have been subject of STM-based investigation of single molecule conductance under electrochemical control. Despite being in the early stages of the field, electrochemical modulation of a junction conductance is now widely accepted.[24a, 24d, 24f, 36a, b, 37] To that end, electrochemical STM studies were performed in order to assess conductance modulation on redox active **30f** (*see* Chapter 4) under the influence of an external, electrochemical 'gate'. A schematic representation of the electrochemical STM (EC-STM) setup employed is shown in Figure 5-7. Despite its added complexity, this method allows one to conveniently adjust the tip and substrate

Fermi levels relative to the molecular orbitals of **30f** by monitoring the substrate potential against a reference electrode.[27, 37b, 38] The ability to control the conductance of the molecular junction brings the field a step closer to the use of molecules as transistors.[24f, 25a]

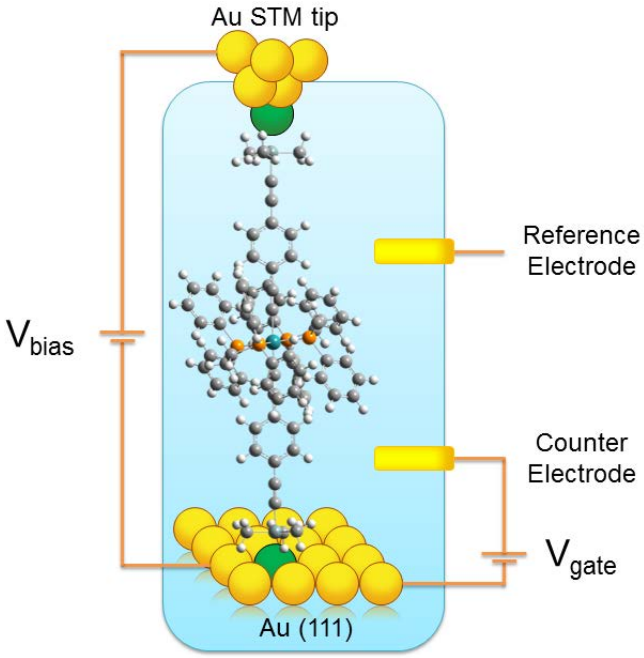


**Figure 5-7.** *Electrochemically controlled STM. $V_{bias}$ and $V_{gate}$ are the tip-substrate bias voltage and the substrate potential with respect to the reference electrode, respectively. Both are controlled by the STM software which operates the device as a bipotentiostat.*

To test the conductance modulation on **30f** the *I*(*s*) STM method was employed to collect current traces at different gating bias. The *I*(*s*) experiments were performed in a 0.1 M $TBAPF_6$ (tetrabutylammonium hexafluorophosphate) DMF electrolyte solution. Figure 5-8 (*top*) summarizes the conductance values obtained for **30f** relative to the gating bias applied. Each value of conductance shown in Figure 5-8, represents the conductance peak found from histograms built out of thousands of *I*(*s*) traces at each different gating potential applied (± 0.7 V). An evident increase in conductance was observed for gating bias between -0.3 V and 0 V. That higher conductance area (Figure 5-8, region II) is delimited by two lower conductance areas (Figure 5-8, regions I and III) leading to a bell-like $G$-$V_{gate}$ plot typically referred to as an off-on-off behaviour. This junction response can

be explained by the two-step electron/hole transfer model including vibrational relaxation developed by Kuznetsov and Ulstrup.[38a, 39] In a few simple words, this model describes how the applied gate voltage can drive the molecular orbitals into resonance with the tip-substrate Fermi levels leading to a conductance increase (Figure 5-8, region II). On the contrary, a conductance drop is expected as the energy levels are brought out of resonance (Figure 5-8, *I and III areas*).

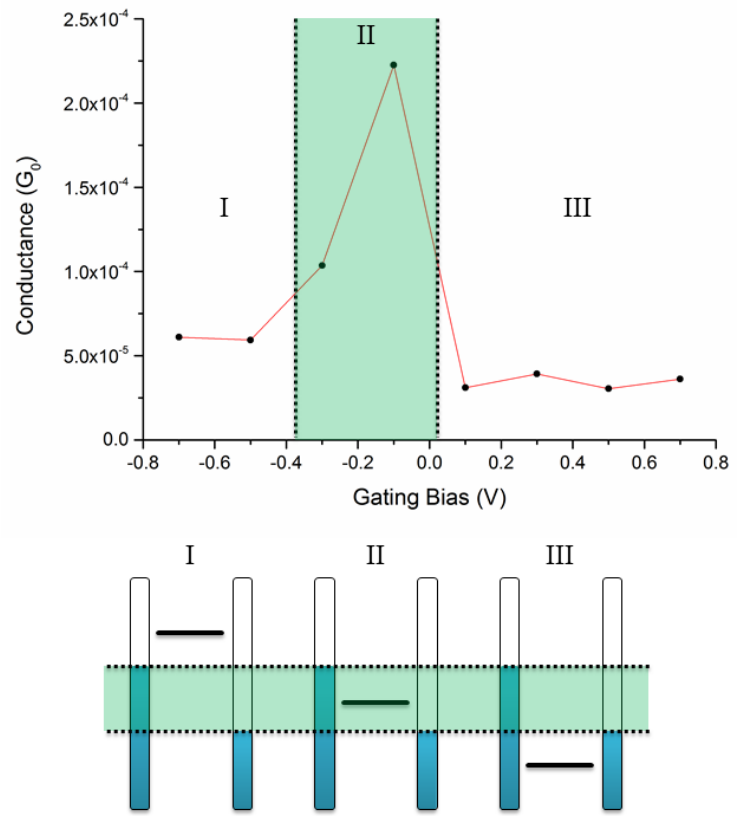


**Figure 5-8.** *Conductance values of **30f** at different gating bias (top). Alignment of the electrode Fermi levels with the molecular orbital responsible of charge transport (bottom). In resonance (II), positive (I) and negative (III) overpotentials.*

Further studies are being performed on **30f**, in collaboration with Prof. Richard Nichols group in order to confirm this transistor-like behaviour and collect more data points in the critical region II and near the I-II and II-III transition regions. In addition, related studies are being performed on related redox derivatives bearing different contact groups such as the amine terminated **30h**.

## 5.4. Conclusions

Effective electrical contacts between conjugated molecules and conducting substrates are important for the continued development of molecular electronic technology. The −C≡CSiMe$_3$ moiety was used to generate contacts on gold substrates with A-type conductance in the same order of magnitude of more traditional linkers (−SH and −NH$_2$) but without the additional complication of multiple conductance signatures. The observed simplification of the conductance profile is an encouraging step towards the integration of molecules in electronic devices. However further studies need to be carried out in order to clarify the C≡CSiMe$_3$···Au interaction and the proposed mode of surface contact at Si which appears to prevent coordination at defect sites. It must also be noted that the −C≡CSiMe$_3$ moiety is optimised for the least conductive A-type junctions. Future work to develop higher conductance contacts may also require concerted optimisation of both the molecular contact group and coarser electrode surfaces in which the under-coordinate sites necessary for B- and C-type contacts can be exploited in a controlled and reliable manner. Finally, encouraging EC-STM studies showed a possible transistor-like behaviour of the redox active organometallic complex **30f**.

## 5.5. Experimental

### *5.5.1. General conditions*

General conditions were reported in Chapter 2. The catalyst Pd(PPh$_3$)$_4$ was prepared following literature methods.[40] The synthesis of 4-ethynylaniline, Me$_3$SiC≡CC$_6$H$_4$C≡CH and **27** (Chapter 3), and HC≡CC$_6$H$_4$C≡CBu$^t$, **30f** and **30h** (Chapter 4) were reported in previous experimental sections of this thesis. Other reagents were purchased commercially and used as received.

### *5.5.2. Synthesis and characterization*

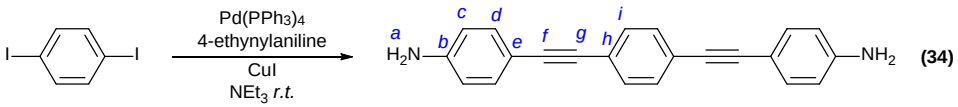


(34)

**Preparation of 34.**[29] To a 100 mL Schlenk charged with $NEt_3$ (80 mL), 4-ethynylaniline (0.37 g, 3.2 mmol), 1, 4-diiodobenzene (0.53 g, 1.6 mmol), $Pd(PPh_3)_4$ (0.09 g, 0.10 mmol) and CuI (0.02 g, 0.10 mmol) were added and the mixture stirred at room temperature overnight. The orange precipitate was collected by filtration washed thoroughly with hexane and purified by column chromatography in neutral alumina (hexane:EtOAc) (*4:6*). The brown powder obtained was then crystallized from hot toluene to obtain the pure product as orange needles. Yield 0.074 g, 0.239 mmol, 15%. $^1$H NMR (400 MHz, $CDCl_3$) δ 7.43 (s, 4H, *i*), 7.33 (d, *J* = 9 Hz, 4H, *d*), 6.63 (d, *J* = 9 Hz, 4H, *c*), 3.82 (s br, 4H, *a*). $^{13}C\{^1H\}$ NMR (101 MHz, $CDCl_3$) δ 146.9 (*b*), 133.2, 131.3 (*d/i*), 123.3, 112.7 (*e/h*), 114.9 (*c*), 92.0, 87.5 (*f/g*). $MS^+$ (ASAP) *m/z* (%): 309.15 (100, $[M+H]^+$). Elemental analysis % calcd. (found): C 85.69 (85.61); H 5.23 (5.12); N 9.08 (9.20).

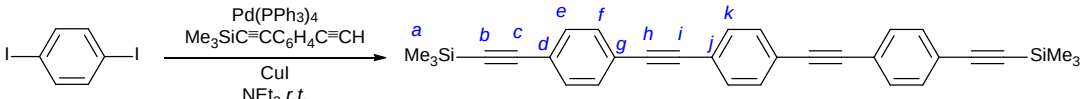


(35)

**Preparation of 35.**[41] A 25 mL Schlenk flask charged with $NEt_3$ (20 mL), $Me_3SiC{\equiv}CC_6H_4C{\equiv}CH$ (0.37 g, 1.5 mmol), 1, 4-diiodobenzene (0.23 g, 0.70 mmol), $Pd(PPh_3)_4$ (0.09 g, 0.10 mmol) and CuI (0.02 g, 0.10 mmol) were added and the resulting suspension stirred at room temperature overnight. The precipitate was collected by filtration and washed thoroughly with hexane. The product was then recrystallized from toluene yielding the pure product as white needles. Yield 0.13 g, 0.28 mmol, 40%. $^1$H NMR (400 MHz, $CDCl_3$) δ 7.50 (s, 4H, *e*), 7.45 (s br, 8H, *f/k*), 0.26 (s, 18H, *a*). $^{13}C\{^1H\}$ NMR (101 MHz, $CDCl_3$) δ 132.1, 131.7, 131.6 (e/*f/k*), 123.4, 123.2, 123.2 (*d/g/j*), 104.8 (*b*), 96.6 (*c*), 91.2, 91.1 (*h/i*), 0.1 (*a*). $MS^+$ (ASAP) *m/z* (%): 470.20 (100, $[M]^+$).

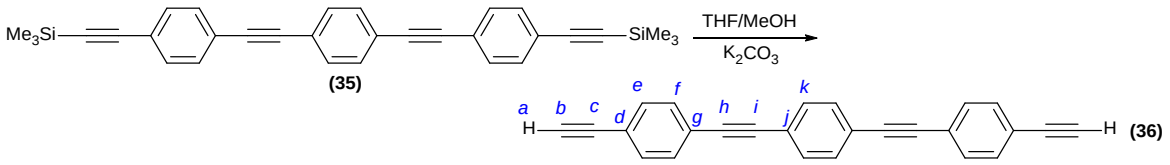


**Preparation of 36.**[42] To a solution of **35** (0.05 g, 0.11 mmol) in THF (35 mL), $K_2CO_3$ (0.04 g, 0.29 mmol) dissolved in MeOH (5 mL) was added and the mixture stirred at room temperature overnight. The mixture was then taken to dryness under reduced pressure and the residue re-dissolved in $CHCl_3$ (50 mL). The organic phase was then washed with water (2×50 mL) and brine (1×25 mL) and dried over $MgSO_4$. The pure product was obtained after taking the organic phase to dryness as an off-white powder. Yield 0.029 g, 0.088 mmol, 81%. $^1$H NMR (400 MHz, $CDCl_3$) δ 7.51 (s, 4H, *e*), 7.48 (s, 8H, *f/k*), 3.18 (s, 2H, *a*). MS$^+$ (ASAP) *m/z* (%): 326.1 (100, $[M]^+$. IR (*nujol*) cm$^{-1}$: 3271 (*m*) ν($C_{sp}$–H); *not observed* ν(C≡C).

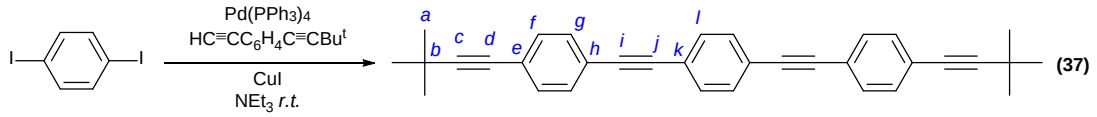


**Preparation of 37.** To a 25 mL Schlenk charged with $NEt_3$ (20 mL), $HC{\equiv}CC_6H_4C{\equiv}CBu^t$ (0.37 g, 1.5 mmol), 1, 4-diiodobenzene (0.25 g, 0.76 mmol), $Pd(PPh_3)_4$ (0.05 g, 0.04 mmol) and CuI (0.01 g, 0.05 mmol) were added and the mixture stirred at room temperature overnight. The white precipitate was collected by filtration and washed with hexane. The product was then crystallized from hot toluene and washed with hexane and EtOH to obtain the pure product as white needles. Yield 0.24 g, 0.56 mmol, 74%. $^1$H NMR (400 MHz, $CDCl_3$) δ 7.49 (s, 4H, *l*), 7.44 (d, *J* = 8 Hz, 4H, *f*), 7.36 (d, *J* = 8 Hz, 4H, *g*), 1.32 (s, 18H, *a*). $^{13}$C{$^1$H} NMR (101 MHz, $CDCl_3$) δ 131.7, 131.7, 131.5 (*f/g/l*), 124.4, 123.2, 122.0 (*e/h/k*), 100.9 (*c*), 91.3, 90.5 (*i/j*), 79.0 (*d*), 31.1 (*a*), 28.2 (*b*). MS$^+$ (ASAP) *m/z* (%): 389.2 (100, $[M]^+$).

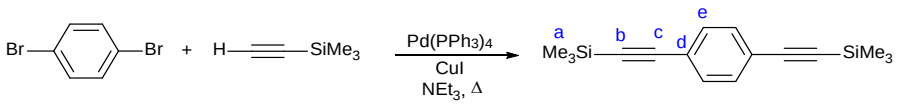


**Preparation of $Me_3SiC{\equiv}CC_6H_4C{\equiv}CSiMe_3$.**[43] In an oven-dried round bottom flask, trimethylsilylacetylene (7.6 mL, 5.2 g, 53 mmol) was added to a solution of 1,4-dibromobenzene (6.37 g, 25.1 mmol), $Pd(PPh_3)_4$ (1.36 g, 1.18 mmol) and CuI (0.23 g, 1.23 mmol) in anhydrous degassed $NEt_3$ (150 mL). The reaction mixture was heated at reflux overnight. Upon completion of the reaction, the black mixture was taken to dryness and purified by silica gel column chromatography (hexane). Removal of solvent from the main fraction yielded the pure product as a white powder. Yield 6.51 g, 24.1 mmol, 96%. $^1$H NMR (400 MHz, $CDCl_3$) δ 7.39 (s, 4H, *e*), 0.24 (s, 18H, *a*). $MS^+$ (ASAP) *m/z* (%): 255.10 (100, $[M\text{-}CH_3]^+$); 270.12 (53.7, $[M]^+$). IR (*nujol*) $cm^{-1}$: 2162 (m) *ν*(C≡C).

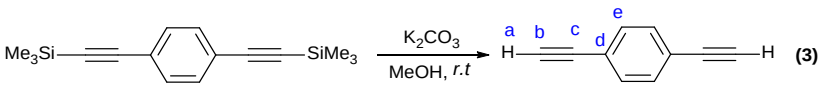


**Preparation of $HC{\equiv}CC_6H_4C{\equiv}CH$.**[44] In a 250 mL round bottom flask $Me_3SiC{\equiv}CC_6H_4C{\equiv}CSiMe_3$ (6.47 g, 24.0 mmol) and $K_2CO_3$ (4,83 g, 35.0 mmol) were dissolved in MeOH (150 mL). The reaction mixture was stirred overnight at room temperature. The mixture was then poured into water and extracted twice with $CH_2Cl_2$. The organic phase was washed with water (2×100 mL), brine (1×100 mL) and dried over $MgSO_4$. Yield 2.2 g, 17.4 mmol, 73%. $^1$H NMR (400 MHz, $CDCl_3$) δ 7.44 (s, 4H, *e*), 3.17 (s, 2H, *a*). $^{13}C\{^1H\}$ NMR (101 MHz, $CDCl_3$) δ 132.2 (*e*), 122.7 (*d*), 83.2 (*c*), 79.2 (*b*). $MS^+$ (ASAP) *m/z* (%): 126.04 (100, $[M]^+$).

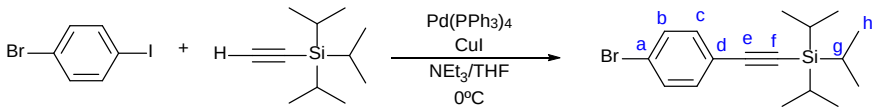


**Preparation of $BrC_6H_4C{\equiv}CSiPr_3^i$.**[45] In a 250 mL Schlenk flask charged 1-bromo-4-iodobenzene (1.01 g, 3.58 mmol), $Pd(PPh_3)_4$ (0.198 g, 0.171 mmol) and CuI (0.032 g, 0.168 mmol) were suspended into an ice cold mixture of THF (100 mL) and $NEt_3$ (10 mL). To that mixture ethynyltriisopropylsilane (0.80 mL, 3.6 mmol) was added drop wise during 15 minutes and the mixture stirred at 0 ºC for 5 hours. The yellow suspension was allowed to warm to room temperature and stirred overnight. The mixture was filtered and the filtrate purified by chromatography on silica gel using hexane as the eluent. Removal of solvent from the main fraction yielded the pure product as a colourless oil. Yield 1.13 g, 3.35 mmol, 94%. $^1$H NMR (400 MHz, $CDCl_3$) δ 7.24 (d, *J* = 9 Hz, 2H, *c*), 7.14 (d, *J* = 9 Hz, 2H, *b*), 0.93 (s, 21 H, g/*h*). $^{13}C\{^1H\}$ NMR (101 MHz, $CDCl_3$) δ 133.6, 131.58 (*b*/c), 122.6 (*a*/d), 106.0, 92.2 (*e*/*f*), 18.8 (*g*), 11.4 (*h*). IR (*nujol*) $cm^{-1}$: 2159 (*s*) ν(C≡C).

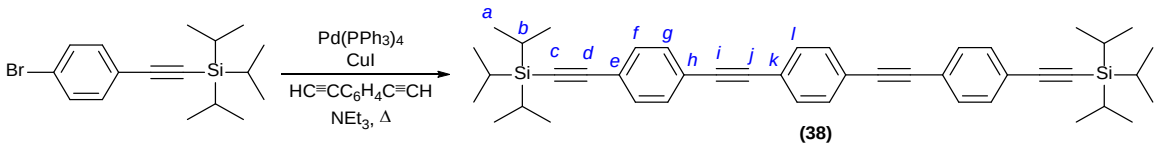


**(38)**

**Preparation of 38.** A 25 mL Schlenk flask charged with $HC{\equiv}CC_6H_4C{\equiv}CH$ (0.054 g, 0.428 mmol), $BrC_6H_4C{\equiv}CSiPr_3^i$ (0.29 g, 0.86 mmol), $Pd(PPh_3)_4$ (0.05 g, 0.04 mmol) and CuI (0.01 g, 0.05 mmol) and $NEt_3$ (15 mL) was stirred at reflux overnight. The reaction mixture was filtered and the yellow filtrate taken to dryness. The residue was purified by silica gel column chromatography (hexane). A yellow residue obtained after solvent evaporation from the main fraction. The pure product was obtained as white needles upon crystallization from hexane. Yield 0.16 g, 0.26 mmol, 61%. $^1$H NMR (400 MHz, $CDCl_3$) δ 7.51 (s, 4H, *f*), 7.45 (s, 8H, *g*/*l*), 1.14 (s, 42H, *a*/*b*). $^{13}C\{^1H\}$ NMR (101 MHz, $CDCl_3$) δ 132.2, 131.7, 131.5 (*f*/*g*/*l*), 123.7, 123.2, 123.0 (*e*/*h*/*k*), 106.8, 93.2 (*c*/*d*), 91.2, 91.0 (*i*/*j*), 18.8 (*b*), 11.5 (*a*). $MS^+$ (ASAP) *m*/*z* (%): 638.36 (100, $[M]^+$).

## 5.6. References


1. (a) Tour, J. M., *Molecular Electronics; Commercial Insights, Chemistry, Devices, Architecture and Programming.* World Scientific Publishing Co: Scientific, 2003; (b) Salomon, A.; Cahen, D.; Lindsay, S.; Tomfohr, J.; Engelkes, V. B.; Frisbie, C. D., *Adv. Mater.*, **2003**, *15*, 1881-1890; (c) Seminario, J. M.; De La Cruz, C.; Derosa, P. A.; Yan, L., *J. Phys. Chem. B*, **2004**, *108*, 17879-17885; (d) McCreery, R. L.; Bergren, A. J., *Adv. Mater.*, **2009**, *21*, 4303-4322.
2. (a) Hong, S.; Reifenberger, R.; Tian, W.; Datta, S.; Henderson, J. I.; Kubiak, C. P., *Superlattices Microstruct.*, **2000**, *28*, 289-303; (b) Ke, S.-H.; Baranger, H. U.; Yang, W., *J. Am. Chem. Soc.*, **2004**, *126*, 15897-15904.
3. (a) Cui, X. D.; Primak, A.; Zarate, X.; Tomfohr, J.; Sankey, O. F.; Moore, A. L.; Moore, T. A.; Gust, D.; Harris, G.; Lindsay, S. M., *Science*, **2001**, *294*, 571-574; (b) Selzer, Y.; Salomon, A.; Cahen, D., *J. Am. Chem. Soc.*, **2002**, *124*, 2886-2887; (c) Seminario, J. M.; Yan, L., *Int. J. Quantum Chem*, **2005**, *102*, 711-723; (d) Kaun, C.-C.; Guo, H., *Nano Lett.*, **2003**, *3*, 1521-1525.
4. Andrews, D. Q.; Van Duyne, R. P.; Ratner, M. A., *Nano Lett.*, **2008**, *8*, 1120-1126.
5. (a) Haiss, W.; Martín, S.; Leary, E.; Zalinge, H. v.; Higgins, S. J.; Bouffier, L.; Nichols, R. J., *J. Phys. Chem. C*, **2009**, *113*, 5823-5833; (b) Huang, M. J.; Hsu, L. Y.; Fu, M. D.; Chuang, S. T.; Tien, F. W.; Chen, C. H., *J. Am. Chem. Soc.*, **2014**, *136*, 1832-1841.
6. Wang, G.; Kim, T. W.; Lee, T.; Wang, W.; Reed, M. A., 4.16 - Electronic Properties of Alkanethiol Molecular Junctions: Conduction Mechanisms, Metal–Molecule Contacts, and Inelastic Transport. In *Comprehensive Nanoscience and Technology*, Andrews, D. L.; Scholes, G. D.; Wiederrecht, G. P., Eds. Academic Press: Amsterdam, 2011; pp 463-487.
7. (a) Rubio, G.; Agraït, N.; Vieira, S., *Phys. Rev. Lett.*, **1996**, *76*, 2302-2305; (b) Krüger, D.; Fuchs, H.; Rousseau, R.; Marx, D.; Parrinello, M., *Phys. Rev. Lett.*, **2002**, *89*, 186402.
8. (a) Rubio-Bollinger, G.; Bahn, S. R.; Agraït, N.; Jacobsen, K. W.; Vieira, S., *Phys. Rev. Lett.*, **2001**, *87*, 026101; (b) Huang; Chen, F.; Bennett, P. A.; Tao, *J. Am. Chem. Soc.*, **2007**, *129*, 13225-13231; (c) Sondag-Huethorst, J. A. M.; Schonenberger, C.; Fokkink, L. G. J., *J. Phys. Chem.*, **1994**, *98*, 6826-6834.
9. Häkkinen, H., *Nat. Chem*, **2012**, *4*, 443–455.
10. (a) Ie, Y.; Hirose, T.; Nakamura, H.; Kiguchi, M.; Takagi, N.; Kawai, M.; Aso, Y., *J. Am. Chem. Soc.*, **2011**, *133*, 3014-3022; (b) Sedghi, G.; Garcia-Suarez, V. M.; Esdaile, L. J.; Anderson, H. L.; Lambert, C. J.; Martin, S.; Bethell, D.; Higgins, S. J.; Elliott, M.; Bennett, N.; Macdonald, J. E.; Nichols, R. J., *Nat. Nano*, **2011**, *6*, 517-523; (c) Xu, B.; Tao, N. J., *Science*, **2003**, *301*, 1221-1223; (d) Zhao, X.; Huang, C.; Gulcur, M.; Batsanov, A. S.; Baghernejad, M.; Hong, W.; Bryce, M. R.; Wandlowski, T., *Chem. Mater.*, **2013**, *25*, 4340-4347; (e) Wang, C.; Batsanov, A. S.; Bryce, M. R.; Martín, S.; Nichols, R. J.; Higgins, S. J.; García-Suárez, V. M.; Lambert, C. J., *J. Am. Chem. Soc.*, **2009**, *131*, 15647-15654.

11. (a) Venkataraman, L.; Park, Y. S.; Whalley, A. C.; Nuckolls, C.; Hybertsen, M. S.; Steigerwald, M. L., *Nano Lett.*, **2007**, *7*, 502-506; (b) Venkataraman, L.; Klare, J. E.; Tam, I. W.; Nuckolls, C.; Hybertsen, M. S.; Steigerwald, M. L., *Nano Lett.*, **2006**, *6*, 458-462; (c) Frei, M.; Aradhya, S. V.; Hybertsen, M. S.; Venkataraman, L., *J. Am. Chem. Soc.*, **2012**, *134*, 4003-4006.
12. Patrone, L.; Palacin, S.; Charlier, J.; Armand, F.; Bourgoin, J. P.; Tang, H.; Gauthier, S., *Phys. Rev. Lett.*, **2003**, *91*, 096802.
13. Moreno-García, P.; Gulcur, M.; Manrique, D. Z.; Pope, T.; Hong, W.; Kaliginedi, V.; Huang, C.; Batsanov, A. S.; Bryce, M. R.; Lambert, C.; Wandlowski, T., *J. Am. Chem. Soc.*, **2013**, *135*, 12228-12240.
14. (a) Chen, F.; Li, X.; Hihath, J.; Huang, Z.; Tao, N., *J. Am. Chem. Soc.*, **2006**, *128*, 15874-15881; (b) Martin, S.; Haiss, W.; Higgins, S. J.; Nichols, R. J., *Nano Lett.*, **2010**, *10*, 2019-2023.
15. Kiguchi, M.; Miura, S.; Hara, K.; Sawamura, M.; Murakoshi, K., *Appl. Phys. Lett.*, **2006**, *89*, 213104.
16. (a) Chen, J.; Calvet, L. C.; Reed, M. A.; Carr, D. W.; Grubisha, D. S.; Bennett, D. W., *Chem. Phys. Lett.*, **1999**, *313*, 741-748; (b) Beebe, J. M.; Engelkes, V. B.; Miller, L. L.; Frisbie, C. D., *J. Am. Chem. Soc.*, **2002**, *124*, 11268-11269.
17. Fu, M.-D.; Chen, I. W. P.; Lu, H.-C.; Kuo, C.-T.; Tseng, W.-H.; Chen, C.-h., *J. Phys. Chem. C*, **2007**, *111*, 11450-11455.
18. Fukazawa, A.; Kiguchi, M.; Tange, S.; Ichihashi, Y.; Zhao, Q.; Takahashi, T.; Konishi, T.; Murakoshi, K.; Tsuji, Y.; Staykov, A.; Yoshizawa, K.; Yamaguchi, S., *Chem. Lett.*, **2011**, *40*, 174-176.
19. Komoto, Y.; Fujii, S.; Hara, K.; Kiguchi, M., *J. Phys. Chem. C*, **2013**, *117*, 24277-24282.
20. (a) Cheng, Z. L.; Skouta, R.; H., V.; Widawsky, J. R.; Schneebeli, S.; Chen, W.; Hybertsen, M. S.; Breslow, R.; Venkataraman, L., *Nat. Nano*, **2011**, *6*, 353-357; (b) Hong, W.; Li, H.; Liu, S.-X.; Fu, Y.; Li, J.; Kaliginedi, V.; Decurtins, S.; Wandlowski, T., *J. Am. Chem. Soc.*, **2012**, *134*, 19425-19431.
21. Su, T. A.; Widawsky, J. R.; Li, H.; Klausen, R. S.; Leighton, J. L.; Steigerwald, M. L.; Venkataraman, L.; Nuckolls, C., *J. Am. Chem. Soc.*, **2013**, *135*, 18331-18334.
22. (a) Marchenko, A.; Katsonis, N.; Fichou, D.; Aubert, C.; Malacria, M., *J. Am. Chem. Soc.*, **2002**, *124*, 9998-9999; (b) Katsonis, N.; Marchenko, A.; Taillemite, S.; Fichou, D.; Chouraqui, G.; Aubert, C.; Malacria, M., *Chem. Eur. J.*, **2003**, *9*, 2574-2581.
23. Katsonis, N.; Marchenko, A.; Fichou, D.; Barrett, N., *Surf. Sci.*, **2008**, *602*, 9-16.
24. (a) Albrecht, T.; Guckian, A.; Ulstrup, J.; Vos, J. G., *Nano Lett.*, **2005**, *5*, 1451-1455; (b) Inkpen, M. S.; White, A. J. P.; Albrecht, T.; Long, N. J., *Chem. Commun.*, **2013**, *49*, 5663-5665; (c) Liu, K.; Wang, X.; Wang, F., *ACS Nano*, **2008**, *2*, 2315-2323; (d) Pobelov, I. V.; Li, Z.; Wandlowski, T., *J. Am. Chem. Soc.*, **2008**, *130*, 16045-16054; (e) Olivier, C.; Kim, B.; Touchard, D.; Rigaut, S., *Organometallics*, **2008**, *27*, 509-518; (f) Kay, N. J.; Higgins, S. J.; Jeppesen, J. O.; Leary, E.; Lycoops, J.; Ulstrup, J.; Nichols, R. J., *J. Am. Chem. Soc.*, **2012**, *134*, 16817-16826.
25. (a) Aviram, A.; Ratner, M. A., *Chem. Phys. Lett.*, **1974**, *29*, 277-283; (b) Joachim, C.; Ratner, M. A., *Proc. Natl. Acad. Sci. U.S.A.*, **2005**, *102*, 8801-8808; (c) Joachim,

C.; Gimzewski, J. K.; Aviram, A., *Nature*, **2000**, *408*, 541-548; (d) Aradhya, S. V.; Venkataraman, L., *Nat. Nano*, **2013**, *8*, 399-410; (e) Bergfield, J. P.; Ratner, M. A., *physica status solidi (b)*, **2013**, *250*, 2249-2266.

26. Haiss, W.; Lackey, D.; Sass, J. K.; Besocke, K. H., *J. Chem. Phys*, **1991**, *95*, 2193-2196.
27. Nichols, R. J.; Haiss, W.; Higgins, S. J.; Leary, E.; Martin, S.; Bethell, D., *Phys. Chem. Chem. Phys.*, **2010**, *12*, 2801-2815.
28. Xiao; Xu; Tao, N. J., *Nano Lett.*, **2004**, *4*, 267-271.
29. Lu, Q.; Liu, K.; Zhang, H.; Du, Z.; Wang, X.; Wang, F., *ACS Nano*, **2009**, *3*, 3861-3868.
30. (a) Haiss, W.; Wang, C.; Grace, I.; Batsanov, A. S.; Schiffrin, D. J.; Higgins, S. J.; Bryce, M. R.; Lambert, C. J.; Nichols, R. J., *Nat. Mater.*, **2006**, *5*, 995-1002; (b) Weibel, N.; Błaszczyk, A.; von Hänisch, C.; Mayor, M.; Pobelov, I.; Wandlowski, T.; Chen, F.; Tao, N., *Eur. J. Org. Chem.*, **2008**, *2008*, 136-149.
31. Watcharinyanon, S.; Nilsson, D.; Moons, E.; Shaporenko, A.; Zharnikov, M.; Albinsson, B.; Martensson, J.; Johansson, L. S. O., *Phys. Chem. Chem. Phys.*, **2008**, *10*, 5264-5275.
32. (a) Tao, N. J., *Phys. Rev. Lett.*, **1996**, *76*, 4066-4069; (b) Kim, B. S.; Beebe, J. M.; Olivier, C.; Rigaut, S.; Touchard, D.; Kushmerick, J. G.; Zhu, X. Y.; Frisbie, C. D., *J. Phys. Chem. C*, **2007**, *111*, 7521-7526; (c) Luo, L.; Benameur, A.; Brignou, P.; Choi, S. H.; Rigaut, S.; Frisbie, C. D., *J. Phys. Chem. C*, **2011**, *115*, 19955-19961.
33. Mayor, M.; von Hänisch, C.; Weber, H. B.; Reichert, J.; Beckmann, D., *Angew. Chem. Int. Ed.*, **2002**, *41*, 1183-1186.
34. Bruce, M. I.; Le Guennic, B.; Scoleri, N.; Zaitseva, N. N.; Halet, J.-F., *Organometallics*, **2012**, *31*, 4701-4706.
35. (a) Haiss, W.; van Zalinge, H.; Higgins, S. J.; Bethell, D.; Höbenreich, H.; Schiffrin, D. J.; Nichols, R. J., *J. Am. Chem. Soc.*, **2003**, *125*, 15294-15295; (b) Haiss, W.; van Zalinge, H.; Höbenreich, H.; Bethell, D.; Schiffrin, D. J.; Higgins, S. J.; Nichols, R. J., *Langmuir*, **2004**, *20*, 7694-7702; (c) Zhihai, L.; Ilya, P.; Bo, H.; Thomas, W.; Alfred, B.; Marcel, M., *Nanotechnology*, **2007**, *18*, 044018; (d) Petrangolini, P.; Alessandrini, A.; Berti, L.; Facci, P., *J. Am. Chem. Soc.*, **2010**, *132*, 7445-7453; (e) Petrangolini, P.; Alessandrini, A.; Navacchia, M. L.; Capobianco, M. L.; Facci, P., *J. Phys. Chem. C*, **2011**, *115*, 19971-19978; (f) Petrangolini, P.; Alessandrini, A.; Facci, P., *J. Phys. Chem. C*, **2013**, *117*, 17451-17461.
36. (a) Albrecht, T.; Guckian, A.; Ulstrup, J.; Vos, J. G., *Nanotechnology, IEEE Transactions on*, **2005**, *4*, 430-434; (b) Ricci, A. M.; Calvo, E. J.; Martin, S.; Nichols, R. J., *J. Am. Chem. Soc.*, **2009**, *132*, 2494-2495; (c) Alessandrini, A.; Corni, S.; Facci, P., *Phys. Chem. Chem. Phys.*, **2006**, *8*, 4383-4397.
37. (a) Leary, E.; Higgins, S. J.; van Zalinge, H.; Haiss, W.; Nichols, R. J.; Nygaard, S.; Jeppesen, J. O.; Ulstrup, J., *J. Am. Chem. Soc.*, **2008**, *130*, 12204-12205; (b) Friis, E. P.; Kharkats, Y. I.; Kuznetsov, A. M.; Ulstrup, J., *J. Phys. Chem. A*, **1998**, *102*, 7851-7859.

38. (a) Kuznetsov, A. M.; Ulstrup, J., *J. Phys. Chem. A*, **2000**, *104*, 11531-11540; (b) Jingdong, Z.; Mikala, G.; Allan, G. H.; Alexander, M. K.; Anja, B.; Hainer, W.; Jens, U., *J. Phys.: Condens. Matter*, **2003**, *15*, S1873.
39. (a) Zhang, J.; Chi, Q.; Kuznetsov, A. M.; Hansen, A. G.; Wackerbarth, H.; Christensen, H. E. M.; Andersen, J. E. T.; Ulstrup, J., *J. Phys. Chem. B*, **2002**, *106*, 1131-1152; (b) Kuznetsov, A. M.; Ulstrup, J., *Surf. Coat. Technol.*, **1994**, *67*, 193-200; (c) Zhang, J.; Chi, Q.; Albrecht, T.; Kuznetsov, A. M.; Grubb, M.; Hansen, A. G.; Wackerbarth, H.; Welinder, A. C.; Ulstrup, J., *Electrochim. Acta*, **2005**, *50*, 3143-3159.
40. Coulson, D. R.; Satek, L. C.; Grim, S. O., Tetrakis(Triphenylphosphine)Palladium(0). In *Inorg. Synth.*, John Wiley & Sons, Inc.: 2007; pp 107-109.
41. Khairul, W.; Porrès, L.; Albesa-Jové, D.; Senn, M.; Jones, M.; Lydon, D.; Howard, J.; Beeby, A.; Marder, T.; Low, P., *J. Cluster Sci.*, **2006**, *17*, 65-85.
42. Coskun, A.; Akkaya, E. U., *J. Am. Chem. Soc.*, **2006**, *128*, 14474-14475.
43. Takahashi, S.; Kuroyama, Y.; Sonogashira, K.; Hagihara, N., *Synthesis*, **1980**, *1980(8)*, 627-630.
44. Demessence, A.; Long, J. R., *Chem. Eur. J.*, **2010**, *16*, 5902-5908.
45. Türp, D.; Wagner, M.; Enkelmann, V.; Müllen, K., *Angew. Chem. Int. Ed.*, **2011**, *50*, 4962-4965.

# 6. SINGLE MOLECULE CONDUCTANCE STUDIES ON POLYYNES

## 6.1. Abstract

In this Chapter the single molecule conductance studies a series of trimethylsilyl terminated oligoyne molecular wires **43 - 46** (*n = 2 - 5*) (Chart 6-1) are discussed. The STM conductance measurements were performed in collaboration with Prof. Richard Nichols and Prof. Walther Schwarzacher groups at the University of Liverpool and Bristol respectively. Preliminary results show that, for all molecular junctions, evaluated under different experimental conditions, conductance is found to be almost independent of molecular length.

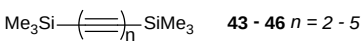


**43 - 46** *n = 2 - 5*

**Chart 6-1.** *Series of polyynes studied in this Chapter.*

## 6.2. Introduction

As previously discussed in Chapter 1, the electrical performance of a molecular junction is dependent on a number of factors, namely the metal|molecule interface (*see* Chapter 5), the junction geometry (tilt angles and tip-substrate gap size), the nature of the molecular bridge and environmental factors such as: temperature; solvent and measuring technique. In this Chapter, we focus our attention on the influence of the molecular bridge in the junction overall performance. Amongst the key molecular features found to influence the junction overall conductance are: the degree of conjugation of the molecular bridge;[1] the different molecular linkers[2] and the insertion of chemical substituents on the molecular backbone.[3] Despite all factors being equally important, perhaps the most intuitive is that related to the molecular bridge conjugation.

Molecular wires with highly delocalized π-systems are known to transport charge more effectively than their non-conjugated analogues. This was first observed in donor-bridge-acceptor (D-B-A) studies in solution[4] and self-assembled monolayers.[5] More recently, several single molecule studies supported the same observation. In their work, Mayor et al.[1a] demonstrated that disrupting the molecular conjugation of an oligophenylene-ethynylene (OPE) derivative by inserting a Pt centre in the molecular backbone lead to a conductance an order of magnitude lower whilst Liu *et al*.[1b] reported the opposite behaviour when a Ru centre was employed in analogue studies. In addition, purely organic conjugated systems have also been subject of study. In this context, OPEs and their parent compounds oligo(phenylenevinylene)s (OPV)s have been subject of a number of single molecule conductance studies.[6] The typically higher conductance found for the OPV derivatives has been explained by the longer vinyl bond C=C (*ca.*1.35 Å) allowing for a better conjugation of the molecular backbone in comparison with the shorter C≡C (*ca.* 1.22 Å), ultimately leading to a smaller energy difference between the frontier orbitals in the case of OPVs.[7]

Although less experimentally exploited, an alternative family of conjugated molecular wire candidates are polyynes. These compounds, which can be considered a carbon allotrope typically referred to as carbyne,[8] consist on a succession of *sp*-hybridized carbons forming a rigid linear chain, with an almost cylindrical orbital delocalization throughout the molecular backbone.[9] Interestingly, due to the great degree of orbital delocalization, the charge transport is independent of the different conformers. On the contrary OPEs and OPVs, where a low energy barrier is present for the rotation of phenyl rings leading to a disruption of the orbital conjugation, may ultimately lead to the coexistence of high and low conductance conformers.[10] This clearly relates to the studies of spectroscopic properties of the bis(arylethynyl) complexes discussed in Chapter 4.

The high transmission and low distance dependence of polyyne based molecular wires was first theoretically proposed by Crljen *et al.*,[11] expanded further by García-Suarez *et al.*[12] and most recently by Lambert *et al.*[13] These theoretical studies were later confirmed experimentally by Wang *et al.*[14] In their work, the conductance of a series of pyridyl terminated polyynes (n = 1, 2 and 4) were obtained by both the STM *I*(*s*) and STM-BJ methods, benchmarked against 4,4´-bipyridyl and supported by computational studies. Multiple conductance values were obtained for every compound ascribed to the different possible pyridine surface binding modes with values ranging from $5 \cdot 10^{-5}$ to $2 \cdot 10^{-3}$ $G_0$. Remarkably, the wires conductance was found to be very weakly dependent on molecular length, with an experimentally obtained attenuation factor $\beta = 0.6 \pm 0.3$ $nm^{-1}$, five times lower than that previously reported for pyridine terminated OPEs (3.3 $nm^{-1}$),[6h] and three times lower than previously reported OPVs (~2 $nm^{-1}$).[6a, 15] Despite the marked differences, it is important to note that, the attenuation factor $\beta$ not only depends on the orbital delocalization of the molecular backbone but on the entire molecular junction, including metal|molecule interface, electrode shape and material, and measuring technique.[15a] Encouraged by these promising studies,[14, 16] a series of symmetric polyynes **43 – 46** *(n = 2 - 5)* were prepared bearing the previously introduced trimethylsilyl group as a molecular linker (*see* Chapter 5), and molecular conductance of these simple wires explored.

## 6.3. Results and discussion

In order to ensure reproducibility and remove measurement specific artefacts conductance studies of compounds **43 - 45** were performed employing both STM-BJ and *I*(*s*) techniques. The experiments were performed employing an Agilent STM controlled using Picoscan 4.19 software. The STM tips were freshly prepared for each experiment by etching a Au wire (99.99%) in a HCl:EtOH (50 v/v) at 2.4 V. The gold-on-glass substrates employed were purchased from Arrandee, Schroeer, Germany. The substrates were flame

annealed with a butane flame immediately before use. This thermal treatment is known to generate atomically flat terraces on the Au(111) substrate.[17] The substrates were immersed in low concentration solutions (~$10^{-5}$ M, $CHCl_3$) of the targeted molecule for ~30 seconds. The low concentrations and short immersion times were chosen to promote a low surface coverage of the gold substrate, encouraging single molecule events instead of molecular aggregates. After adsorption, the sample was rinsed thoroughly with $CHCl_3$ and blown dry in a stream of $N_2$ gas. Figure 6-1 presents the conductance histograms, referenced to the $G_0$, constructed from early STM studies performed in collaboration with the Liverpool group for compounds **43 – 45** *(n = 2 - 4)* employing both *I*(*s*) *(left)* and STM-BJ techniques *(right)*. In every case, a single conductance value *ca.* $0.8 \cdot 10^{-4}$ $G_0$ was obtained, supporting the hypothesis of the C≡CSiMe$_3$ moiety enabling a single contact mode, and in good agreement with previously reported values for the pyridine terminated polyynes ($5 \cdot 10^{-5}$ to $2 \cdot 10^{-3}$ $G_0$).[14]

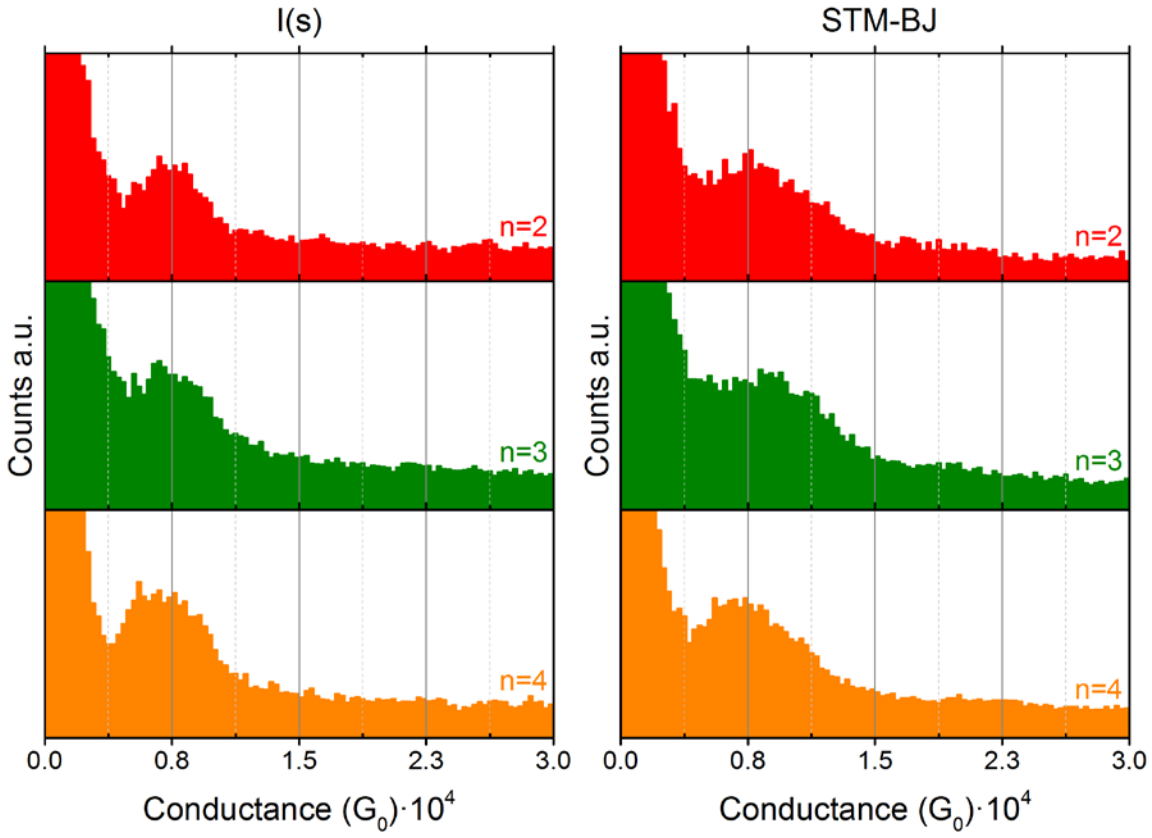


**Figure 6-1.** *Histograms obtained for **43 - 45** (n=2 - 4) by I(s) (left) and STM-BJ (right).*

Remarkably, the conductance values obtained were found to be almost independent of the molecular length (Table 6-1). Despite these results being consistent with the previously reported low values of $\beta$ for pyridyl terminated polyynes, the substantial broadness of the conductance histograms obtained lead us evaluate the statistical significance of the results.

**Table 6-1.** *Values of BJ and I(s) STM analyses.*

| **Compound** | **Molecular length Si···Si (nm)*** | **Conductance ($G_0$) · $10^4$** | |
|---|---|---|---|
| | | *I(s) method* | *STM-BJ* |
| **43** *(n = 2)* | ~ 0.74 | 0.72 ± 0.38 | 0.73 ± 0.74 |
| **44** *(n = 3)* | ~ 0.98 | 0.71 ± 0.51 | 0.83 ± 0.71 |
| **45** *(n = 4)* | ~ 1.22 | 0.68 ± 0.50 | 0.70 ± 0.66 |

** MM2 energy minimizations*

In order to statistically assess the molecular length influence on conductance, the conductance data obtained for the shortest **43** (n = 2) and longest **45** (n = 4) compounds was subjected to a *t*-test. The *t*-test offers a quick and simple alternative to the analysis of variance in order to determine if two sets of data are significantly different from each other. The value of *t* for a given dataset can be calculated using Eq. 6-1.

$$t = \frac{|\bar{x}_1 - \bar{x}_2|}{\sqrt{\frac{\sigma_1^2}{n_1} + \frac{\sigma_2^2}{n_2}}} \qquad \text{Eq. 6-1}$$

where $\bar{x}$ is the mean of each normal distribution, and *n* the degrees of freedom of the system under study, in this case the number of STM experiments per dataset minus one. Once *t* is calculated for the pair of normal distributions under study, its value is compared against tabulated values of *t* for the total number of degrees of freedom ($n_1 + n_2$) and a given level of significance (typically 95%). If the tabulated value of *t* exceeds that of the calculated for the system under study, then both distributions can be treated as identical with a 95% confidence.

A summary of the *t*-test for compounds **43** *(n = 2)* and **45** *(n = 4)* employing both STM-BJ and *I*(*s*) methods are shown in Table 6-2. A value of $t = 0.18$ and $t = 0.25$ was obtained from the analysis of the pair of normal distributions obtained by STM-BJ and *I*(*s*). In both cases, the calculated *t* is smaller than that of the tabulated value ($t \sim 1.97$) for a 95% significance level and over 250 degrees of freedom. According to these results, it can be stated with a 95% confidence that there is no statistically significant difference between the conductance values obtained for **43** *(n = 2)* and **45** *(n = 4)*. Hence, despite the small differences in the conductance means, the distance dependence in this series of compounds was found to be statistically insignificant for both measuring methods.

**Table 6-2.** *Student's t-test for compounds **43** and **45** obtained using I(s) and STM-BJ.*

| | **STM-BJ** | | ***I*(*s*)** | |
|---|---|---|---|---|
| | **43** *(n = 2)* | **45** *(n = 4)* | **43** *(n = 2)* | **45** *(n = 4)* |
| $\bar{x}$ | 0.73 | 0.70 | 0.72 | 0.68 |
| $\sigma$ | 0.37 | 0.33 | 0.19 | 0.25 |
| Number of experiments | 152 | 151 | 125 | 131 |
| Calculated *t (Eq. 6-1)* | 0.18 | | 0.25 | |
| Tabulated *t* (95%) | ~1.97 | | | |

In the light of these results, a more complete set of studies was designed to help with the identification of the molecular length influence in the junction conductance. The new studies were performed in parallel by our colleagues at the University of Liverpool and Bristol in order cross-check the results. Furthermore, compound **46** *(n = 5)* was prepared by Ms. Marie-Christine Oerthel (PhD candidate, Bryce and Low groups) and included in the new studies in order to have an extra dataset to explore the attenuation factor $\beta$ for trimethylsilyl terminated polyynes. In this occasion, the thermally annealed gold substrates were immersed in solutions (~$10^{-3}$ M) of the targeted molecule in dry 1,2,4-trichlorobenzene (TCB) for 1 minute. After the incubation time, the sample was rinsed

thoroughly with EtOH and blown dry in a stream of Ar gas. Once the substrate is placed on the STM holder, a few drops of TCB are placed on the substrate in order to perform the measurements in solution. In addition, an atmospheric chamber is fitted and purged with Ar gas for an hour before the measurements start. A brief summary of the ongoing *I*(*s*) studies obtained by the Liverpool group are shown in Figure 6-2. When compared with the conductance values obtained from the early *I*(*s*) studies ~ $0.7 \cdot 10^{-4}$ $G_0$, a slightly higher conductance was observed for every compound of the series ~ $1 \cdot 10^{-4}$ $G_0$. This slight shift to higher conductance values can be attributed to the different experimental conditions employed. Importantly, the conductance value seems almost independent from the molecular length consistent with the previous studies (Table 6-3).

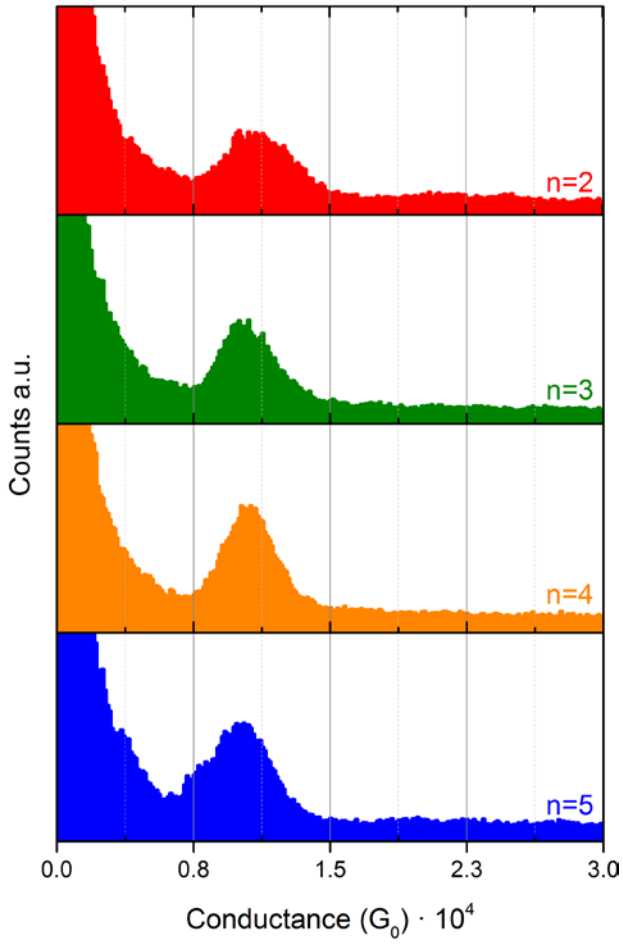


**Figure 6-2.** Preliminary c*onductance studies of compounds **43 - 46** obtained by the Liverpool group employing the I(s) method in solution (TCB).*

In a parallel way to the previous statistical analysis, a *t*-test was performed for the conductance histograms of the shortest **43** *(n = 2)* and longest **46** *(n = 5)* compounds of the series. In this case, the large number of experiments employed in the construction of the conductance histograms of **43** (342) and **46** (327) led to sharp conductance peaks following a narrow normal distribution. In this case, the value of *t* calculated employing Eq. 6-1 ($t$ = 2.30) was found to exceed the tabulated *t* for a 95% significance ($t$ = 1.96). Therefore, for these studies, molecular length was found to play a statistically significant role with a calculated attenuation factor $\beta \sim 0.12$ nm$^{-1}$ of the same order of magnitude of that reported for pyridine terminated polyynes ($\beta = 0.6 \pm 0.3$ nm$^{-1}$).[14]

**Table 6-3.** *Summary of the on-going conductance studies of compounds **43 - 46** obtained by the I(s) method in TCB.*

| **Compound** | **Molecular length** *Si···Si d(nm)** | **Number of experiments** | **Conductance ($G_0$) · $10^4$** *I(s) method in TCB* |
|---|---|---|---|
| **43** *(n = 2)* | ~ 0.74 | 342 | 1.09 ± 0.38 |
| **44** *(n = 3)* | ~ 0.98 | 401 | 1.03 ± 0.28 |
| **45** *(n = 4)* | ~ 1.22 | 419 | 1.05 ± 0.28 |
| **46** *(n = 5)* | ~ 1.46 | 327 | 0.99 ± 0.37 |

**MM2 energy minimizations*

In addition to these STM *I*(*s*) studies in-solution, the electrical performance of compounds **43 - 46** are being studied by our collaborators at the University of Bristol, employing the STM-BJ method in order to verify the low $\beta$ value obtained by the *I*(*s*) technique.

## 6.4. Conclusions

A series of polyynes **43** – **46** *(n = 2 - 5)* were prepared and their electrical performance studied by means of STM-BJ and *I*(*s*). The recently introduced −C≡CSiMe$_3$ moiety was employed to generate contacts on gold substrates. The presence of a single

conductance value is consistent with the previously observed ability of the −C≡CSiMe$_3$ group to form A-type only contacts. The very low distance dependence observed in the early studies, was found to be statistically insignificant leading to a redesign of the studies in order to clarify the role of molecular length in the junction conductance. Preliminary studies from our collaborators at the University of Liverpool, involving a larger number of STM experiments, confirmed the previously reported weak distance dependence in polyynes with a calculated attenuation factor $\beta \sim 0.12$ nm$^{-1}$. Finally, on-going STM-BJ experiments are being performed on compounds **43 - 46** at the Univeristy of Bristol in order to confirm the low $\beta$ when the BJ technique is employed.

## 6.5. Experimental

### *6.5.1. General conditions*

General conditions were reported in Chapter 2. Compounds **45** and **46** were synthesized by Marie-Christine Oerthel in the University of Durham. Other reagents were purchased commercially and used as received.

### *6.5.2. Synthesis and characterization*

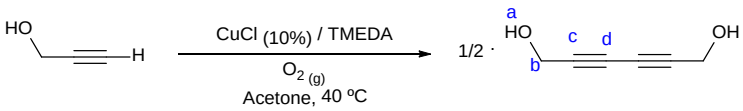


**Preparation of HOH$_2$CC≡CC≡CCH$_2$OH.**[18] A 250 mL Schlenk flask was charged with acetone (150 mL) and CuCl (5 g, 51 mmol) and purged with nitrogen. To that, freshly distilled N, N, N', N'-tetramethylethylenediamine (TMEDA) (2.5 mL, 16.6 mmol) was added and the mixture stirred at room temperature for 30 minutes. After that time, the mixture was allowed to settle leaving a clear deep-blue solution of the catalyst used in the coupling reaction. A 1 L four-necked flask, equipped with a reflux condenser, a gas

sintered inlet, a thermometer and a rubber septum was charged with acetone (300 mL) and prop-2-yn-1-ol (29 mL, 500 mmol). The mixture was stirred and a stream of oxygen was passed through the solution. The blue supernatant solution containing the catalyst was added in 5 mL portions into the reaction vessel, during the addition, the flask was cooled occasionally to keep the temperature constant at 30 ºC. After three hours, the solvent was removed by evaporation and the residue extracted with hexane. The extract was washed with 3M HCl (150 mL) and the aqueous phase extracted with EtOAc (2 × 200 mL). The combined organic phases were washed with brine (200 mL), dried over $MgSO_4$ and taken to dryness to yield the pure product as a light brown solid. Yield 21.6 g, 196 mmol, 78%. $^{1}H$ NMR (400 MHz, Acetone-$d_6$) δ 4.46 (s *br*, 2H, *a*), 4.26 (s, 4H, *b*). $^{13}C^{19}$ NMR (101 MHz, Acetone-$d_6$) δ 79.4, 69.0 (c/d), 50.8 (*b*). IR (*nujol*) $cm^{-1}$: 3500-3100 (br. s) *v*(OH); *not observed v*(C≡C).

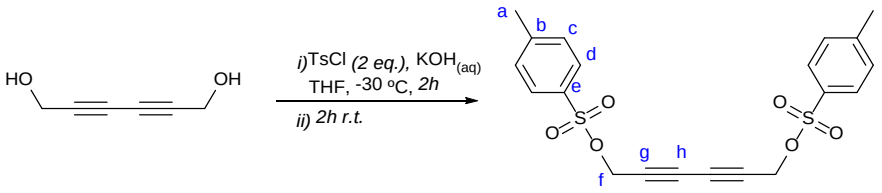


**Preparation of $TsOH_2CC{\equiv}CC{\equiv}CCH_2OTs$.**[20] To a 500 mL flask charged with a solution of $HOH_2CC{\equiv}CC{\equiv}CCH_2OH$ (11 g, 100 mmol) in THF (250 mL) at -30 ºC, 4-toluenesulfonyl chloride (TsCl) (42 g, 220 mmol) was added and the suspension stirred at that temperature for 15 minutes. To the cooled reaction mixture, a KOH (13g, 231 mmol) aqueous solution (40 mL) was added in small portions. The orange mixture evolved to a deep red suspension while stirring at -30 ºC for 2 hours. The reaction was stirred at room temperature for another 2 hours and then poured into an ice-water mixture yielding a light yellow precipitate. As the precipitate was filtered under reduced pressure the yellow colour turned into pink. The precipitate was washed thoroughly with MeOH and dried in air. The

pure product was obtained as a pink powder. Yield 35 g, 84 mmol, 84%. $^{1}$H NMR (400 MHz, $CDCl_3$) δ 7.77 (d, *J* = 8.3 Hz, 4H, *c*), 7.35 (d, *J* = 7.9 Hz, 4H, *d*), 4.72 (s, 4H, *f*), 2.45 (s, 6H, *a*). $^{13}$C{$^{1}$H} NMR (101 MHz, $CDCl_3$) δ 145.7 (*e*), 132.7 (*b*), 130.1, 128.2 (*c/d*), 72.4, 72.0 (*g/h*), 57.6 (*f*), 21.8 (*a*). IR (*nujol*) cm$^{-1}$: 2167 *v*(C≡C).

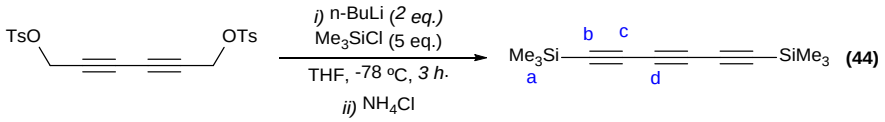


**Preparation of 44 (*n* = *3*).**[21] To a three necked 500 mL flask charged with a solution of $TsOH_2CC{\equiv}CC{\equiv}CCH_2OTs$ (15 g, 36 mmol) in dry degassed THF (250 mL) at -78 ºC, n-butyllithium (n-BuLi) 1.5 M in hexane (80 mL, 120 mmol) was added drop wise for one hour. After three hours stirring at -78 ºC the brown suspension was allowed to warm to -20 ºC before the addition of an aqueous saturated solution of $NH_4Cl$ (200 mL). The mixture was poured into a separation funnel and the red organic phase collected, washed with brine (1×150mL) and dried over $MgSO_4$. The clear red solution was then taken to dryness and purified by silica gel column chromatography using hexane as eluent. The final product was obtained as an oil that crystallizes on standing after solvent evaporation of the first yellow fraction. High purity crystals of **44** were obtained after several re-crystallizations of the compound from saturated hexane solutions. Yield 3.9 g, 17.8 mmol, 50%. $^{1}$H NMR (400 MHz, $CDCl_3$) δ 0.20 (s, 9H, *a*). $^{13}$C{$^{1}$H} NMR (101 MHz, $CDCl_3$) δ 88.1, 87.5 (*b/c*), 62.0 (d), -0.4 (*a*). IR (*nujol*) cm$^{-1}$: 2158 (m), 2112 (w) *v*(C≡C).

## 6.6. References


1. (a) Mayor, M.; von Hänisch, C.; Weber, H. B.; Reichert, J.; Beckmann, D., *Angew. Chem. Int. Ed.*, **2002**, *41*, 1183-1186; (b) Liu, K.; Wang, X.; Wang, F., *ACS Nano*, **2008**, *2*, 2315-2323; (c) Salomon, A.; Cahen, D.; Lindsay, S.; Tomfohr, J.; Engelkes, V. B.; Frisbie, C. D., *Adv. Mater.*, **2003**, *15*, 1881-1890.
2. (a) Cheng, Z. L.; Skouta, R.; H., V.; Widawsky, J. R.; Schneebeli, S.; Chen, W.; Hybertsen, M. S.; Breslow, R.; Venkataraman, L., *Nat. Nano*, **2011**, *6*, 353-357; (b) Su, T. A.; Widawsky, J. R.; Li, H.; Klausen, R. S.; Leighton, J. L.; Steigerwald, M. L.; Venkataraman, L.; Nuckolls, C., *J. Am. Chem. Soc.*, **2013**, *135*, 18331-18334; (c) Frei, M.; Aradhya, S. V.; Hybertsen, M. S.; Venkataraman, L., *J. Am. Chem. Soc.*, **2012**, *134*, 4003-4006; (d) Chen, F.; Li, X.; Hihath, J.; Huang, Z.; Tao, N., *J. Am. Chem. Soc.*, **2006**, *128*, 15874-15881; (e) Hong, S.; Reifenberger, R.; Tian, W.; Datta, S.; Henderson, J. I.; Kubiak, C. P., *Superlattices Microstruct.*, **2000**, *28*, 289-303; (f) Ke, S.-H.; Baranger, H. U.; Yang, W., *J. Am. Chem. Soc.*, **2004**, *126*, 15897-15904.
3. (a) Li, Z.; Han, B.; Meszaros, G.; Pobelov, I.; Wandlowski, T.; Blaszczyk, A.; Mayor, M., *Faraday Discuss.*, **2006**, *131*, 121-143; (b) Quinn, J. R.; Foss, F. W.; Venkataraman, L.; Breslow, R., *J. Am. Chem. Soc.*, **2007**, *129*, 12376-12377.
4. Ward, M. D., *Chem. Soc. Rev.*, **1995**, *24*, 121-134.
5. Rampi, M. A.; Whitesides, G. M., *Chem. Phys.*, **2002**, *281*, 373-391.
6. (a) He, J.; Chen, F.; Li, J.; Sankey, O. F.; Terazono, Y.; Herrero, C.; Gust, D.; Moore, T. A.; Moore, A. L.; Lindsay, S. M., *J. Am. Chem. Soc.*, **2005**, *127*, 1384-1385; (b) Seferos, D. S.; Trammell, S. A.; Bazan, G. C.; Kushmerick, J. G., *Proc. Natl. Acad. Sci. U.S.A.*, **2005**, *102*, 8821-8825; (c) Reed, M. A.; Chen, J.; Rawlett, A. M.; Price, D. W.; Tour, J. M., *Appl. Phys. Lett.*, **2001**, *78*, 3735-3737; (d) Kaliginedi, V.; Moreno-García, P.; Valkenier, H.; Hong, W.; García-Suárez, V. M.; Buiter, P.; Otten, J. L. H.; Hummelen, J. C.; Lambert, C. J.; Wandlowski, T., *J. Am. Chem. Soc.*, **2012**, *134*, 5262-5275; (e) Martín, S.; Grace, I.; Bryce, M. R.; Wang, C.; Jitchati, R.; Batsanov, A. S.; Higgins, S. J.; Lambert, C. J.; Nichols, R. J., *J. Am. Chem. Soc.*, **2010**, *132*, 9157-9164; (f) Haiss, W.; Wang, C.; Grace, I.; Batsanov, A. S.; Schiffrin, D. J.; Higgins, S. J.; Bryce, M. R.; Lambert, C. J.; Nichols, R. J., *Nat. Mater.*, **2006**, *5*, 995-1002; (g) Martin, S.; Haiss, W.; Higgins, S. J.; Nichols, R. J., *Nano Lett.*, **2010**, *10*, 2019-2023; (h) Zhao, X.; Huang, C.; Gulcur, M.; Batsanov, A. S.; Baghernejad, M.; Hong, W.; Bryce, M. R.; Wandlowski, T., *Chem. Mater.*, **2013**, *25*, 4340-4347; (i) Hong, W.; Li, H.; Liu, S.-X.; Fu, Y.; Li, J.; Kaliginedi, V.; Decurtins, S.; Wandlowski, T., *J. Am. Chem. Soc.*, **2012**, *134*, 19425-19431.
7. Kushmerick, J. G.; Holt, D. B.; Pollack, S. K.; Ratner, M. A.; Yang, J. C.; Schull, T. L.; Naciri, J.; Moore, M. H.; Shashidhar, R., *J. Am. Chem. Soc.*, **2002**, *124*, 10654-10655.
8. Liu, M.; Artyukhov, V. I.; Lee, H.; Xu, F.; Yakobson, B. I., *ACS Nano*, **2013**, *7*, 10075-10082.

9. (a) Szafert, S.; Gladysz, J. A., *Chem. Rev.*, **2003**, *103*, 4175-4206; (b) Szafert, S.; Gladysz, J. A., *Chem. Rev.*, **2006**, *106*, PR1-PR33.
10. (a) Taylor, J.; Brandbyge, M.; Stokbro, K., *Phys. Rev. B: Condens. Matter*, **2003**, *68*, 121101; (b) James, P. V.; Sudeep, P. K.; Suresh, C. H.; Thomas, K. G., *J. Phys. Chem. A*, **2006**, *110*, 4329-4337.
11. Crljen, Ž.; Baranović, G., *Phys. Rev. Lett.*, **2007**, *98*, 116801.
12. García-Suárez, V. M.; Lambert, C. J., *Nanotechnology*, **2008**, *19*, 455203.
13. Al-Backri, A.; Zólyomi, V.; Lambert, C. J., *eprint arXiv:1402.5812*, **2014**,
14. Wang, C.; Batsanov, A. S.; Bryce, M. R.; Martín, S.; Nichols, R. J.; Higgins, S. J.; García-Suárez, V. M.; Lambert, C. J., *J. Am. Chem. Soc.*, **2009**, *131*, 15647-15654.
15. (a) Liu, H.; Wang, N.; Zhao, J.; Guo, Y.; Yin, X.; Boey, F. Y. C.; Zhang, H., *ChemPhysChem*, **2008**, *9*, 1416-1424; (b) Newton, M. D.; Smalley, J. F., *Phys. Chem. Chem. Phys.*, **2007**, *9*, 555-572.
16. Moreno-García, P.; Gulcur, M.; Manrique, D. Z.; Pope, T.; Hong, W.; Kaliginedi, V.; Huang, C.; Batsanov, A. S.; Bryce, M. R.; Lambert, C.; Wandlowski, T., *J. Am. Chem. Soc.*, **2013**, *135*, 12228-12240.
17. Haiss, W.; Lackey, D.; Sass, J. K.; Besocke, K. H., *J. Chem. Phys*, **1991**, *95*, 2193-2196.
18. Jones, G. E.; Kendrick, D. A.; Holmes, A. B., 1,4-BIS(TRIMETHYLSILYL)BUTA-1,3-DIYNE. In *Organic Syntheses*, 1993; Vol. Coll. Vol. 8, p 63.
19. Berners-Price, S. J.; Ronconi, L.; Sadler, P. J., *Prog. Nucl. Magn. Reson. Spectrosc.*, **2006**, *49*, 65-98.
20. Dickschat, J. S.; Reichenbach, H.; Wagner-Döbler, I.; Schulz, S., *Eur. J. Org. Chem.*, **2005**, *2005*, 4141-4153.
21. Alberts, A. H., *Recl. Trav. Chim. Pays-Bas*, **1989**, *108*, 242-243.

# 7. CONCLUSIONS AND FUTURE PERSPECTIVES

The work detailed here embodies a multidisciplinary approach to some of the challenges that molecular electronics faces nowadays. Initially, the synthesis of conjugated oligo(phenylene-ethynylene)s (OPEs) has been reviewed in detail. Despite the synthetic difficulties encountered deriving from solubility issues, OPEs were found to be a good workhorse for molecular electronic studies as their modular synthesis allowed the systematic study of the linker's influence on the overall junction conductance. In that regard, a novel molecular linker, C≡CSiMe$_3$ was introduced and its electrical and mechanical properties benchmarked against literature known molecular anchoring groups *i.e.* NH$_2$, pyridine, SH. Despite the former presenting a lower conductance than that of the more traditional anchoring groups, the introduction of geometrical constraints to the junction formation may be of great relevance to improve the reproducibility of single molecule studies.

In addition to OPEs, polyynes also been prepared and studied as alternative molecular wire candidates with preliminary conductance studies showing a comparatively higher conductance than that of the OPEs, together with a remarkably low distance dependence showing the great potential of polyynes as highly conductive molecular wires.

The synthesis of bis(ethynyl) complexes *trans*-Ru(C≡CR)$_2$(dppe)$_2$ and unsymmetrically substituted derivatives *trans*-Ru(C≡CR$^1$)(C≡CR$^2$)(dppe)$_2$ has been reviewed in detail. Preliminary single molecule electrochemical STM studies performed on **3f** presented a transistor-like behaviour paving the way towards the design, development and integration of molecular transistors.

Furthermore, a detailed structural and spectroelectrochemical study of the *trans*-$Ru(C{\equiv}CR)_2(dppe)_2$ complexes, supported by TD-DFT calculations demonstrated the relationships between the underlying electronic transitions that are responsible for the NIR absorption band shape and the relative orientations of the metal fragment and arylethynyl moieties in the oxidized species, providing a very detailed insight into the charge transfer processes occurring at the molecular level.

In addition, two novel approaches to the formation of the top electrode on sandwich like metal|molecule|metal devices, based on the in-situ decomposition of gold complexes, were developed. Despite the process not yielding a smooth metallic film atop the molecular film, the formation of gold islands leading to defect-free molecular junctions was observed. Future work will be directed to the integration of a larger number of Au atoms in order to promote the formation of a smooth metallic electrode, and the integration of different metals such as Ag, Cu and Pt.

Finally, some of the main challenges deriving from the statistical treatment of the conductance (STM) and force (AFM) measurements were detailed and addressed with the development of Visual Basic (VBA) codes able to lighten the processing and analysis of the large datasets obtained.

To sum up, this work provides a wide view of the molecular electronics, from the initial design and preparation of the molecular wire candidates, to their reliable integration on molecular devices, in an attempt to provide a solid platform from which to ultimately lead to the improved design of the next generation of molecular devices.

# APPENDIX A. STM DATA ANALYSIS

## A.1. Introduction

As a result of many efforts made over many years, the reliable preparation and electrical measurements of single molecule junctions is now possible. However, the data generated by the different STM, AFM or MCBJ methods still require a sophisticated numerical treatment in order to extract the electrical response in a meaningful way. For example, during single molecule studies using the *I*(*s*) method employed in this thesis, the current flow (nA) between the two electrodes (STM tip and substrate) is measured as a function of electrode separation in the absence of molecular candidates in the first instance (Figure A-1). An exponential current decay is typically registered in these blank experiments deriving from the exponential relationship of the tunnelling regime with distance. However, when these experiments are conducted in the presence of the molecules under study, the molecules can spontaneously bridge the gap between the two electrodes leading to junction formation to the metallic tip. The presence of the molecule in the newly formed metal|molecule|metal junction provides a wire-like connection between the electrodes and a constant current plateau is registered in the current decay trace at a particular electrode separation. As the STM tip continues to be withdrawn the junction eventually ruptures and current-distance response falls back to the exponential decay profile. The point of rupture, referred to as the break-off distance, often but not necessarily corresponds to the molecular length. Despite the plateau being considered a direct measurement of the molecular conductance, in order to acquire a statistically relevant dataset the junction formation and rupture process is repeated thousands of times. To facilitate the analysis of the large data sets generated, the series of electrical current traces are typically plotted as conductance histograms. Electrical conductance *G* (nS) is defined

as the inverse of resistance (hence $G = 1/R = I/V$) and gives an indication of the "ease" with which electrical current flows through a material. A conductance histogram is built by binning the raw electrical current traces into discrete divisions of $I$ (nA) and dividing the electrical current axis by the experimental bias. Typically, the conductance results are further converted in terms of the quantum of conductance $G_0 = 2e^2/h = 77480$ nS. In the histograms built this way, peaks for the most frequently occurring conductance values can be seen. In addition, a clear peak at $G_0$ conductance can be seen for the BJ techniques as a direct proof of the formation of a point contact.

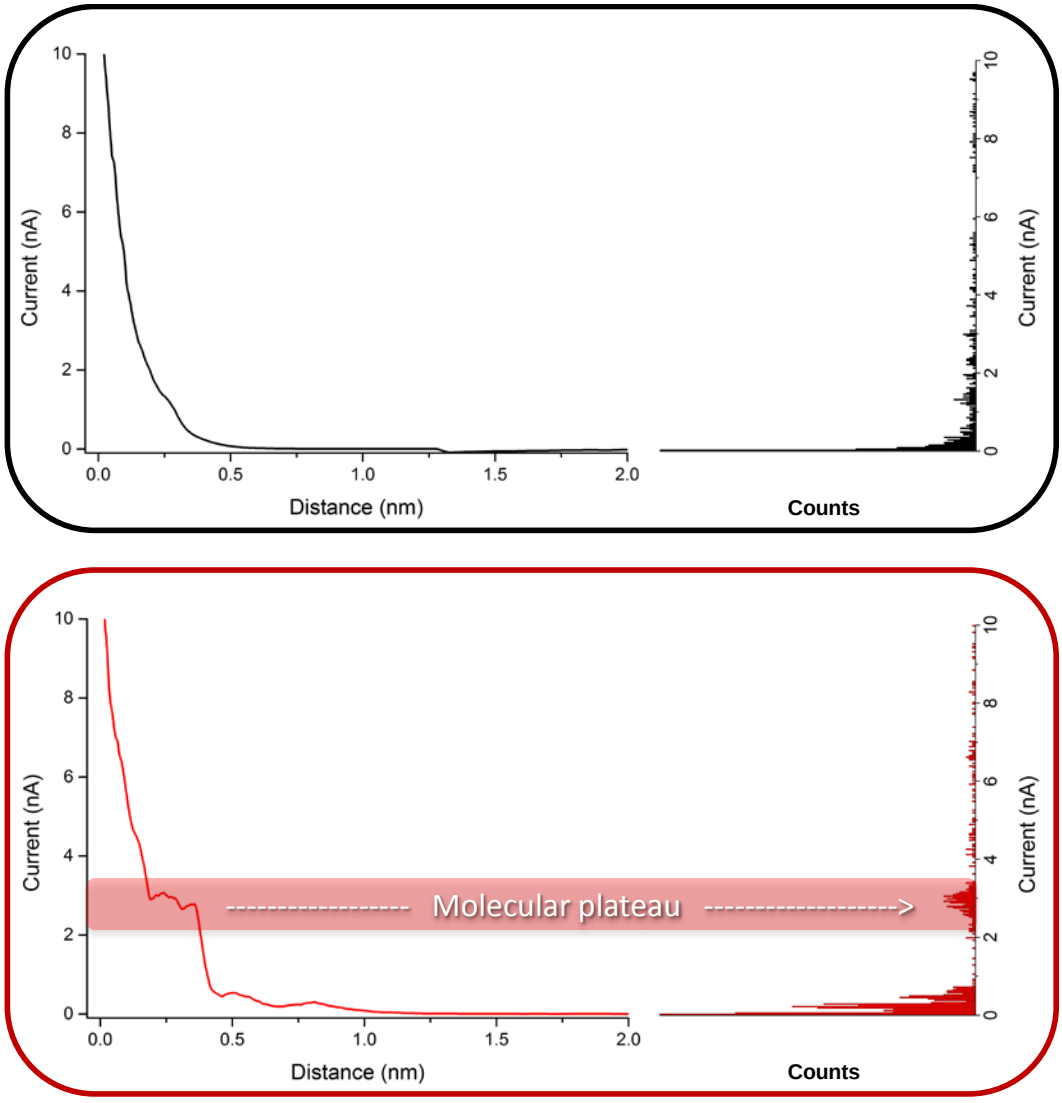


**Figure A-1.** *STM traces and histograms associated: clean exponential decay (black) and constant current plateaus corresponding to a molecule bridging the electrodes (red).*

Although the use of conductance histograms is very common, no information about the junction geometry can be extracted from them.[1] In order to obtain further insight into the nature of the molecular junction, 2D distance-conductance binning is becoming established as an alternative method of analysis.[2] Despite its additional complexity, 2D mapping reveals important information about the junction formation as well as its electrical properties (Figure A-2).

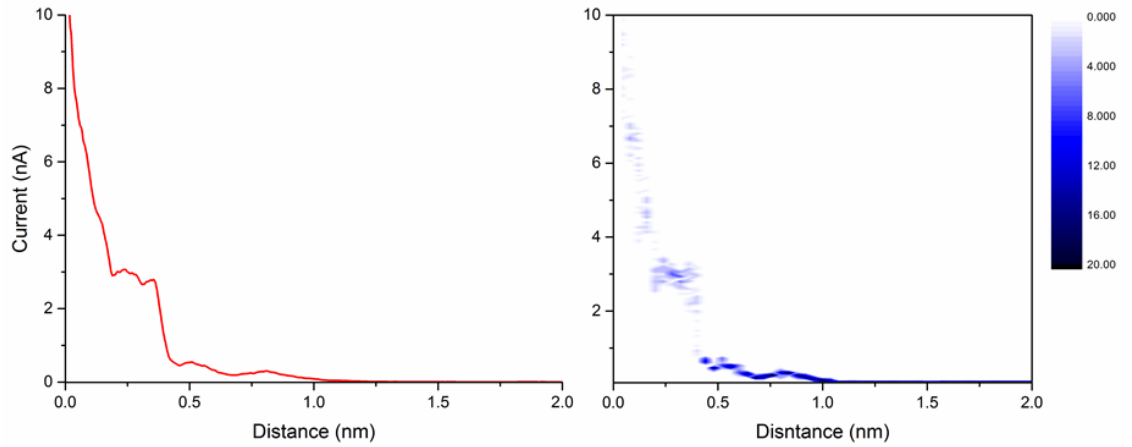


**Figure A-2.** *STM I(s) trace (left) and corresponding 2D binning plot (right).*

## A.2. Calibration of the BJ data for 2D plotting

Despite the relevant information that can be extracted from the 2D conductance-distance mapping, the plotting of data in a useful form can sometimes be a challenge. Electrical current traces obtained by the *I*(*s*) STM method have a common origin in both axis (current and distance) that facilitates 2D mapping. However, in order to build the 2D maps from the raw data obtained from other methods such as STM-BJ or MCBJ may require preconditioning as the electrode shape is changed in every experiment leading to a random distribution in the tip-substrate separation. Therefore, in contrast to data generated from *I*(*s*) studies, the break-off distance in BJ methods may differ by several nanometers on a run to run basis as a result of the repetitive electrode reforming rendering the 2D map

useless (Figure A-3, *top*). Because data sets can contain over thousands of conductance traces, manual calibration of the traces becomes unfeasible. In order to facilitate this task an open code computer program was written. The code (*vide infra*) is able to read through the collected traces, distinguish the electrode breaking point of each trace and reference the data accordingly. In addition, the calibrated traces are automatically transformed to conductance, and the output data arranged into columns to allow direct plotting. The program is able to run through a dataset of 100 traces in a few seconds allowing immediate data analysis. Once the calibration process is finished, a 2D map can be built from the BJ data allowing further analysis of the junction formation process (Figure A-3, *bottom*).

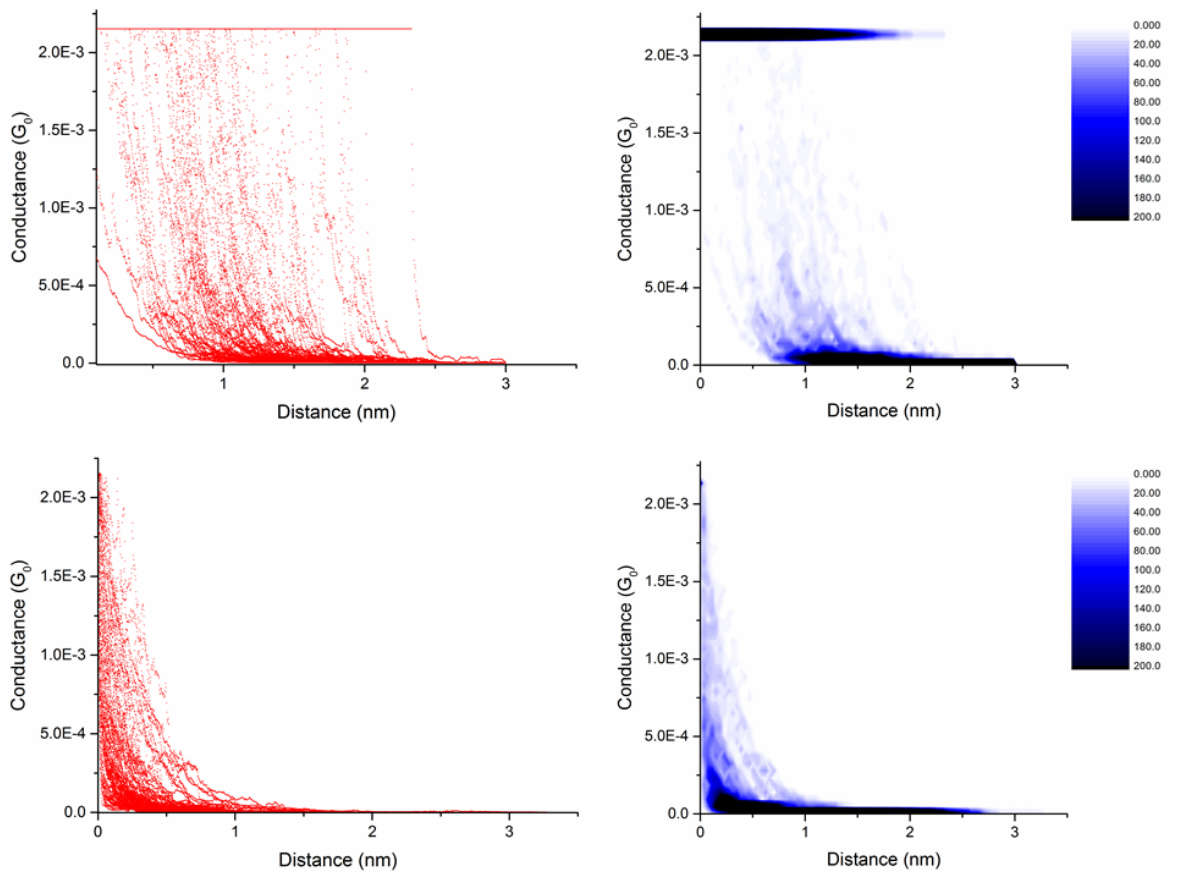


**Figure A-3.** *Effect of the data calibration program developed on 100 BJ traces 2D plotting (right): raw data from the STM (top) and after distance calibration (bottom).*

As an example of the importance of this process, both 2D maps in Figure A-3 were built from the same raw data (*top*) before and (*bottom*) after calibration. Thanks to the calibration program, a distance-conductance map can be built allowing for important information about the junction formation in correlation with its electrical properties. At this point it is important to note that, despite the clear scattering of the raw BJ data along the electrode displacement axis in the raw data (Figure A-3, *top*), this has no influence on the preparation of conductance histograms. The fact that both data sets (*top*) and (*bottom*), would display the same electrical fingerprint in a conductance histogram is a good proof of the importance of the 2D plotting for single molecule studies. Importantly, the calibrated 2D map also allows for easy detection of experimental errors and datasets with exceptional inconsistency. The ability to analyze these results in real time also allows for corrections to be made in the experimental setup when required.

## A.3. VBA code

The BJ calibration program was written in Visual Basic language for Microsoft Excel 2010. The code can be run on PC versions of Microsoft Excel 2007 or later. The code is provided with the electronic content associated with this thesis. The reader is encouraged to copy, modify and share this code for academic and educational purposes only.

## A.4. References


1. (a) Williams, P. D.; Reuter, M. G., *J. Phys. Chem. C*, **2013**, *117*, 5937-5942; (b) Natelson, D., *ACS Nano*, **2012**, *6*, 2871-2876.
2. Makk, P.; Tomaszewski, D.; Martinek, J.; Balogh, Z.; Csonka, S.; Wawrzyniak, M.; Frei, M.; Venkataraman, L.; Halbritter, A., *ACS Nano*, **2012**, *6*, 3411-3423.

# APPENDIX B. NANOFABRICATION OF MOLECULAR MATERIALS AND INELASTIC TUNNELLING INDUCED FLUORESCENCE

## B.1. Introduction

Despite the many advances in scanning probe microscopies, one of the main challenges towards the development of the molecular electronics field is the controlled assembly of molecules into more complex architectures with the required function (*see* Chapter 1). In this context, the ability of molecules to self-assemble on surfaces into complex structures by supramolecular interactions (hydrogen bonding, π-π stacking, dipolar and van der Waals) has attracted considerable attention in the last decade.[1] In contrast to intermolecular interactions, a covalent bond offers a great chemical stability and an efficient charge transport.[2] Although the generation of such intermolecular interactions can be done employing a scanning tunnelling microscope (STM), a fabrication procedure where each molecule needs to be addressed individually is clearly impractical for the construction of systems involving a large number of molecules.[3] An alternative to this tedious step-wise approach was first introduced by Grill *et al.*[4] In their pioneering work, they demonstrated the formation of covalently bound porphyrin based structures on a gold surface, by thermal activation and subsequent reaction of bromide substituted porphyrin building blocks.

In addition to these recent nanofabrication developments, electron transport studies at the nanoscale involving a few atoms or molecules, have recently revealed unusual junction properties which may be of great relevance in the fabrication of electronic devices. The generation of light induced by inelastic electron tunnelling was first reported by Lambe and McCarthy for metal-insulator-metal junctions.[5] When a voltage was applied to such junctions, visible light was seen to emanate from the device that ranged from red to

orange to blue upon increasing voltage. This process was explained in terms of inelastic tunnelling excitation of optically coupled surface plasmon modes in the junction. An electron tunnelling between metal electrodes, can excite an optically coupled surface plasmon mode with frequency ν provided that the applied voltage $|eV| \geq h\nu$. This quantum condition can be experimentally observed as a sharp cutoff at $|eV|$ on the fluorescence spectra of the STM junction. The experimentally observed photon efficiency of this process is of the order of $10^{-4}$ photons per electron.[6] When a molecule is placed bridging the tip-substrate gap intramolecular photon emission can be observed.[7] Amongst the most relevant STM single molecule fluorescence studies present in the literature are: $C_{60}$ on Au (110);[8] Cu phthalocyanine on Au (111);[9] and alkanethiols on Au (111).[10] However, no direct evidence of molecular fluorescence was encountered in any of these studies due to the strong emission observed from the metallic substrates. In addition, the non-radiative energy transfer from an excited molecular state to the metal substrate is often an efficient decay process.[11] Therefore, the nature of the emission process at molecular junctions remains unknown. In order to study further the single molecule luminescence in STM molecular junction experiments OPEs **47 - 50** were synthesized (Chart B-1, *see experimental Chapter*). In collaboration with Prof. Jose Ignacio Pascual and Dr. Jincheng Li at the Free University of Berlin, and Dr Luz Marina Ballesteros and Dr Pilar Cea at the University of Zaragoza, the halogen substituted **50** was thermally coupled *in-situ* to fabricate more complex molecular structures, a process of nanofabrication deserving of further attention in its own right. The light emission from those extended 1D structures when addressed with the STM tip was recorded, and analysed within the framework of inelastic tunnelling induced fluorescence.

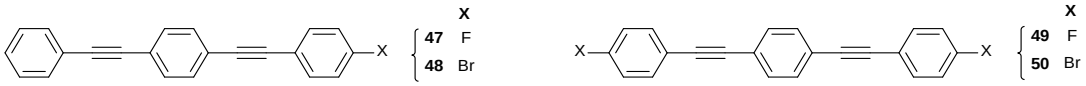


**Chart B-1.** *Halogen-terminated OPEs **47 – 50**.*

## B.2. Sample preparation

Amongst the halogenated OPEs tested **47**− **50**, the dibromo substituted derivative **50** was chosen for these experiments because of its higher reactivity towards thermal coupling and its ability to generate extended linear structures. The thermal coupling of **50** was conducted in a low-temperature STM (LT-STM) under ultrahigh vacuum conditions (UHV). The working temperature was 4.8 K and the substrate of choice was a single crystal of Ag (111). Compound **50** was deposited on the substrate by sublimation. The optimum sublimation temperature of **50** was obtained from a series of QCM experiments performed in UHV conditions, in which a significant shift in the oscillator frequency was obtained at temperatures ~160 ºC. Hence, the sublimation of **50** on the Ag substrate was performed with a Knudsen cell at temperatures ranging 160-170 ºC under UHV conditions. After the deposition process was completed, the substrate was in some cases subject of a thermal treatment and then transferred into the STM chamber and cooled down to working temperatures (4.8 K). Table B-1 presents a summary of the molecular structures resulting from the different sublimation and thermal annealing conditions employed

**Table B-1.** *Sample preparation conditions and STM imaging of the resulting product.*

| | $T_{subl}$ (ºC) | $t_{subl}$ (min) | $T_{subs}$ (ºC) | $P$ (mbar) | $T_{ann}$ (ºC) | $t_{ann}$ (min) | RESULTS |
|---|---|---|---|---|---|---|---|
| **A** | 168 | 3 | 15 | $1.5\cdot10^{-9}$ | --- | --- | *Complete coverage* |
| **B** | 160 | 20 | 8 | $1.4\cdot10^{-9}$ | --- | --- | *Short chains / easy Br dissociation* |
| **C** | 160 | 20 | 6 | $1.9\cdot10^{-9}$ | --- | --- | *2D honeycomb network* |
| **D** | | | | | 142 | Flash | *Long chain grid* |
| **E** | 167 | 5 | 13 | $1.5\cdot10^{-9}$ | --- | --- | *Molecular network* |
| **F** | 170 | 5 | 5 | $7.0\cdot10^{-10}$ | --- | --- | *2D honeycomb network* |
| **G** | | | | | 27 | Flash | *Long chain and 2D networks* |
| **H** | | | | | 125 | Flash | *Long chain / no Br dissociation* |
| **I** | 162 | 20 | 8 | $1.1\cdot10^{-9}$ | --- | --- | *Complete coverage* |
| **J** | 162 | 3 | 5 | $9.9\cdot10^{-10}$ | 52 | Flash | *Long chain / easy Br dissociation* |
| **K** | 163 | 3 | 7 | $1.7\cdot10^{-9}$ | | | *Long chain / easy Br dissociation* |
| **L** | 162 | 3 | 6 | $1.2\cdot10^{-9}$ | | | *Longest chain / easy Br dissociation* |

*subl = sublimation, subs = substrate, P = chamber pressure, ann = annealing.*

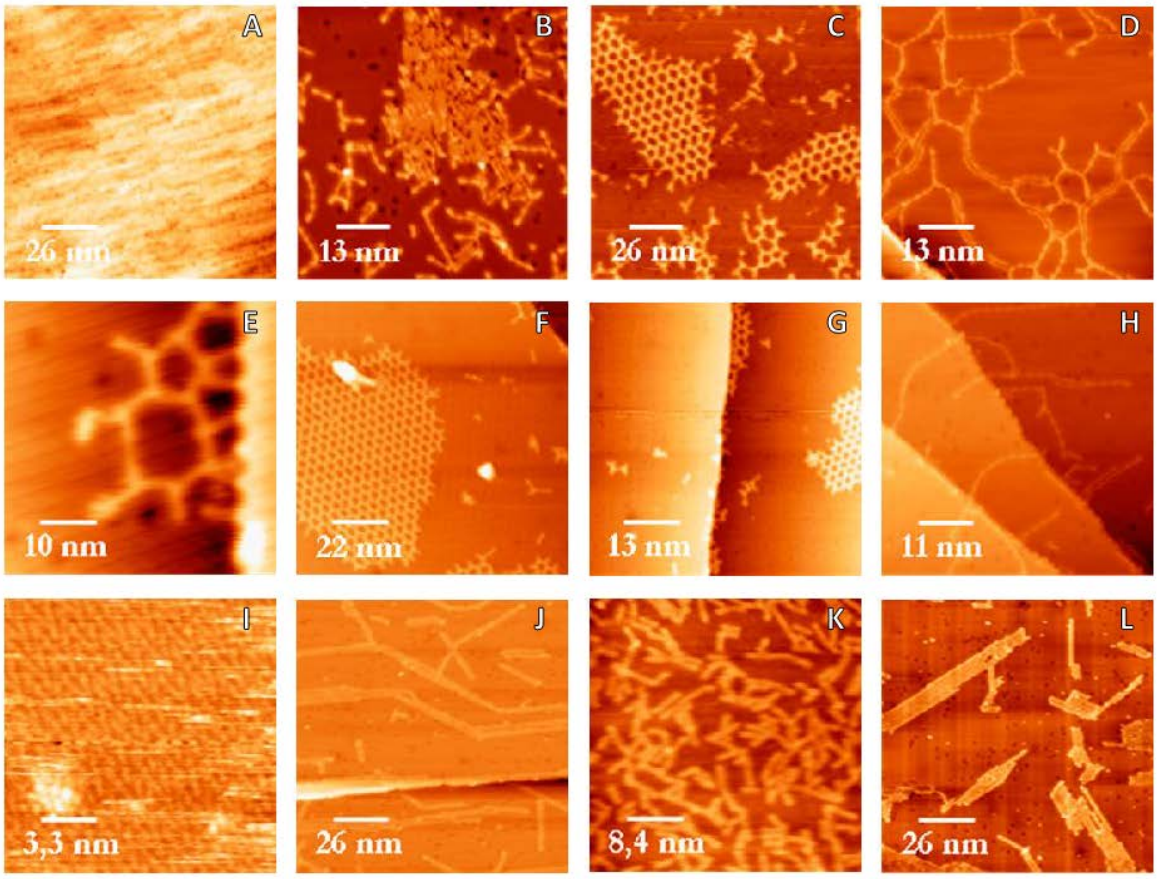


### B.3. Bromide dissociation

Molecular bond dissociation triggered by tunnelling electrons has been previously reported and represents a powerful tool towards the manipulation of matter at the molecular level.[12] In this work, the weaker C−Br bonds in OPE **50** are the more susceptible to cleavage, hence a bias pulse was applied at the molecular termini and the chemical process was monitored by observing changes on the tunnelling current. Typically, when a bias pulse of 2.2 V was applied on the Br termini, a marked drop of the tunnelling decay was found. In addition, Figure B-1 shows the STM imaging obtained before (*left*) and after (*right*) the bias pulse. Interestingly this process was not possible for samples prepared after a thermal annealing at temperatures over 55 ºC (Table B-1, *entries D, H and I*). These differences were ascribed to the formation of a strong bond between the molecular radical and the metallic surface generated upon thermal annealing.[4]

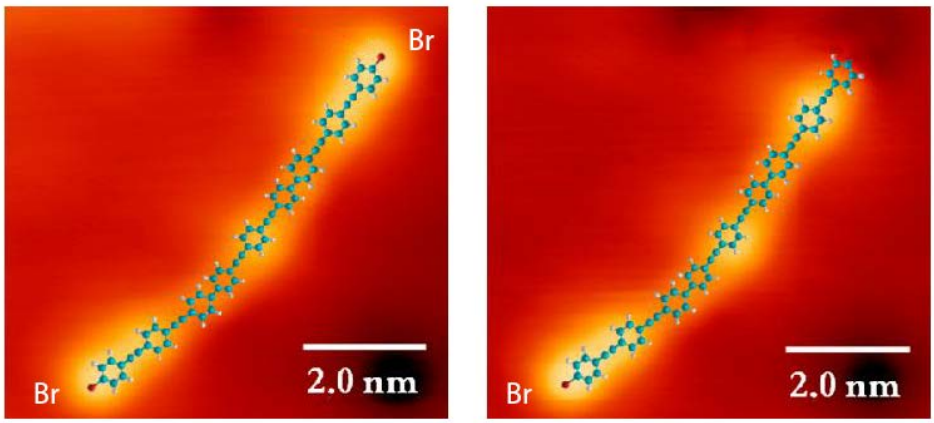


**Figure B-1.** *STM imaging sequence before (left) and after (right) applying a current pulse of 2.2 V over the terminal bromide atom of a molecular chain present on the substrate.*

## B.4. Molecular chain manipulation

As it was described in the introduction of this Chapter, in order to measure the photoelectrical properties of molecular junctions, the molecules need to be electronically decoupled from the metallic substrate to avoid quenching radiative transitions.[11] This has typically been achieved by placing a thin oxide layer on the metallic substrate, however even under these conditions the high intensity of the surface emission process dominates the fluorescence spectra. In this work, the electronic decoupling of the molecular chains was done by lifting the nanostructures from the Ag(111) substrate with the STM tip and placing them vertically while the light emission is monitored. In order to lift the molecules of interest, the molecular terminus was addressed with the STM tip (-0.1 V) and the STM tip retracted 13 Å while monitoring the tunnelling current decay.[13] A typical current-distance (*I*-*s*) profile registered for these experiments is shown in Figure B-2. The several current jumps observed along the exponential decay were assigned to different molecular conformations adopted upon lifting of the molecular chain.

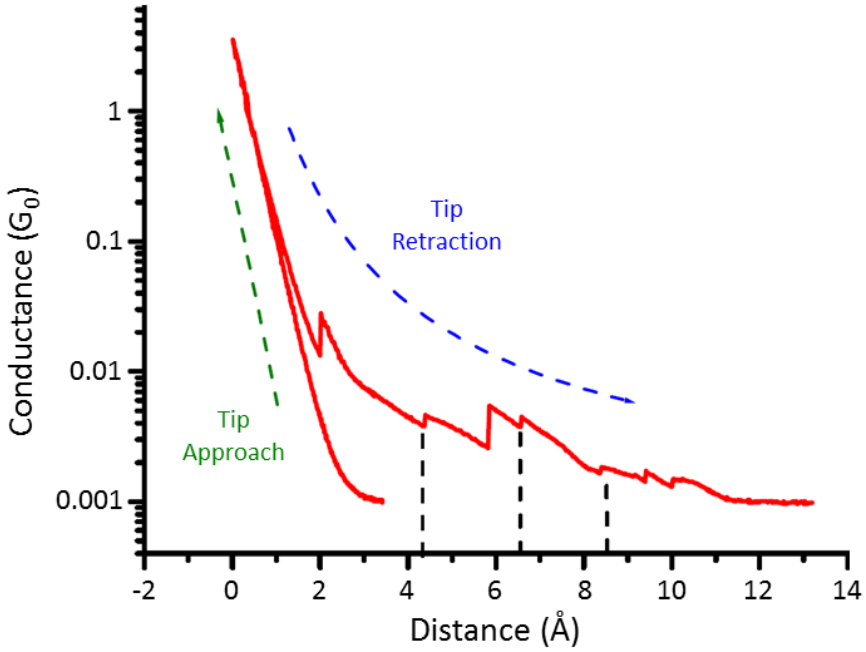


**Figure B-2.** *Typical tunnelling current dependence on tip-substrate gap, for experiments where molecular chains are lifted from the surface.*

## B.5. Scanning Tunnelling Spectroscopy (STS)

In order to probe the local density of electronic states (LDOS) several scanning tunnelling spectroscopy (STS) experiments were performed. The I-V curves of the naked substrate, a single molecule and a long polymer chain were collected while holding the STM tip at a fixed distance. For clarity, the dependence of the slope of the I-V curve (d*I*/d*V*) on the bias (± 2 V) is shown in Figure B-3. For the naked Ag (111) substrate a surface state can be observed at -0.65 mV characterized by a significant slope change in the STS spectra (*green*). On the other hand, the spectra recorded for a single molecule of **50** (*red*) presents two important features at 0.75 V and 1.5 V that were ascribed to the LUMO and LUMO +1 orbital levels. Interestingly, for the polymer chain only one feature was observed 1.5 V. These differences between the monomer and the coupled structures were ascribed to changes in the density of states upon polymerization.

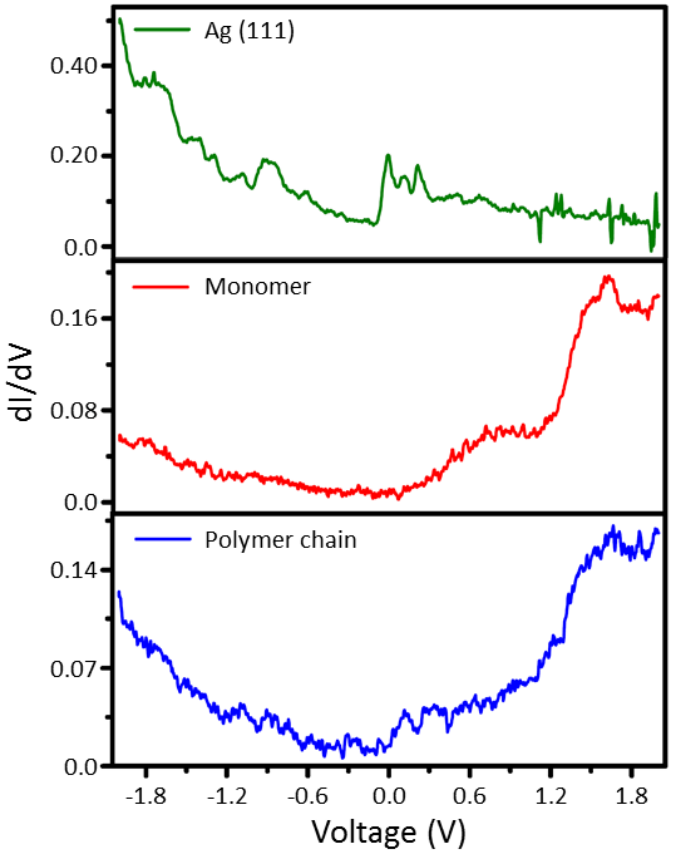


**Figure B-3.** *STS spectra (± 2 V) collected at constant height for the Ag(111) substrate (green), a monomer **50** (red) and a polymer chain (blue).*

## B.6. Tunnelling induced molecular junction luminescence

As described in the introduction of this Appendix, a tunnelling electron can excite an optically coupled surface plasmon mode with frequency ν provided that the applied voltage $|eV| \geq h\nu$. Hence, a sharp cutoff at $|eV|$ is expected on the fluorescence spectra of the STM junction for the naked substrate. Figure B-4 presents the fluorescence spectra of the Ag (111) observed at bias ranging 1.5 - 2.5 V employing a constant set point current of 6 nA and a detector exposure time of 4 minutes.

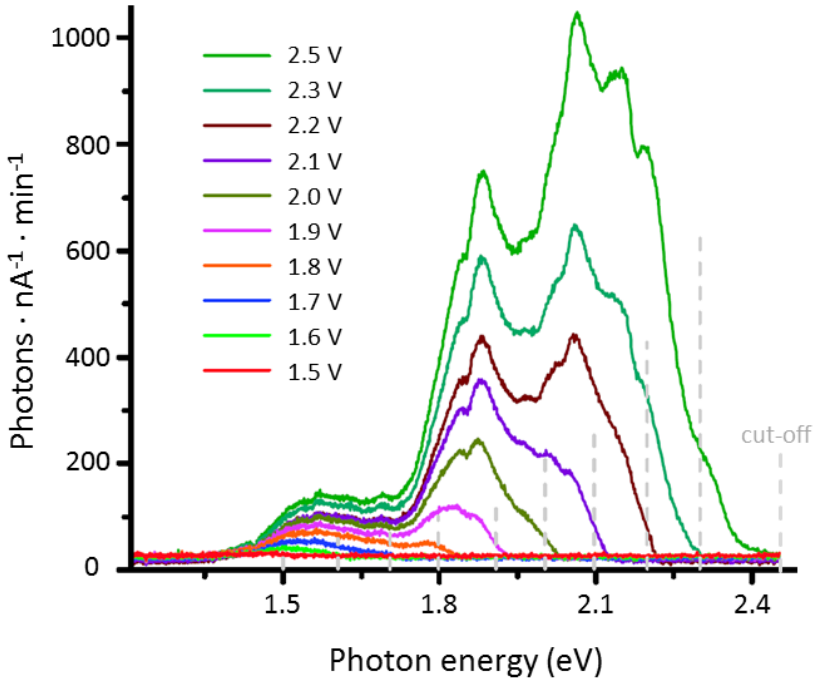


**Figure B-4.** *Tunnelling induced fluorescence spectra obtained for Ag(111) substrate at 1.5-2.5 V (6nA, 4 min).*

Tunnelling induced fluorescence on the single-molecule level offers a unique opportunity to study the optical properties of molecular adsorbates.[7a, 14] However, light emission from molecular junctions is only measurable for molecules electronically decoupled from the metallic surface. For molecules directly adsorbed on a metal surface, intramolecular radiative transitions are quenched and the surface plasmon emission dominates the optical spectra.[7a, 11] In order to electronically decouple the molecular chains of **50** from the Ag (111) substrate, the nanostructures were addressed with the STM tip and positioned vertically on the substrate. Figure B-5 shows the spectra recorded for a single molecular chain of **50** lifted 5.2 Å from the surface at bias ranging 1.6 - 2.0 V. The great similarity between the emission spectra of the molecular junction and that of the naked Ag (111) substrate (Figure B-4) is indicative of the dominance of the plasmon emission process. The competition between the two emissive processes makes the assessment of the molecular contribution to the fluorescence spectra very complicated.

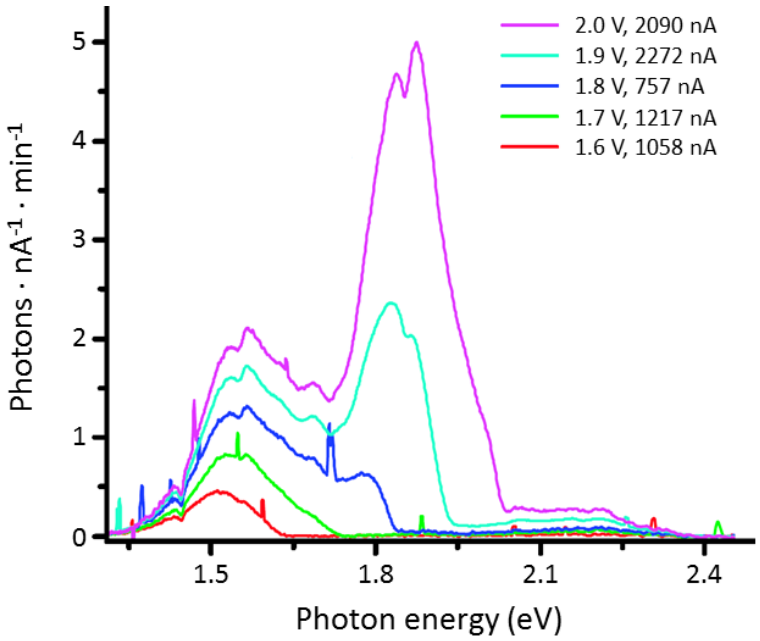


**Figure B-5.** *Emission spectra of **50** (polymer), lifted 5.2 Å at bias ranging 1.8 - 2.0 V.*

In order to facilitate a detailed comparison between the emission spectra recorded for a single molecule and that of the bare Ag(111) substrate, both spectra collected at 1.8 V were plotted on a logarithmic scale in Figure B-6. In both cases, the low energy region of the spectra *i.e* 1.2 - 1.8 *e*V presents a broad emission although for the molecular junction the emission process is clearly shifted to higher energies (*ca.* 1.7 *e*V).

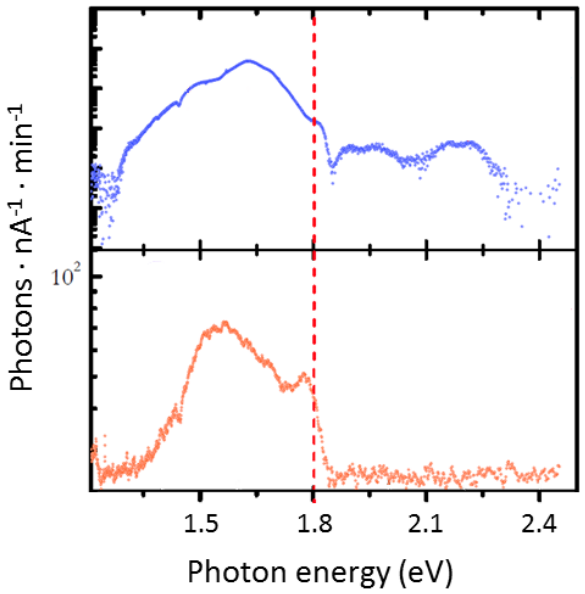


**Figure B-6.** *Logarithmic scale fluorescence spectra obtained from a single molecular chain of **50** (top) and that of the naked Ag(111) substrate (bottom).*

Remarkably, the emission spectra obtained for the molecular junction show two clear emission processes at energies higher than the quantum limit $h\nu \geq |eV|$. The "forbidden" emission of photons with energy exceeding the energy of the tunnelling electron has been previously reported for different metallic STM junctions.[15] Two mechanisms have been proposed in order to explain this possibility: a coherent Auger-like process where the energy of a tunnelling electron is transferred to another; and the decay of hot holes injected into the tip as a result of the tunnelling current passing through the lower quantum well state.[15] However, the role of the molecular bridge in this process is not clear. Ongoing research is focused in clarifying the molecular contribution to the emission spectra for energies under and over the cut-off energy.

## B.7. Conclusions

Dibromo substituted OPE **50** was deposited and thermally coupled under UHV conditions on a single crystal of Ag (111) to form extended 1D molecular structures. The molecular chains of **50** were characterized and manipulated employing an STM tip at low temperatures. The dissociation of the bromide termini of a linear molecular structure employing a current pulse was demonstrated. The tunnelling induced emission spectra of a single crystal of Ag (111) and a molecular chain of **50** were collected. Further studies are required to shed light on the molecular influence in the light emission process.

## B.8. Experimental

### *B.8.1. General conditions*

General experimental conditions were reported in Chapter 2. The synthesis of $BrC_6H_4C{\equiv}CSiMe_3$ (Chapter 2) and $HC{\equiv}CC_6H_4C{\equiv}CH$ (Chapter 5) were reported in previous experimental sections of this thesis. Other reagents were purchased commercially and used as received.

### *B.8.2. Synthesis and characterization*

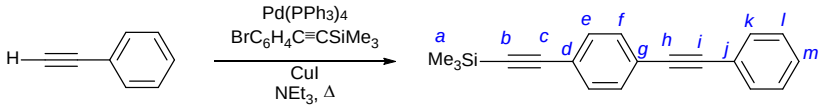


**Preparation of $Me_3SiC{\equiv}CC_6H_4C{\equiv}CC_6H_5$.**[16] In a 100 mL Schlenk flask, phenylacetylene (2.285 g, 22.37 mmol), $BrC_6H_4C{\equiv}CSiMe_3$ (4.693 g, 18.53 mmol), $Pd(PPh_3)_4$ (1.101 g, 0.953 mmol) and CuI (0.179 g, 0.940 mmol) were dissolved in $NEt_3$ (80 mL) and the resulting suspension was heated at reflux for 48 h. The reaction mixture was then taken to dryness and the residue purified by silica gel column chromatography using hexane as eluent. The product was obtained as a white powder upon solvent evaporation of the main fraction. Yield 4.23 g, 15.4 mmol, 83%. $^1$H NMR (400 MHz, $CDCl_3$) δ 7.55 – 7.49 (m, 2H, *e*), 7.45 (d, *J* = 3 Hz, 4H, *f*/*k*), 7.35 (m, 3H, *l*/*m*), 0.25 (s, 9H, *a*). $^{13}$C NMR (126 MHz, $CDCl_3$) δ 132.0, 131.7, 131.5, 128.6, 128.5 (*e*/*f*/*k*/*l*/*m*), 123.5, 123.1, 123.0 (*d*/*g*/*j*), 104.8, 96.3 (*b*/*c*), 91.5, 89.2 (*h*/*i*), 0.1 (*a*). $MS^+$ (ASAP) *m*/*z* (%): 274.10 (100, $[M]^+$).

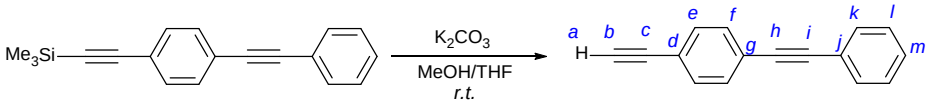


**Preparation of $HC{\equiv}CC_6H_4C{\equiv}CC_6H_5$.**[16] In a 100 mL round bottom flask, $Me_3SiC{\equiv}CC_6H_4C{\equiv}CC_6H_5$ (2.94 g, 10.7 mmol) and $K_2CO_3$ (4.04 g, 29.2 mmol) were dissolved in MeOH:THF (1:1) (100 mL) and stirred overnight at room temperature. The mixture was then poured into water and extracted with $CH_2Cl_2$ (3×50 mL). The organic extracts were then washed with water (2×100 mL) and brine (1×100 mL) and dried over $MgSO_4$. The pure product was obtained as a white solid after removal of the solvent. Yield 2.04 g, 10.1 mmol, 94%.$^1$H NMR (400 MHz, $CDCl_3$) δ 7.56 – 7.51 (m, 2H, *e*), 7.51 – 7.45 (m, 4H, *f/k*), 7.39 – 7.33 (m, 3H, *l/m*), 3.18 (s, 1H, *a*).$^{13}$C NMR (126 MHz, $CDCl_3$) δ 132.2, 131.7, 131.6, 128.6, 128.5 (*e/f/k/l/m*), 123.9, 123.0, 122.0 (*d/g/j*), 91.5, 90.0 (*h/i*), 83.4, 79.1 (*b/c*). $MS^+$ (ASAP) *m/z* (%): 202.3 (100, $[M]^+$).

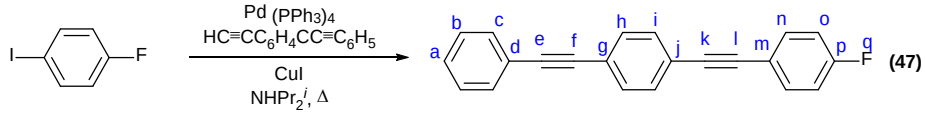


**Preparation of 47.**[17] To a 100 mL Schlenk flask charged with $NHPr^i_2$ (50 mL), $HC{\equiv}CC_6H_4C{\equiv}CC_6H_5$ (0.205 g, 1.01 mmol), 1,4-iodofluorobenzene (0.279 g, 1.25 mmol), $Pd(PPh_3)_4$ (0.062 g, 0.053 mmol) and CuI (0.010 g, 0.052 mmol) were added. The resulting mixture was heated at reflux overnight and then taken to dryness and purified by silica gel column chromatography using hexane:$CH_2Cl_2$ (8:2) as the eluent. The product was crystallized from $CH_2Cl_2$:MeOH. Yield 0.051 g, 0.172 mmol, 17%. $^1$H NMR (400 MHz, $CDCl_3$) δ 7.56 – 7.47 (m, 8H), 7.36 (m, 3H), 7.09 – 7.04 (m, 2H, *o*). $^{19}$F NMR (376 MHz, $CDCl_3$) δ -110.5 (tt, *J'*= 8 Hz, *J''*= 5 Hz, *q*). $MS^+$ (ASAP) *m/z* (%): 296.06 (100, $[M]^+$).

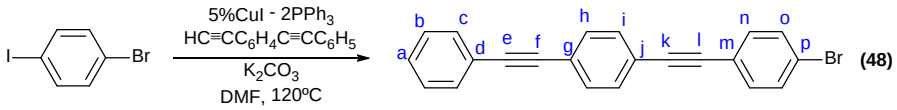

(48)

**Preparation of 48.**[17] To a 50 mL Schlenk flask charged with DMF (40 mL), $HC{\equiv}CC_6H_4C{\equiv}CC_6H_5$ (0.198 g, 0.980 mmol), 1,4-iodobromobenzene (0.287 g, 1.01 mmol), CuI (0.011 g, 0.058 mol), $PPh_3$ (0.031 g, 0.118 mmol) and $K_2CO_3$ (0.182 g, 1.31 mmol), were added. The mixture was stirred at 120ºC overnight and then poured into water and extracted with $CH_2Cl_2$ (50 mL). The organic phase was then washed with water (2×50 mL) and brine (1×50 mL), and dried over $MgSO_4$. The pure product was dissolved in $CH_2Cl_2$ and isolated by precipitation upon addition of MeOH. Yield 0.112 g, 0.314 mmol, 32%. $^1$H NMR (700 MHz, $CDCl_3$) δ 7.57 – 7.47 (m, 8H, *c/h/i/n*), 7.39 (d, *J* = 8.3 Hz, 2H, *o*), 7.38 – 7.33 (m, 3H, *a-b*). $MS^+$ (ASAP) *m/z* (%): 355.99 (100, $[M]^+$).

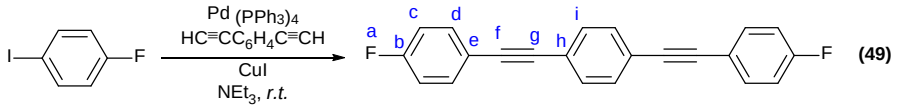

(49)

**Preparation of 49.**[18] In a 50 mL round bottom flask 4-fluoroiodobenzene (1.60 g, 7.23 mmol), $HC{\equiv}CC_6H_4C{\equiv}CH$, 0.397 g, 3.15 mmol), $Pd(PPh_3)_4$ (0.362 g, 0.313 mmol) and CuI (0.062 g, 0.326 mmol) were dissolved anhydrous degassed $NEt_3$ (25 mL). The reaction mixture was stirred overnight at room temperature. The light-brown precipitate was collected by filtration and crystallized from hot toluene yielding the pure product as yellow needles. Yield 0.32 g, 1.0 mmol, 32%. $^1$H NMR (400 MHz, $CDCl_3$) δ 7.54 – 7.47 (m, 8H, *d/i*), 7.09 – 7.04 (m, 4H, *c*). $^{19}$F NMR (376 MHz, $CDCl_3$) δ -110.5 (m, *a*). $MS^+$ (ASAP) *m/z* (%): 314.26 (100, $[M]^+$).

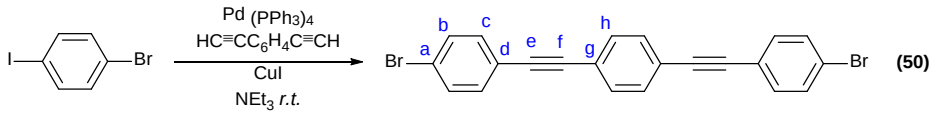

(50)

**Preparation of 50.**[19] To a 25 mL Schlenk flask charged with $NEt_3$ (25 mL), 1-bromo-4-iodobenzene (1.012 g, 3.577 mmol), $HC{\equiv}CC_6H_4C{\equiv}CH$ (0.205 g, 1.625 mmol), $Pd(PPh_3)_4$ (0.090 g, 0.078 mmol) and CuI (0.021 g, 0.110 mmol) were added. The reaction mixture was stirred overnight at room temperature. Upon completion of the reaction, the precipitate was collected by filtration and washed thoroughly with $CH_2Cl_2$ yielding the pure product as a white powder. Yield 0.610 g, 1.40 mmol, 86%. $^1$H NMR (400 MHz, $CDCl_3$) δ 7.52-7.46 (m, 8H, *c/h*); 7.39 (d, *J* =9 Hz, 4H, *b*). $MS^+$ (ASAP) *m/z* (%): 435.91 (100, $[M]^+$). Elemental analysis % calcd. (found): C 60.59 (60.43); H 2.77 (2.81).

## B.9. References


1. (a) Pawin, G.; Wong, K. L.; Kwon, K.-Y.; Bartels, L., *Science*, **2006**, *313*, 961-962; (b) Whitesides, G. M.; Grzybowski, B., *Science*, **2002**, *295*, 2418-2421; (c) Barth, J. V.; Weckesser, J.; Lin, N.; Dmitriev, A.; Kern, K., *Appl. Phys. A*, **2003**, *76*, 645-652.
2. (a) Kiguchi, M.; Murakoshi, K., *Thin Solid Films*, **2009**, *518*, 466-469; (b) Cheng, Z. L.; Skouta, R.; H., V.; Widawsky, J. R.; Schneebeli, S.; Chen, W.; Hybertsen, M. S.; Breslow, R.; Venkataraman, L., *Nat. Nano*, **2011**, *6*, 353-357.
3. Hla, S.-W.; Bartels, L.; Meyer, G.; Rieder, K.-H., *Phys. Rev. Lett.*, **2000**, *85*, 2777-2780.
4. Grill, L.; Dyer, M.; Lafferentz, L.; Persson, M.; Peters, M. V.; Hecht, S., *Nat. Nano*, **2007**, *2*, 687-691.
5. Lambe, J.; McCarthy, S. L., *Phys. Rev. Lett.*, **1976**, *37*, 923-925.
6. Johansson, P.; Monreal, R.; Apell, P., *Phys. Rev. B: Condens. Matter*, **1990**, *42*, 9210-9213.
7. (a) Hoffmann, G.; Libioulle, L.; Berndt, R., *Phys. Rev. B: Condens. Matter*, **2002**, *65*, 212107; (b) Poirier, G. E., *Phys. Rev. Lett.*, **2001**, *86*, 83-86; (c) Galperin, M.; Nitzan, A., *Phys. Chem. Chem. Phys.*, **2012**, *14*, 9421-9438.
8. Chen, C.; Chu, P.; Bobisch, C. A.; Mills, D. L.; Ho, W., *Phys. Rev. Lett.*, **2010**, *105*, 217402.
9. Uemura, T.; Furumoto, M.; Nakano, T.; Akai-Kasaya, M.; Saito, A.; Aono, M.; Kuwahara, Y., *Chem. Phys. Lett.*, **2007**, *448*, 232-236.
10. Liu, H. W.; Ie, Y.; Nishitani, R.; Aso, Y.; Iwasaki, H., *Phys. Rev. B: Condens. Matter*, **2007**, *75*, 115429.
11. Wu, S. W.; Nazin, G. V.; Ho, W., *Phys. Rev. B: Condens. Matter*, **2008**, *77*, 205430.

12. (a) Stipe, B. C.; Rezaei, M. A.; Ho, W.; Gao, S.; Persson, M.; Lundqvist, B. I., *Phys. Rev. Lett.*, **1997**, *78*, 4410-4413; (b) Hla, S.-W.; Meyer, G.; Rieder, K.-H., *Chem. Phys. Lett.*, **2003**, *370*, 431-436.
13. (a) Dujardin, G.; Mayne, A.; Robert, O.; Rose, F.; Joachim, C.; Tang, H., *Phys. Rev. Lett.*, **1998**, *80*, 3085-3088; (b) Kelly, K. F.; Sarkar, D.; Hale, G. D.; Oldenburg, S. J.; Halas, N. J., *Science*, **1996**, *273*, 1371-1373.
14. (a) Dong, Z. C.; Guo, X. L.; Trifonov, A. S.; Dorozhkin, P. S.; Miki, K.; Kimura, K.; Yokoyama, S.; Mashiko, S., *Phys. Rev. Lett.*, **2004**, *92*, 086801; (b) Ćavar, E.; Blüm, M.-C.; Pivetta, M.; Patthey, F.; Chergui, M.; Schneider, W.-D., *Phys. Rev. Lett.*, **2005**, *95*, 196102.
15. (a) Schull, G.; Néel, N.; Johansson, P.; Berndt, R., *Phys. Rev. Lett.*, **2009**, *102*, 057401; (b) Hoffmann, G.; Berndt, R.; Johansson, P., *Phys. Rev. Lett.*, **2003**, *90*, 046803.
16. Li, K.; Wang, Q., *Chem. Commun.*, **2005**, 4786-4788.
17. Doi, T.; Orita, A.; Matsuo, D.; Saijo, R.; Otera, J., *Synlett*, **2008**, *2008*, 55,60.
18. Keshtov, M.; Petrovskii, P.; Stakhanov, A.; Kochurov, V.; Khokhlov, A., *Doklady Chemistry*, **2009**, *429*, 277-282.
19. Ito, Y.; Miyazaki, A.; Takai, K.; Sivamurugan, V.; Maeno, T.; Kadono, T.; Kitano, M.; Ogawa, Y.; Nakamura, N.; Hara, M.; Valiyaveettil, S.; Enoki, T., *J. Am. Chem. Soc.*, **2011**, *133*, 11470-11473.

# APPENDIX C. LINKER DEPENDENT BOND RUPTURE FORCE MEASUREMENTS IN SELF-ASSEMBLED MONOLAYERS

## C.1. Introduction

In collaboration with Dr. Thomas Becker at Curtin University, Western Australia, a series of AFM experiments were conducted in order to assess the force required to rupture the junction formed by symmetrically substituted OPEs terminated with three different molecular linkers, *i.e.* $NH_2$ (**34**), C≡CSiMe$_3$ (**35**) and C≡CH (**36**) (Chart C-1) and hence again further information about the nature of the linker-substrate interaction in this series. Preliminary results show a well-defined trend for the break-off force where $NH_2$ > C≡CSiMe$_3$ > C≡CH. A Visual Basic (VBA) code was designed in order to allow a quick and effective analysis of the large datasets collected, revealing experimental artefacts that were not detected using the AFM software alone. Future AFM investigations following this work are briefly described.

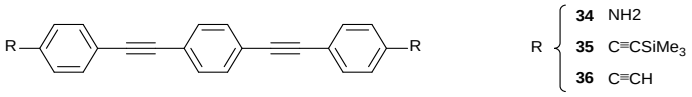


**Chart C-1.** *Compounds employed to generate SA monolayers and test the strength of the metal|molecule interaction.*

## C.2. Sample preparation

A Bruker Dimension FastScan AFM controlled using FastScan NanoScope software was used to conduct all of the measurements described here. The gold-on-glass substrates employed were purchased from Arrandee, Schroeer, Germany. The substrates were flame annealed with a propane flame immediately before use. This thermal treatment is known to generate atomically flat terraces on the Au(111) substrate.[1] The substrates

were immersed in low concentration solutions (~$10^{-5}$ M, $CHCl_3$) of compounds **34 - 36** for 24 hours to ensure full coverage of the gold substrate. After incubation, the samples were rinsed thoroughly with $CHCl_3$ and blown dry in a stream of $N_2$ gas, immediately before placing them on the AFM holder for their analysis. The force rupture experiments were performed in water by placing a few drops of mili-Q water on the substrate with a gold coated silicon nitride probe with radius < 25 nm.

## C.3. Results and discussion

As it was discussed in detail in Chapter 5, the metal|molecule interface is now considered an essential factor in the electrical performance of a molecular junction.[2] As a clarifying example, a difference in conductance of up to three orders of magnitude between chemisorbed and a physisorbed molecules has been reported.[3] However, whilst the influence of the contacting group on junction behaviour is widely recognised, the physical properties of the metal-molecule interactions are often overlooked. Here we present the preliminary results obtained from a series of AFM experiments, evaluating the strength of the metal|molecule interaction of the same molecular backbone terminated with three different linkers (Chart C-1), which have special relevance to the on-going investigations of the nature of the Au$\cdots$ $Me_3SiC{\equiv}C$ contact disclosed in this thesis.

A typical force-distance plot, showing the cantilever deflection (force) relative to the tip vertical movement (*z*) is displayed in Figure C-1. Generally, as the AFM tip is brought into contact with the molecular film (Figure C-1, *extension*) a small negative kink is observed as a result of the tip jumping into contact with the substrate in what is referred to as the “snap-in effect” due to short-range attractive interactions. After contacting the sample, as the tip is pushed into the surface, a monotonic increase of the repulsive (positive) force is recorded deriving from the deflection of the cantilever. When the

process is reversed, as the piezo is retracts from the surface, the adhesive forces generated between tip and substrate hold the tip in contact with the surface causing a large deflection of the cantilever. At a given distance, the cantilever force becomes enough to overcome the adhesive forces and as the tip breaks free, a marked force jump is recorded ($\Delta F$).

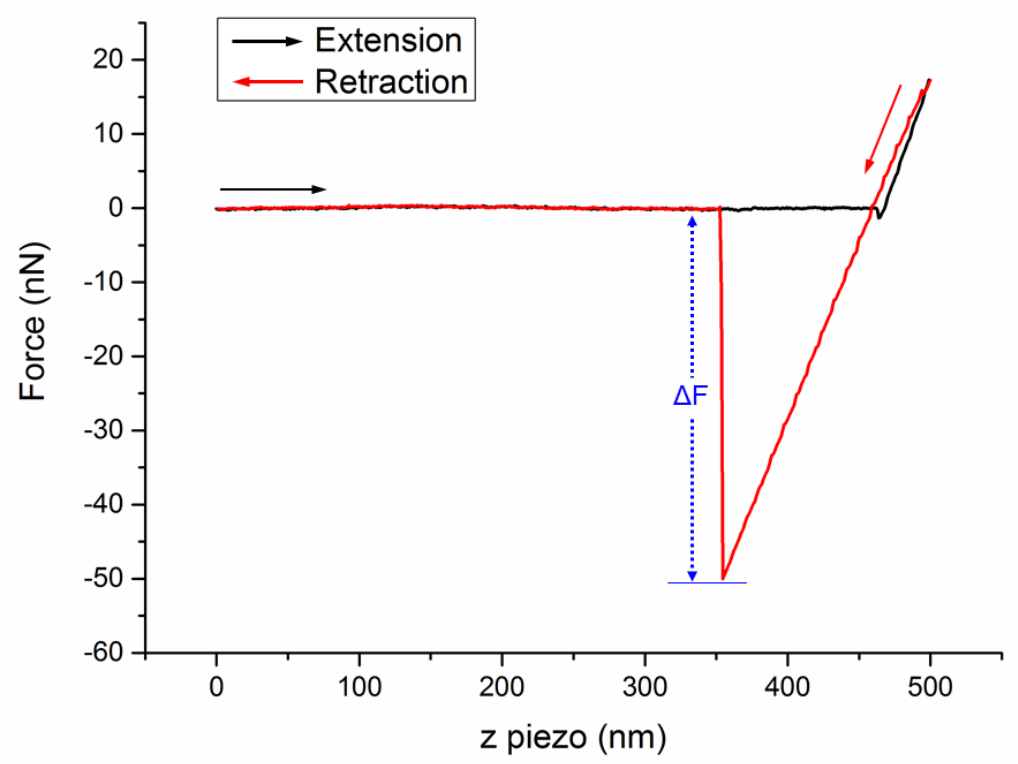


**Figure C-1.** *Typical force-distance AFM plot. Negative forces representing adhesive tip-substrate interactions.*

For molecular films, $\Delta F$ represents the adhesive force generated from the summation of the molecule|metal interaction from every individual molecule in the junction. For naked gold substrates, the rupture force $\Delta F$, of the metallic tip|substrate junction was determined to be 1.4 nN.[4] In contrast, for molecular junctions, the force required to break a *single* metal|molecule interaction was recently determined to be less than 1 nN.[4a] Figure C-2 presents the bond rupture histograms obtained for monolayers of compounds **34 – 36** employing a gold coated AFM tip (< 25 nm radius).

The values obtained from the NanoScope analysis software were 35.27 ± 10.36 nN for **34** ($NH_2$), 23.24 ± 4.73 nN for **35** ($C{\equiv}CSiMe_3$), and 10.35 ± 4.28 nN for **36** ($C{\equiv}CH$). Despite the large variability encountered, and the uncertainty in the number of molecules within each junction that makes quantitative analysis of the data unclear, a marked trend $NH_2$ > $C{\equiv}CSiMe_3$ > $C{\equiv}CH$ can be observed where the adhesive force is greatest for the more traditional amine linker. Hence, although only qualitatively, the results follow the expected trend for the series, if one makes the assumption that a similar number of molecules are contacted to the tip in each case.

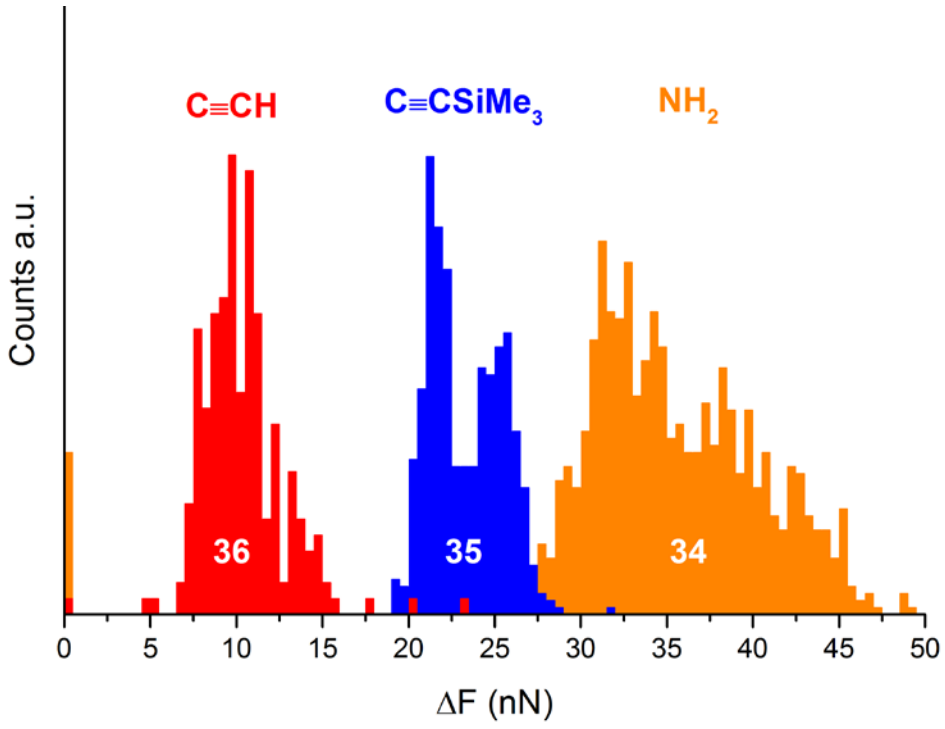


**Figure C-2.** *Rupture force histograms corresponding to compounds **34 - 36** in water.*

Despite the clear trend observed, we turned our attention to the causes of the great deviation registered for these experiments. This becomes evident for **35** where the results obtained show a marked double normal distribution with their centre at $\Delta F_1$ ~ 22 nN and $\Delta F_2$ ~ 26 nN (Figure C-2). In an analogous manner to the STM experiments, we found that, the commercial software provided with the AFM resulted impractical for the

treatment of large datasets. Hence, in order to gain further insight into the origin of the significative data dispersion, a Visual Basic (VBA) code for Excel (*vide infra*) was developed to enable statistical treatment of the raw AFM data. The code is designed to import large datasets (*i.e.* over 1000 traces per sample), read, calibrate the distance axis, update the baseline, extract $\Delta F$ and rearrange the data to facilitate plotting with third party software. The efficiency of this code to analyse large datasets enabled quicker and deeper analysis of the experimental results leading us to conclude that the significant and sharp deviation obtained for individual data sets within these experiments was a consequence of experimental artefacts and not intrinsic of the metal|molecule interaction.

As an example of the possibilities enabled by the VBA code analysis, the drift of the bond rupture force ($\Delta F$) extracted by the VBA code for compound **35**, was examined in detail. Figure C-3 shows the bond rupture force recorded in chronological order. As it is evident from the figure, the first 250 experiments display a bond rupture force value in the range of 21 - 23 nN ($\Delta F_1$). However, a sudden increase in the rupture force is observed for the second half of the data with values ranging from 26 - 28 nN ($\Delta F_2$). This results undoubtedly ascribe the origin of the two normal distributions present in the rupture force histogram of compound **35** (Figure C-2) to experimental artefacts. Although less evident, similar step-wise deviations were also found for compounds **34** and **36** when the raw data was examined employing the developed VBA code.

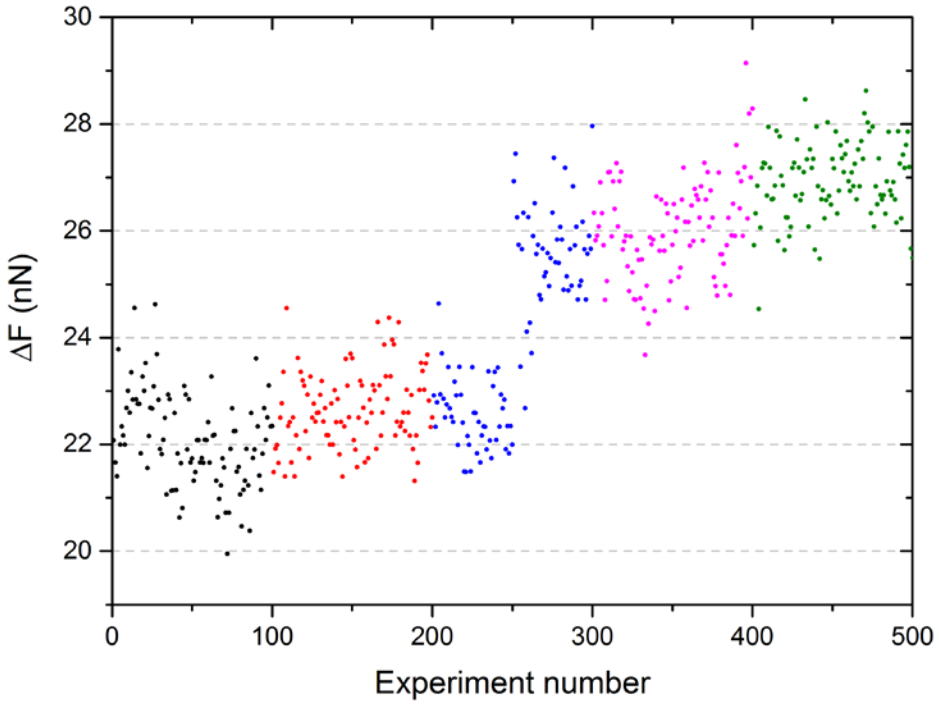


**Figure C-3.** *Bond rupture force trend obtained for **35** (500 experiments).*

In an analogous way to that described for the STM conductance traces (*see* Appendix A), the VBA code developed here allows 2D plotting of the calibrated data. Figure C-4, presents the 2D map of the force-distance VBA calibrated retraction traces recorded for **35**, clearly showing the origin of $\Delta F_1$ and $\Delta F_2$ responsible for the double normal distribution seen in the force histogram (Figure C-2) The origin of this step-wise change is not entirely clear, but may be due to either drift in the experimental system, a change in the shape of the tip or some other as yet unidentified experimental variation. It is difficult to correlate such clear step-wise change to a molecular effect, given the underlying molecular ensemble giving rise to the data.

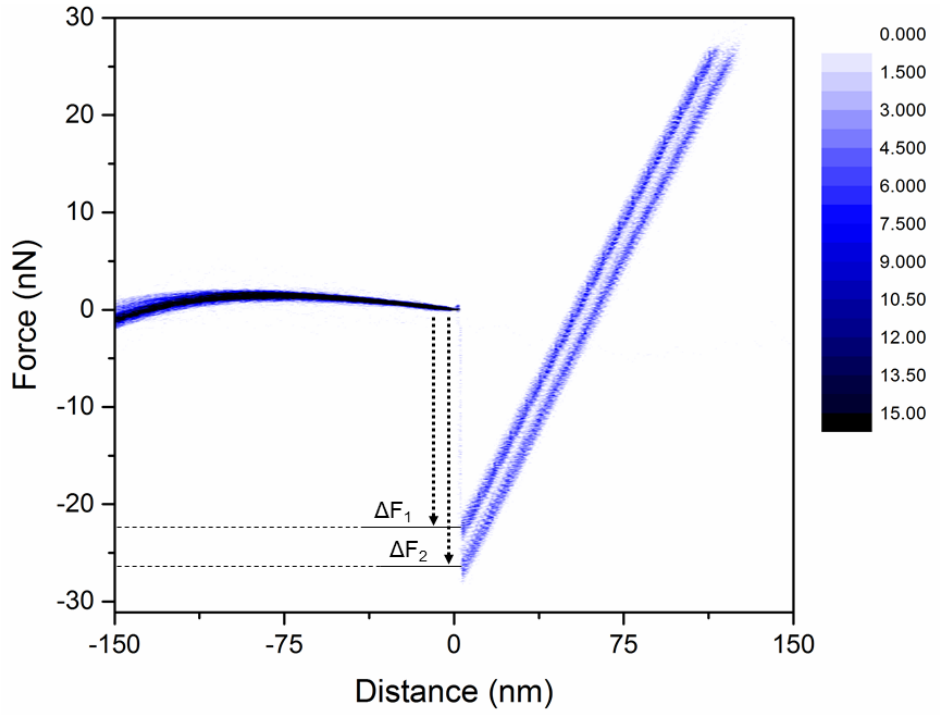


**Figure C-4.** *2D binning the force-distance retraction traces of **35** showing a marked splitting in the bond rupture force values.*

Despite, the step-wise variability encountered which hampers quantitative analysis of these results, qualitatively the data shows a marked trend for the strength of the metal|molecule interaction $NH_2$ > C≡C$SiMe_3$ > C≡CH. However further experiments are required to clarify these results. A series of AFM experiments have been designed, in which the SA monolayers of the compounds of interest will be both imaged and the forces simultaneously determined in dry mesitylene, a common solvent for such work, and the data will be analysed with help of the VBA code. In addition, compounds **39** (SAc) and **51** (Py) (Chart C-2) have been prepared and will be introduced in the next series experiments in order to obtain a wider comparative study between the different linkers. However at this stage of the investigation it can be concluded that the novel trimethylsilylethynyl (C≡C$SiMe_3$) contact introduced in this thesis is comparable with that of the amine group, and given the significant difference in contact force between compounds **34** and **36**,

desilylation in the junction can be largely discounted. This is entirely in agreement with the other results concerning junctions involving novel contacting group described in the thesis.

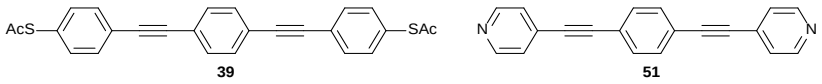


**Chart C-2.** *Compounds prepared to be included into the next series of experiments.*

## C.4. VBA code

The BJ calibration program was written in Visual Basic language for Microsoft Excel 2010. The code can be run on PC versions of Microsoft Excel 2007 or later. The code is provided with the electronic content associated with this thesis. The reader is encouraged to copy, modify and share this code for academic and educational purposes only.

## C.5. Experimental

### *C.5.1. General conditions*

General experimental conditions were reported in Chapter 2. The synthesis of HC≡CC$_6$H$_4$C≡CH and **34 - 36** (Chapter 5) were reported in previous experimental sections of this thesis. Other reagents were purchased commercially and used as received.

### *C.5.2. Synthesis and characterization*

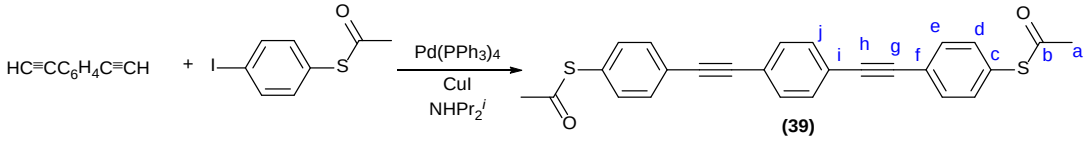


**Preparation of 39.**[5] To a 25 mL Schlenk flask charged with NHPr$_2^i$ (15 mL), HC≡CC$_6$H$_4$C≡CH (0.068 g, 0.539 mmol), 1-iodo-4-acetylthiobenzene (0.301 g, 1.08 mmol), Pd(PPh$_3$)$_4$ (0.057 g, 0.049 mmol) and CuI (0.010 g, 0.052 mmol) were added. The

mixture was stirred overnight at room temperature. The orange precipitate was collected by filtration and washed with hexane. The product was purified by silica gel column chromatography hexane: $CH_2Cl_2$ (6:4). The targeted compound was obtained after solvent evaporation of the main fraction, as an off-white powder. Yield 0.151 g, 0.354 mmol, 66 %. $^1$H NMR (500 MHz, $CDCl_3$) δ 7.56 (d, *J* = 8 Hz, 4H, *e*), 7.52 (s, 4H, *j*), 7.41 (d, *J* = 8 Hz, 4H, *d*), 2.44 (s, 6H, *a*). $^{13}$C{$^1$H} NMR (126 MHz, $CDCl_3$) δ 193.4 (*b*), 134.3, 132.2, 131.66 (*d*/*e*/*j*), 128.4 (*c*), 124.2, 123.0 (*f*/*i*), 90.7, 90.6 (*h*/*g*), 30.3 (*a*). MS$^+$ (ESI) *m*/*z* (%): 172.0 (100, [M-2COMe+2H]$^{2+}$). IR ($CH_2Cl_2$) cm$^{-1}$: 2217 (w), 2204 (w) *ν*(C≡C); 1707 (br. s) *ν*(C=O).

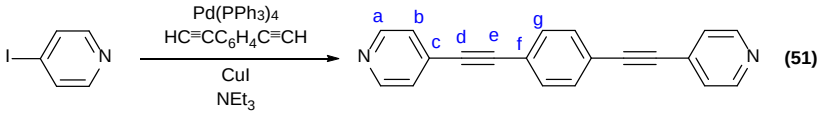

**(51)**

**Preparation of 51.**[6] To a 100 mL Schlenk flask charged with $NEt_3$ (100 mL), 4-iodopyridine (0.334 g, 1.63 mmol), HC≡C$C_6H_4$C≡CH (0.101 g, 0.801 mmol), $Pd(PPh_3)_4$ (0.045 g, 0.039 mmol) and CuI (0.008 g, 0.042 mmol) were added. The suspension was stirred overnight at room temperature. The mixture was filtered and the colourless filtrate taken to dryness. The off-white solids were dissolved in $Et_2O$ (100 mL). Addition of trifluoroacetic acid generated a precipitate that was collected by filtration, washed thoroughly with $Et_2O$ and dried in air. The solids were re-dissolved in $CH_2Cl_2$ (25 mL) and extracted with KOH (0.1 M, 1 × 25 mL), water (1 × 25 mL) and brine (1 × 25 mL). The organic phase was collected, dried over $MgSO_4$ and taken to dryness. The pure product was obtained as an off-white powder. Yield 0.156 g, 0.556 mmol, 69 %. $^1$H NMR (400 MHz, $CDCl_3$) δ 8.62 (d, *J* = 5 Hz, 4H, *a*), 7.56 (s, 4H, *g*), 7.38 (d, *J* = 5 Hz, 4H, *b*). $^{13}$C{$^1$H} NMR (101 MHz, $CDCl_3$) δ 150.0 (*a*), 132.1(*g*), 131.2 (*c*), 125.6 (*b*), 123.0 (*f*), 93.3, 89.0 (*d*/*e*). MS$^+$ (ASAP) *m*/*z* (%): 281.17 (100, [M+H]$^+$).

## C.6. References


1. Haiss, W.; Lackey, D.; Sass, J. K.; Besocke, K. H., *J. Chem. Phys*, **1991**, *95*, 2193-2196.
2. Liu, H.; Wang, N.; Zhao, J.; Guo, Y.; Yin, X.; Boey, F. Y. C.; Zhang, H., *ChemPhysChem*, **2008**, *9*, 1416-1424.
3. (a) Salomon, A.; Cahen, D.; Lindsay, S.; Tomfohr, J.; Engelkes, V. B.; Frisbie, C. D., *Adv. Mater.*, **2003**, *15*, 1881-1890; (b) Cui, X. D.; Primak, A.; Zarate, X.; Tomfohr, J.; Sankey, O. F.; Moore, A. L.; Moore, T. A.; Gust, D.; Harris, G.; Lindsay, S. M., *Science*, **2001**, *294*, 571-574; (c) Selzer, Y.; Salomon, A.; Cahen, D., *J. Am. Chem. Soc.*, **2002**, *124*, 2886-2887; (d) Seminario, J. M.; Yan, L., *Int. J. Quantum Chem*, **2005**, *102*, 711-723; (e) Kaun, C.-C.; Guo, H., *Nano Lett.*, **2003**, *3*, 1521-1525.
4. (a) Frei, M.; Aradhya, S. V.; Hybertsen, M. S.; Venkataraman, L., *J. Am. Chem. Soc.*, **2012**, *134*, 4003-4006; (b) Rubio, G.; Agraït, N.; Vieira, S., *Phys. Rev. Lett.*, **1996**, *76*, 2302-2305; (c) Rubio-Bollinger, G.; Bahn, S. R.; Agraït, N.; Jacobsen, K. W.; Vieira, S., *Phys. Rev. Lett.*, **2001**, *87*, 026101.
5. Haiss, W.; Wang, C.; Grace, I.; Batsanov, A. S.; Schiffrin, D. J.; Higgins, S. J.; Bryce, M. R.; Lambert, C. J.; Nichols, R. J., *Nat. Mater.*, **2006**, *5*, 995-1002.
6. Zhao, X.; Huang, C.; Gulcur, M.; Batsanov, A. S.; Baghernejad, M.; Hong, W.; Bryce, M. R.; Wandlowski, T., *Chem. Mater.*, **2013**, *25*, 4340-4347.

*“It is a miracle that curiosity survives formal education”*

**Albert Einstein**